



<https://theses.gla.ac.uk/>

Theses Digitisation:

<https://www.gla.ac.uk/myglasgow/research/enlighten/theses/digitisation/>

This is a digitised version of the original print thesis.

Copyright and moral rights for this work are retained by the author

A copy can be downloaded for personal non-commercial research or study, without prior permission or charge

This work cannot be reproduced or quoted extensively from without first obtaining permission in writing from the author

The content must not be changed in any way or sold commercially in any format or medium without the formal permission of the author

When referring to this work, full bibliographic details including the author, title, awarding institution and date of the thesis must be given

Enlighten: Theses

<https://theses.gla.ac.uk/>
research-enlighten@glasgow.ac.uk

**Structure and function studies on the LH1-RC core
complex from a range of photosynthetic purple
bacteria**

by

Christopher J. Law

A thesis submitted for the degree of Doctor of Philosophy

University of Glasgow

Department of Biochemistry & Molecular Biology

December 1998

ProQuest Number: 10391135

All rights reserved

INFORMATION TO ALL USERS

The quality of this reproduction is dependent upon the quality of the copy submitted.

In the unlikely event that the author did not send a complete manuscript and there are missing pages, these will be noted. Also, if material had to be removed, a note will indicate the deletion.



ProQuest 10391135

Published by ProQuest LLC (2017). Copyright of the Dissertation is held by the Author.

All rights reserved.

This work is protected against unauthorized copying under Title 17, United States Code
Microform Edition © ProQuest LLC.

ProQuest LLC.
789 East Eisenhower Parkway
P.O. Box 1346
Ann Arbor, MI 48106 – 1346

GLASGOW
UNIVERSITY
LIBRARY

11444 (copy 2)

Abstract

The LH1-RC core complexes from a range of purple bacterial species were investigated. The complexes were isolated by solubilisation with the detergent LDAO, then purified using a combination of techniques such as sucrose gradient centrifugation, anion exchange and gel filtration chromatography. The integrity of the complexes during purification was monitored by means of absorption spectroscopy. This showed that the stability of the detergent solubilised cores was species dependent. The most stable cores were obtained from *Rps. acidophila*, *Rps. cryptolactis*, *Rps. palustris* and *Chr. vinosum*. The least stable core complexes were from *Rv. gelatinosus* and *Rs. rubrum*. The intactness and stability of the purified cores was further investigated by circular dichroism (CD) spectroscopy. This technique provided a much more sensitive spectral test for intactness than that offered by absorption spectroscopy. CD spectra in the NIR region confirmed that the cores from *Rv. gelatinosus* and *Rs. rubrum* denatured during purification.

The purified core complexes were screened for their suitability for forming 3-D crystals using vapour diffusion methods. Core complex crystals did not form when LDAO was used as detergent or when ammonium sulphate and potassium phosphate were used as precipitants. However, when LDAO was exchanged for other detergents, such as cholate and heptyl thioglucoside, and PEG was used as a precipitant core complex crystals did form. The presence of $MgCl_2$ and other small additives seemed an absolute requirement for crystal formation. The best crystals were obtained using core complex from *Rps. acidophila* strain 10050. Preliminary characterisation of one of these crystals showed it diffracted X-rays to a resolution of 7.6\AA . Data analysis suggested a space group with putative tetragonal P4 symmetry and unit cell dimensions of $a=b=156.56\text{\AA}$ and $c=181.11\text{\AA}$, and $\alpha=\beta=\gamma=90.0^\circ$. Due to a problem of irreproducibility the crystallisation experiments failed to yield crystals of a sufficient quality to allow a structural determination of the LH1-RC core.

The LH1 (B880) complex from *Rh. marinum* was also isolated and purified, and the effects of chemical oxidation on its absorption and fluorescence emission spectra was investigated. Mild chemical oxidation of the LH1 complex, by addition of 10mM potassium ferricyanide, caused a 2-3% bleaching of the 880nm Q_y absorption band. In contrast, at the same ferricyanide concentration, fluorescence emission intensity of the complex was quenched by about 50%. This result demonstrated that oxidation of a very few bacteriochlorophyll molecules in the LH1 ring is enough to completely quench its fluorescence. This suggests the possibility of redox control of energy transfer.

The antenna arrangement in the photosynthetic membrane of the 7750 strain of the purple bacterium *Rps. acidophila* was investigated by means of fluorescence induction spectroscopy. The membrane of this species is thought to be composed of LH1-RC core complexes which are surrounded by peripheral LH2 complexes. The sigmoidicity of fluorescence induction curves was used to probe the excitonic connectivity of RC's, and this information were used to gain information on the structural arrangement of the antennae. The data obtained excluded models of the *Rps. acidophila* photosynthetic unit (PSU) that assume aggregates of LH1-RC complexes or linear chains of LH1-RC complexes to which LH2 complexes are attached on the periphery. Rather, they support the model suggested by Papiz *et al.* (1996) (Trends in Plant Science 1, 198-206) in which peripheral LH2 rings tightly surround each core complex circumferentially.

Acknowledgements

I would like to extend my gratitude to my supervisor, Prof. Richard Cogdell, for giving me the opportunity of studying in his laboratory, for his encouragement and advice, and for beers in the Aragon on a Friday night. Thanks too to the people who work (or worked) in the Lab B4a during the time I spent there working on this thesis. They are (in no particular order!) Evelyn Johnstone, Tina Howard, Niall Fraser, Paul Fyfe, Katherine McAuley-Hecht, Karen McLuskey, Juan Arellano and Kim McKendrick. A special mention will go to Stuart Barrett for the laughs we have had (remember Budapest!!!) and for being a fan of the Simpsons. Thanks also to all the friends I have made in the Depts of Botany and Crystallography - hopefully you are too many to mention individually but you will know who you are. I am also indebted to Steve Prince and Peter Dominy for always making time for discussion and for keeping an eye on me when Richard was on sabbatical in Berlin. Thanks guys.

During my studies I was fortunate enough to spend time in Osnabrück, Germany working with Prof. Hawi Trissl - a physicist and a gentleman. Hawi gave me a different appreciation of some of the more biophysical aspects of photosynthesis and he was always willing to spend time to teach me the theory behind them. Thanks also to Dr. Werner Kühnbrandt who allowed me to study in his lab at Frankfurt to learn 2-D crystallisation and electron microscopy techniques. At this point I must mention Alastair Gardiner. During my stay in Frankfurt, Alastair met me at the airport, arranged my accommodation and showed me the best eating houses (read as pubs) even though he had much more important issues to deal with. Get well soon Alastair.

I must acknowledge the BBSRC for funding my research studentship, and the ESF and EMBO for providing the fellowships that allowed me to work in Germany. Finally, I would like to dedicate this thesis to my mother and late father. Without their support and encouragement this work would never have been completed.

Abbreviations

The S.I. standard is used where possible throughout this thesis. Most of the abbreviations used are explained in the text. The most common ones are:

λ	wavelength
ϕ	bacteriopheophytin
Å	Angstrom
Bchl	bacteriochlorophyll
BPhe	bacteriopheophytin
Car	carotenoid
CD	circular dichroism
cyt	cytochrome
Da	Dalton
EM	electron microscopy
ICM	intracytoplasmic membrane
LDAO	lauryl dimethylamine- <i>N</i> -oxide
LH1	light-harvesting complex 1
LH2	light-harvesting complex 2
LH1-RC	light-harvesting complex 1-reaction centre
NIR	near infrared
OD	optical density
PS	photosynthetic
β -OG	n-octyl- β -D-glucopyranoside
P870	special pair bacteriochlorophylls
PEG	polyethylene glycol
ps	picosecond
PSM	photosynthetic membrane
PSU	photosynthetic unit
Q	quinone
RC	reaction centre
SDS	sodium dodecyl sulphate
UV	ultraviolet

INDEX

Abstract	ii
Acknowledgements	iv
Abbreviations	v
Declaration	vi
Table of Contents	vii
Table of Figures	xi

TABLE OF CONTENTS

Chapter One: Introduction

1.1..An overview of photosynthesis	1
1.2..A brief history of photosynthesis research	3
1.3..Physiology of the phototrophic purple bacteria	4
1.4. Taxonomy of the phototrophic purple bacteria	6
1.5. The purple bacterial photosynthetic apparatus	9
1.5.1. The bacteriochlorophylls	9
1.5.2. Purple bacterial antenna complexes	13
1.5.3. General aspects of antenna complex structure	16
1.5.4. Peripheral antenna complex variability	20
1.5.5. The carotenoids	24
1.5.5.1. Photoprotection	25
1.5.5.2. Accessory light harvesting	27
1.5.5.3. Structure stabilisation	28
1.6. The photochemical reaction centre	29
1.6.1. The RC protein subunits	33
1.6.2. Arrangement of the cofactors and electron flow through the RC	35
1.6.3. Electron flow beyond the RC	37

1.7. Structure of the LH2 (b800-850) antenna complex	39
1.7.1. Binding and arrangement of the Bchl <i>a</i> molecules	42
1.7.2. The bacteriochlorophyll phytyl tails	45
1.7.3. Structure and arrangement of the carotenoids	46
1.8. Structure of the LH1-RC 'core' complex	47
1.8.1. The <i>Rhodopseudomonas viridis</i> core complex	48
1.8.2. The <i>Rhodospirillum rubrum</i> core complex	50
1.8.3. The size of the LH1 ring	52
1.8.4. The role of the pufX protein	55
1.8.5. Structure and topology within the membrane of the pufX protein	56
1.9. The concept of the photosynthetic unit	57
1.9.1. The purple bacterial PSU	58
1.10. Energy transfer within the PSU	65
1.11. 3-D crystallisation of proteins	68
1.11.1. Physical chemistry of protein crystallisation	68
1.11.2. The strategy of crystallisation	71
1.11.3. Methods for producing supersaturation	72
1.11.4. 3-D crystallisation of membrane proteins	75
1.12. Thesis aims	82
 <u>Chapter Two: Cell culture and protein purification</u>	
2.1. Cell culture	83
2.1.1. General culture conditions	83
2.1.2. <i>Rhodobium marinum</i> strain 2698	84
2.1.3. <i>Rhodopseudomonas acidophila</i> strain 7750	85
2.1.4. <i>Rhodopseudomonas cryptolactis</i>	85
2.2. Cell harvesting	86
2.3. Preparation of photosynthetic membranes and chromatophores	86
2.3.1. Preparation of <i>Rhodopseudomonas acidophila</i> photosynthetic membranes for	

fluorescence induction studies	87
2.4. Purification of the LH1-RC core complex	88
2.4.1. Solubilisation of photosynthetic membranes and chromatophores	88
2.4.2. Sucrose gradient centrifugation	90
2.4.3. Anion exchange chromatography	90
2.4.4. Gel filtration chromatography	91
2.4.5. Detergent exchange	92
2.5. Purification of <i>Rhodobium marinum</i> B880 complex	93
2.6. 3-D crystallisation of the LH1-RC core and B880 complexes	94
2.6.1. Purification of PEG	97
2.6.2. Crystal characterisation and X-ray diffraction studies	98
 <u>Chapter Three: Spectroscopic and analytical techniques</u>	
3.1. Absorption spectroscopy	100
3.2. Fluorescence emission spectroscopy	101
3.3. Fluorescence induction spectroscopy	101
3.3.1. Spectral decomposition	105
3.4. Circular dichroism spectroscopy	107
3.5. Polypeptide analysis	108
3.5.1. Determination of protein concentration	108
3.5.2. SDS-PAGE	108
3.6. Electron microscopy	111
 <u>Chapter Four: Purification and characterisation of the LH1-RC core complex</u>	
4.1. Purification and characterisation of the LH1-RC core complex	113
4.2. <i>Rhodospseudomonas acidophila</i> strain 10050	113
4.3. <i>Rhodospseudomonas palustris</i> strain French	132
4.4. <i>Rhodospseudomonas cryptolactis</i>	137
4.5. <i>Rubrivivax gelatinosus</i>	141

4.6. <i>Chromatium vinosum</i> strain D	147
4.7. <i>Rhodospirillum rubrum</i> strain S1	152
4.8. <i>Rhodobium marnum</i> strain DSM 2698	155
4.9. <i>Rhodobium marinum</i> DSM 2698 B880 complex	158

Chapter Five: Circular dichroism (CD) spectroscopy of the LH1-RC core complexes

5.1. Circular dichroism (CD) spectroscopy of the LH1-RC core complexes	165
5.2. <i>Rhodopseudomonas acidophila</i> strain 10050 core complex	167
5.3. <i>Rhodopseudomonas palustris</i> strains French and 1a1 core complexes	171
5.4. <i>Rhodopseudomonas cryptolactis</i> core complex	174
5.5. <i>Rubrivivax gelatinosus</i> strains DSM 149 and DSM 151 core complexes	176
5.6. <i>Chromatium vinosum</i> strain D core complex	179
5.7. <i>Rhodospirillum rubrum</i> and <i>Rhodobium marinum</i> core complexes	181

Chapter Six: The effect of chemical oxidation on the fluorescence of the LH1 (B880) complex from *Rhodobium marinum*

6.1. The effect of chemical oxidation on the fluorescence of the LH1 (B880) complex from <i>Rhodobium marinum</i>	185
---	-----

Chapter Seven. Antenna organisation in the purple bacterium *Rhodopseudomonas acidophila* strain 7750 studied by fluorescence induction

7.1. Fluorescence induction spectroscopy as a probe of PSU structure	196
7.2. Antenna organisation in the purple bacterium <i>Rhodopseudomonas acidophila</i> strain 7750 studied by fluorescence induction	199

Chapter Eight. 3-D crystallisation of the LH1-RC core complex

8.1. 3-D crystallisation of the LH1-RC core complex	210
8.2. <i>Rhodopseudomonas acidophila</i> strain 10050 core complex	213
8.3. <i>Rhodopseudomonas acidophila</i> strains 7750 and 7050 core complexes	243
8.4. <i>Rhodopseudomonas palustris</i> strains 1a1 and French core complexes	246

8.5. <i>Rhodospseudomonas cryptolactis</i> core complex	247
8.6. <i>Chromatium vinosum</i> strain D core complex	249
8.7. <i>Rhodospirillum rubrum</i> S1 core complex	250
8.8. <i>Rhodobium marinum</i> core and LH1-only complexes	253
<u>Chapter Nine. Discussion</u>	258
<u>Appendices</u>	
Appendix A: Composition of growth media	272
Appendix B: SDS-PAGE stock solutions	277
Appendix C: Crystallisation screens, detergents and additives	279
<u>References</u>	285

LIST OF FIGURES AND TABLES

Figure 1.1. Taxonomic tree of the Rhodospirillales	7
Figure 1.2. Different types of photosynthetic membrane	10
Figure 1.3. The chemical structure and absorption spectrum of bacteriochlorophyll <i>a</i>	12
Figure 1.4. NIR absorption spectrum of photosynthetic membranes of <i>Rps. acidophila</i>	13
Figure 1.5. Absorption spectra of an LH1-RC core and LH2 complex	15
Figure 1.6. Schematic diagram of the minimal structural units of an LH1 and LH2 complex	17
Figure 1.7. Absorption spectra of high and low-light grown LH2 from <i>Rps. palustris</i>	23
Figure 1.8. Structure of the <i>Rps. viridis</i> reaction centre	31
Figure 1.9. Cartoon of the reaction centre from <i>Rb. sphaeroides</i>	32
Figure 1.10. Diagram showing the spatial arrangement of cofactors in the RC of <i>Rb. sphaeroides</i>	36
Figure 1.11. Schematic diagram of the electron and proton transport pathway in purple bacteria	38
Figure 1.12. Schematic representation of the <i>Rps. acidophila</i> LH2 complex	41
Figure 1.13. Arrangement of the Bchl <i>a</i> molecules within the LH2 complex	43
Figure 1.14. Arrangement of pigments in the LH2 complex of <i>Rps. acidophila</i>	46
Figure 1.15. Contour map of the <i>Rps. viridis</i> photosynthetic membrane	49
Figure 1.16. Projection map of the LH1-RC complex from <i>Rps. viridis</i>	50
Figure 1.17. Projection map of the LH1 complex from <i>Rs. rubrum</i>	51
Figure 1.18. Model of the PSU	60
Figure 1.19. Models of the postulated PSU from <i>Rps. acidophila</i>	61
Figure 1.20. Schematic diagram of the PSU in a low-light grown purple bacterium	62
Figure 1.21. Schematic models of antenna organisation within different species of purple bacteria	63

Figure 1.22. Schematic diagram summarising timescales of energy transfer in purple bacteria	67
Figure 1.23. Typical solubility diagram	70
Figure 1.24. Schematic representation of hanging, sitting and sandwich drops	74
Figure 1.25. Schematic representation of a cross-section through a membrane protein	76
Figure 1.26. Schematic diagram showing two basic types of membrane protein crystals	79
Figure 1.27. Schematic phase diagrams	81
Figure 2.1. Absorption spectrum of LH1-RC complex from <i>Chr. vinosum</i> strain D	89
Figure 2.2. Discontinuous sucrose gradient of solubilised <i>Rps. cryptolactis</i> membranes	91
Figure 3.1. Schematic diagram of fluorescence induction apparatus	103
Figure 3.2. Spectral decomposition of <i>Rps. acidophila</i> strain 7750 photosynthetic membranes	106
Figure 3.3. Protein concentration calibration curve	109
Figure 4.1. Absorption spectrum of <i>Rps. acidophila</i> strain 10050 membranes	114
Table 4.1. Purification table for the LH1-RC complex from <i>Rps. acidophila</i> strain 10050	115
Figure 4.2. Sucrose gradient of solubilised membranes from <i>Rps. acidophila</i> strain 10050	117
Figure 4.3. Absorption spectra of <i>Rps. acidophila</i> strain 10050 LH2 and LH1-RC	118
Figure 4.4. Profile of the protein distribution in discontinuous sucrose gradients	120
Figure 4.5. Elution profile of <i>Rps. acidophila</i> core complex from an anion exchange column	121
Figure 4.6. Absorption spectrum of <i>Rps. acidophila</i> strain 10050 core aliquots	123
Figure 4.7. Elution profile of <i>Rps. acidophila</i> core complex from a gel filtration column	125
Figure 4.8. Absorption spectrum of fully purified core complex from <i>Rps. acidophila</i> strain 10050	126
Figure 4.9. SDS-PAGE gel of antenna complexes from <i>Rps. acidophila</i> strain 10050	128
Figure 4.10. Electron micrograph of LH1-RC core complexes from <i>Rps. acidophila</i>	129
Figure 4.11. Absorption spectrum of solubilised membranes from <i>Rps. palustris</i> strain French	133
Figure 4.12. Absorption spectrum of pigmented bands from sucrose gradient centrifugation of solubilised membranes of <i>Rps. palustris</i>	134
Table 4.2. Purification table for the LH1-RC complex from <i>Rps. palustris</i> strain French	135
Figure 4.13. Absorption spectrum of fully purified LH1-RC from <i>Rps. palustris</i> strain French	136
Figure 4.14. Absorption spectrum of core complex from <i>Rps. palustris</i> strain 1a1	137
Figure 4.15. Absorption spectrum of solubilised membranes from high light <i>Rps. cryptolactis</i>	138
Figure 4.16. Absorption spectra of <i>Rps. cryptolactis</i> complexes from sucrose gradients	139
Figure 4.17. Absorption spectrum of fully purified LH1-RC from <i>Rps. cryptolactis</i>	140
Table 4.3. Purification table for the LH1-RC complex from <i>Rps. cryptolactis</i>	142
Figure 4.18. Absorption spectrum of unsolubilised membranes from <i>Rv. gelatinosus</i>	143
Figure 4.19. Absorption spectra of <i>Rv. gelatinosus</i> complexes from sucrose gradients	144
Table 4.4. Purification table for the LH1-RC complex from <i>Rv. gelatinosus</i>	145
Figure 4.20. Absorption spectrum of fully purified LH1-RC from <i>Rv. gelatinosus</i>	146
Figure 4.21. Absorption spectrum of chromatophores from <i>Chr. vinosum</i> strain D	148
Figure 4.22. Absorption spectra of <i>Chr. vinosum</i> strain D complexes from sucrose gradients	149
Table 4.5. Purification table for the LH1-RC complex from <i>Chr. vinosum</i> strain D	150
Figure 4.23. Absorption spectrum of fully purified LH1-RC from <i>Chr. vinosum</i> strain D	151
Table 4.6. Purification table for the LH1-RC complex from <i>Rs. rubrum</i>	153
Figure 4.24. Absorption spectrum of fully purified LH1-RC from <i>Rs. rubrum</i> strain S1	154
Figure 4.25. Absorption spectrum of solubilised membranes from <i>Rh. marinum</i>	157

Table 4.7. Purification table for the LH1-RC complex from <i>Rh. marinum</i>	158
Figure 4.26. Absorption spectrum of fully purified LH1-RC from <i>Rh. marinum</i>	159
Table 4.8. Purification table for the LH1 complex from <i>Rh. marinum</i>	160
Figure 4.27. Absorption spectrum of isolated B880 (LH1) complex from <i>Rh. marinum</i>	161
Table 4.9. Summary of the purification results	163
Figure 5.1. CD spectrum of the LH1-RC complex from <i>Rps. acidophila</i> strain 10050	168
Table 5.1. Summary of the results of analysis of CD spectra of the core complex	169
Figure 5.2. CD spectra of the LH1-RC complexes from <i>Rps. palustris</i> strains French and 1a1	172
Figure 5.3. CD spectrum of the LH1-RC complex from <i>Rps. cryptolactis</i>	175
Figure 5.4. CD spectra of the LH1-RC complexes from <i>Rv. gelatinosus</i> DSM 149 and 151	177
Figure 5.5. CD spectrum of the LH1-RC complex from <i>Chr. vinosum</i> strain D	180
Figure 5.6. CD spectra of the LH1-RC complexes from <i>Rs. rubrum</i> and <i>Rh. marinum</i>	182
Figure 6.1. Absorption spectra of the LH1-RC and LH1-only complexes from <i>Rh. marinum</i>	187
Figure 6.2. Effect of oxidation on the NIR absorption spectrum of <i>Rh. marinum</i> LH1	189
Figure 6.3. Evolution with time of the NIR absorption spectrum of <i>Rh. marinum</i> LH1	190
Figure 6.4. Effect of illumination on the NIR absorption spectrum of <i>Rh. marinum</i> LH1	191
Figure 6.5. Effect of chemical oxidation on fluorescence emission of <i>Rh. marinum</i> LH1	192
Figure 6.6. Comparison of the effect of chemical oxidation on the transmission and fluorescence emission intensity of the LH1 complex from <i>Rh. marinum</i>	194
Figure 7.1. Absorption and fluorescence emission spectra of <i>Rps. acidophila</i> membranes	200
Figure 7.2. Absorption change of P870 of <i>Rps. acidophila</i> 7750 membranes	202
Figure 7.3. Time courses of excitation flash and fluorescence emission	204
Figure 7.4. Normalised fluorescence induction curve and residuals	206
Table 7.1. Number of Bchl pigments in a pigment pool	208
Table 7.2. Summary of averaged fit parameters from analysis of fluorescence induction curves	208
Figures 8.1. and 8.2. 3-D crystals of <i>Rps. acidophila</i> strain 10050 core complex	217
Figures 8.3. and 8.4. 3-D crystals of <i>Rps. acidophila</i> strain 10050 core complex	218
Figures 8.5. and 8.6. 3-D crystals of <i>Rps. acidophila</i> strain 10050 core complex	219
Figures 8.7. and 8.8. 3-D crystals of <i>Rps. acidophila</i> strain 10050 core complex	220
Figures 8.9. and 8.10. 3-D crystals of <i>Rps. acidophila</i> strain 10050 core complex	222
Figures 8.11. and 8.12. 3-D crystals of <i>Rps. acidophila</i> strain 10050 core complex	223
Figures 8.13. and 8.14. 3-D crystals of <i>Rps. acidophila</i> strain 10050 core complex	225
Figures 8.15. and 8.16. 3-D crystals of <i>Rps. acidophila</i> strain 10050 core complex	227
Figures 8.17. and 8.18. 3-D crystals of <i>Rps. acidophila</i> strain 10050 core complex	229
Figures 8.19. and 8.20. 3-D crystals of <i>Rps. acidophila</i> strain 10050 core complex	230
Figures 8.21. and 8.22. 3-D crystals of <i>Rps. acidophila</i> strain 10050 core complex	232
Figures 8.23. and 8.24. 3-D crystals of <i>Rps. acidophila</i> strain 10050 core complex	234
Figures 8.25. and 8.26. 3-D crystals of <i>Rps. acidophila</i> strain 10050 core complex	236
Figures 8.27. and 8.28. 3-D crystals of <i>Rps. acidophila</i> strain 10050 core complex	237
Figures 8.29. and 8.30. 3-D crystals of <i>Rps. acidophila</i> strain 10050 core complex	238
Figure 8.31. 3-D crystals of <i>Rps. acidophila</i> strain 10050 core complex	240
Figure 8.32. Absorption spectrum of <i>Rps. acidophila</i> strain 10050 core complex crystals	242
Figure 8.33. 3-D crystals of <i>Rps. acidophila</i> strain 7750 core complex	244

Figure 8.34. 3-D crystals of <i>Rps. acidophila</i> strain 7050 core complex	244
Figures 8.35. and 8.36. 3-D crystals of <i>Rps. acidophila</i> strain 7050 core complex	245
Figure 8.37. 3-D crystals of <i>Rps. palustris</i> core complex	248
Figure 8.38. 3-D crystals of <i>Rps. cryptolactis</i> core complex	248
Figures 8.39. and 8.40. 3-D crystals of <i>Chr. vinosum</i> strain D core complex	251
Figure 8.41. 3-D crystals of <i>Chr. vinosum</i> strain D core complex	252
Figure 8.42. 3-D crystals of <i>Rs. rubrum</i> S1 core complex	252
Figure 8.43. 3-D crystals of the <i>Rh. marinum</i> core complex	255
Figure 8.43. 3-D crystals of the <i>Rh. marinum</i> LH1 (B880) complex	255
Table 8.1. List of precipitants, detergents and additives used in successful crystallisation trials	256
Figure 9.1. Models of the antenna organisation in <i>Rps. acidophila</i> strain 7750	270

CHAPTER ONE

INTRODUCTION

1.1. An overview of photosynthesis

Photosynthesis is the process by which plants and some bacteria convert solar energy into chemically useful energy. This fundamental process is virtually the only mechanism of net energy input into the biosphere. The only exceptions occur in chemosynthetic bacteria that derive energy by the oxidation of inorganic substrates, such as ferrous ions and sulphur, leached from the earth's crust or H_2S released by volcanic activity (Stetter, 1996). Additionally, energy can be put into biological systems in the form of heat by hydrothermal vents (Prieur, 1997). However, these non-photosynthetic processes represent only a small fraction of the energy flow in the biosphere.

Photosynthesis is the largest scale synthetic process on earth. Annually, phototrophs fix $\sim 2 \times 10^{11}$ tonnes of carbon into organic compounds (Salisbury, 1991). Green plants, algae and cyanobacteria perform oxygenic photosynthesis during which carbon, in the form of CO_2 , is fixed into carbohydrates and water is oxidised to yield molecular oxygen as a by-product. This mode of photosynthesis is responsible for replenishing the entire atmospheric oxygen content every 2,000 years (Barber & Andersson, 1994).

The green and purple bacteria, the latter group which are divided into the purple sulphur bacteria and purple non-sulphur bacteria and form the basis of this thesis, are capable of anoxygenic photosynthesis. Like the green plants and algae these organisms also fix CO_2 into organic compounds. However, they do not oxidise water or evolve oxygen. Instead, the green and purple sulphur bacteria utilise inorganic sulphur compounds as electron donors for the reduction of CO_2 . In the purple non-sulphur bacteria organic compounds such as succinate replace sulphur (Pfennig, 1978).

Although the green and purple bacteria are regarded as being of little importance ecologically compared to the higher plants and algae, the study of bacterial photosynthesis has made landmark contributions to our understanding of photosynthesis in general.

Photosynthesis is not a single reaction and water, inorganic sulphur or organic compounds do not directly reduce CO_2 . Rather, the overall photosynthetic process is both chemically and physically separated into two sub-processes: the light and dark reactions (Gregory, 1989). During the light reactions, light energy absorbed by the pigments of the photosynthetic apparatus is used to generate ATP and reducing equivalents in the form of NADPH (or, in photosynthetic bacteria, NADH). Both the reducing equivalents and ATP are then utilised during the dark reactions in the reductive synthesis of carbohydrate from CO_2 .

The ability of phototrophs to convert solar energy into chemical energy supports almost all other life on earth. Heterotrophic organisms can only derive energy by the controlled oxidation of carbohydrates and similar organic compounds furnished by phototrophs. Thus, the importance of photosynthesis cannot be overstated: without it virtually all life on earth would become extinct.

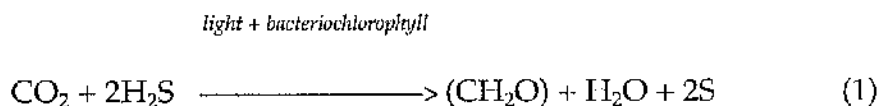
1.2. A brief history of photosynthesis research

Since the time of the ancient Greeks it was generally believed that plants derived all their matter from soil. This concept went unchallenged until 1648, when a simple experiment prompted van Helmont to guess that most of a plant's mass was derived from water. It was not until the early 18th century that Hales suggested plants actually gained nourishment from

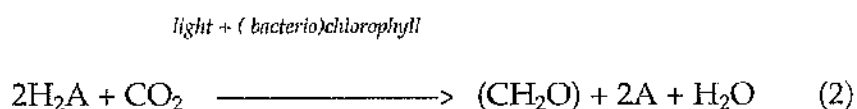
the atmosphere and that light was involved in this process. For a good review of Hales's and other early work on photosynthesis see Gest (1988).

In 1771, an interest in the study of gases and their effect on animals led an English clergyman and chemist, Joseph Priestly, to design a series of elegant experiments which showed that green plants could restore air made 'bad' by the burning of candles or breathing of animals. Thus, Priestly's experiments were the first demonstration that green plants produce oxygen, or, as he termed it, dephlogisticated air. At the time, Priestly did not know that oxygen was a molecule or light was essential for this process. However, in 1779, the Dutch physician Jan Ingenhousz, credited as the discoverer of photosynthesis, not only determined that light was required for oxygen production but also identified leaves as the site of photosynthesis (for a review see Gest, 1997). Three years later, Jean Senebier showed that plants required what he called 'fixed air' (or CO_2) to dephlogisticate the air. Thus, by the end of the 18th century it was known that at least two gases participated in photosynthesis. The work of Lavoisier and others showed that these gases were indeed oxygen and CO_2 . Adopting Lavoisier's ideas, Ingenhousz proposed that the organic matter in plants was derived from CO_2 . The nature of this organic matter was reported by von Sachs. In 1864 he observed the formation of starch grains in illuminated chloroplasts. This observation also implied a role for chlorophyll in the photosynthetic process.

In the 1920's, C.B. van Niel embarked on a study of bacterial photosynthesis that gave rise to the essentially correct view of the overall photosynthetic reaction. van Niel studied photosynthetic bacteria that utilised H_2S as an electron source and deposited elemental sulphur as a by-product (van Niel, 1941). The photosynthetic equation for these bacteria is:



Comparison of this photosynthetic reaction scheme with that of green plants stimulated van Niel to postulate that O_2 released during oxygenic photosynthesis was derived from H_2O , not CO_2 as was believed at the time. His reasoning was based on analogies between the roles of H_2S , H_2O and O_2 and elemental sulphur. Thus, both anoxygenic bacterial and oxygenic plant photosynthesis can be represented by the general equation:



where H_2A is water in the green plants, algae and cyanobacteria, hydrogen sulphide in sulphur bacteria and simple organic compounds in the purple non-sulphur bacteria. The oxidised product, 2A , is molecular oxygen in the oxygenic phototrophs and elemental sulphur in the sulphur bacteria. In the non-sulphur bacteria, 2A represents oxidised organic compounds. van Niel's view of photosynthesis as a redox reaction, driven by light and mediated by (bacterio)chlorophyll, still forms the basis of contemporary descriptions of the photosynthetic process.

1.3. Physiology of the phototrophic purple bacteria

Both the phototrophic purple and green bacteria share the capacity to perform anoxygenic photosynthesis utilising light energy absorbed by bacteriochlorophylls (Pfennig & Trüper, 1974; Trüper, 1976). However, in

contrast to the green bacteria, which are metabolic specialists, the purple bacteria exhibit a great diversity in their metabolic capabilities. This diversity allows them to adapt to a wide range of environmental and growth conditions (Imhoff, 1995). With regard to their metabolic capabilities, the purple bacteria can be divided into the purple sulphur and purple non-sulphur bacteria (Trüper & Pfennig, 1978).

Typically, the purple sulphur bacteria grow photoautotrophically using either reduced sulphur compounds or molecular hydrogen as electron donors for the reduction of CO₂. The purple non-sulphur bacteria grow preferentially under photoheterotrophic conditions utilising a variety of organic substrates as both electron donors and carbon sources. However, some of the purple non-sulphur bacteria can also grow photoautotrophically using sulphide or molecular hydrogen as electron donors and CO₂ as a carbon source. Most of the species which perform this particular type of anoxygenic photosynthesis oxidise sulphide to elemental sulphur only (Hansen & van Gemerden, 1972). Others, such as *Rhodopseudomonas sulfidophila*, oxidise sulphide to sulphate without accumulation of elemental sulphur (Hansen & Veldkamp, 1973).

Although some species of purple non-sulphur bacteria are extremely oxygen sensitive, most can grow aerobically in the dark (Madigan & Gest, 1979; Kämpf & Pfennig, 1980). Under these chemolithotrophic conditions, the cultures are either faintly pigmented or colourless due to the repression of synthesis of the photosynthetic pigments by oxygen (Cohen-Bazire *et al.*, 1957). Such is the metabolic versatility of the purple non-sulphur bacteria that some species, such as *Rhodospirillum rubrum*, are even capable of fermentation under anaerobic conditions in the dark (Gorrell & Uffen, 1977). This metabolic versatility is further illustrated by the recent discovery of a new species of phototrophic bacteria with the proposed name of

Porphyrobacter tepidaris (Hanada *et al.*, 1997). This bacterium is a thermophilic obligate aerobe.

1.4. Taxonomy of the phototrophic purple bacteria

Historically, classification of the phototrophic bacteria was based on a variety of characteristics such as cell morphology and ultrastructure, pigment composition, physiological properties and DNA base ratio (Pfennig & Trüper, 1974; Trüper & Pfennig, 1981; Imhoff & Trüper, 1989). Chemotaxonomic methods, in which the cellular composition of quinones (Imhoff, 1984a) and the lipid A structure of lipopolysaccharides (Mayer, 1984) were investigated, have also been applied to the taxonomic characterisation of the phototrophic bacteria. More recently, sequence analyses of proteins and nucleic acids have been used to determine taxonomic relationships between species (Fowler *et al.*, 1984; Woese *et al.*, 1985; Stackebrandt *et al.*, 1988). Indeed, the first phylogenetic tree of the purple bacteria was constructed using the primary sequence data and tertiary structure of *c*-type cytochromes (Dickerson, 1980).

The phototrophic bacteria belong to the order Rhodospirillales (Trüper & Pfennig, 1978). This order is divided into the suborders Chlorobiineae and Rhodospirillineae (Figure 1.1). The suborder Chlorobiineae comprises what are commonly termed the green photosynthetic bacteria. These bacteria contain bacteriochlorophyll *c*, *d* or *e*, which is located in specialised organelles called chlorosomes (Staehlin *et al.*, 1980).

The suborder Rhodospirillineae, which comprises the purple phototrophic bacteria, is divided into families which contain the purple sulphur and purple non-sulphur bacteria (Trüper & Pfennig, 1978).

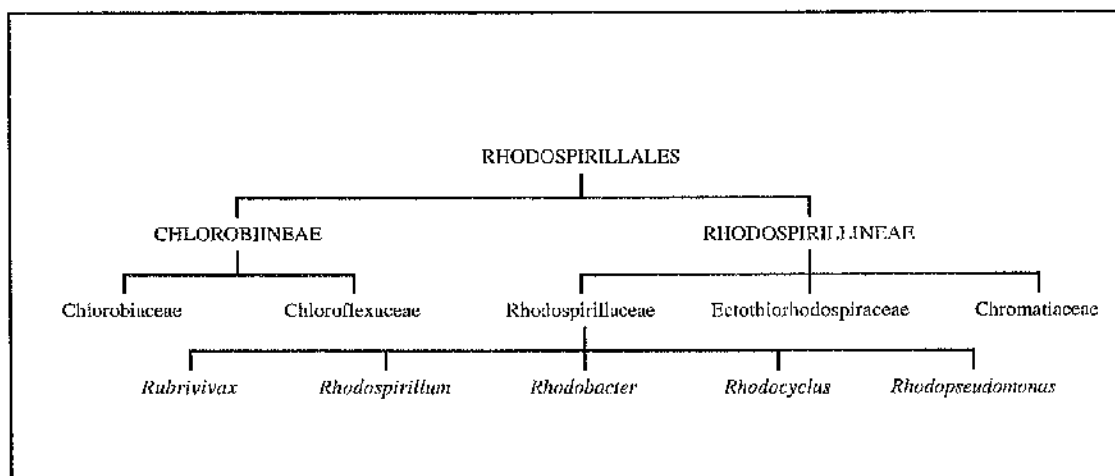


Figure 1.1. Taxonomic tree showing the relationship between members of the order Rhodospirillales. This order is divided into two sub-orders, the Chlorobiineae (green bacteria) and the Rhodospirillineae (purple bacteria). The sub-orders are split into families based on the ability to utilise sulphur. The Rhodospirillaceae family of purple and brown non-sulphur bacteria contains representatives of the genera investigated in this thesis.

Originally, all the purple bacteria that accumulated elemental sulphur intracellularly were grouped into the family Thiorodaceae (Molisch, 1907). The remaining purple bacteria were placed in the family Athiorhodaceae. These two groups were later renamed Chromatiaceae (Bavendamm, 1924) and Rhodospirillaceae (Pfennig & Trüper, 1971). A new family, the Ectothiorhodospiraceae, was formed to account for those purple sulphur bacteria that deposit elemental sulphur globules extracellularly (Imhoff, 1984b).

All members of the Rhodospirillineae contain the pigments bacteriochlorophyll *a* or *b* (Thornber *et al.*, 1978). These pigments are non-covalently bound to light-harvesting or reaction centre polypeptides that

are housed in an extended intracytoplasmic membrane system which originates from the cytoplasmic membrane (Remsen, 1978). The structure of the intracytoplasmic membrane varies between species and can consist of fingerlike invaginations, vesicles, tubules or lamellae (Figure 1.2). Intracytoplasmic membrane (ICM) structure has been used in the past as a means of differentiating the purple bacteria. However, 16S rRNA analyses of several species of purple non-sulphur bacteria and a non-phototrophic bacteria have demonstrated that ICM structure is not a sufficient criterion to distinguish between these bacteria at the genus level (Kawasaki *et al.*, 1993).

16S rRNA sequence analysis led Stackebrandt *et al.*, (1988) to propose a new class - the Proteobacteria - for all the purple bacteria and their relatives. This class has been divided into four subgroups called α , β , γ and δ (Woese *et al.*, 1985). The α branch contains genera of the purple non-sulphur bacteria such as *Rhodobacter*, *Rhodospirillum*, *Rhodopseudomonas*, *Rhodomicrobium* and *Rhodophila*. Another genera of the purple bacteria, *Rhodocyclus*, is placed in the β branch. The purple sulphur bacteria are classified in the γ branch, which has sub-branches for the Chromatiaceae and Ectothiorhodospiraceae. The aerobic phototroph, *Porphyrobacter tepidaris*, has been assigned to the δ branch.

Recently, the use of molecular techniques to classify organisms has led to a number of species being reassigned and renamed. For example, the marine bacterium *Rhodopseudomonas marina* has been assigned to a new genus and renamed *Rhodobium marinum* (Hiraishi *et al.*, 1995). The taxonomy of the purple bacteria is under constant review as new techniques give greater insight into the phylogenetic relationships between species. The constant name changes, however, make following the literature very difficult.

1.5. The purple bacterial photosynthetic apparatus

The primary event of photosynthesis is the absorption of light energy. In the photosynthetic purple bacteria, this occurs in the highly pigmented intracytoplasmic membrane (Figure 1.2). The major light absorbing pigments are the bacteriochlorophylls (Bchls) *a* and *b*, and the carotenoids. Although many different species of Bchl *a*-containing bacteria have been characterised, only a few Bchl *b*-containing species, such as *Rhodopseudomonas (Rps.) viridis* and *Ectothiorhodospira halochloris* (Steiner & Scheer, 1985) have been reasonably well studied. The photosynthetic pigments are non-covalently bound to two different types of integral membrane proteins to form the light-harvesting (LH) or antenna complexes and the photochemical reaction centres (RCs) (Drews, 1985; Hawthornthwaite & Cogdell, 1991; Zuber & Brunisholz, 1991; Kuhlbrandt, 1995; Zuber & Cogdell, 1995; Fyfe & Cogdell, 1996). Most of the pigments serve as light-harvesters and are responsible for the collection and subsequent rapid funneling of absorbed light energy to a specialised few Bchls located in the RCs. Once in the RC the energy is used to drive the initial charge separation reaction (see review by Feher *et al.*, 1989). Ultimately, this results in formation of a membrane potential and proton gradient which is used to drive the ATP synthesis and generation of reducing equivalents necessary for growth and maintenance of the organism.

1.5.1. The bacteriochlorophylls

When dissolved in an organic solvent such as 7:2 (v/v) acetone:methanol, monomeric Bchl *a* exhibits two characteristic

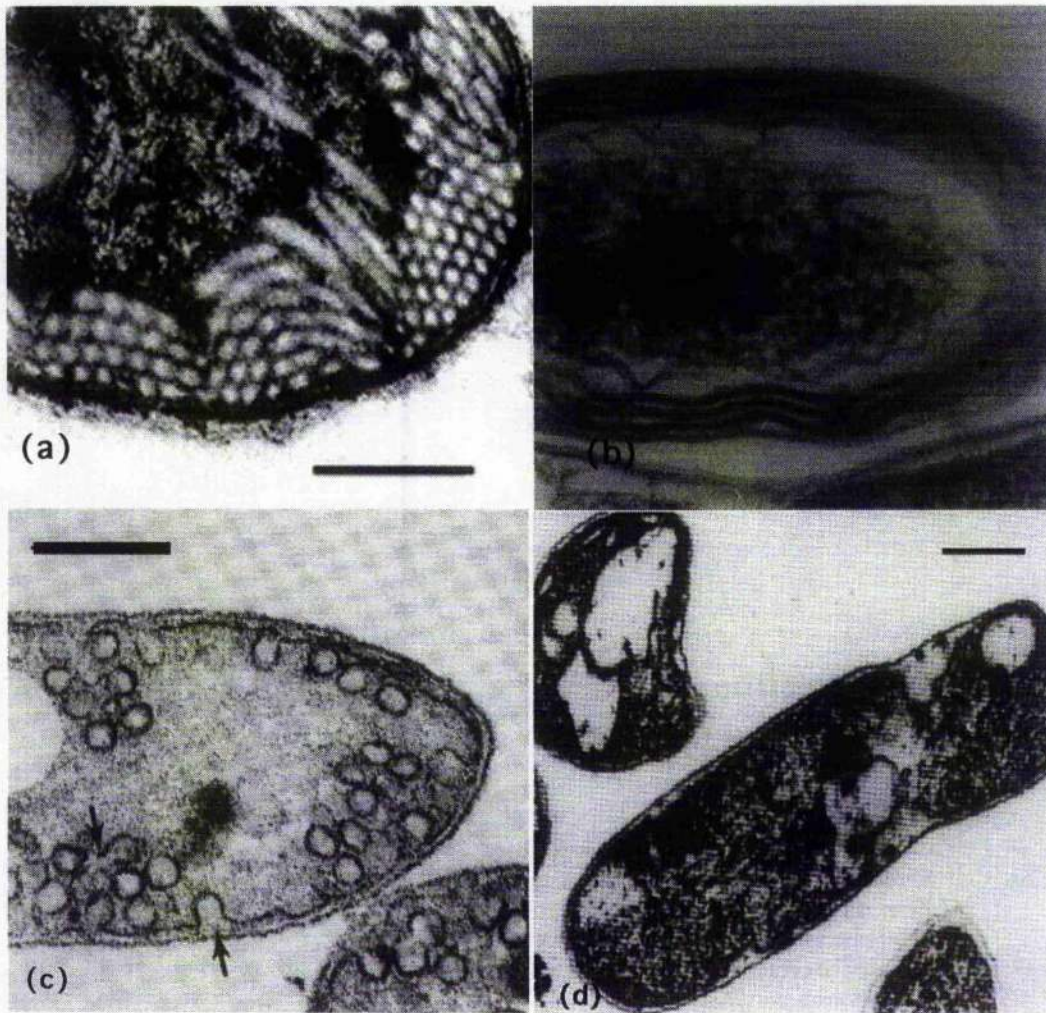


Figure 1.2. Types of intracytoplasmic membranes. (a) A section through a cell of *Thiocapsa pfennigii*, showing a tubular type of intracytoplasmic membrane. Scale bar represents 500nm. (b) A section through *Rps. palustris* containing lamellae. Magnification is x 90, 000. (c) A section through *Rb. sphaeroides* showing the vesicular type of intracytoplasmic membrane. The arrow indicates the origin of the intracytoplasmic membrane by invagination of the cytoplasmic membrane. The scale bar represents 200nm. (d) A cross section through whole cells of *Rps. acidophila* strain 7050 that were grown aerobically. Such cells do not possess invaginations of the membrane. Scale bar represents 200nm. (a) was adapted from Clayton & Sistrom (1978), (b) adapted from Gall (1994), (c) from Clayton (1980), and (d) from Cogdell & Hawthornthwaite (1993).

absorption bands (Figure 1.3b). One of these bands is located in the NIR at 772nm and the other in the visible at 590nm. The 772nm band is due to the Q_y transition and the 590nm band to the Q_x transition of the Bchl *a* molecule. These transitions are polarised along the N_I and N_{III} nitrogens and N_{II} and N_{IV} nitrogens of the molecule, respectively (Figure 1.3a). A strong absorption band located near 390nm, known as the Soret band, results from the B_x transition of the Bchl molecule (Clayton, 1980).

In vivo, when Bchl *a* is non-covalently bound to the antenna complex protein scaffold, the near infrared (NIR) absorption band is red-shifted to between 800nm-940nm, depending on species (Thornber *et al.*, 1978; Hawthornthwaite & Cogdell, 1991). In the case of Bchl *b*-containing species such as *Rps. viridis*, the red-shift is even more dramatic, the NIR absorption maximum being located at 1012nm (Hawthornthwaite & Cogdell, 1991). At low temperature the absorption maximum is shifted even further to the red. This red-shift is a result of pigment-pigment and pigment-protein interactions in the antenna (Thornber *et al.*, 1978). Bchl-Bchl and Bchl-protein interactions predominate in generating the red-shift (Sturgis & Robert, 1996; Freer *et al.*, 1996) but Bchl-carotenoid interactions also contribute to it (Parkes-Loach *et al.*, 1988). Commonly associated with the red-shift is an increase in spectral complexity with several peaks and shoulders appearing in the absorption spectrum (Figure 1.4) (Thornber *et al.*, 1978). The *in vivo* Bchl absorption spectrum can be used as a 'fingerprint' for identifying antenna complexes and is routinely used as a method for monitoring their integrity (see Materials and Methods). The precise form of the NIR absorption spectrum (location of absorption maxima, relative peak heights and presence or absence of shoulders) is dependent on a variety of factors including strain of organism, growth conditions, carbon source, age of culture and source of reducing power

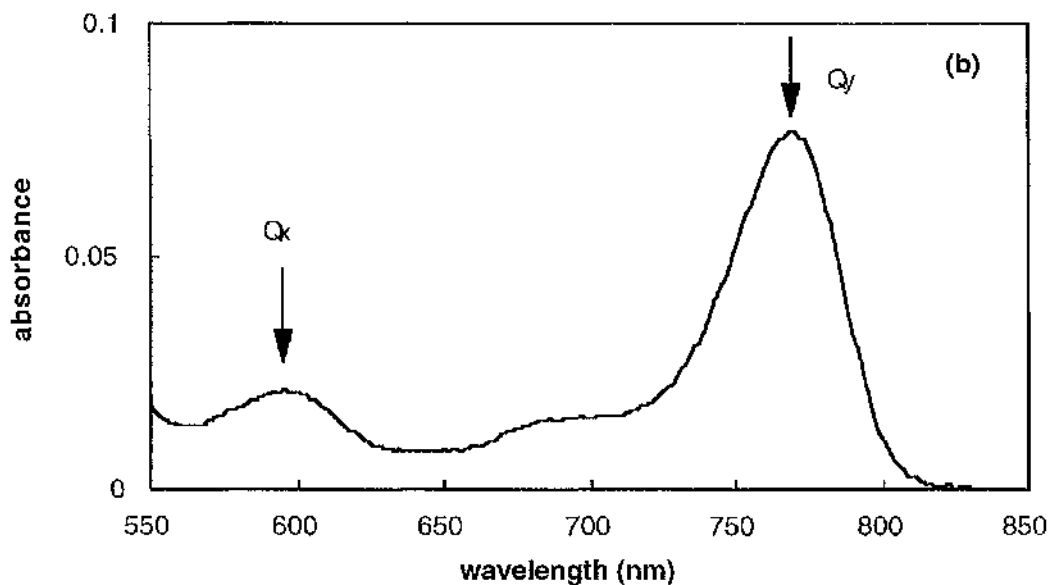
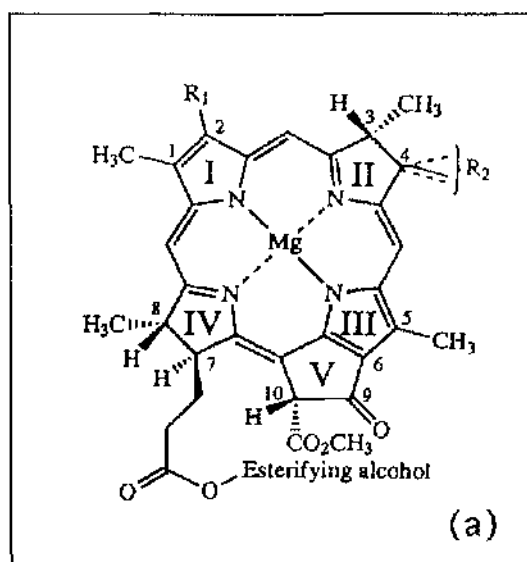


Figure 1.3. (a) The chemical structure of Bchl a. $R_1 = \text{COCH}_3$ and $R_2 = \text{CH}_2\text{CH}_3$ and H. Bchl molecules are large, macrocyclic π electron systems which can be photochemically promoted to an electronically excited state. (b) Absorption spectrum of Bchl a extracted from chromatophores of *Rs. rubrum* in 7:2 acetone:methanol. The arrows indicate the major electronic transitions of the molecule. The small peak at 680nm is due to an oxidised breakdown product of Bchl a.

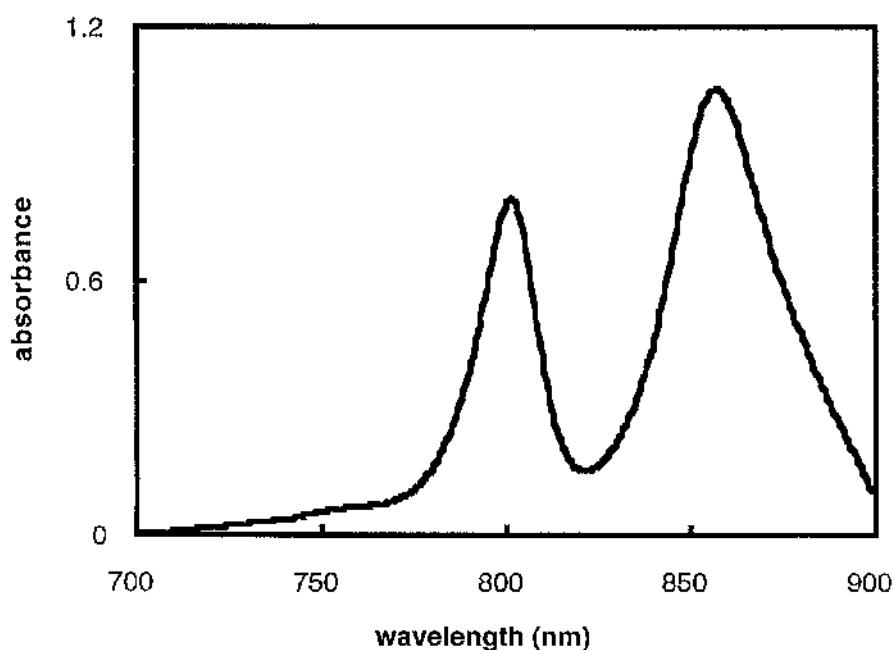


Figure 1.4. NIR absorption spectrum of photosynthetic membranes of *Rps. acidophila* strain 10050. The spectrum shows two main absorption bands located at 800nm and 858nm. The shoulder to the red of the 858nm band is due to the contribution of the Q_y absorption of the LH1 antenna Bchl as.

(Thornber *et al.*, 1978).

1.5.2. Purple bacterial antenna complexes

In most species of purple bacteria, solubilisation of the photosynthetic membrane with a suitable detergent and subsequent fractionation by sucrose density gradient centrifugation reveals the existence of two main types of antenna complex (Figure 2.2) (Firsow & Drews, 1977). These complexes are named LH1 and LH2. The LH1 complex is intimately

associated with the RC to form the so called LH1-RC 'core' complex and all wild-type purple bacteria contain it. Species of purple bacteria like *Rhodobacter (Rb.) sphaeroides*, *Rps. acidophila*, *Rps. palustris* and *Chromatium (Chr.) vinosum* contain both LH1-RC core and LH2 complexes (Hawthornthwaite & Cogdell, 1991). However, some species such as *Rps. viridis*, *Rhodospirillum (Rs.) rubrum* and *Rhodobium (Rh.) marinum* possess LH1 as the only light-harvesting complex (Zuber & Cogdell, 1995). Electron micrographs of membranes of *Rps.viridis* (Stark *et al.*, 1984; Stark *et al.*, 1986) and *Rh.marinum* (Meckenstock *et al.*, 1992b) and, more recently, image analysis of 2-D crystals of LH1-RC core complex from *Rh. marinum* (Meckenstock *et al.*, 1994), *Rs. rubrum* (Walz & Ghosh, 1997), *Rps. viridis* (Ikedu-Yamasaki *et al.*, 1998) and *Rb. sphaeroides* (Walz *et al.*, 1998) show that the LH1 antenna forms a ring around the RC. When present, the LH2 complex, sometimes referred to as the 'variable' or 'peripheral' antenna complex, is located around the periphery of the core complex (Zuber & Cogdell, 1995). The combination of antenna complexes with a RC constitutes the bacterial photosynthetic unit (PSU) (Cogdell *et al.*, 1996; Papiz *et al.*, 1996). The concept of the PSU is discussed in section 1.9.

LH1 complexes only have a single strong NIR absorption band that, depending on species and type of Bchl, is located between 870nm-1020nm (Figure 1.5). These complexes are denoted 'B' (for 'bulk') followed by the number of the room temperature NIR absorption maximum in nanometers (Cogdell *et al.*, 1985). Species such as the Bchl *a*-containing *Rs. rubrum* (Garcia *et al.*, 1966) and the Bchl *b*-containing *Rps.viridis* (Hawthornthwaite & Cogdell, 1991), which only contain the LH1-RC core complex, have LH1 absorption maxima located at 880nm and 1012nm, respectively. Hence, the LH1 complexes from these species are termed B880 and B1012.

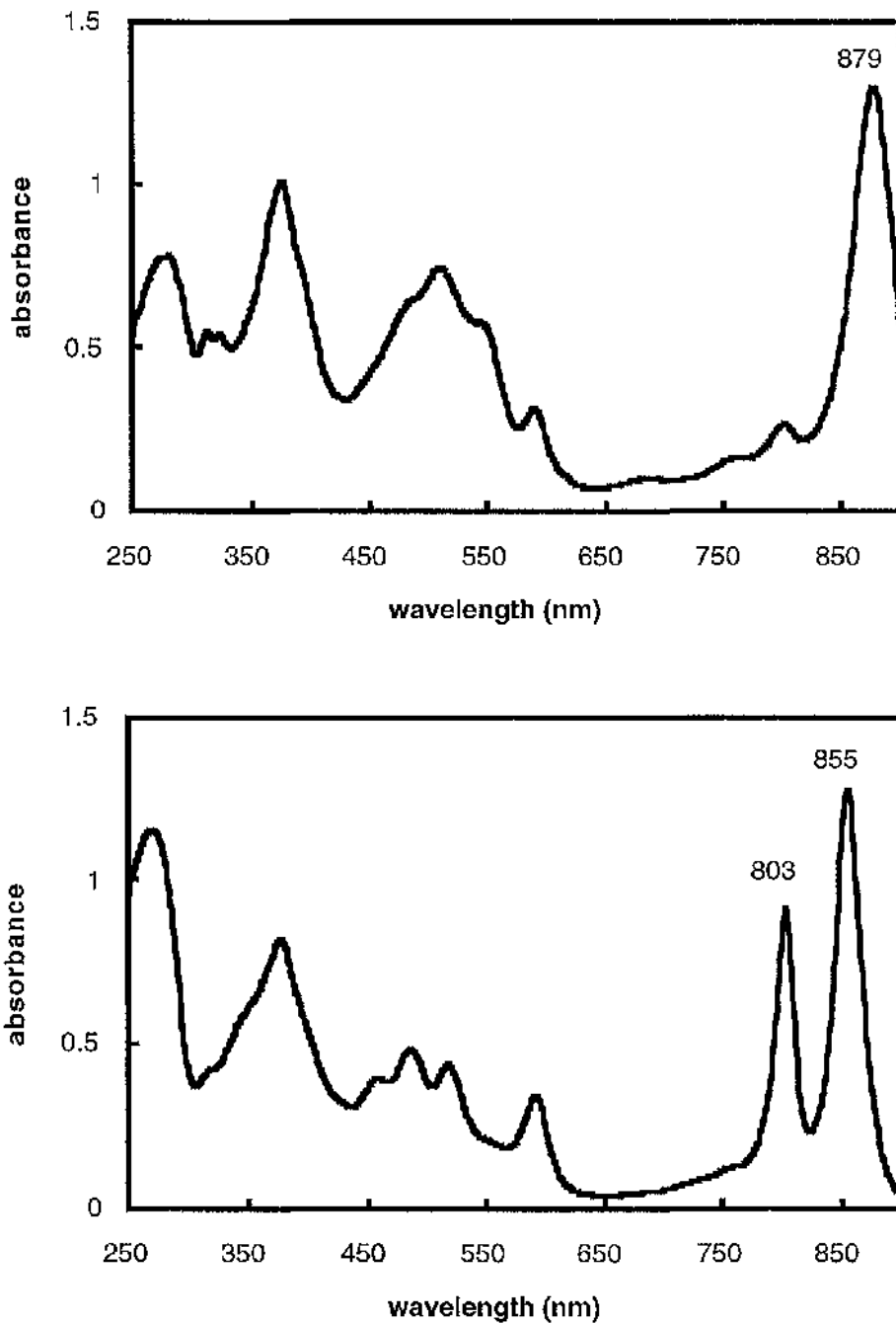


Figure 1.5. Absorption spectra of the Bchl *a*-containing LH1-RC core complex from *Rs. rubrum* (top) and LH2 complex from *Rv. gelatinosus* DSM 149 (bottom). Core complexes have a single NIR absorption band which, in *Rs. rubrum*, is located at 879nm. The small peak near 800nm represents absorption by the RC Bchl *a*s. LH2 complexes possess two strong NIR absorption bands which are located at 855nm and 803nm in *Rv. gelatinosus*.

In contrast to LH1, the LH2 complexes have two NIR absorption bands located between 800nm-860nm (Figure 1.5) (Hawthornthwaite & Cogdell, 1991; Zuber & Brunisholz, 1991). These complexes are generically termed B800-850 irrespective of the exact location of their NIR absorption maxima. Since LH2 complexes absorb energy at shorter wavelengths than LH1 complexes, the photosynthetic light-harvesting system acts as a funnel to direct energy to the RC.

1.5.3. *General aspects of antenna complex structure*

In the 10 years prior to the publication of the first 3-D structure of a purple bacterial antenna complex (McDermott *et al.*, 1995), a great deal of work involving the use of a combination of biochemical and biophysical methods was conducted in order to construct models of these complexes (Kramer *et al.*, 1984; Donnelly & Cogdell, 1993; Zuber & Brunisholz, 1991; Olsen & Hunter, 1994; Zuber & Cogdell, 1995). Included in this work was the determination of the primary structures of a large number of antenna polypeptides from both LH1 and LH2 complexes (Zuber & Brunisholz, 1991). Analyses of these primary structures showed that all antenna complexes are built on the same modular principle. The minimal structural and functional unit of antenna complexes is a heterodimer of low molecular weight (4-7kDa) α - and β -polypeptides, each consisting of 40-70 amino acid residues (Zuber & Brunisholz, 1991; Zuber & Cogdell, 1995). Typically, both polypeptides have a tripartite structure consisting of a central hydrophobic domain and polar (charged) N- and C-terminal domains (Fig.1.6) (Zuber, 1985a; 1985b). IR, UV-CD and labeling experiments (Jay *et al.*, 1983; Breton & Navedryk, 1984) indicated that the hydrophobic domain forms a transmembrane α -helix whereas the N- and C-terminal

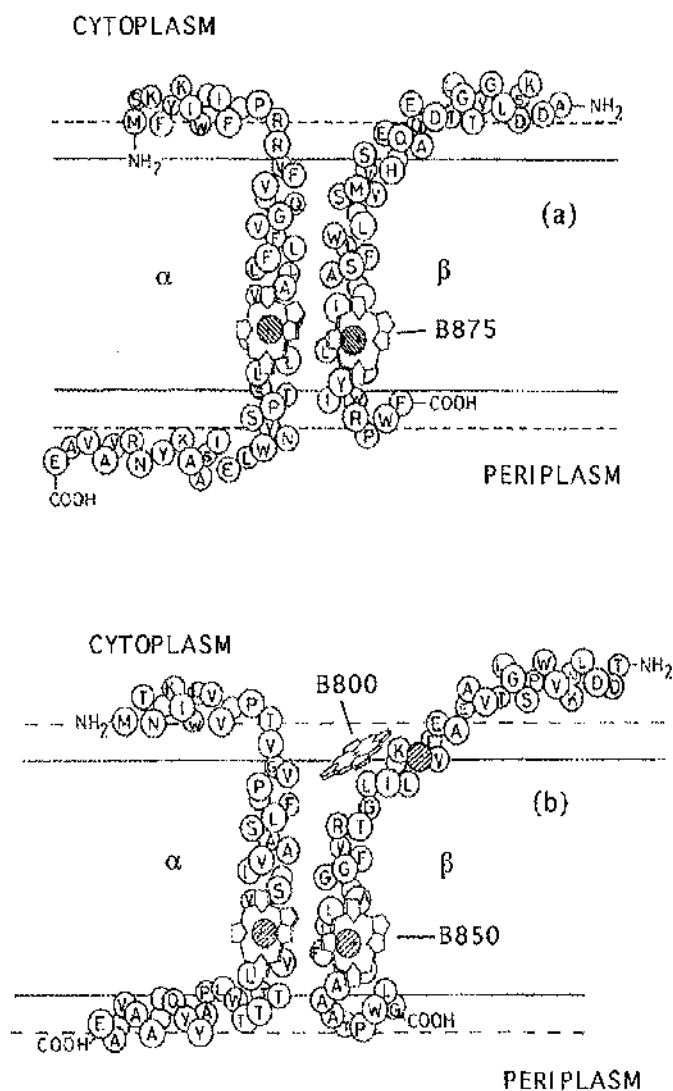


Figure 1.6. Schematic diagram of the minimal structural units of (a) the LH1 and (b) the LH2 antenna complexes of *Rhodospira rubra*. The tripartite structure of the polypeptides, consisting of a central membrane-spanning domain and polar N- and C-terminal domains, can be clearly seen. The general aspects of this diagram are equally applicable to the antenna complexes of other species of the purple bacteria. The conserved His residues which bind the B850 and B875 molecules are shaded in grey. The second conserved His residue of the LH2 β -polypeptide is also shaded grey, even though it is not directly involved in binding B800. Amino acid lettering follows IUPAC nomenclature. Adapted from Olsen & Hunter (1994).

domains are located in the polar head region or surface of the membrane. Proteolytic cleavage (Brunisholz *et al.*, 1984; Brunisholz *et al.*, 1986) and labeling experiments (Wiemken *et al.*, 1983; Peters & Drews, 1983; Jay *et al.*, 1984) showed that the C-terminal domain lies on the periplasmic side and the N-terminal domain on the cytoplasmic side of the membrane. The primary structure of the N-terminal domain suggested that it forms an amphipathic helix which lies parallel to the membrane plane (Theiler & Zuber, 1984).

Native antenna complexes are 'ring-like' structures composed of oligomers of the $\alpha\beta$ -polypeptide minimal unit. LH2 complexes consist of either nonamers (McDermott *et al.*, 1995; Savage *et al.*, 1996) or octamers (Koepeke *et al.*, 1996) of these minimal units while LH1 complexes consist of 16mers (Karrasch *et al.*, 1995; Walz & Ghosh, 1997). The structures of these complexes are discussed in detail in sections 1.7 and 1.8.

The antenna polypeptides are responsible for binding the photosynthetic pigments. Generally, each pair of LH2 α - and β - polypeptides bind three Bchl and one or two carotenoid molecules (Drews, 1985; Cogdell *et al.*, 1997). Generally, each pair of LH1 antenna polypeptides bind two Bchl and one or two carotenoid molecules (Drews, 1985; Cogdell & Frank, 1987). Both the α - and β -polypeptides of each type of antenna complex contain a highly conserved histidine (His) residue located 1-2 α -helix turns from the boundary between the central membrane-spanning domain and the polar C-terminal domain (Olsen & Hunter, 1994; Zuber & Cogdell, 1995). These central His residues are liganded to the central magnesium atoms of the exciton-coupled Bchl macrocycles which give rise to the absorption bands at $\sim 850\text{nm}$ and $\sim 875\text{nm}$ in the LH2 and LH1 antenna complexes, respectively. A second, usually conserved His residue is found near the N-terminal domain of the β -polypeptide although it is not directly involved in binding

of Bchl (Robert & Lutz, 1985). This conserved His is also present in the LH1 β -polypeptide, even though the additional Bchl is absent in this antenna complex (Zuber & Cogdell, 1995).

In both the α - and β -polypeptides several other conserved amino acid residues are found in the vicinity of the conserved central His residue. There is usually a leucine (α -polypeptide) or large aromatic residue (β -polypeptide) located at His+4 (numbered relative to the conserved His, considered as position 0) and, located about one α -helix turn away at His-4, a small hydrophobic residue (Brunisholz *et al.*, 1984; Theiler & Zuber, 1984). Conserved tyrosine (Tyr) or tryptophan (Trp) residues are found at positions His+4, +6 and +9 in the LH1, or His +9 in the LH2 β -polypeptides and at position His +11 in the LH1 and His +9 and +14 in the LH2 α -polypeptides (Zuber & Cogdell, 1995). These aromatic amino acid residues create a particular micro-environment for the His-bound Bchl molecules, thereby influencing their spectral characteristics. They may also act as secondary binding sites for the Bchl molecules (Sturgis *et al.*, 1995). The functional role of these conserved aromatic amino acid residues was demonstrated by site-directed mutagenesis experiments. Substitution of one or two of the conserved aromatic residues resulted in a blue shift of the Bchl Q_y absorption band (Babst *et al.*, 1991; Fowler *et al.*, 1992; Hunter, 1995).

The LH1 antenna polypeptides of Bchl *b*-containing species like *Rps. viridis* and *Ec. halochloris* are similar to the analogous polypeptides of other purple bacteria. However, these polypeptides possess additional aromatic amino acid residues located at two important positions in the α - and β -polypeptides (Zuber & Cogdell, 1995). Another factor of structural and functional significance in these complexes is the presence of an additional, non-pigment binding polypeptide (γ) which is present in a ratio of 1:1:1 with respect to the α - and β -polypeptides (Brunisholz *et al.*, 1985; Jay *et al.*, 1984).

The conserved aromatic amino acid residues and the γ -polypeptides may account for the large red-shift of Bchl-*b* absorbance observed in the core complexes of these species.

It is clear that the absorption characteristics of the light-harvesting antenna are influenced by intricate interactions between the photosynthetic pigments and their protein environment. These interactions enable a fast, efficient transfer of excitation energy from the antenna complexes to the photochemical RC.

1.5.4. *Peripheral antenna complex variability*

While native LH1 complexes are present in a fixed stoichiometric ratio of 1:1 with respect to the RC (Aagard & Sistrom, 1972), the size of the peripheral LH2 antenna pool can vary depending upon the species, strain and growth conditions. In addition to altering the amount of LH2 synthesised some species like *Rps. acidophila* strains 7050 and 7750 (Cogdell *et al.*, 1983) and *Rps. cryptolactis* (Stadtwald-Demchick *et al.*, 1990; Halloren *et al.*, 1995) are able to modulate their absorption characteristics by synthesising different types of LH2. This occurs mainly as a response to changes in light intensity and temperature (Angerhofer *et al.*, 1986; Takaichi *et al.*, 1993; Gardiner *et al.*, 1993). When grown under high light conditions ($150\mu\text{mols/s/m}^2$), *Rps. acidophila* strains 7050 and 7750 synthesise, in addition to the LH1-RC core complex, the typical B800-850 peripheral antenna complex (Cogdell *et al.*, 1983) (see Figure 7.1). If the light intensity is decreased to approximately $40\mu\text{mols/s/m}^2$ during cell growth the B800-850 LH2 complex is replaced successively by a B800-820 LH2 complex (see Figure 7.1) (Takaichi *et al.*, 1993). The changeover from B800-850 to B800-820 is never complete when the cells are grown at 30°C (Gardiner *et al.*, 1993). If

however, low light intensities are combined with a decrease in temperature to 22°C strain 7750 completely replaces its complement of B800-850 antenna with B800-820 (see Figure 7.1) (Gardiner *et al.*, 1993). Such variation of the peripheral antenna pool allows these bacteria to maximise their light-harvesting capacity to suit the prevailing light conditions.

The α -polypeptide of the B800-850 complex of *Rps. acidophila* strains 7750 and 7050 contains a conserved structural element, Tyr-Trp, located in the vicinity of the B850 Bchls at His +13 and His +14. In the B800-820 complex these aromatic residues are modified to Phe-Leu in strain 7050 and Phe-Thr in strain 7750. Brunisholz & Zuber (1988) suggested that these modifications provided a structural basis for the blue-shifting of the 850nm component of the B800-850 complex to 820nm when *Rps. acidophila* was grown under low light and/or low temperature conditions (reviewed in Zuber & Brunisholz, 1991).

Subsequent work using Fourier Transform resonance Raman spectroscopy of a range of purple bacterial peripheral complexes (Sturgis *et al.*, 1995) implicated the contribution of hydrogen bonds to the Bchl molecules in modulating the location of the Bchl *a* Q_y absorption. Three amino acid residues in the α -polypeptide of the B800-850 complexes were identified as candidates for involvement in the hydrogen bonding of the 9-keto carbonyl group of one of the 850nm-absorbing Bchl molecules. Furthermore, it was found that the two 2-acetyl groups of the 820nm-absorbing Bchl *a* molecules of B800-820 complexes are free from hydrogen bonding interactions. Considering previous site-directed mutagenesis studies (Fowler *et al.*, 1992; 1994) it was concluded that lack of such hydrogen bonds to the B820 molecules is generally responsible for eliciting the blue-shift from 850nm to 820nm. More recently, a similar conclusion was presented in the work of Sauer *et al.* (1996) who compared amino acid

sequences of both the B800-850 and B800-820 antenna complexes of *Rps. acidophila* and *Rs. molischianum*. These results confirmed the suggestions of Brunisholz & Zuber (1988) and highlighted the structural basis for the blue-shift of Bchl *a* absorption.

Rps. palustris is another species of purple bacteria that can vary its NIR absorption characteristics in response to different light conditions (Miyazaki & Morita, 1981; Hayashi *et al.*, 1982a; Hayashi *et al.*, 1982b). This species tunes its spectroscopic properties not by synthesising a B800-820 antenna complex but by varying the absorption characteristics of the B800-850 complex (Hayashi *et al.*, 1982a; Hayashi *et al.*, 1982b; Evans *et al.*, 1990). When grown at high light intensities, *Rps. palustris* strain 2.1.6 cells have an NIR absorption spectrum rather similar to that seen in wild type *Rb. sphaeroides* or *Rb. capsulatus* (Figure 1.7a) (Garcia *et al.*, 1968). Under such conditions the 850nm absorption band is more intense than the 800nm band (Hayashi *et al.*, 1982a; Evans *et al.*, 1990). However, in low light grown cells the 800nm band becomes much more intense than the 850nm band (Figure 1.7b) (Hayashi *et al.*, 1982a; Robert *et al.*, 1985; Evans *et al.*, 1990; van Mourik *et al.*, 1992). Biophysical and biochemical studies have shown that this spectral variation is due to differences in the pigment organisation and polypeptide composition between the B800-850 complexes from high light and low light grown cells (Hayashi *et al.*, 1982a; Robert *et al.*, 1985; Evans *et al.*, 1990; van Mourik *et al.*, 1992). Indeed, under low light conditions a completely different B800-850 complex is synthesised (Evans *et al.*, 1990). The increase in intensity of the 800nm absorption band in the LL complexes was explained by an increase in B800 pigment density (van Mourik *et al.*, 1992).

Perhaps the one of the most complex peripheral antenna systems is seen in the purple sulphur bacterium *Chromatium vinosum*. The light-

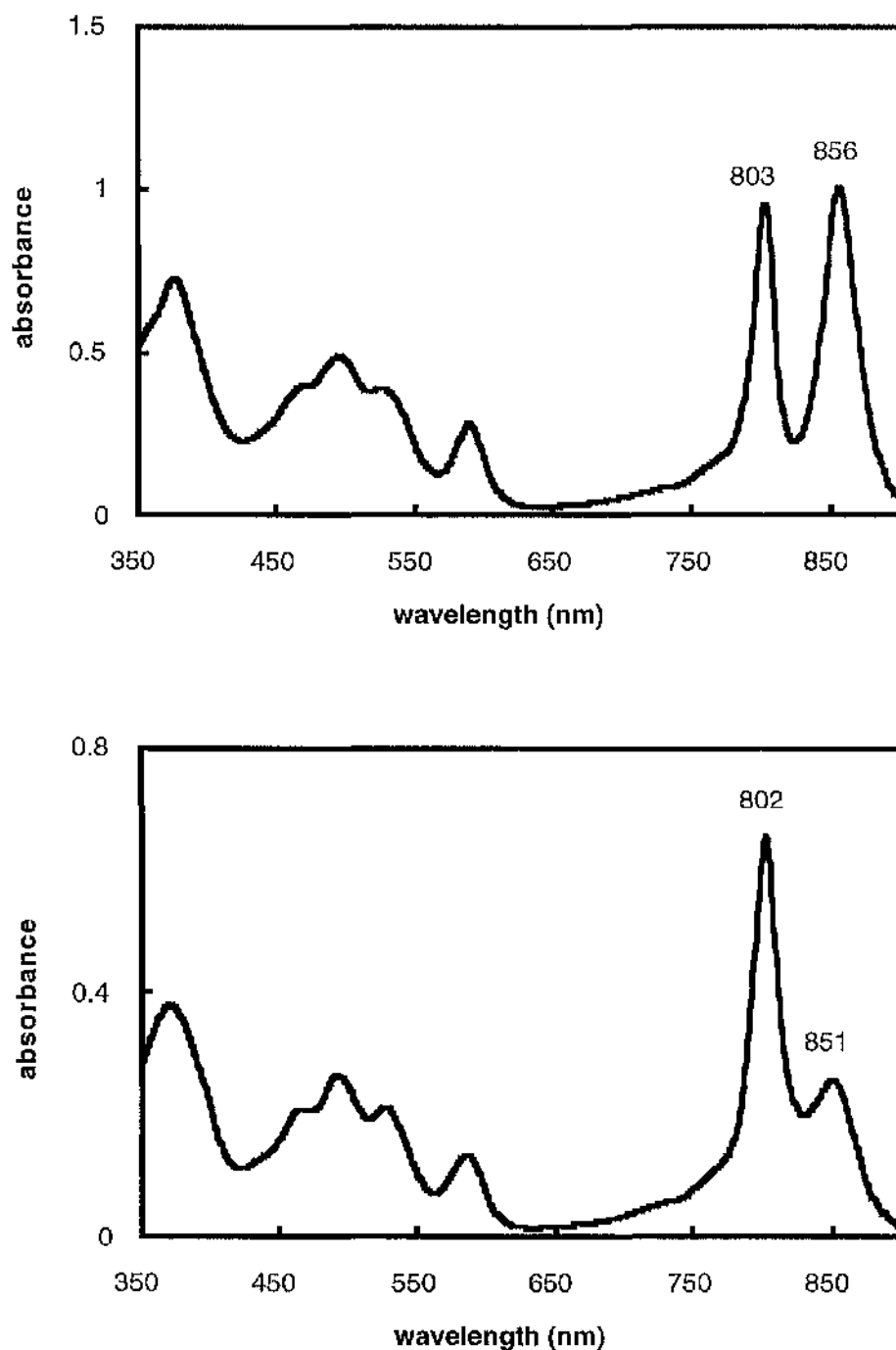


Figure 1.7. Absorption spectra of the LH2 complex from *Rps. palustris* grown under high light (HL) conditions (top) and low light conditions (bottom). The B800 absorption band of the LH2 complex becomes much more intense when the organism is grown under weak illumination. This effect is accompanied by a small blue-shift in the positions of the absorption maxima.

harvesting Bchl_s in chromatophores of *Chr. vinosum* strain D occur in at least five different spectral forms: B795, B805, B820, B850 (845) and B890 (Thornber, 1970; Hayashi *et al.*, 1981). The spectral response of *Chr. vinosum* cells to low light or low temperature (below ~35°C) conditions is similar to that observed in *Rps. acidophila* and *Rps. palustris* (Zuber & Brunisholz, 1991). Interestingly, the extent of the NIR spectral variations were found to be dependent mainly upon light intensity only when the cells were grown autotrophically (Mechler & Oelze, 1978; Hayashi & Morita, 1980). Temperature dependent spectral variations were observed only when the cells were grown heterotrophically (Mechler & Oelze, 1978). The reasons for these spectral adaptations to growth conditions are not yet understood.

Structural analyses have shown that *Chr. vinosum* synthesises at least ten different antenna polypeptides (Bissig *et al.*, 1989). Three α -peripheral antenna complex polypeptides and four β -polypeptides have been isolated and sequenced. The α -polypeptides show additional structural features, located in the elongated N-terminal domain, which are not present in any of the Rhodospirillaceae peripheral antenna complexes studied to date. Furthermore, in contrast to the CD spectra of B800-850 and B880 complexes from the Rhodospirillaceae, which exhibit double CD signals (Sauer & Austin, 1978), the CD spectra of *Chr. vinosum* B800-850 and B890 complexes exhibit mainly single, negative CD bands (Hayashi *et al.*, 1981). This clearly indicates that although Bchl in different species may exhibit absorption bands with the same maxima, the Bchl-Bchl and Bchl-protein interactions are not the same.

1.5.5. *The carotenoids*

The carotenoids are a group of unsaturated hydrocarbons and their

oxygenated derivatives which consist of eight isoprenoid units (Cogdell & Frank, 1987). In the purple bacteria about 1-2 carotenoid molecules are non-covalently bound to each antenna complex $\alpha\beta$ -apoprotein (Drews, 1985) while a single carotenoid molecule is bound to each wild type RC (Cogdell *et al.*, 1976).

Carotenoids perform a variety of functions in photosynthesis (Krinsky, 1971). The major ones are (i) photoprotection, (ii) accessory light harvesting and (iii) structure stabilisation. These and other functions of carotenoids in photosynthesis are reviewed in Frank & Cogdell (1996) and will be discussed only briefly here.

1.5.5.1. Photoprotection

It has long been established that photosynthetic organisms lacking in carotenoids, such as the carotenoidless mutant of *Rb. sphaeroides* R26, are killed if illuminated in the presence of oxygen (Griffiths *et al.*, 1955). This photo-oxidative death results from the production of singlet oxygen ($^1\Delta_g^*O_2$) which occurs when triplet excited state Bchl (or Chl) donates energy to molecular oxygen (Krinsky, 1971; Borland *et al.*, 1987). This reaction can be summarised as follows:



It is possible for carotenoids to quench this reaction in two ways. Firstly, they can directly interact with singlet oxygen and quench it in a 'scavenging'

reaction (Foote & Denny, 1968):



In solution, in order for this reaction to proceed, the energy of the carotenoid triplet state must be equal to or lower than that of singlet oxygen. Only carotenoids with more than seven conjugated carbon-carbon double bonds can perform this reaction (Foote *et al.*, 1970).

Secondly, carotenoids can quench Bchl or Chl triplet states before they can interact with molecular oxygen in what is called a 'trapping' reaction (Foote & Denny, 1968):



In both cases the ${}^3\text{Car}^*$ state is too low in energy to sensitise formation of singlet oxygen and it decays in just a few μs releasing the excess energy as heat. Whether the scavenging or trapping reaction predominates *in vivo* depends upon the type of carotenoid present and the various pigment-pigment and pigment-protein interactions that exist within the different pigment-protein complexes (Cogdell & Frank, 1987). However, it is obvious that without the photoprotective mechanisms provided by carotenoids photosynthesis could not take place.

1.5.5.2. Accessory light harvesting

Carotenoids absorb light energy in the 450-570nm region and transfer this absorbed energy to the Bchl molecules (Goedheer, 1959). As such, carotenoids increase the wavelength range over which light can be harvested for use during photosynthesis (Cogdell & Frank, 1987). The accessory light-harvesting function of carotenoids in purple bacterial antenna complexes involves a singlet-singlet energy transfer process (Cogdell *et al.*, 1994; Andersson *et al.*, 1996). Efficiencies of carotenoid to Bchl singlet-singlet energy transfer in LH2 complexes can range from 100% in the spheroidene-containing complex of *Rb. sphaeroides* strain 2.4.1 (Cogdell *et al.*, 1981) to ~55% in the rhodopin glucoside containing *Rps. acidophila* strain 10050 (Angerhofer *et al.*, 1995).

Carotenoids possess two low-lying electronic excited singlet states - S_1 and S_2 (Hudson & Kohler, 1974). The S_1 state possesses A_g symmetry. Transitions between this state and the ground state, S_0 , which also has A_g symmetry, are optically forbidden. In contrast, transitions from the ground state to S_2 are allowed because the latter possesses B_u symmetry (Frank & Cogdell, 1996). The S_0 to S_2 transition is responsible for the strong absorption of carotenoids in the visible region. The energy of this allowed transition decreases as the extent of double bond conjugation in the carotenoid molecule increases (Cogdell *et al.*, 1994).

Determination of the molecular mechanisms involved in the carotenoid to Bchl singlet-singlet transfer require a knowledge of the dynamics and energy levels of both the S_2 and S_1 states (Frank & Cogdell, 1996; Koyama *et al.*, 1996). The energy level of the S_2 state can be determined from the absorption and weak fluorescence emission spectra (Gillbro & Cogdell, 1989). However, the symmetry forbiddenness of the ground to S_1

state transition has hampered the direct determination of the S_1 energy level (Frank & Christensen, 1995). This obstacle has recently been overcome and the S_1 energies of several biologically important carotenoids have been deduced (Chynwat & Frank, 1995). The lack of observable fluorescence from the S_1 state of carotenoids containing more than 9 conjugated double bonds has proved to be another obstacle (Koyama *et al.*, 1996) although now it too appears to have been overcome (Wantanabe *et al.*, 1993; Bondarev *et al.*, 1994; Fujii *et al.*, 1998).

Cogdell *et al.*, (1997) have suggested that most of the carotenoid to Bchl energy transfer in the LH2 complex of *Rps. acidophila* strain 10050 occurs from the carotenoid S_2 state to Q_x band of the B850 Bchls, via a Förster mechanism (Förster, 1948). Only a diminutive fraction comes to the Bchl Q_y transition, via the S_1 state, by a mechanism such as Coulombic coupling (Nagae *et al.*, 1993). This could explain the rather low (~55%) efficiency of rhodopin glucoside to Bchl *a* transfer in this complex.

1.5.5.3. Structure stabilisation

Since the 1950's it has been suggested that carotenoids are essential for the correct assembly and stability of purple bacterial antenna complexes (Griffiths & Stanier, 1956). *Rhodobacter* mutants which were unable to synthesise carotenoids showed a loss of the absorption peaks associated with LII2. It was suggested that this reduction in antenna size was an adaptive response to limit the size of the photosynthetic antenna in the absence of photoprotective carotenoids (Bartley & Scolnik, 1989).

More recently, both biochemical and genetic approaches have been used to investigate the structural role of carotenoids in antenna complexes.

Zurdo *et al.* (1993) observed that the partial depletion of the carotenoid complement of the LH2 antenna from *Rb. capsulatus* resulted in a range of spectroscopic changes in the LH2 Bchl *a* absorption. These spectral changes were interpreted as being due to a conformational change in the protein component of the antenna complex associated with a loss of stability resulting from carotenoid removal.

Using a genetic approach, Lang & Hunter (1994) have shown that mutants of *Rb. sphaeroides* which lack 'coloured' carotenoids can still synthesise LH2 polypeptides. Mutants capable of LH2 polypeptide synthesis, but with carotenoid biosynthesis blocked by removal of the *crtI* gene, could not synthesise intact LH2 complexes. Complementation of these mutants with a functional *crtI* gene, which encodes for the enzyme phytoene desaturase that catalyses the conversion of phytoene into 'coloured' carotenoids (Giuliano *et al.*, 1986), resulted in the appearance of stable LH2 complexes.

Reconstitution experiments have also underlined the important role of carotenoids in stabilising and maintaining the structural integrity of purple bacterial antenna complexes. Jiraskova & Reiss-Husson (1994) reconstituted the LH1 (or B875) complex from *Rv. gelatinosus* from its B820 subunit form. However, this reconstitution was successful only if the carotenoid, hydroxyspheroidene, which is non-covalently bound to the native LH1 complex, was added to the B820 subunits. The success of the reconstitution was demonstrated by the identical CD and absorption spectra displayed by the reconstituted and native LH1 complexes.

1.6. The photochemical reaction centre

The photochemical reaction centre (RC) of purple bacteria is a membrane bound pigment-protein complex that catalyses the conversion of light energy into chemical energy by stabilising the primary photochemical charge separation. The bacterial RC from *Rps. viridis* was the first membrane protein to have its structure determined at high resolution (Deisenhofer *et al.*, 1984; Deisenhofer *et al.*, 1985). The 1988 Nobel Prize for Chemistry was awarded to Deisenhofer, Huber and Michel for this seminal work. Since this breakthrough the crystal structures of the RC from *Rb. sphaeroides* strain R-26 (Chang *et al.*, 1986; Allen *et al.*, 1987a; Allen *et al.*, 1987b; Yeates *et al.*, 1987; Chang *et al.*, 1991), strain 2.4.1 (Allen *et al.*, 1988a; Yeates *et al.*, 1988) and wild type strain Y (Reiss-Husson *et al.*, 1992; Buchanan *et al.*, 1993) as well as several site directed RC mutants (Chirino *et al.*, 1994; Iyfe *et al.*, 1998) have been determined. Preliminary X-ray crystallographic studies of the RC from the thermophilic sulphur bacterium *Chromatium tepidum* (Katayama *et al.*, 1994) and the green bacterium *Chloroflexus aurantiacus* (Feick *et al.*, 1996) have also been undertaken in recent years.

The RCs from *Rps. viridis* (Fig. 1.9) and *Rb. sphaeroides* (Fig. 1.10) are closely related in both structure and function (El-Kabbani *et al.*, 1991). Indeed, the preliminary structures of the RCs from *Rb. sphaeroides* were elucidated by the method of molecular replacement using the co-ordinates of the *Rps. viridis* RC (Allen *et al.*, 1986a). The RCs from both species contain three polypeptide subunits termed H (heavy), M (medium) and L (light) according to their electrophoretic mobilities in SDS-PAGE. These subunits are present in a molar ratio of 1:1:1 (Feher & Okamura, 1978). The *Rps. viridis* RC also possesses a fourth subunit - a tightly bound 45 kDa tetrahaem cytochrome *c* subunit (Deisenhofer *et al.*, 1984; Deisenhofer *et al.*, 1985). In addition to *Rb. sphaeroides*, only a few other species of purple

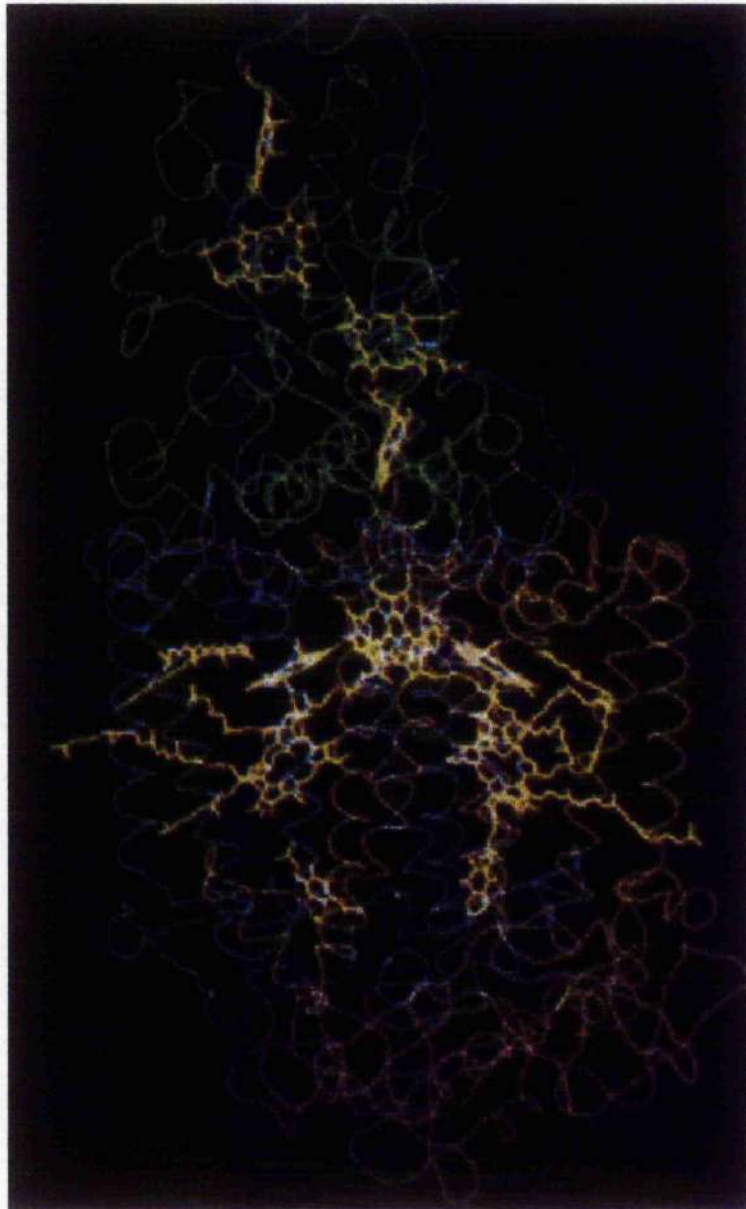


Figure 1.8. Structure of the *Rps. viridis* reaction centre. The polypeptides are represented as smoothed backbone drawings. The tightly bound tetrahaem cytochrome c, which is located on the periplasmic side of the membrane, is coloured green; M subunit, blue; L subunit, brown; H subunit, purple. The cofactors are shown in yellow. A ubiquinone molecule is located towards the bottom left of the figure, whereas a menaquinone is located towards the bottom right. The total length of the RC is about 130 Å. The core of the RC has an elliptical cross-section with axes of 70 and 30 Å. Redrawn from Deisenhofer and Michel (1989).

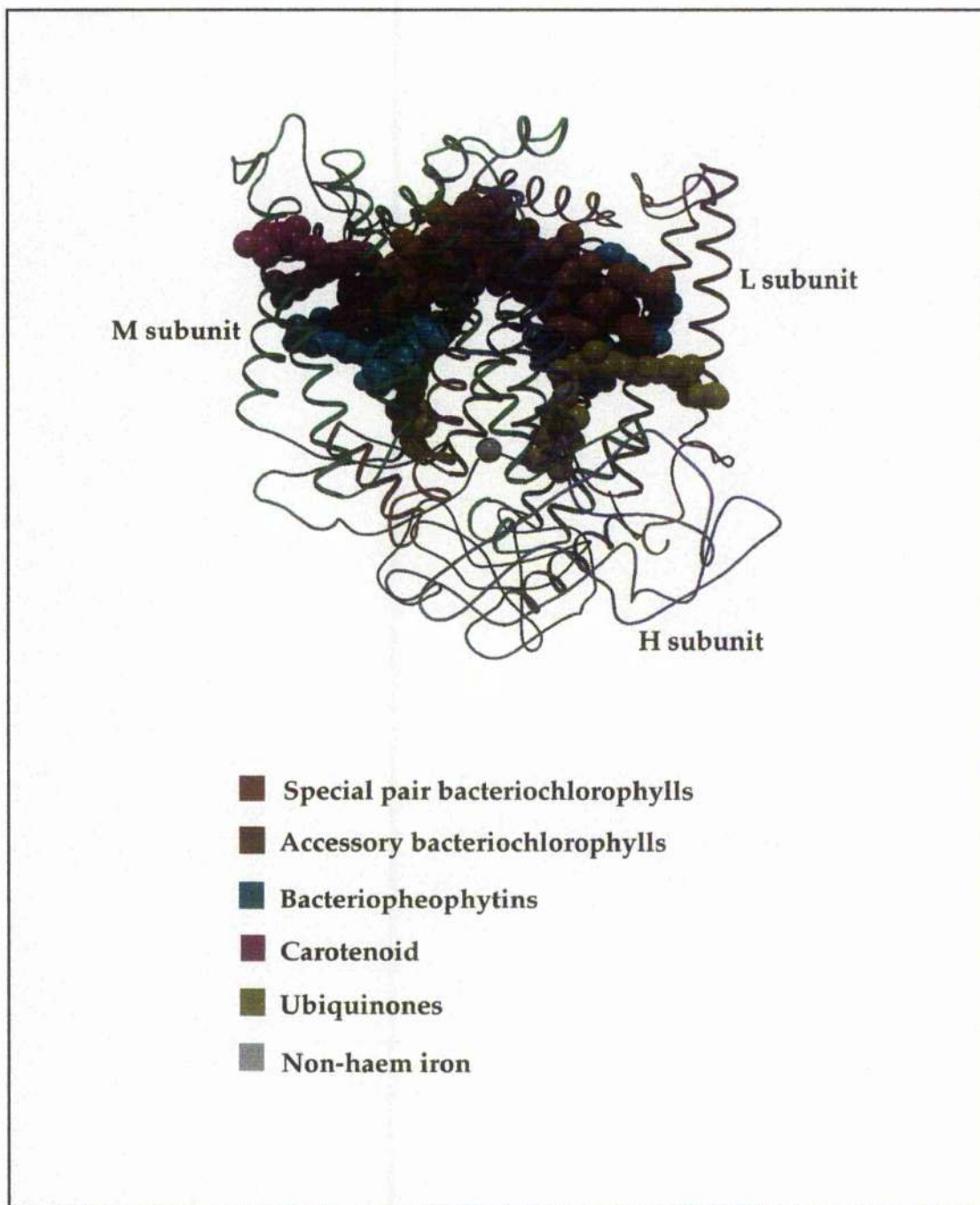


Figure 1.9. Cartoon of the photochemical reaction centre from *Rhodospirillum rubrum* (*Rb. sphaeroides*). The H, M and L subunits are represented as ribbons whereas the cofactors are shown in a space-filling form. A two-fold axis of symmetry extends from the iron atom to the Bchl special pair. The cofactors are bound to the L and M subunits. In contrast to the *Rps. viridis* RC, the *Rb. sphaeroides* RC lacks a tightly bound cytochrome subunit.

bacteria such as *Rb. capsulatus* (Jones *et al.*, 1990), *Rs. rubrum* (Rickle & Cusanovich, 1979) and *Rps. palustris* (Matsuura & Shimada, 1986) lack a tightly bound cytochrome *c* subunit in the RC.

A number of nonprotein cofactors are associated with the L and M subunits of the RC (Feher & Okamura, 1978; Parson, 1987). The *Rps. viridis* RC contains four Bchl *b* molecules, two bacteriopheophytin (BPhe) *b* molecules, a menaquinone, an ubiquinone, a non-haem high spin iron (Fe^{2+}), and a single carotenoid molecule (Deisenhofer & Michel, 1989) (Fig. 1.9). The *Rb. sphaeroides* RC contains four Bchl *as*, two bacteriopheophytin *as*, two ubiquinones (Q_A and Q_B), a non-haem iron atom and, in the wild type bacterium, a single molecule of the carotenoid spheroidene (Arnoux *et al.*, 1989) (Fig. 1.10). For reviews of the structure and function of bacterial RCs refer to Feher *et al.* (1989), Deisenhofer & Michel (1989), Ermiler *et al.* (1994) and Lancaster *et al.* (1995).

1.6.1. The RC protein subunits

The L and M subunits of both the *Rps. viridis* and *Rb. sphaeroides* RC are transmembrane proteins with homologous structure and amino acid sequences (Allen *et al.*, 1986b; El-Kabbani *et al.*, 1991). 59% of the amino acids are identical in the L subunits and, in the M subunits, 50% of the amino acid residues are identical (Williams *et al.*, 1983). In the *Rps. viridis* RC the M chain contains 18 more amino acid residues at its C-terminal end compared with the same subunit of the *Rb. sphaeroides* RC. These extra residues are involved in binding the cytochrome subunit of the *Rps. viridis* RC (Deisenhofer *et al.*, 1985). Both the L and M subunits contain 5 transmembrane helices labelled A to E (Deisenhofer *et al.*, 1985; Allen *et al.*, 1987b). The transmembrane helices are connected by short amphipathic

helical regions which run parallel to the membrane surfaces. In *Rb. sphaeroides* the polar sides of the amphipathic helical regions on the periplasmic surface of the L and M subunits form the docking site for the soluble cytochrome c_2 molecule (Allen *et al.*, 1987b; Chang *et al.*, 1991; Caffrey *et al.*, 1992).

The L and M subunits interact to form an elliptical core with quasi two-fold symmetry which binds all the cofactors involved in photochemistry and primary charge separation (Allen *et al.*, 1987a; 1987b). The core region contains a bundle of 4 α -helices, each of which contains a conserved His residue that ligands to the Fe^{2+} ion. This suggests that the Fe^{2+} has a role in the stabilisation of the core region of the RC (Deisenhofer & Michel, 1989).

In contrast to the L and M subunits the H subunit possesses only one transmembrane helix. This helix may function in maintaining the proper orientation of the RC complex in the membrane (Chang *et al.*, 1991). The majority of the H subunit is located on the cytoplasmic side of the membrane (see Figures 1.8 & 1.9). The cytoplasmic part of the H subunit forms a globular, soluble domain with a polar exterior and hydrophobic interior. Extensive contacts are formed between the H subunit and the cytoplasmic side of the L and M subunits. These contacts probably serve to stabilise the tertiary structure of the whole RC complex (Debus *et al.*, 1985).

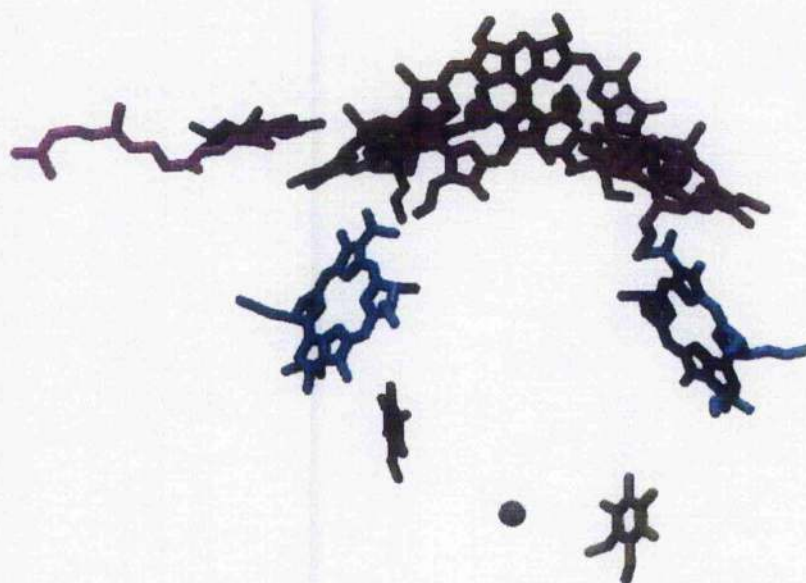
Removal of the H subunit from the RC still results in a photochemically active complex (Agalidis & Reiss-Husson, 1983; Feher & Okamura, 1984) although the efficiency of electron transfer from Q_A^- to Q_B is diminished (Debus *et al.*, 1985). This may be due to a loosening of the structure of the LM complex which, in turn, lowers the binding constant of Q_B (Feher *et al.*, 1989).

1.6.2. Arrangement of the cofactors and electron flow through the RC

The structure of the cofactors of the *Rb. sphaeroides* RC is shown in Figure 1.10. The cofactors are arranged in two symmetric branches referred to as A and B (or L and M in *Rps. viridis*). The two-fold symmetry axis extends from the iron atom to the two strongly coupled Bchls (D_A and D_B or P870), known as the 'special pair', that constitute the primary electron donor (Feher *et al.*, 1989). The most striking property of the RC complex is that, despite its symmetry, electron transfer proceeds through only the A branch of the complex (Michel-Beyerle *et al.*, 1988). Although the reason for this is not known, it has been postulated that the unidirectionality of electron transport may be caused by the different protein environments of the cofactors (Allen *et al.*, 1987a; Nakagawa *et al.*, 1995).

Located downstream from the primary donor are two monomeric Bchl molecules (B_A and B_B), two BPhe molecules (ϕ_A and ϕ_B) and a pair of quinones (Q_A and Q_B) (Allen *et al.*, 1988b; Yeates *et al.*, 1988). The quinones, Q_A and Q_B , act as the primary and secondary electron acceptors, respectively (Yeates *et al.*, 1988). These quinones are located in different environments in the LM core of the RC with the Q_A binding site being more apolar than the Q_B site (Allen *et al.*, 1988b). Located between the quinones is a single high-spin Fe^{2+} ion. Originally it was thought that this ion played an important role in electron transfer from Q_A to Q_B . However, later experiments showed that removal of the Fe^{2+} does not significantly affect the rate of electron transfer to Q_B (Debus *et al.*, 1986). The arrangement of pigments along the A branch is in concert with the electron pathway as predicted from spectroscopic measurements (reviewed in Parson & Ke, 1982).

A single carotenoid molecule is non-covalently bound to the RC. The X-



- Special pair bacteriochlorophylls
- Accessory bacteriochlorophylls
- Bacteriopheophytins
- Carotenoid
- Ubiquinones
- Non-haem iron

Figure 1.10. Stick and ball diagram showing the spacial arrangement of the cofactors in the RC of *Rb. sphaeroides*. The two fold symmetry of the arrangement, which extends from the iron atom to the Bchl special pair, can be clearly seen. Despite this symmetry, electron transfer generally occurs down the A branch (right hand side of the diagram). The special pair Bchl's are closely coupled whereas the accessory Bchl's are monomeric. The single molecule of the carotenoid, spheroidene, is located at the upper left corner of the diagram. The primary and secondary quinones are located to the right and left of the iron atom, respectively.

ray structure of the *Rb. sphaeroides* RC locates the carotenoid next to the B branch (Arnoux *et al.*, 1989). This carotenoid is not known to be involved in the primary photochemical events (Parson & Monger, 1976; Chadwick & Frank, 1986). However, it does perform a photoprotective function by quenching triplet state Bchl before it can sensitise formation of singlet oxygen (Krinsky, 1971; Cogdell *et al.*, 1975).

Upon excitation of the primary donor, a photochemical reaction is triggered in which an electron is transferred from the primary donor, P870, to ϕ_A . This process occurs in about 3 ps. The electron transfer to ϕ_A is facilitated by the monomeric B_A molecule. In both *Rb. sphaeroides* and *Rps. viridis* the electron is then transferred to the primary acceptor, Q_A , in about 200 ps. The secondary quinone, Q_B , is the final electron acceptor of the RC complex. Electron transfer from Q_A to Q_B occurs in 100 μ s (see reviews by Cogdell, 1983; Kirmaier & Holten, 1987; Feher *et al.*, 1989; Shinkarev & Wraight, 1993). This series of events results in a charge separation across the membrane.

1.6.3. Electron flow beyond the RC

Charge separation alone cannot be converted directly into useful chemical energy in the form of ATP as, according to the chemiosmotic theory, this requires formation of a proton gradient (Mitchell, 1961). A proton gradient can only form after the secondary quinone is reduced by a second electron to form Q_B^{2-} (reviewed in Okamura & Feher, 1995). Subsequently, two protons are picked up by the doubly-reduced quinone which then dissociates from the RC and diffuses into the membrane. The now empty Q_B binding site is re-occupied by one of a pool of exogenous neutral quinones. The electrons are transferred to a membrane-bound

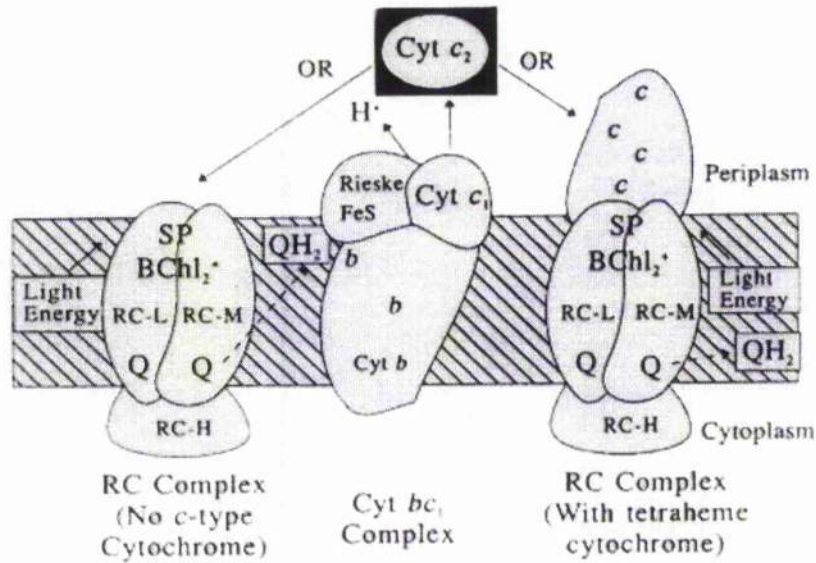


Figure 1.11. Schematic diagram of the electron and proton transport pathway in purple bacteria. The Cyt c_2 complex accepts electrons from the membrane bound Cyt bc_1 complex (centre). The reduced Cyt c_2 then donates electrons either directly to the RC (left) or to an RC bound tetraheme (right). Protons picked up by doubly reduced quinone are translocated across the photosynthetic membrane (represented by diagonal shading) to form a proton gradient. This gradient is utilised for ATP formation. Abbreviations: RC-H, RC-M and RC-L, reaction center heavy, medium and light subunits; SP Bchl, bacteriochlorophyll special pair; Q, quinone; QH $_2$, quinol; Rieske FeS, Rieske 2-Fe-S subunit of the Cyt bc_1 complex; Cyt c_1 , Cyt c_1 subunit of the Cyt bc_1 complex; Cyt b , membrane spanning Cyt b subunit of the Cyt bc_1 complex. Redrawn from Meyer & Donohue (1995).

cytochrome bc_1 complex and the protons are translocated across the membrane to form the proton gradient necessary for ATP formation (Fig. 1.11). The electrons from Q $_B^{2-}$ are used to reduce the cyt bc_1 complex, which in turn reduces a soluble cyt c_2 complex (reviewed in Meyer & Donohue, 1995). The cycle is completed when the cyt c_2 migrates to the oxidised RC and donates electrons back to the special pair (Dutton *et al.*, 1975). The RC is

now returned to a photochemically active state and ready to absorb another photon.

In *Rb. sphaeroides* the soluble cyt c_2 binds only transiently to the RC core subunits (Dutton & Prince, 1978; Dutton *et al.*, 1975), whereas in *Rps. viridis* electrons are passed from cyt c_2 to the 2-haem group of the bound tetrahaem cytochrome (Bartsch, 1978). As RC complexes that contain a tightly bound cytochrome subunit appear to be more commonplace than those in which a soluble cyt c_2 interacts directly with the RC, it has been suggested that the former is a more efficient method of reducing the special pair (Meyer & Donohue, 1995).

Recent studies, using mutants of *Rb. sphaeroides* and *Rb. capsulatus*, have implicated another membrane-associated cytochrome (termed cyt c_y) in the mediation of electron transfer during photosynthetic growth (Jenney & Daldal, 1993). For a comprehensive review of the role of cytochromes in cyclic electron transfer refer to Meyer & Donohue (1995).

1.7. Structure of the LH2 (B800-850) antenna complex

In the past, our understanding of light-energy capture and transfer in the purple bacteria has been hampered by the lack of detailed structural information about the light-harvesting complexes. However, this situation has changed dramatically with the elucidation, by X-ray crystallography, of high resolution 3-D structures of the B800-850 complexes from *Rps. acidophila* strain 10050 (McDermott *et al.*, 1995) and *Rs. molischianum* (Koepke *et al.*, 1996).

As shown in Figure 1.12 the B800-850 complex from *Rps. acidophila* consists of a nonamer of $\alpha\beta$ -apoproteins arranged in a ring-like structure

(McDermott *et al.*, 1995). The transmembrane helices of the nine α - and β -apoproteins form two concentric rings with radii of 18Å and 34Å, respectively. The hole in the centre of the structure is thought to be filled with lipid (R.J. Cogdell, personal communication). The α -apoprotein helices lie perpendicular to the proposed plane of the membrane while those of the β -apoproteins are tilted by about 15° with respect to the membrane plane. There is no $\alpha\beta$ -helix-helix interaction within the transmembrane domain of the structure and this may explain the failure of detailed models of LH2 (Olsen & Hunter, 1994) prior to the determination of the crystal structure (Cogdell *et al.*, 1997). However, the N- and C-termini of both apoproteins, which are located on the cytoplasmic and periplasmic sides of the membrane, respectively, fold over and interact with each other to enclose the top and bottom of the structure. Large aromatic residues located at the C-termini of both apoproteins interact, via hydrogen bonds and hydrophobic interactions, to interlock the whole structure (Cogdell *et al.*, 1997). This protein structure acts as a scaffold for the photosynthetic pigments.

The structure of the LH2 complex from *Rs. molischianum* is very similar to that of *Rps. acidophila* but instead of a nonamer it consists of an octamer of $\alpha\beta$ -apoproteins (Koepke *et al.*, 1996). The α - and β -apoproteins of the *Rs. molischianum* complex are longer than those of the *Rps. acidophila* complex, consisting of 56 and 45 amino acid residues, respectively. The $\alpha\beta$ -dimers of the LH2 complex from both species show the same basic protein folds even though there is only a 26% and 31% sequence similarity for the α - and β -apoproteins, respectively (Cogdell *et al.*, 1997).

Electron diffraction of 2-D crystals of the LH2 complexes from

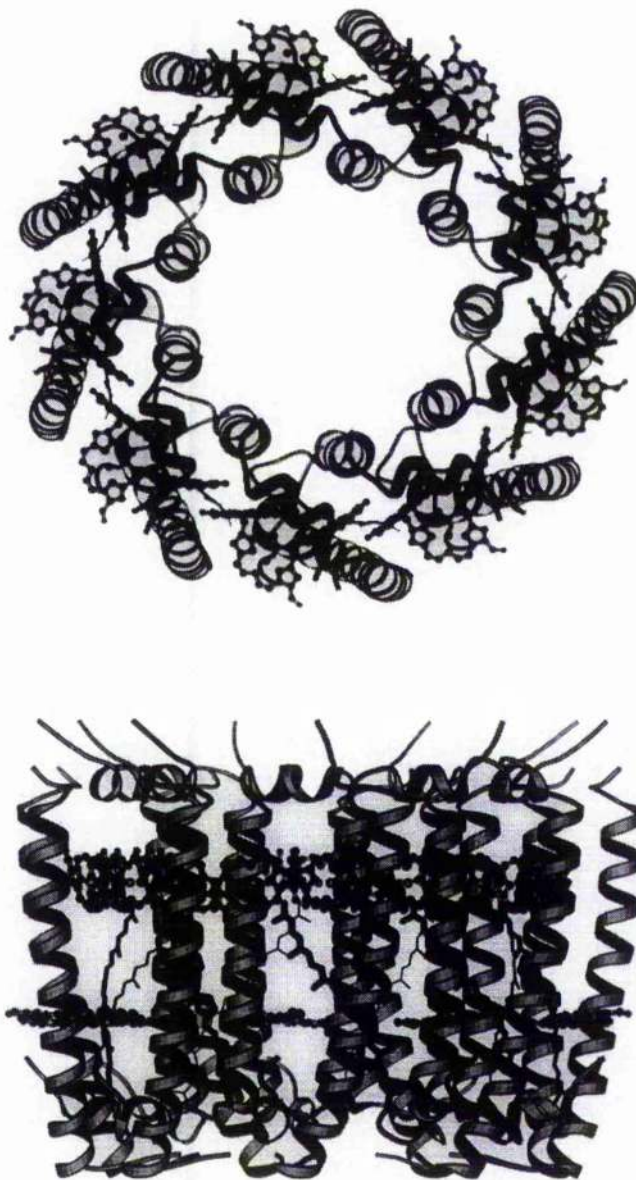


Figure 1.12. Schematic representation of the nonameric LH2 complex from *Rps. acidophila* strain 10050 (McDermott *et al.*, 1995) viewed from the periplasmic side of the membrane (top) and from within the membrane (bottom). The apoproteins are shown as ribbons and the carotenoids and Bchl *a* molecules as ball and stick representations. Only the photoactive moieties of the chromophores are shown. The figures were produced by Dr. S.M. Prince, Dept. of Chemistry, University of Glasgow, using the modelling package 'Molscript' (Kraulis, 1991).

Rhodovulum sulfidophilum (Savage *et al.*, 1995), *Rb. sphaeroides* (Walz *et al.*, 1998), *Rb. capsulatus* and an *Ectothiorhodospira* species (Oling *et al.*, 1996) have shown that these complexes too are ring-like. The first three are nonameric in arrangement, the latter octameric. It is not yet understood what controls the oligomeric size of these complexes but it has been suggested it may be a function of the exact primary sequence at the N- and C-termini where the α - and β -apoproteins interact (Cogdell *et al.*, 1996).

1.7.1. Binding and arrangement of the Bchl *a* molecules

The Bchl *a* molecules of the LH2 complexes from both *Rps. acidophila* and *Rs. molischianum* are arranged into two distinct populations. In *Rps. acidophila*, one of these populations consists of eighteen tightly coupled Bchl's that are sandwiched, in a very hydrophobic environment, between the concentric rings formed by the transmembrane helices of the α - and β -apoproteins (Fig. 1.13). These Bchl's are liganded to one or other of the conserved α -(His 31) and β -(His 30) of the apoproteins and their bacteriochlorin rings lie perpendicular to the plane of the membrane. The centres of the bacteriochlorin rings are located about 10Å from the periplasmic surface of the membrane. Nine other Bchls are arranged between the β -apoprotein α -helices about 16.5Å further into the membrane. The binding pocket of these Bchl's is rather hydrophilic (Cogdell *et al.*, 1997). The planes of their bacteriochlorin rings lie more or less parallel to the presumed plane of the membrane (McDermott *et al.*, 1995). In contrast to the 18 tightly coupled Bchls, the central Mg²⁺ atoms of the 9 Bchl's that lie between the β -apoproteins are not liganded to a His residue. It was originally thought that they were liganded to an N-formyl methionine residue (McDermott *et al.*, 1995). Current thinking, however, suggests that

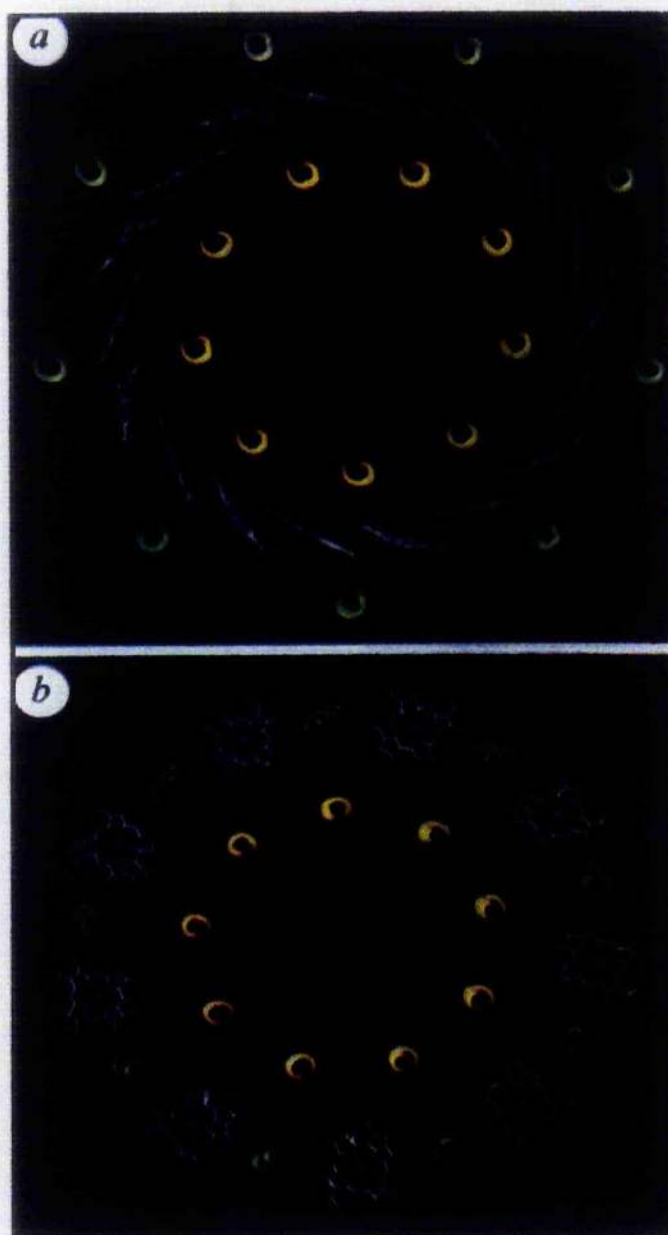


Figure 1.13. Arrangement of the Bchl *a* molecules within the LH2 complex of *Rps. acidophila* strain 10050. The α -apoproteins are coloured yellow and the β -apoproteins are green. (a) A top view of the complex showing the ring of coupled B850 Bchl *a*'s sandwiched between the apoproteins with their bacteriochlorin rings perpendicular to the membrane surface. (b) A view further into the membrane showing the B800 Bchl *a*'s with their bacteriochlorin rings parallel to the membrane surface. Adapted from McDermott *et al.* (1995).

this may not be the case (R.J. Cogdell, personal communication). The Mg^{2+} - Mg^{2+} distance between each of these Bchl's is 21.2Å. Based on previous spectroscopic studies of the *Rps. acidophila* LH2 complex, the group of 18 Bchls were identified as those absorbing at about 863nm (B850) and the group of 9 Bchls as those absorbing at about 801nm (B800) (Cogdell & Scheer, 1985; Robert & Lutz, 1985). Spectroscopic studies by Visschers *et al.* (1995) confirmed a similar arrangement of the B850 and B800 Bchl's in *Rs. molischianum*.

In the *Rps. acidophila* LH2 complex the individual environments and conformations of the B850 Bchl's are not all equivalent (McDermott *et al.*, 1995; Freer *et al.*, 1996; Cogdell *et al.*, 1997; Prince *et al.*, 1997). The Mg^{2+} - Mg^{2+} distance between the two B850 Bchl's of each $\alpha\beta$ - apoprotein is 9.6Å. However, the Mg^{2+} - Mg^{2+} distance between the nearest B850 Bchl's of adjacent $\alpha\beta$ - apoproteins is only 8.9Å (S.M. Prince, personal communication). The orientation of the Bchl's also alternates going around the ring. The face of the α B850 Bchl bacteriochlorin ring is presented to the inside of the complex whereas that of the β B850 Bchl is presented to the outside (Freer *et al.*, 1996).

The configuration of each type of Bchl also differs (Freer *et al.*, 1996; Cogdell *et al.*, 1997). The bacteriochlorin ring of the α B850 is almost planar while that of the β B850 shows a significant 'bowing' along the direction of the Q_y transition. The bacteriochlorin of the peripheral B800 Bchl's is slightly 'domed'.

The Bchl's of the *Rs. molischianum* LH2 complex are more tightly and evenly distributed in the ring compared to those of *Rps. acidophila*. (Koepke *et al.*, 1996). In *Rs. molischianum* the B850 Bchl's are also sandwiched between the helical apoproteins with their bacteriochlorin

rings perpendicular to the plane of the membrane (Koepke *et al.*, 1996). The central magnesium atoms of these sixteen coupled B850 Bchl's are liganded to one or other of the conserved α -(His 34) and β -(His 35) residues of the apoproteins. The eight B800 Bchl's form a ring around the periphery of the complex. The B800 Bchl's are located between the β -apoproteins and the planes of their bacteriochlorin rings are tilted away from the membrane plane by 38°. The B800 Bchl macrocycle itself is rotated by 90° compared that of the *Rps. acidophila* LH2 complex. The central Mg²⁺ atom of each B800 is liganded to the γ oxygen of the α Asp6 residue (Koepke *et al.*, 1996). This is a consequence of the greater length of the α -apoprotein in the *Rs. molischianum* complex (Cogdell *et al.*, 1997).

1.7.2. The bacteriochlorophyll phytyl tails

The Bchl molecules play an important role in maintaining the structural integrity of the LH2 complex (Klug *et al.*, 1986). The phytyl chains of the Bchl's also aid in the alignment of the bacteriochlorin rings (Cogdell *et al.*, 1997; Freer *et al.*, 1996). In *Rps. acidophila*, the B800 phytyl chain travels through the complex, wraps around the phytyl chain of the β B850 Bchl then passes across the face of the β B850 Bchl macrocycle (Fig. 1.14). The phytyl tail of the β B850 Bchl passes across the face of the B800 Bchl, effectively holding the latter in place within the complex. In contrast, the phytyl chain of the α -B850 Bchl is almost fully extended and does not pass across the face of a bacteriochlorin ring. Instead, it makes several contacts with the carotenoid and probably functions to orient the carotenoid within the complex (Freer *et al.*, 1996).

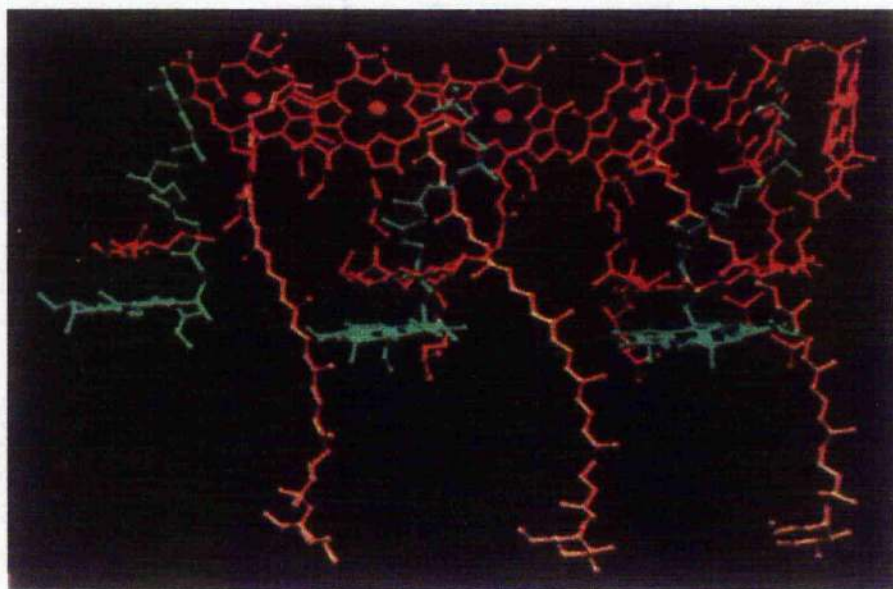


Figure 1.14. Arrangement of the pigments (carotenoids and Bchl *a*'s) in the LH2 complex of *Rps. acidophila* strain 10050. This figure represents the pigments bound to 3 $\alpha\beta$ -polypeptide pairs. Carotenoids are shown in yellow; B800 Bchl, green; α B850 Bchl, orange; β B850 Bchl, red. The carotenoid molecules traverse the depth of the membrane passing close to both the B800 and B850 Bchl's. It was thought that two carotenoids were present in the refined model of the complex but this now appears to be wrong. The phytol chains of the B800 Bchl's twist up and pass across the face of the α B850 macrocycles. The phytol chains of the β B850 molecules trail down across the face of the B800 Bchl rings. Adapted from McDermott *et al.* (1995).

1.7.3. Structure and arrangement of the carotenoids

The original electron density map of the *Rps. acidophila* LH2 complex only identified one molecule of the carotenoid, rhodopin glucoside, $per\alpha\beta$ dimer (McDermott *et al.*, 1995). This carotenoid, which is well ordered, has a

typical all *trans* conformation and spans the depth of the complex. The glucoside ring interacts with polar residues on the N-terminal of the α -apoprotein, and the hydrocarbon chain passes across the face of the β -B850 macrocycle in the adjacent $\alpha\beta$ -dimer. Viewed down its axis, the carotenoid is twisted and this probably gives rise to the strong circular dichroism (CD) observed in the visible region of the spectrum (Cogdell *et al.*, 1997).

A refined model of the LH2 complex was thought to show the existence of a second molecule of rhodopin glucoside per $\alpha\beta$ -dimer (Cogdell *et al.*, 1997; Freer *et al.*, 1996). Current opinion, however, indicates this may not be correct (R.J. Cogdell, personal communication) although the existence of a second carotenoid seems to be provided by the projection map of 2-D crystals of LH2 from *Rhodovulum sulfidophilus* (Montoya *et al.*, 1995; Savage *et al.*, 1995).

Like the Bchl's, the carotenoids also play an important role in the stabilisation of the LH2 structure (see section 1.5.5.3). Studies using carotenoid deletion mutants of purple bacteria have shown that LH2 either fails to assemble (Griffiths & Stanier, 1956; Zurdo *et al.*, 1993) or is rapidly turned over (Lang & Hunter, 1994).

1.8. Structure of the LH1-RC 'core' complex

Unfortunately, no high resolution 3-D structure of either the isolated LH1 antenna or LH1-RC core complex yet exists. However, several low resolution structures, based on single particle analyses of isolated LH1-RC cores (Boonstra *et al.*, 1994) and electron microscopy of photosynthetic membranes and 2-D crystals, and have been proposed (Ikedu-Yamasaki *et al.*, 1998; Karrasch *et al.*, 1995; Meckenstock *et al.*, 1994; Miller, 1982; Stark *et*

al., 1984; Walz & Ghosh, 1997; Walz *et al.*, 1998). These studies have shown that the LH1 complex consists of a ring-like structure which encircles the photochemical reaction centre.

1.8.1. *The Rhodospseudomonas viridis* core complex

LH1-RC core complexes were first visualised in electron microscopy (EM) studies of the photosynthetic (PS) membranes of the Bchl *b*-containing 'core only' bacterium *Rps. viridis* (Miller, 1979; Wehrli & Kübler, 1980; Welte & Kreutz, 1982; Miller, 1982; Stark *et al.*, 1984). This species is useful for EM studies as its PS membrane contains extensive, quasi-crystalline 2-D arrays of core complexes (Garcia *et al.*, 1968). Fourier processing and averaging of the membrane images gave a map with a resolution of $\sim 20\text{\AA}$ which revealed the *Rps. viridis* photoreceptor unit to be a roughly circular structure with hexagonal symmetry. This unit consisted of a core of 45\AA diameter surrounded by a ring of about 20\AA wide (Stark *et al.*, 1984) (Fig. 1.15). The whole structure was $100\text{-}120\text{\AA}$ in diameter. The central core, which extended through the PS membrane and protruded $\sim 40\text{\AA}$ above its surface on the exoplasmic side, was postulated to be the photochemical RC. The surrounding ring was proposed to be the LH1 antenna which consisted of 12 and 6 subunits on the cytoplasmic and exoplasmic sides, respectively. Similar results were obtained from EM studies of the PS membrane of *Ectothiorhodospira halochloris* (Engelhardt *et al.*, 1983). This suggested that this type of structure was a feature common to all Bchl *b*-containing PS membranes (Stark *et al.*, 1984).

A more recent study of 2-D crystals of the LH1-RC complex from *Rps. viridis* using cryo-electron microscopy produced a higher resolution (10\AA) projection map of the core complex structure (Ikedu-Yamasaki *et al.*, 1998).

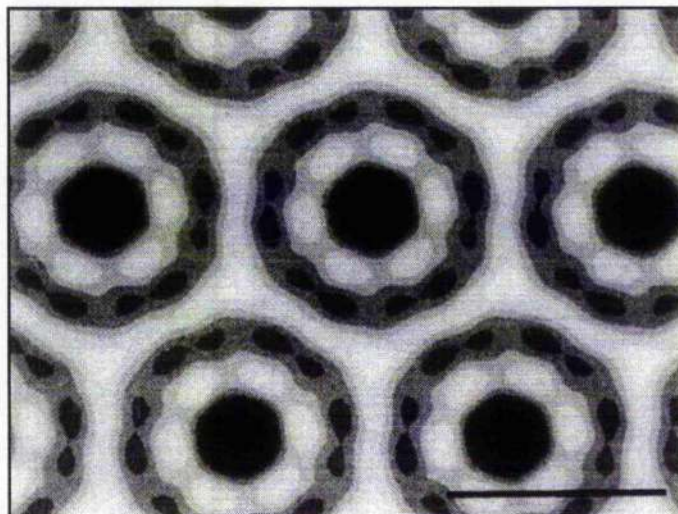


Figure 1.15. Fourier processed contour map of an electron micrograph of tantalum/tungsten rotary-shadowed, Triton X-100 treated photosynthetic membrane of *Rps. viridis*. The structural unit appears to consist of a ring with a diameter of 120 Å (the LH1 antenna) with a central core (the RC) measuring about 45 Å across. The ring consists of 12 subunits and the whole complex possesses a six fold symmetry. Bar= 10nm. Reproduced from Stark *et al.* (1984).

This map also revealed three regions of density (an asymmetric central core and two concentric rings surrounding it) which were equated to a RC surrounded by an LH1 ring (Fig. 1.16). Despite the improvement in resolution the projection map could not give unambiguous evidence as to the number of subunits in the LH1 ring. However, the density of the outer LH1 ring appeared to be significantly higher than that of the inner one. As each subunit of the LH1 complex from *Rps. viridis* consists of three polypeptides (α , β and γ) in a stoichiometric ratio of 1:1:1 (Jay *et al.*, 1984; Brunisholz *et al.*, 1985) the higher density of the outer ring was interpreted as being due to the presence of two membrane-spanning helices per

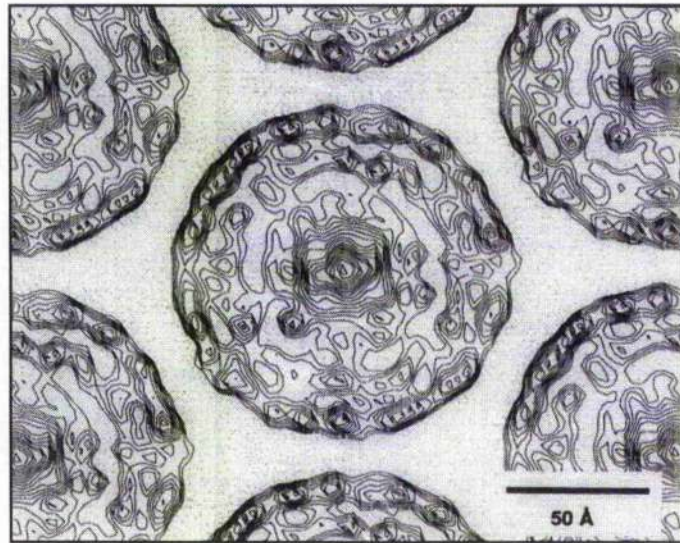


Figure 1.16. 10Å projection map of the LH1-RC core complex from *Rps. viridis*. The map clearly shows the complex to consist of a central core surrounded by a ring. However, the resolution is not good enough to determine the number of subunits which make up the ring. Refer to the text for details. Reproduced from Ikeda-Yamasaki *et al.* (1998).

subunit. Accordingly, the inner, lower density ring was due to the third transmembrane helix of the subunit (Ikeda-Yamasaki *et al.*, 1998). Analogous with the LH2 complex from *Rps. acidophila* (McDermott *et al.*, 1995), the Bchl *b* molecules of the *Rps. viridis* LH1 complex were assumed to be sandwiched between the helices of the α - and β -polypeptides. This implied a total of 24 Bchl's per core complex.

1.8.2. The *Rhodospirillum rubrum* core complex

Recently, Karrasch *et al.* (1995) produced 2-D crystals of highly purified LH1 antenna from *Rs. rubrum* which, when studied by cryo-electron

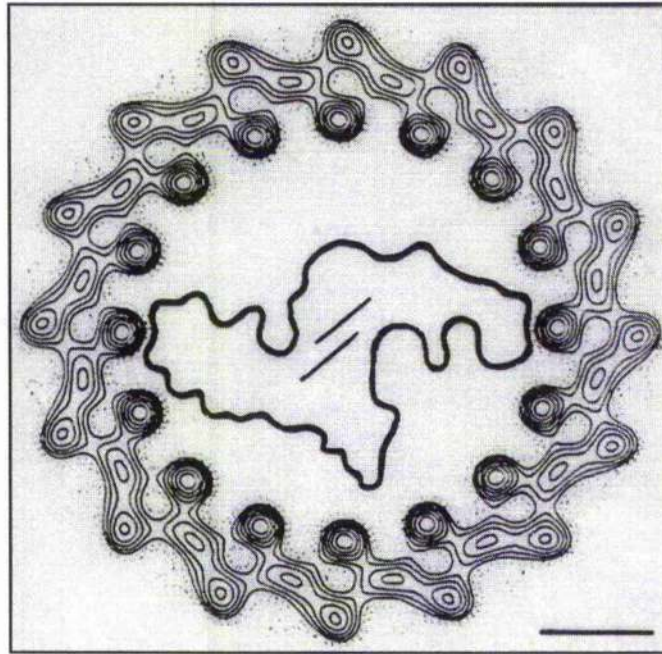


Figure 1.17. 8.5Å projection map of 2-D crystals of the LH1 antenna complex from *Rs. rubrum* viewed from above the membrane. An approximate van der Waals projection of the LM dimer and the single transmembrane helix of the H subunit of the *Rps. viridis* RC (Deisenhofer *et al.*, 1985) has been arbitrarily placed within the LH1 ring. The antenna appears to consist of a ring of 16 $\alpha\beta$ -subunits which completely encircle the RC. The density between each α - and β -subunit probably represents the Bchl *a* and carotenoid pigments. Scale bar=20Å. Adapted from Karrasch *et al.* (1995).

microscopy techniques, yielded an 8.5Å resolution projection map of the LH1 complex. The map showed the complex to consist of a closed ring of 16 $\alpha\beta$ -subunits. This ring had an overall diameter of 116Å with a 68Å diameter hole in the centre. The hole in the centre of the structure was just large enough to house a RC *in vivo* (Fig. 1.17). Three domains of density could be resolved within each subunit of the averaged projection map of the LH1 ring. The inner face of the ring showed 16 large peaks separated by a distance of ~15Å. These peaks were proposed to be due to the α -apoproteins

of the complex. The outer face of the ring showed 16 less dense peaks, separated from each other by $\sim 20\text{\AA}$ and from the inner peaks by $\sim 15\text{\AA}$, which were assigned to the β -apoproteins of the complex. The lower density of the β -apoproteins was thought to be due to their helices being more tilted than those of the α -apoproteins. The density between the inner and outer peaks of the ring was attributed to the Bchl *a* and carotenoid molecules of the complex (Karrasch *et al.*, 1995). This model therefore implied a ratio of 32 Bchl *a*'s per RC.

A criticism of the above work was that the LH1 complexes were reconstituted from their $\alpha\beta$ -subunits prior to crystallisation and, therefore, the ring-like structure may not reflect the actual *in vivo* structure of the LH1 complex. However, this problem was addressed by Walz & Ghosh (1997) who grew 2-D crystals of the complete LH1-RC complex from a carotenoidless strain of *Rs. rubrum*. Image analysis of these crystals supported a model of the core complex in which the LH1 ring completely surrounded a RC which was probably free to assume various orientations within the ring.

1.8.3. The size of the LH1 ring

Although the 8.5\AA projection map of the LH1 complex from *Rs. rubrum* indicated it consisted of 16 $\alpha\beta$ -subunits, previous EM studies of the core complexes from the Bchl *a*-containing species *Rb. sphaeroides* (Boonstra *et al.*, 1993), *Rs. molischianum* (Boonstra *et al.*, 1994), and isolated LH1 from *Rh. marinum* (Meckenstock *et al.*, 1994) suggested the LH1 ring was, like that of *Rps. viridis*, composed of 12 $\alpha\beta$ -subunits. However, the resolution of these images was very low ($40\text{-}50\text{\AA}$) and analysis of them may have necessitated symmetrisation according to a preconceived model (Walz

& Ghosh, 1997). Due to the lack of high resolution data the size of the LH1 ring remains the subject of debate.

In the past, a biochemical approach has been used to ascertain the size of the LH1 ring. Since there is a definite relationship between the size of an LH1 ring and its capacity to completely surround a RC, the stoichiometry of the LH1 antenna Bchl's per RC provides a method to calculate the LH1 ring size (assuming each $\alpha\beta$ -subunit of the LH1 ring binds two Bchl molecules). Indeed, this method was used in several studies which encompassed a wide range of species (Dawkins *et al.*, 1988; Gall, 1994; Franke & Ames, 1995). Dawkins *et al.* (1988) investigated the LH1 ring size of nine different species and strains of Bchl *a*-containing purple bacteria, and obtained Bchl *a*:RC ratios of between 21:1 to 41:1 with an average of ~30:1. The latter value was similar to that reported by Ueda *et al.* (1985) for the Bchl *a*-containing species *Rb. sphaeroides*, *Chr. vinosum* and *Rs. rubrum*. Due to the variability in the values it was difficult to assign a ring size for the LH1 complex, although the average value of ~30:1 would suggest an LH1 ring consisting of 16 $\alpha\beta$ -subunits. There may be several reasons for the variability in the measurements: (i) the ring size may vary between species; (ii) the instability of some of the isolated core complexes in detergent (Dawkins *et al.*, 1988), and; (iii) there may be a heterogeneity in the ring size within a given species (Kühlbrandt, 1995). Although no direct evidence exists for the latter *in vivo*, Karrasch *et al.* (1995) reported that LH1 forms 2-D crystals of two different types. One consisted of rings with a diameter of 116Å and the other of rings with a diameter of 80Å. The larger ring consisted of 16 $\alpha\beta$ -subunits, whereas the smaller rings probably consisted of ~9 $\alpha\beta$ -subunits. However, the smaller rings may simply be an artefact of the isolation and crystallisation protocol.

Careful measurements of the LH1 Bchl *a*:RC ratio for seven species of

purple bacteria were made by Gall (1994). Although the data again showed some variability, an average value of $33 \pm 4:1$ was obtained. These data were consistent with the $16\alpha\beta$ -subunit model of the LH1 complex described by Karrasch *et al.* (1995) assuming that each apoprotein dimer bound two Bchl's. In contrast, measurements conducted by Franke and Amesz (1995) on six Bchl *a*-containing and one Bchl *b*-containing species of purple bacteria yielded values that were more consistent with a ring composed of 12 $\alpha\beta$ -subunits. However, using molecular modelling techniques, Papiz *et al.* (1996) demonstrated that a ring consisting of 12 $\alpha\beta$ -subunits is not sufficient to completely enclose the RC. Given these conflicting data, it seems that the determination of the exact ring size of the LH1 antenna will have to await the arrival of a high resolution structure.

One way to justify a LH1 Bchl:RC ratio of less than 32:1 while at the same time addressing the requirement of the LH1 ring to encircle the RC would be to include a non-pigment-binding component, equivalent to 2 $\alpha\beta$ -subunits, in the ring (Kramer *et al.*, 1998). However, a structure of the core complex in which the LH1 ring encircles the RC is at odds with the well established dogma that electron transfer between the RC and cytochrome *bc₁* complex occurs via the diffusion of a membrane-bound quinone between them (reviewed in Meyer & Donohue, 1995). This contradiction could be resolved if the non-pigment-binding component of the ring acted as a quinone channel. In fact, a strong body of evidence suggests that a protein, termed PufX, may perform such a role in the LH1 antenna of *Rb. sphaeroides* and *Rb. capsulatus* (Bauer *et al.*, 1988; Farchaus & Oesterhelt, 1989; Lilburn *et al.*, 1992; McGlynn *et al.*, 1994, 1996; Barz *et al.*, 1995a,b; Kramer *et al.*, 1998; Recchia *et al.*, 1998; Pugh *et al.*, 1998). In *Rs. rubrum* no gene (or gene product) homologous to *pufX* has been found (Bélanger *et al.*, 1988). However, a small 4kDa polypeptide, termed the Ω -polypeptide, which

copurifies with the LH1 $\alpha\beta$ dimer may be a candidate for this role (Ghosh *et al.*, 1994a; 1994b).

1.8.4. The role of the PufX protein

The importance of the PufX protein in bacterial photosynthesis was evident from experiments which showed that deletion of the *pufX* gene of strains of *Rb. sphaeroides* resulted in a loss of photosynthetic competence (Farchaus *et al.* 1990a; 1992). Addition of *pufX* back to *pufX*⁻ strains resulted in a recovery of photosynthetic competence (Farchaus *et al.*, 1990b). Furthermore, PufX is necessary for photosynthetic growth only in strains that contain the LH1 antenna (McGlynn *et al.*, 1994). Photosynthetic growth was not compromised by the deletion of the *pufX* gene in RC-only mutants (McGlynn *et al.*, 1994). These observations, along with another which showed that deletion of *pufX* caused a change in LH1 content (Klug & Cohen, 1988), supported the suggestion that PufX functions in the structural organisation of the PSU, thereby allowing a free exchange of quinone between the RC and the cytochrome *bc*₁ complex (Lilburn *et al.*, 1992; McGlynn *et al.*, 1994; Barz *et al.*, 1995a; Barz *et al.*, 1995b). This postulated function of PufX was further illustrated by studies on suppressor mutants of *Rb. capsulatus* and *Rb. sphaeroides* which lacked the *pufX* gene. These mutants were shown to have mutations in the α - and β -polypeptides of the LH1 antenna which apparently compensated for the loss of PufX (Lilburn & Beatty, 1992; Barz & Oesterhelt, 1994; Lilburn *et al.*, 1995).

The use of genetically modified strains of *Rb. sphaeroides*, in which the C-terminal region of the LH1 α -polypeptide was progressively truncated, allowed McGlynn *et al.* (1996) to demonstrate that a lack of PufX did not prevent photosynthetic growth if the LH1 antenna size was reduced below

21 Bchl *a*'s per RC. Additionally, the loss of *pufX* caused an increase of 1-2 Bchl *a*'s per RC. These results were in accordance with those of Kramer *et al.* (1998) who found that a *pufX* deletion mutant of an LH1-only strain of *Rb. sphaeroides* contained 29.5 Bchl *a*'s per RC, whereas in the presence of *pufX* the control mutant contained 25 Bchl *a*'s per RC. The difference of ~4 Bchl *a*'s indicated that 2 $\alpha\beta$ -subunits in the LH1 ring of the control were replaced by the non-pigment binding *pufX* protein. This reconciled the results of Franke & Amesz (1995) and Karrasch *et al.* (1995), and supported the postulated 'gateway' function of the *pufX* protein.

Very recently, the *pufX* protein from *Rb. capsulatus* and *Rb. sphaeroides* has been isolated and used in reconstitution experiments to examine its effect on LH1 antenna formation (Recchia *et al.*, 1998). For a review of reconstitution experiments refer to Loach & Parkes-Loach (1995). The isolated *pufX* protein was shown to have a specific, high affinity for the LH1 α -polypeptides and was inhibitory to LH1 formation at low concentrations. Once again, these results were in agreement with the idea that *pufX* modifies the molecular architecture of the LH1 ring, thereby allowing the quinone free movement between the RC and cytochrome *bc*₁ (Barz *et al.*, 1995a; Lilburn *et al.*, 1995).

1.8.5. Structure and topology within the membrane of the *pufX* protein

The circular dichroism (CD) spectrum of the *pufX* protein from *Rb. capsulatus* indicated that it contained ~19% α -helical structure (Recchia *et al.*, 1998). This compared with 56% α -helical structure for the LH1 α -polypeptide. The amount of α -helical structure in the *pufX* protein would be insufficient to allow it to span the membrane. However, there are 7 glycine residues in the middle section of the protein which suggests a rather

unusual structure, perhaps involving a series of turns or even a U-shaped membrane anchor that extends only a short way into the membrane (Recchia *et al.*, 1998). One way in which the *pufX* polypeptides could achieve their task without actually spanning the membrane, but only partially extending into it, would be for them to form a lipid-containing 'porthole' near the Q_B quinone binding site of the RC. Such a scenario would require specific interactions between *pufX*, LH1 and the RC (Recchia *et al.*, 1998). However, no evidence yet exists for an interaction between the L, M or H subunit of the RC and *pufX*.

Proteolytic treatment of membrane vesicles of *Rb. sphaeroides*, followed by N-terminal sequencing, showed that the *pufX* protein was inserted into the membrane with its N-terminus exposed on the cytoplasmic surface (Pugh *et al.*, 1998). Such a topology suggested the possibility of the C-terminal end of an LH1 α -polypeptide acting as a recognition or binding site for the C-terminal end of the PufX protein (Pugh *et al.*, 1998). However, the exact structural role of *pufX* and its interactions with other components of the PSU will probably have to await the arrival of a high resolution, 3-D structure of a *pufX*-containing core complex.

1.9. The concept of the photosynthetic unit

The concept of the photosynthetic unit (PSU), which forms the basis of modern thinking of the primary processes of photosynthesis, originated from the studies of Emerson & Arnold (1932). They determined that when *Chlorella* cells were exposed to illumination by a single flash of saturating intensity, one oxygen molecule was formed per 2500 Chl molecules. When the latter number was divided by 8 (the minimum number of light quanta per oxygen molecule evolved) it was concluded that ~300 Chl molecules

collaborated in the production of oxygen. This collaboration was explained by the ability of an absorbed quantum to be transferred between Chl's until it became trapped at a specific site where the energy was used to drive the primary photochemical reaction. This trap is now known to be the RC. The combination of a RC and the light-harvesting pigments that contribute excitation energy to that RC, is defined as the PSU (reviewed by Mauzerall & Greenbaum, 1989; Freiberg, 1995).

1.9.1. *The purple bacterial PSU*

Studies performed on *Rs. rubrum* and *Rb. sphaeroides* enabled Aagard and Sistrom (1972) to show that the size of the purple bacterial PSU is variable in many species, and that in some cases this variability arose from environmental factors such as light intensity (refer to section 1.5.4). In *Rb. sphaeroides* the size of the PSU varied from 30 Bchl *a* molecules per RC when cells were grown under high light conditions, to ~200-250 Bchl *a*'s per RC when cells were grown under low illumination. This demonstrated that at least some of the purple bacteria are able to tune their capacity for photon capture, not only in terms of the wavelengths of light absorbed, but also by increasing the amount of (and thereby the physical area occupied by) antenna complexes within the photosynthetic membrane. The employment of such a strategy ensures the RC is supplied with sufficient photons while at the same time keeping expenditure on protein and pigment biosynthesis to a minimum.

As discussed previously (section 1.5) the antenna system of purple bacteria is relatively simple, consisting of two main types of antenna complex referred to as LH1 and LH2 (Firsow & Drews, 1977). In species such as *Rps. viridis* and *Rs. rubrum*, which possess LH1 as the only antenna

complex, the LH1-RC core complex represents the maximal size of the PSU (Zuber & Brunisholz, 1991). In such cases the size of the PSU is fixed within a given species (Aagard & Siström, 1972). However, in species such as *Rb. sphaeroides*, which can synthesise peripheral LH2 as well as core complexes, the core complex represents the minimal size of the PSU. In these cases the LH2 complexes are arranged around the periphery of the core complexes and the ratio of LH2:RC is variable. Generally, the lower the light intensity at which the cells are grown the greater the ratio of LH2:RC. Yet other species, such as *Rps. acidophila*, *Chr. vinosum* and *Rps. cryptolactis*, can adapt to low light conditions by synthesising different types of LH2 complex (refer to section 1.5.4 and references therein).

Although many structural details are known about antenna complexes reconstituted in various systems, much less is known about their organisation within the natural photosynthetic membrane. To date, knowledge about antenna organisation has been derived mostly from methods based on picosecond absorption (Kramer *et al.*, 1995), fluorescence decay kinetics and fluorescence yield measurements (Monger & Parson, 1977; Deinum *et al.*, 1991; Kramer & Ames, 1996), as well as microscopic techniques (Miller, 1982; Stark *et al.*, 1984). More recently, research in this area has been advanced by the determination of the 3-D crystal structures of LH2 from *Rps. acidophila* (McDermott *et al.*, 1995) and *Rs. molischianum* (Koepke *et al.*, 1996), and a projection map of the LH1 complex from *Rs. rubrum* (Karrasch *et al.*, 1995). Using this structural information, Papiz *et al.* (1996) proposed an elegant model of the PSU of purple bacteria. In this model the structure of the *Rb. sphaeroides* RC (Allen *et al.*, 1987) was built into an LH1 ring of 16 $\alpha\beta$ -apoproteins (Fig. 1.18a). The structure of this ring was based on a combination of the known structure of LH2 (McDermott *et al.*, 1995) and the 8.5Å projection map of the *Rs. rubrum* LH1 (Karrasch *et*

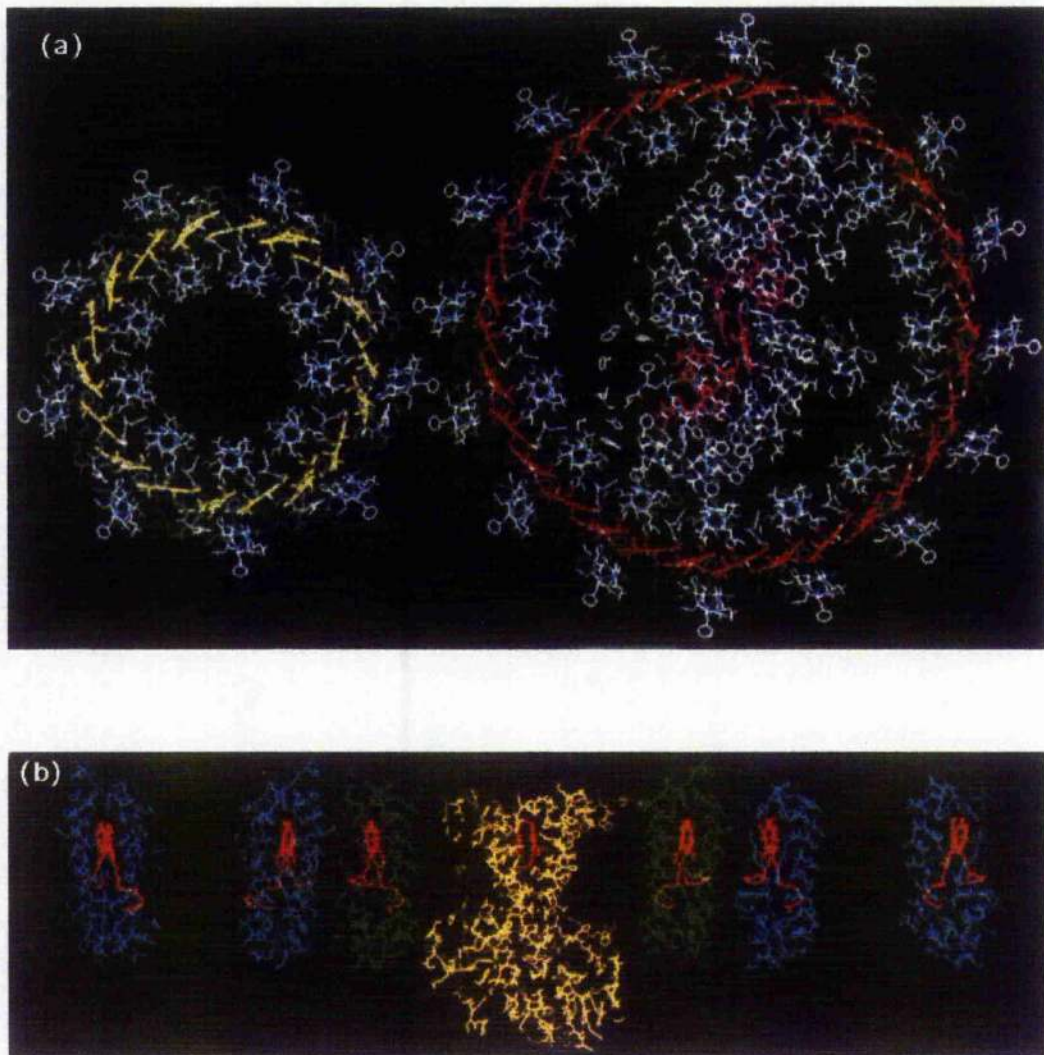


Figure 1.18. (a) View to the normal of the membrane surface looking onto a core LH1-RC complex composed of the RC from *Rb. sphaeroides* (Allen *et al.*, 1987) surrounded by an LH1 ring composed of 16 $\alpha\beta$ -subunits based on an analogy with the LH2 complex of *Rps. acidophila* strain 10050. An LH2 structure (McDermott *et al.*, 1995) is shown next to it. The B850 Bchl *a*'s are shown in yellow, the B875 Bchl *a*'s in red, and the RC pigments in purple. All other colours represent protein. (b) View along the membrane, with the periplasmic surface at the top of the diagram, of the putative PSU consisting of a core complex surrounded by LH2 complexes. The RC is yellow, LH1 complex is green, LH2 is blue. All the Bchl *a* pigments are shown in red, apart from the B800 pigments which are omitted for clarity. Reproduced from Papiz *et al.* (1996).

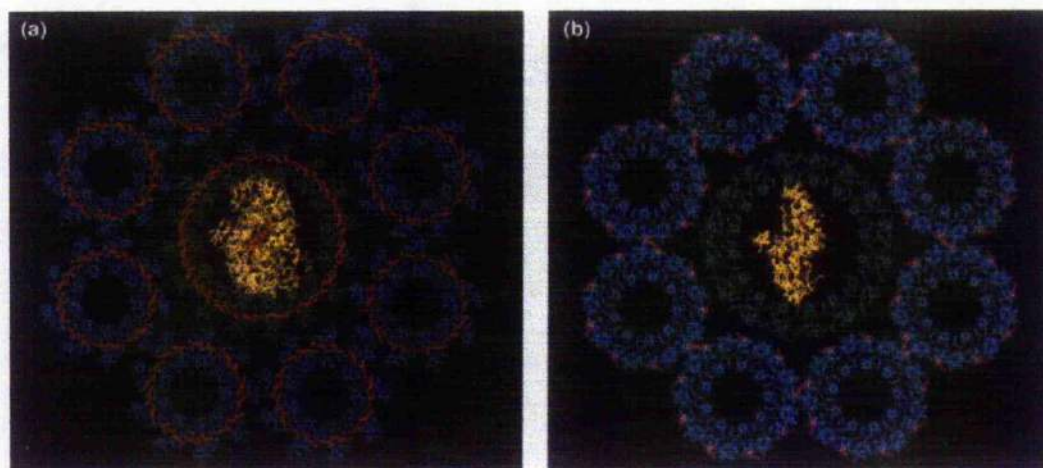


Figure 1.19. A postulated PSU consisting of a core complex surrounded by 8 LH2 complexes. (a) A section of a view through the membrane around the B850 and B875 Bchl *a* rings of the LH2 and LH1 rings, respectively, and the RC special pair. (b) View into the membrane of the structure around the Asp17 and Arg20 residues (in magenta) of the β -apoproteins of the LH2 complex. Some of these residues can be seen to form links between LH2 complexes. LH2 complexes are shown in blue, LH1 complex in green, RC polypeptides in yellow and the Bchl *a* B850, B875 and RC special pair in red. Both views are perpendicular to the membrane and represent a narrow section of about 5Å in thickness. Reproduced from Papiz *et al.* (1995).

al., 1995). When an LH2 ring is placed next to this model of the LH1-RC core complex the rings of B850 and B875 Bchl *a* molecules line up at a depth in the membrane which corresponds closely to that where the RC special pair Bchl *a*'s are located (Fig. 1.18b). This is an important feature of the model as it minimises the distance between Bchl *a* molecules, thereby ensuring a fast and efficient energy transfer from LH2 to LH1 and from LH1 to the RC. This type of information allowed Papiz *et al.* (1996) to construct a model of the PSU of LH2-containing purple bacteria grown under low light conditions in which 8 LH2 complexes surround each LH1-RC core complex in a lattice with hexagonal symmetry (Fig.1.19). However, in reality the lattice can only

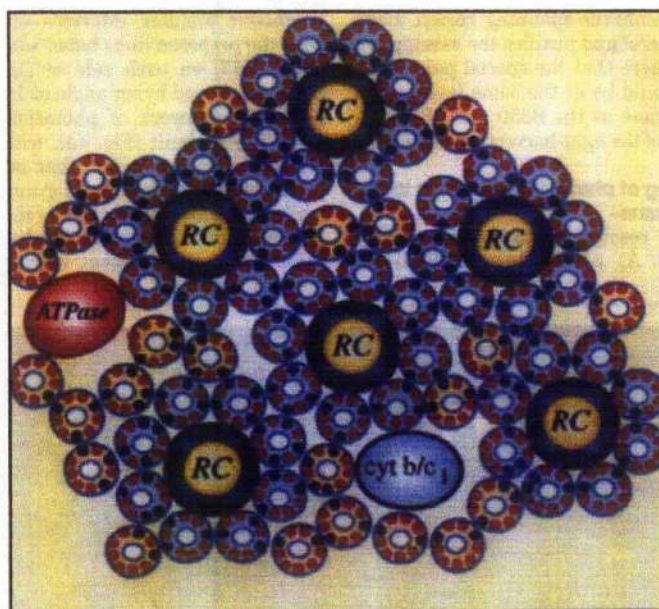


Figure 1.20. Schematic representation of the postulated antenna organisation within the photosynthetic membrane of a low-light grown purple bacterium. The PSU's are embedded in bulk LH2 and other membrane proteins. The RC (yellow circle) and LH1 antenna (large blue ring) are surrounded by LH2 complexes. The latter have the Asp and Arg residues displayed as blue or red spots. The red spots represent ion-pair links that cannot be made between complexes, whereas blue spots represent links that can be made. This allows a network of interactions involving asp-Arg links to be formed. LH2 complexes that possess LH1 complexes as neighbours are shown in light blue. Those that are only neighbours to other LH2 complexes are shown in light orange. Reproduced from Papiz *et al.* (1996).

be approximately regular as other membrane proteins, such as ATPases and cytochromes, must also be incorporated into the membrane (Fig. 1.20). No evidence exists to either confirm or disprove such a model. Therefore, more detailed EM studies on intact photosynthetic membranes are required to test it.

Several other models have been proposed for the antenna organisation

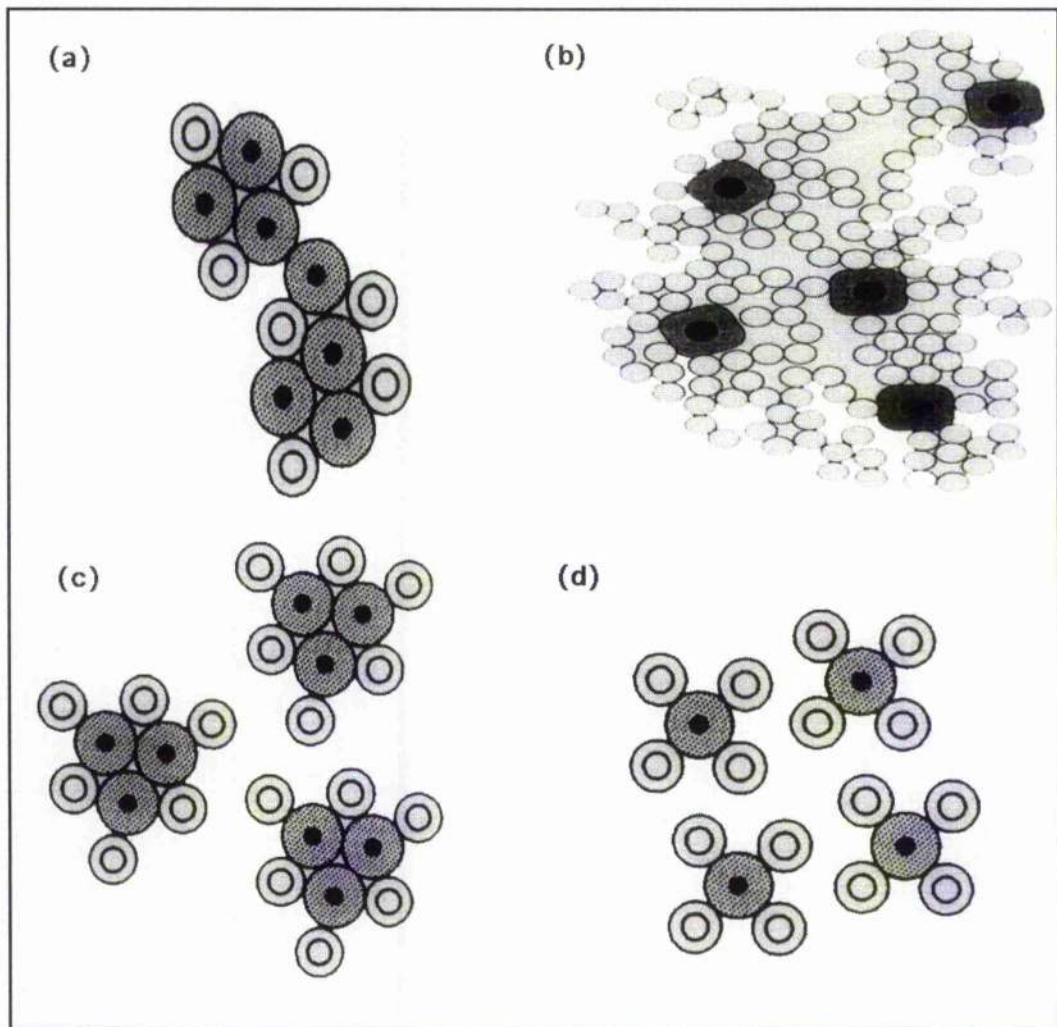


Figure 1.21. Schematic models of the antenna organisation within different species of purple bacteria. The reaction centres are represented by black circles, the LH1 antenna by dark rings, and the LH2 complexes by light rings. Model (a) represents a 'lake' model of the PSU as postulated by Monger and Parson (1977), model (b) the antenna arrangement in *Rps. acidophila* strain 7750 (Deinum *et al.*, 1991), model (c) the antenna arrangement in *Rps. cryptolactis* grown at high light intensity (Kramer *et al.*, 1995) and model (d) the organisation of the PSU in the purple sulphur bacterium *Chr. tepidum* (Kramer and Amesz, 1996). Adapted from Deinum *et al.*(1991) and Kramer and Amesz (1996).

in LH2-containing purple bacteria. Vredenberg and Duysens (1963) showed that the relationship between the fluorescence yield and the fraction of closed reaction centres is hyperbolic. This could be understood by assuming that several reaction centres share a common network of antenna Bchl's. This 'lake model', in which several PSU's are energetically interconnected to form so-called domains, seemed to be experimentally confirmed by Monger and Parson (1977), who studied the effect of singlet-triplet quenching on the low intensity fluorescence yield in chromatophores of *Rb. sphaeroides*. In this model the LH1-RC core complexes formed large aggregates surrounded by LH2 (Fig. 1.21a). Purple bacteria containing LH1 as the only antenna complex are also thought to have a functional antenna organisation of a 'lake' (van Grondelle, 1985) implying the PSU's are extremely densely packed. This would allow for the rapid energy transfer required by the 'lake model' approach.

A study of the antenna organisation in *Rps. acidophila* using singlet-singlet annihilation produced a model in which small clusters of B880, the size of one PSU, were separated by a more or less continuous array of B800-820 or B800-850 LH2 complexes (Deinum *et al.*, 1991) (Fig. 1.21b). The postulated clusters could now be equated with the LH1 ring. However, neither this nor the 'lake' model of Monger and Parson (1977) seemed to apply to *Rps. cryptolactis* for which the data suggest a close association of each LH1-RC unit with its own complement of LH2 and the absence of an interconnecting network of LH2 (Kramer *et al.*, 1995) (Fig. 1.21c). In *Chr. tepidum* the PSU consists of isolated arrays of core-reaction centre-LH2 complexes containing one or more RC's (Kramer & Amesz, 1996) (Fig. 1.21d).

1.10. Energy transfer within the PSU

The purple bacterial photosynthetic apparatus is arranged in such a way that it is able to participate in the ultrafast transfer of excitation energy to the RC, where charge separation takes place (van Grondelle *et al.*, 1994). The development of pico- and femtosecond laser spectroscopy has allowed the study of the dynamics of this energy transfer (reviewed in Pullerits & Sundström, 1996; van Grondelle *et al.*, 1994).

Energy transfer processes can be described in terms of two distinct transfer mechanisms. Each of these mechanisms represents an extreme and the actual situation *in vivo* is probably represented by an intermediate process. The first type of energy transfer process is the Förster induced dipole-dipole resonance transfer mechanism (refer to Borisov, 1978). This mechanism, which typically applies to weakly coupled pigments ~20-80Å apart, occurs via a non-radiative resonance process that can be thought of as equivalent to a donor molecule emitting absorbed photons as fluorescence and the acceptor molecule re-absorbing the emitted photons (Förster, 1948). Energy transfer by this mechanism is governed by several factors: (i) the magnitude of the spectral overlap of the fluorescence of the donor and the absorbance of the acceptor; (ii) the distance, R , between the donor and acceptor; (iii) geometry of the donor and acceptor transition dipoles; and, (iv) the refractive index of the medium between the donor and acceptor. There is a $1/R^6$ dependence of energy transfer by the Förster mechanism.

The strong Coulombic coupling of the transition dipoles of closely interacting pigments, such as those in the B850 ring, gives rise to the second type of energy transfer process (Davydov, 1962). A third possible mechanism of energy transfer can occur when pigments are in van der Waals contact. In

this case energy transfer, via electron exchange, occurs in a Dexter-type process (Dexter, 1953). Such an exchange is of crucial importance for the deactivation of triplet state Bchl's (refer to section 1.5.5.1).

The physical mechanisms of energy transfer within the purple bacterial PSU depend upon which pigments are involved and whether they are strongly coupled or weakly interacting. Once a Bchl pigment has absorbed a photon it must transfer that energy to another pigment before the absorbed energy can be lost in a wasteful process such as fluorescence. Therefore, the organisation of pigments in an antenna system is an important factor and the time required for energy migration from pigment to pigment must be short compared to the time required for a non-productive process. As the lifetime of the first excited singlet state of a Bchl *a* molecule is in the order of several hundreds of picoseconds to a few nanoseconds, antenna pigments must transfer energy to the RC in less than ~100ps (Sundström & van Grondelle, 1995; Pullerits & Sundström, 1996). Energy transfer within the PSU is a directed process which is guided by the energy gradient going from B800 to B850 to B880 and then to the RC (Pullerits & Sundström, 1996).

Examination of the structure of LH2 from *Rps. acidophila* (McDermott *et al.*, 1995; Freer *et al.*, 1996) reveals an organisation which is beautifully adapted to optimise the orientation of the Bchl *a*'s for a rapid and efficient energy transfer (refer to Figure 1.12). Use of low energy pump-probe techniques allowed the energy transfer kinetics in LH2 complexes from *Rb. sphaeroides* and *Rps. palustris* to be investigated (Hess *et al.*, 1995). The experiments showed that energy transfer from B800 to B850 takes place with a rate constant of 0.7ps at room temperature, and 1.8ps at 77K. The decay of the anisotropy of excited B800 at room temperature indicated a rapid, but limited B800 to B800 energy transfer with a time constant of 0.3ps. The B800 to B850 energy transfer has been modelled in terms of a Förster process

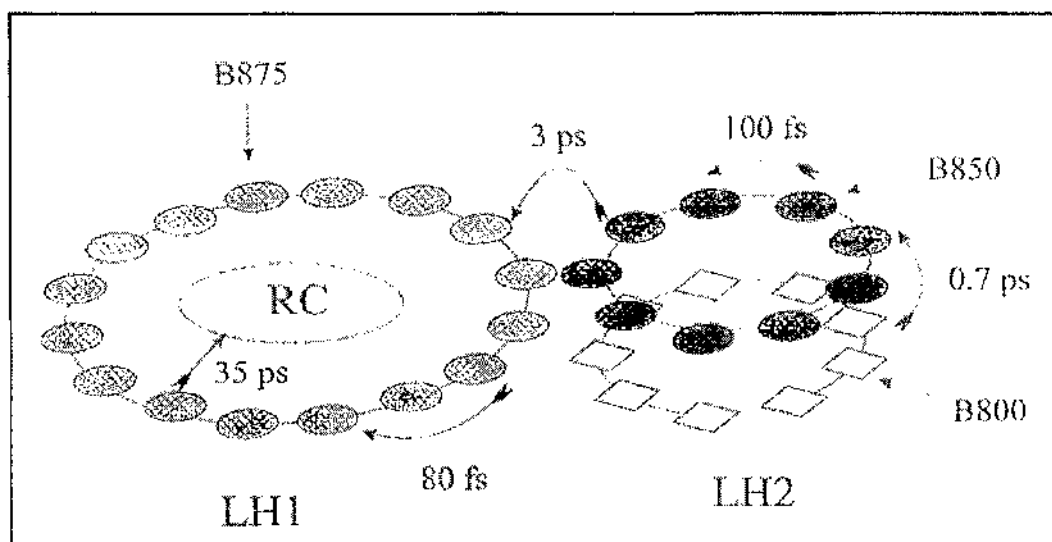


Figure 1.22. Schematic diagram summarising the timescales for energy transfer in the purple bacteria. The carotenoid to Bchl transfer times, which are of the order of 100fs in LH2 are not shown. The B875 (or B880) and B850 Bchl's are shown as dimers (ovals), and the monomeric B800 Bchl's are shown as diamonds. From Fleming and van Grondelle (1997).

(Laan *et al.*, 1990; Monshouwer *et al.*, 1995; van Grondelle *et al.*, 1982).

When excitation energy arrives at the B850 ring it can remain there for > 1 ns, provided no other antenna complex is nearby. The energy is rapidly mobile within the B850 ring and transfers between Bchl a 's occur on the 50-150fs timescale (Jiminez *et al.*, 1996). Such a fast delocalisation is a result of the strong coupling between B850 Bchl a 's (Alden *et al.*, 1997). The rapid delocalisation around the circumference of the whole ring, the timescale of which is much faster than that of energy transfer to neighbouring antenna complexes, means that energy is available for transfer from any part of the ring to any part of a neighbouring ring, provided they are close enough. Thus, the rings of B850 act as 'storage rings'. (Pullerits & Sundström, 1996).

The extent of the exciton delocalisation is still the subject of debate (see review by Fleming & van Grondelle, 1997) and diverging values have been reported for it (Chachisvilis *et al.*, 1997; Monshouwer *et al.*, 1997; Pullerits *et al.*, 1996). For the next energy transfer step, B850 to B880, rather diverging times ranging from 2-40ps and even some biphasic kinetics have been reported (Hess *et al.*, 1995; Kennis *et al.*, 1995; McDermott *et al.*, 1995; Nagarajan & Parson, 1997; Pullerits & Sundström, 1996; Sundström *et al.*, 1986; Zhang *et al.*, 1992). Once again, when the energy reaches the circular array of B880 molecules it is rapidly delocalised with B880 to B880 transfers occurring in about 80fs (Visser *et al.*, 1995). The final, and slowest energy transfer step, from B880 to the RC, occurs in about 20-40ps (Visscher *et al.*, 1989; Bergström *et al.*, 1989). The relatively slow rate of this transfer is a consequence of the distance between the RC special pair Bchl *a*'s and the antenna Bchl *a*'s (Pullerits & Sundström, 1996). The timescales for energy transfer within the purple bacterial PSU are summarised in Figure 1.22.

1.11. 3-D crystallisation of proteins

1.11.1. *Physical chemistry of protein crystallisation*

In principle, the crystallisation of a protein is the same as the crystallisation of conventional small molecules (Hermans, 1982) and involves three stages; (i) formation of stable nuclei, (ii) growth of nuclei to form crystals, and (iii) termination of growth (Kam *et al.*, 1978). The crystallisation of a protein, as with any other molecule, in a given solvent requires the formation of a supersaturated solution followed by a change from the liquid to the solid phase (McPherson, 1991). The solid phase is called a crystal if the change occurs in a uniform manner.

A solution is said to be saturated if a thermodynamic equilibrium exists between the liquid and solid phases. At equilibrium no increase in the proportion of the solid phase can occur since it would be counteracted by a concomitant dissolution. As such, crystals cannot form from a saturated solution. For crystals to grow, the solution must be in a non-equilibrium state with a driving force toward the establishment of equilibrium. Such a solution is supersaturated. Supersaturation is attained when the concentration of a molecule (protein) in solution is greater than the solubility of that molecule should allow (McPherson, 1991). This can be achieved by altering some or other physical property of the system (refer to section 1.11.2). However, crystals cannot form out of all supersaturated solutions. For a second phase to be created the system must overcome an energy barrier called the free energy of germination, ΔG_g (Mikol & Giegé, 1992). The second phase is either a stable nucleus of a crystal or a precipitate.

Once a stable nucleus is formed it will continue to grow provided the system does not regain equilibrium. As long as non-equilibrium is maintained and supersaturation exists a crystal will grow or precipitate will form. Many nuclei can form spontaneously once supersaturation is achieved. However, many are unstable and will redissolve as quickly as they form. In order to be regarded as stable, a nucleus must be a molecular aggregate of sufficient size and physical integrity that it will recruit new molecules to its growing surfaces faster than others are lost to the solution (McPherson, 1991).

As illustrated in Figure 1.23, the region of supersaturation can be divided into two parts - the labile and the metastable (Miers & Isaac, 1907). The metastable region cannot support spontaneous nucleation but crystals can grow in it if a stable nucleus is introduced. The labile region can spontaneously produce nucleation sites and crystals. If crystals do form in

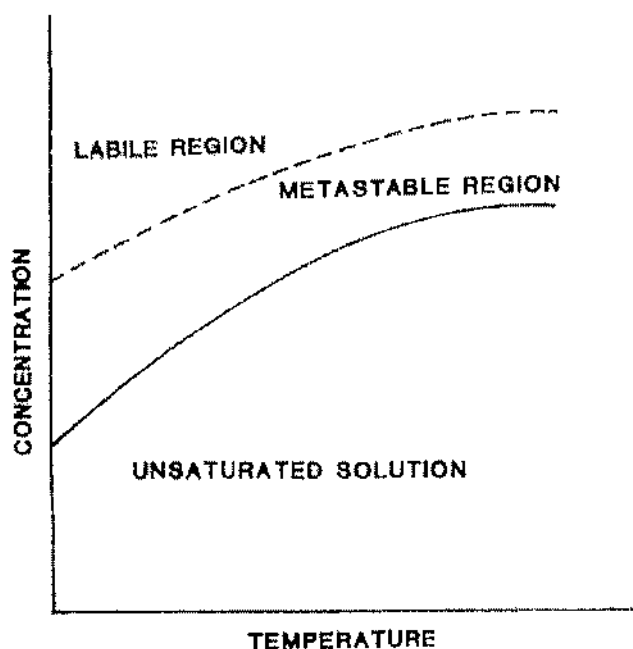


Figure 1.23. A typical solubility diagram showing the labile, metastable, and unsaturated regions. The solid line represents the saturation boundary. This diagram illustrates the case for concentration as a function of temperature, although other factors which can effect solubility can be treated in a similar manner. In this case, for any given temperature, as the solute concentration is increased a phase change occurs. Refer to text for details. Adapted from McPherson (1991).

this region they can also redissolve into the solution. It may appear, therefore, that the best strategy for producing crystals is to push the system as far into the labile region as possible, where the speed of crystal growth is greatest. However, the probability of spontaneous and uncontrolled nucleation is also increased, often resulting in 'showers' of crystals or small crystals with defects and flaws which are unsuitable for X-ray diffraction studies. Ideally, when growing crystals for structural analysis the strategy is to form nucleation sites and crystals in the labile region then

to transport the supersaturated solution into the metastable region. Such a strategy should produce slow growing, large, well ordered crystals. However, if the move from the labile to the metastable region is too fast, the protein will come out of solution as an amorphous precipitate. This should be avoided and one must attempt to approach the metastable state very slowly to allow the protein molecules to order themselves into a crystalline lattice (McPherson, 1991).

1.11.2. *The strategy of crystallisation*

The formation of crystals in a supersaturated solution is achieved by gradually altering some of the physical properties of the system. These properties may include protein concentration, temperature, pH, type and concentration of precipitant, and in the case of membrane proteins the type and concentration of detergent, to name but a few (McPherson, 1991). As biological macromolecules can be unstable outside a small range of temperature and pH, the alteration of these two parameters should be kept within a fairly narrow range to prevent denaturation of the macromolecule. This is especially true in the case of the purple bacterial light-harvesting complexes (Gall, 1994).

The alteration of the physical properties of the system is intended to deprive the protein molecules of sufficient water to maintain hydration, to disrupt the hydration layers, or to exclude the proteins from the bulk solvent (Arakawa & Timasheff, 1985b). Alternatively, the addition of organic solvent can be used to decrease the dielectric properties of a solution, thereby reducing the electrostatic shielding between protein molecules and encouraging them to aggregate and form crystals (McPherson, 1982).

The most commonly used approach for inducing proteins to come out of solution and to enter a solid state is to increase the level of saturation of a salt. Usually the salts ammonium sulphate and potassium phosphate are used. This approach utilises a phenomenon known as 'salting out' (Cohn *et al.*, , 1947). This phenomenon can be explained by the fact that at a certain ionic strength, protein-protein aggregation suddenly becomes predominant over protein-water and protein-salt interactions. Crystallisation systems using salts have probably yielded more protein crystals than any other (Gilliland, 1988; Carter, 1992).

Synthetic polymers such as polyethylene glycol (PEG) have also been used to produce protein crystals (McPherson, 1991). PEG acts in a similar manner to salts but also perturbs the solvent structure by creating a more complex network having both water and itself as structural elements (Arakawa & Timasheff, 1985a; McPherson, 1991). A major advantage of PEG as a precipitant is that once crystallisation conditions have been found, crystals can still be produced within a 2-3% range of the optimal PEG concentration. Additionally, crystals grown in PEG are usually formed quicker than those precipitated by use of salts or organic solvents (McPherson, 1991).

1.11.3. *Methods for producing supersaturation*

If the protein of interest is available in sufficient quantities (*i.e.* ml quantities of 10-20mg/ml protein solution) then batch methods may be used to produce crystals. However, as many proteins are often difficult to obtain in the quantities necessary for bulk crystallisation using batch methods several microcrystallisation techniques, which use only μ l quantities of protein solution, have been developed (McPherson, 1991;

Ducruix & Giegé, 1992). These techniques include vapour diffusion (reviewed in McPherson, 1990; 1991), microdialysis (Zeppenauer, 1971) and diffusion in lipidic cubic phases (Landau & Rosenbusch, 1996). Vapour diffusion, which was first used for the crystallisation of tRNA (Hampel *et al.*, 1968), is the most commonly used technique for the crystallisation of proteins and was the favoured technique for producing LH1-RC core complex crystals (see Chapter 8).

Vapour diffusion relies on the equilibration, in a sealed environment, of a protein solution droplet against a reservoir of greater precipitant concentration. Equilibration occurs by diffusion of the volatile solvent (water or organic solvent), via the vapour phase, from the droplet to the reservoir until vapour pressure in the droplet equals that of the reservoir. As equilibration proceeds, the concentration of the protein and precipitating agent in the droplet increase until supersaturation occurs. This ultimately results in either crystal formation or general precipitation (Green *et al.*, 1954).

There are three experimental methods that utilise vapour diffusion: (i) hanging drop; (ii) sitting drop; and, (iii) the sandwich drop (Fig. 1.24) (reviewed in McPherson, 1991; Ducruix and Giegé, 1992). The hanging drop method requires that a droplet of protein solution, which is adhered to the underside of a siliconised glass microscope coverslip by surface tension, is suspended over a reservoir solution. The disadvantage of this method is that only small droplets (~10 μ l) can be used. If the droplet is too large it could fall into the equilibrating reservoir. This method is of restricted use in the crystallisation of membrane proteins because detergents lower the surface tension of the droplet, again causing it to drop into the reservoir. Therefore, only small volumes (<10 μ l) of protein-detergent solution can be safely used in such cases. In the sitting drop method, the protein solution is

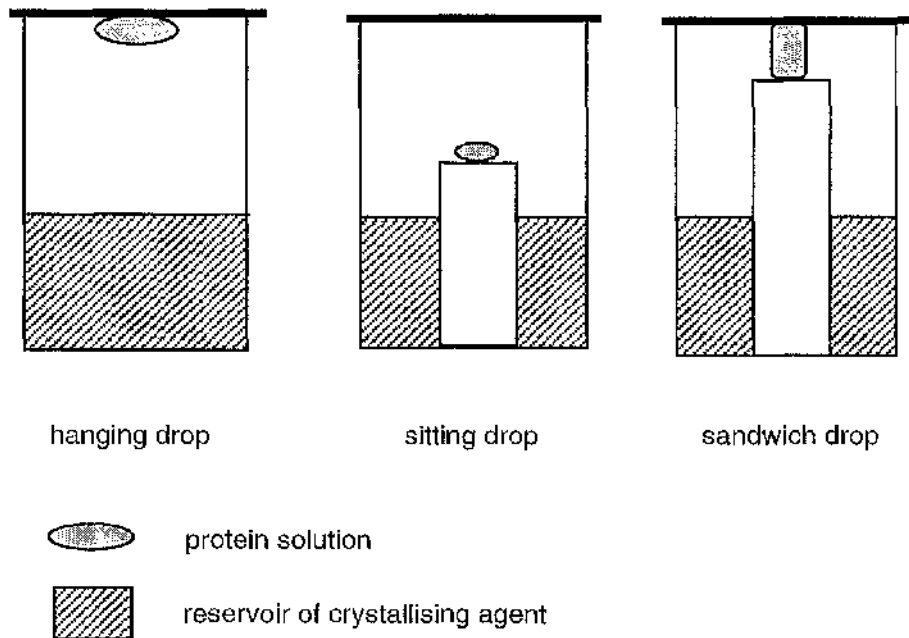


Figure 1.24. Schematic representation of the hanging, sitting and sandwich drop methods for use in vapour diffusion crystallisation experiments. Refer to text for details.

placed in a well surrounded by a moat containing the precipitant (Fig. 1.24). This method has the advantage that larger drop volumes (10-20 μ l) can be used compared to the hanging drop method. It also avoids the problem of decreased surface tension, caused by detergents, when crystallising membrane proteins. The sandwich method is really a combination of the hanging and sitting drop methods (Fig. 1.24). All these methods allow a wide range of crystallisation trials to be undertaken using only small amounts of protein.

1.11.4. 3-D crystallisation of membrane proteins

Although many hundreds of proteins have been crystallised (in both 2- and 3-dimensions) and the structures of over four hundred are known to atomic resolution, only a handful of these are membrane proteins or complexes of membrane proteins (reviewed in Kühlbrandt, 1988; McPherson, 1991; Reiss-Husson, 1992). The first integral membrane proteins to be successfully crystallised were bacteriorhodopsin (Michel & Oesterhelt, 1980) and porin (Garavito & Rosenbusch, 1980). Since then over twenty membrane proteins, such as the chlorophyll *a/b* protein complex from pea chloroplasts (Kühlbrandt, 1987), have yielded 3-D crystals. The first membrane protein to have its structure determined to atomic resolution was the photosynthetic reaction centre from purple bacteria (Deisenhofer *et al.*, 1985). Since this was described the 3-D crystallisation of membrane proteins has become a very active field with the structures of the RCs from other bacterial species (Chang *et al.*, 1985; Yeates *et al.*, 1987; Arnoux *et al.*, 1989), porin (Weiss *et al.*, 1991), and the LH2 complexes from two species of purple bacteria (McDermott *et al.*, 1995; Koepke *et al.*, 1996) having been determined. This area has been reviewed by Michel (1991), Reiss-Husson (1992) and Garavito *et al.* (1996). However, despite the increasing number of crystal structures of membrane proteins their crystallisation is hampered due to their peculiar solubility properties.

Integral membrane proteins are amphipathic molecules. They possess two polar surface domains located on either side of the lipid bilayer. These domains are separated by a hydrophobic region which is buried in the lipid bilayer core (refer to review in Eisenberg, 1984). As such, membrane proteins are not soluble in aqueous buffers and require the presence of detergents for their solubilisation. For the crystallisation of membrane

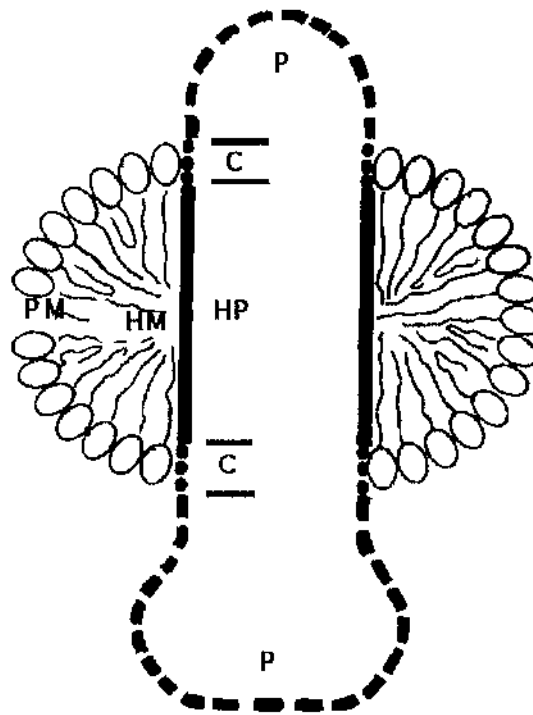


Figure 1.25. Schematic representation of a cross-section through a membrane protein-containing detergent micelle. The detergent molecules form a belt around the hydrophobic transmembrane region of the protein with their polar heads facing out into the aqueous solution. The hydrophilic surface regions (HP) are represented as solid lines, the exposed polar surface regions (P) as dashed lines, and the polar surface regions (C) of the protein which interact with the polar head groups (PM) of the detergent as dotted lines. The hydrophobic interior of the micelle is indicated by HM. Reproduced from Michel (1991).

proteins it is crucial to find a detergent that can completely replace the lipids of the membrane without affecting the structure or stability of the protein (Michel, 1991). The successful crystallisation of membrane proteins are usually performed starting from their detergent solubilised state.

Detergents, like lipids, are generally amphipathic molecules with a

distinct polar head group and hydrophobic tail. Detergents used in the crystallisation of membrane proteins are usually nonionic or zwitterionic surfactants with a single head group and single unbranched, saturated alkyl tail (Garavito, 1991). At low concentrations, detergents are soluble in water as a monomeric species. However, at a critical concentration, known as the critical micelle concentration (CMC) the detergent molecules associate into disordered aggregates called micelles. The CMC varies with the type of detergent (Tanford, 1980). When at concentrations greater than their CMC, detergents bind to the hydrophobic surfaces of the protein via mainly hydrophobic interactions. The hydrophobic effect causes the polar heads of the detergent molecules to face the aqueous environment (Fig. 1.25) (Tanford, 1980). As the protein-detergent complex is the species that crystallises it is important to understand the characteristics and behaviour of the complex in solution.

Most of the detergent found in the protein-detergent complex appears to be distributed as a belt around the hydrophobic transmembrane surface of the protein (Le Maire *et al.*, 1983). This was confirmed by crystallographic analysis of crystals of bacterial reaction centre (Roth *et al.*, 1989; 1991). The actual amount of detergent bound to the protein can vary depending on the characteristics of the detergent, the solvent environment and the protein itself (Reiss-Husson, 1992). The behaviour of a specific detergent is dependent on number of characteristics such as the polar head group size and the length of the alkyl chain. The importance of the latter was demonstrated by the crystallisation of the chloroplast LHC II complex. This complex crystallised reliably with nonyl- β -D-glucopyranoside but very poorly when octyl- β -D-glucopyranoside was used (Kühlbrandt, 1988). Nevertheless, the choice of detergent for use in crystallisation experiments is still very much an empirical process and some membrane proteins will

crystallise in a variety of detergents. Indeed, the *E. coli* porin, Omp F, was found to crystallise in 16 different nonionic detergents (Eisele & Rosenbusch, 1989). For extensive reviews on the roles of detergents in the crystallisation of membrane proteins refer to Garavito *et al.* (1996), Michel (1991) and Zulauf (1991).

The successful crystallisation of membrane proteins often requires that the starting protein be as pure and homogeneous as possible (Giegé *et al.*, 1986). After purification the protein preparation should consist of a single, monodisperse species consisting of a stably solubilised protein-detergent complex (Garavito *et al.*, 1996). If this is not the case, the complex will probably not crystallise. The improvement in purity of the Omp F porin (Garavito *et al.*, 1983), prostaglandin H synthase (Picot *et al.*, 1994) the bacterial RC (Deisenhofer *et al.*, 1985), and the bacterial IH2 complex (McDermott *et al.*, 1995) was a crucial factor in the formation of large, good quality crystals suitable for analysis by X-rays. The light harvesting complex from a marine alga was also found to be difficult to crystallise until an improved purification procedure was developed (Welte *et al.*, 1995).

Once a protein has been solubilised in a suitable detergent system the traditional methods for inducing crystallisation can be used (refer to section 1.11.3). Membrane proteins can form two different types of 3-D crystals (Michel, 1983; 1991) (Fig. 1.26). Type I crystals are basically stacks of 2-D crystals. These crystals are held together by polar interactions as well as hydrophobic ones. These crystals are usually formed by the removal of detergent, via dialysis at raised ionic strength, from the solubilised membrane protein (Henderson & Shotton, 1980). Type I crystals, however, are never well ordered or large enough for X-ray structure analysis (Michel, 1991). In type II crystals, the membrane proteins are crystallised with their hydrophobic surface coated by detergent (Fig. 1.26). In this case the crystal

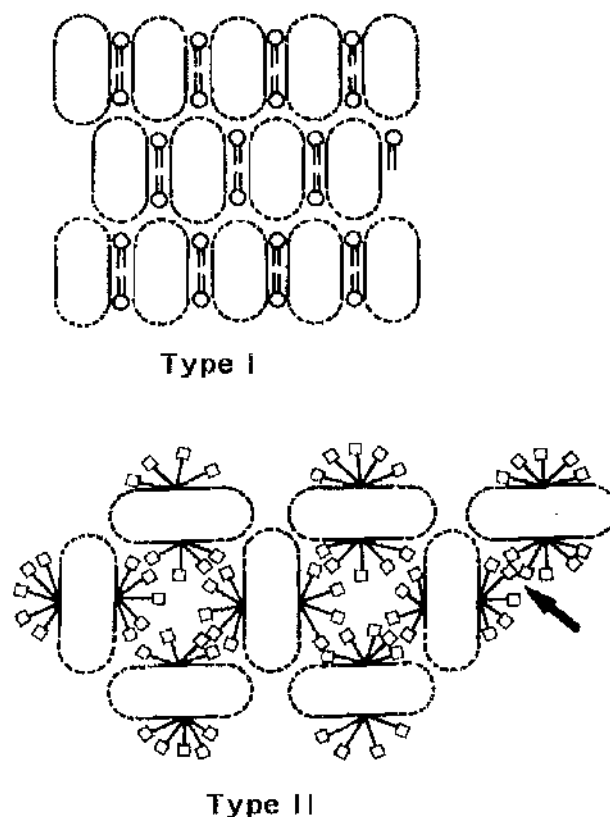


Figure 1.26. Schematic diagram showing cross-sections of the two basic types of membrane protein crystals. Type I crystals are basically stacks of 2-D crystalline arrays which are ordered in the third dimension. Type II crystals are membrane protein-detergent complexes ordered in a such a way that contacts are made between the hydrophilic parts of the protein and polar heads of the detergent molecules. The polar surfaces of the proteins are indicated by dashed lines, and the hydrophobic transmembrane regions as solid lines. Lipid molecules are shown as circles attached to two straight lines, and detergent molecules as squares attached to a single straight line. From Michel (1983).

lattice is formed by polar interactions between the hydrophilic surface domains of the protein. These type of crystals can be grown using the same techniques as crystals of soluble proteins (Michel, 1991).

One of the major hurdles to the crystallisation of membrane proteins is the tendency of the detergent to form a separate, detergent rich phase into which the proteins migrate. This phenomenon is called phase separation (Zulauf, 1991). Phase separation of the detergent can affect nucleation, crystal growth and stability. Most proteins usually undergo rapid denaturation in the detergent rich phase although some, such as the LH2 complex from *Rps. molischianum*, can actually be crystallised in it (Michel, 1991). Phase separation can be induced by a number of variables such as the detergent type and concentration, salt type, temperature, and type of precipitant to name just some (Reiss-Husson, 1992). The temperature and concentration at which phase separation occurs is defined by a curve called the consolution boundary (Fig. 1.27). Depending on the detergent type, this boundary can be reached starting from the micellar solution either by increasing or decreasing the temperature.

Phase separation proved to be a major problem in the crystallisation of bacteriorhodopsin (Michel & Oesterhelt, 1980). However, it was overcome by the addition of glycerol, proline or piperidine-2-carboxylic acid (Michel, 1983). This led to the concept of using small amphiphiles to suppress phase separation and promote the quality of membrane protein crystals. Amphiphiles affect the behaviour of detergents by interacting with the detergent micelles to form mixed micelles (Wennerström & Lindman, 1979). These micelles are smaller than pure detergent micelles. This allows a larger area of the polar surface of the protein molecule to protrude from the micelle thereby increasing interactions between proteins in the crystal. Amphiphiles can also reduce stress in the protein crystal lattice by filling in gaps between the detergent and proteins. Additionally, amphiphiles are thought to change the consolution boundary of detergents and bring them within a favourable range.

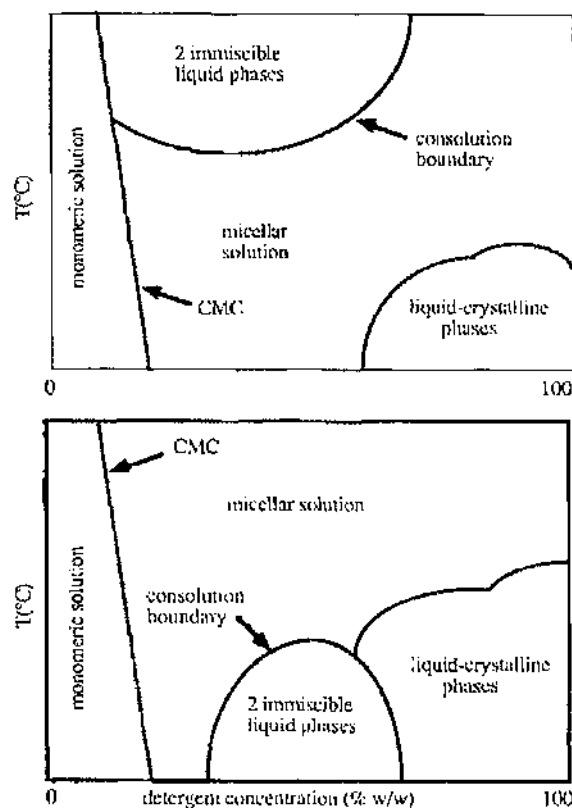


Figure 1.27. Schematic phase diagrams commonly observed for nonionic detergent-water mixtures. The micellar solution of a detergent only exists in a limited range of concentration and temperature which is defined by the phase diagram. Outside this range the micellar solution dissociates into two phases. One of these is enriched in detergent and the other depleted. The temperature and concentration at which phase separation occurs is defined by a curve called the consolution boundary. Depending on the detergent type, the region occupied by two immiscible liquid phases may be situated either above (upper diagram) or below (lower diagram) the consolution boundary, and the boundary can be reached by either increasing or decreasing the temperature. Reproduced from Reiss-Husson (1992).

The best examples of the pros and cons of amphiphiles come from crystallisation experiments on the pigment-protein complexes from photosynthetic bacteria (Michel, 1982; Papiz *et al.*, 1989; Cogdell *et al.*, 1991;

Buchanan *et al.*, 1993). The small amphiphile heptane-1,2,3-triol (high melting point isomer) was an absolute requirement for the successful crystallisation of the *Rps. viridis* RC in LDAO (Michel, 1982). Although crystals of the RC from *Rb. sphaeroides* formed in the absence of heptane-1,2,3-triol, its addition improved their quality (Allen *et al.*, 1987; Chang *et al.*, 1985; Buchanan *et al.*, 1993). LH2 from *Rps. acidophila* was crystallised in β -OG with benzamidine hydrochloride as an amphiphile (Papiz *et al.*, 1989; McDermott *et al.*, 1995). In some cases, such as the crystallisation of *E. coli* porin in β -OG, the presence of amphiphiles has no effect (Reiss-Husson, 1992).

Due to the relatively high concentrations (1-5% w/v) at which they are needed to have an influence on the crystallisation process, amphiphiles also have their drawbacks. These include protein denaturation, irreproducible nucleation and crystal metastability (Garavito *et al.*, 1996). Indeed, unwanted amphiphile effects can themselves prove a hindrance to the formation of X-ray quality crystals (Garavito *et al.*, 1996). As such, the use of these additives is not the cure-all for membrane protein crystallisation.

1.12. Thesis aims

This aim of this thesis was to investigate the structure and function of the LH1-RC core complex from a range of purple photosynthetic bacteria using a range of biochemical and biophysical techniques. The antenna complex organisation within the photosynthetic membrane was also investigated in order to elucidate the architecture of the purple bacterial PSU.

CHAPTER TWO

MATERIALS & METHODS PART A:

CELL CULTURE, PROTEIN PURIFICATION AND 3-D CRYSTALLISATION

2.1. Cell culture

Several species of Rhodospirillineae were investigated in this study: *Rhodopseudomonas* (*Rps.*) *acidophila* strains 10050, 7050 and 7750, *Rps. palustris* 'French' and strain 1a1, *Rhodospirillum* (*Rs.*) *rubrum* strain S1, *Chromatium* (*Chr.*) *vinosum* strain D, *Rps. cryptolactis*, *Rubrivivax* (*Rv.*) *gelatinosus* strains DSM 149 and 151, and *Rhodobium* (*Rh.*) *marinum* strain DSM 2698. *Rps. acidophila* strains were grown in Pfennig's medium (Pfennig, 1969). *Rh. marinum* was grown in modified DSM-27 Rhodospirillaceae medium supplemented with 3% NaCl (Imhoff, 1983), *Rps. cryptolactis* in THERMED medium (Stadtwald-Demchick *et al.*, 1990) and *Chr. vinosum* in Fuller's medium (Fuller, 1963). The other species were grown in C-succinate medium (Bose, 1969). The composition of each medium is listed in Appendix A.

2.1.1. General culture conditions

All cultures were stored either as glycerol stocks at -70°C or as agar stabs at room temperature. The agar stabs consisted of 25ml McCartney bottles half-filled with 1.5% agar and medium. When liquid cultures were required the appropriate stabs were flooded with medium, resealed and grown photoheterotrophically in a growth room maintained at a constant temperature of 28°C±2°C. A high light intensity of about 150µmols/s/m² was provided by positioning the cultures between two arrays of 150W incandescent electric lamps (Crompton). After 3-4 days growth the liquid culture was removed and used to inoculate a 500ml flat sided glass medical bottle. This culture was incubated for a further 24-28 hours then either harvested or used as inocula for a 10l pyrex flask or a series of 500ml bottles. All inoculations were performed under aseptic conditions using sterile

materials in a laminar air-flow cabinet. Due to the low level of irradiation produced in the centre of cultures growing in flasks, these cultures were circulated by stirring with a large magnetic stirring bar. Cells of all species studied (except those of *Rps. acidophila* strain 7750 for use in fluorescence induction studies, *Rh. marinum* strain 2698 and *Rps. cryptolactis*) were cultured in this manner.

As a check for cross contamination air dried agar plates, supplemented with the appropriate medium, were regularly inoculated with serially diluted cultures. The plates were transferred to GasPak[®] containers (Merck) which provided an anaerobic environment suitable for photoheterotrophic growth. The cultures were placed in a growth room under high illumination. After 5 days the plates were examined and single, pure bacterial colonies were picked off and used as inocula for fresh agar stabs.

2.1.2. *Rhodobium marinum* strain 2698

The marine bacterium *Rh. marinum* was purchased as a liquid culture from DSMZ, Braunschweig, Germany. This culture was used to inoculate a 500ml glass medical bottle containing modified DSM-27 Rhodospirillaceae medium. The 500ml culture was grown anaerobically at $28^{\circ}\text{C}\pm 2^{\circ}\text{C}$ under high light ($\sim 150\mu\text{mol/s/m}^2$). The cultures grew slowly in small volumes of medium and 4-6 days of incubation were required before the cells were dense enough to be sub-cultured. These cells were then used as inocula for a series of 500ml bottles which were again incubated for 4-6 days under high illumination. As this species of bacteria preferred to be cultured in large volumes, six 500ml bottles were used to heavily inoculate a 20l pyrex flask of medium.

Autoclaving often caused the NaCl in the medium to come out of

solution. Therefore, the salt was redissolved by vigorously stirring the medium for several hours prior to inoculation. Vigorous stirring was continued after inoculation to ensure a good circulation of the growing culture. This helped to prevent the formation of flocculent aggregates of bacteria that were observed in cultures which were not circulated. The 20l culture required 5 days incubation at $28^{\circ}\text{C}\pm 2^{\circ}\text{C}$ under high illumination ($\sim 150\mu\text{mol/s/m}^2$) before the cells were of a sufficient density to be harvested.

2.1.3. *Rhodospseudomonas acidophila* strain 7750

Rps. acidophila strain 7750 for use in fluorescence induction studies was grown photoheterotrophically at different light intensities and temperatures (Angerhofer *et al.*, 1986; Gardiner, 1992). Strain 7750 high light cells were grown under conditions described in section 2.1.1 and harvested after 24 hours growth. Initially, strain 7750 low light cells were grown under the same conditions but after 24 hours growth they were sub-cultured and grown at a lower light intensity of $40\mu\text{mol/s/m}^2$ provided by a bank of two 100W electric lamps. The cells were harvested after the third sub-culture. One of these sub-cultures was used as a starter culture for production of low light/low temperature cells. This culture was placed in a glass water tank with a thermostatically controlled heater maintaining a temperature of 22°C in a cold room. The tank was illuminated by two 40W electric lamps and protected from extraneous light sources. Cells were sub-cultured every 24 hours and harvested after the third sub-culture.

2.1.4. *Rhodospseudomonas cryptolactis*

The thermotolerant bacterium *Rps. cryptolactis* was grown under high light conditions at a thermostatically controlled temperature of 42°C in a glass water tank. Starter cultures were prepared using flooded agar stabs as described in section 2.1.1. The liquid cultures were then transferred to 100ml glass bottles which were placed in the water tank. High light conditions (150µmols/s/m²) were provided by illuminating the tank with a bank of six 100W incandescent electric lamps. After 72 hours growth the 100ml cultures were used to inoculate a series of 500ml bottles of media. The cells were then grown for a further 72 hours before harvesting.

2.2 . Cell harvesting

Cells were harvested in mid-log phase with a low speed spin (2,500 x g, 30min, 4°C) in a Mistral 6000 Coolspin centrifuge (Fison). The pelleted cells were resuspended in the minimum volume of 20mM Tris-HCl, pH8.0. The resuspended cells were either frozen at -20°C until required or used immediately to prepare photosynthetic membranes or chromatophores.

2.3. Preparation of photosynthetic membranes and chromatophores

Photosynthetic membranes and chromatophores were prepared essentially as described by Cogdell *et al.*, (1983). The harvested cell suspension was homogenised and a few grains of DNase (bovine pancreas deoxyribonuclease I, Sigma Chemical Co.) and MgCl₂ (Fluka Biochemicals) were added to digest DNA. This reduced the viscosity of the homogenate during cell disruption. Cells were disrupted by two passes through a pre-cooled French pressure cell at 950 p.s.i. Cells of *Rs. rubrum* and *Chr. vinosum* contain vesicular intracytoplasmic membranes which yield

chromatophores when French pressed (Niederman & Gibson, 1978). In these cases, unbroken cells and large cell debris were removed with a low speed spin (12,000 x g, 10min, 4°C) in a Sigma 3K20 benchtop centrifuge. The resulting supernatant, which contained the chromatophores, was centrifuged at high speed (240,000 x g, 1h, 4°C) using a pre-cooled T-865 fixed-angle rotor in a Sorvall OTD-65B ultracentrifuge. The other bacterial species studied possess lamellar or, in the case of *Rv. gelatinosus*, tubular intracytoplasmic membranes (Remsen, 1978). French pressing of these cells produces photosynthetic membrane fragments. The membranes were collected with a single high speed spin (240,000 x g, 1h, 4°C) in a Sorvall OTD-65B ultracentrifuge. The pelleted chromatophores and photosynthetic membranes were resuspended in the minimum volume of 20mM Tris-HCl, pH8.0, then homogenised. Prior to solubilisation the absorption spectrum of the homogenate was measured and the optical density adjusted to 50cm⁻¹ at the NIR absorption maximum.

2.3.1. Preparation of *Rhodopseudomonas acidophila* photosynthetic membranes for fluorescence induction studies

Photosynthetic membranes of *Rps. acidophila* strain 7750 for use in fluorescence induction studies were prepared in the laboratory of Dr. H.-W. Trissl, Dept. of Biophysics, University of Osnabrück, Germany. Due to the unavailability of a French pressure cell, the protocol described in section 2.3 was modified. DNase and MgCl₂ were not added to the harvested cell suspension and the cells were disrupted by sonication with a Branson Sonifier B15 fitted with a microtip. The cells were kept on ice and subjected to 3 x 3 min periods of pulsed sonication with a 5 min interval between each period. Unbroken cells were removed with a low speed spin (12,000 x

g, 10min, 4°C). The photosynthetic membranes were pelleted with a high speed spin (240,000 × g, 1h, 4°C), resuspended in 20mM Tris-HCl, pH8.0, homogenised then either used immediately for fluorescence induction experiments or stored at -20°C until required.

2.4. Purification of the LH1-RC core complex

The purification protocol for LH1-RC complexes was based on that described by Dawkins *et al.*, (1988) and Gall (1994) and, for LH2-containing species, consisted of four stages: (i) solubilisation of the photosynthetic membranes in detergent; (ii) sucrose gradient centrifugation; (iii) anion exchange chromatography, and; (iv) gel filtration chromatography. The sucrose gradient centrifugation step was omitted from the protocol for species which synthesise LH1 as the only light-harvesting complex.

Each stage of the purification process was monitored spectroscopically by measuring the absorption spectrum of each sample between 900nm and 250nm (Figure 2.1). Samples were also retained for analysis by SDS-PAGE.

2.4.1. Solubilisation of photosynthetic membranes and chromatophores

Photosynthetic membranes and chromatophores were solubilised by the addition of *N,N*-dimethyldodecylamine-*N*-oxide (LDAO) supplied by Fluka Biochemicals. The concentration of detergent used for the solubilisation was species dependent (Dawkins *et al.*, 1988). *Rs. rubrum* chromatophores and *Rps. palustris* membranes were solubilised by the addition of 0.5% and 0.75% (v/v) LDAO, respectively. The chromatophores and membranes of the other species studied were solubilised with 1% (v/v) LDAO. Each mixture was stirred in the dark for 15 mins at room temperature.

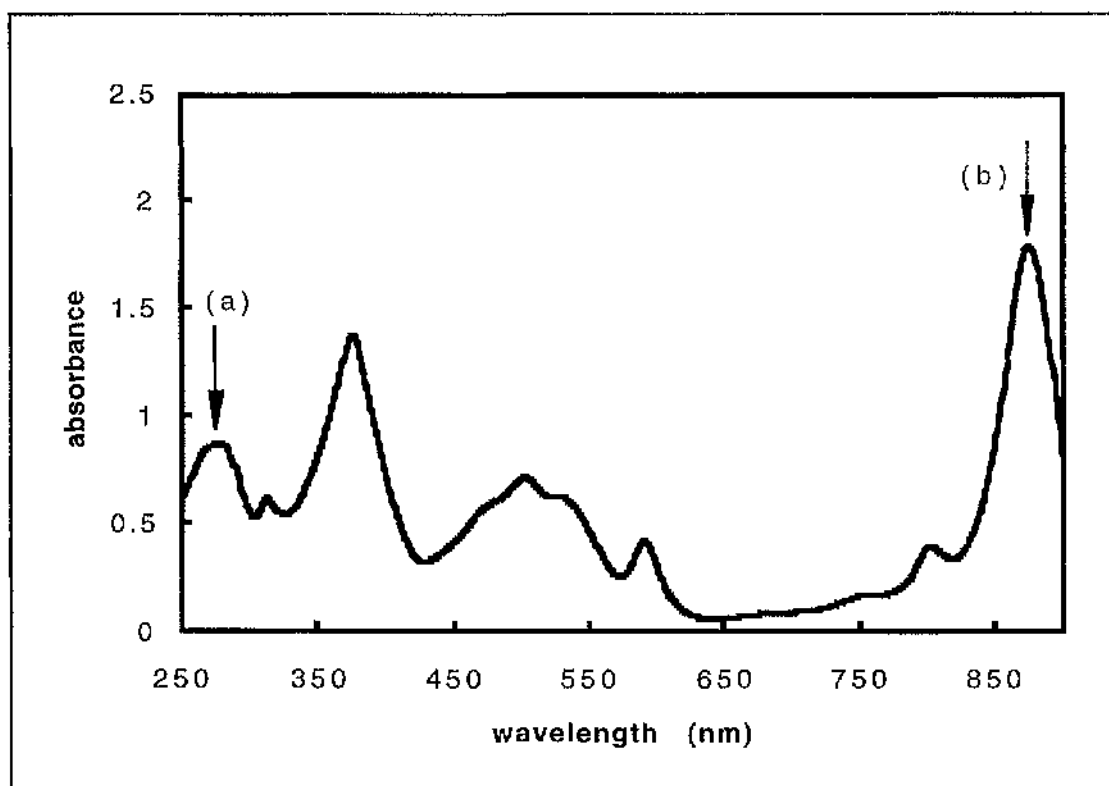


Figure 2.1. Absorption spectrum of purified LH1-RC core complex, in this case from the purple sulphur bacterium *Chromatium vinosum* strain D. Arrow (a) indicates the absorption band due to aromatic amino acid residues of the core complex. Arrow (b) indicates the NIR absorption band which is due to the LH1 Bchl *a* molecules. In this species the NIR absorption maximum is located at 878nm. The ratio of the absorbance at the NIR maximum to that at 280nm was used as an indicator of sample purity. Generally, ratios of about 2 were considered to represent fully purified core complex.

Unsolubilised material was removed with a low speed spin ($12,000 \times g$, 10mins, 4°C) in a Sigma 3K20 centrifuge. To prevent dissociation of the RC from the LH1 complex, which can sometimes occur in the presence of high concentrations of detergent, the clear, pigmented supernatant was immediately diluted with 20mM Tris-HCl, pH8.0, to reduce the LDAO concentration to 0.2% (v/v).

2.4.2. Sucrose gradient centrifugation

Sucrose gradient centrifugation was used to separate LH1-RC from LH2 complexes (Firsow & Drews, 1977). Discontinuous sucrose density gradients were prepared by carefully layering 8ml each of 1.0M, 0.6M and 0.3M sucrose (in 20mM Tris-HCl, pH8.0, containing 0.2% (v/v) LDAO) into 28ml polycarbonate centrifuge tubes (Du Pont or Nalgene). 4ml of solubilised membranes were layered on top of the sucrose and the tubes were centrifuged at high speed ($197,000 \times g$, 16hrs, 4°C) in a Sorvall OTD-65B or Beckman L7 ultracentrifuge. After centrifugation two discrete pigmented bands could be discerned (Figure 2.2). The bottom band, which contained LH1-RC, was removed using a Pasteur pipette and purified further by anion exchange chromatography.

2.4.3. Anion exchange chromatography

Anion exchange chromatography was performed in a cold room at 4°C under low illumination using a hand poured, gravity-flow DEAE-cellulose anion exchange column (DE52™, Whatman). Columns were prepared and equilibrated using one column volume of 20mM Tris-HCl, pH8.0. Once equilibrated two column volumes of 20mM Tris-HCl, pH8.0, containing 0.1% (v/v) LDAO were run through the column to provide a homogeneous environment for the solubilised complex. LH1-RC complex from the sucrose gradients or, in the case of LH1-RC only species, solubilised photosynthetic membranes or chromatophores were then loaded onto the column. These were eluted by a discontinuous salt gradient covering the range from 50mM NaCl to 320mM NaCl dissolved in 20mM Tris-HCl, pH8.0, containing 0.1% (v/v) LDAO. The exact elution point varied between each preparation and each species. The progress of the LH1-RC complex

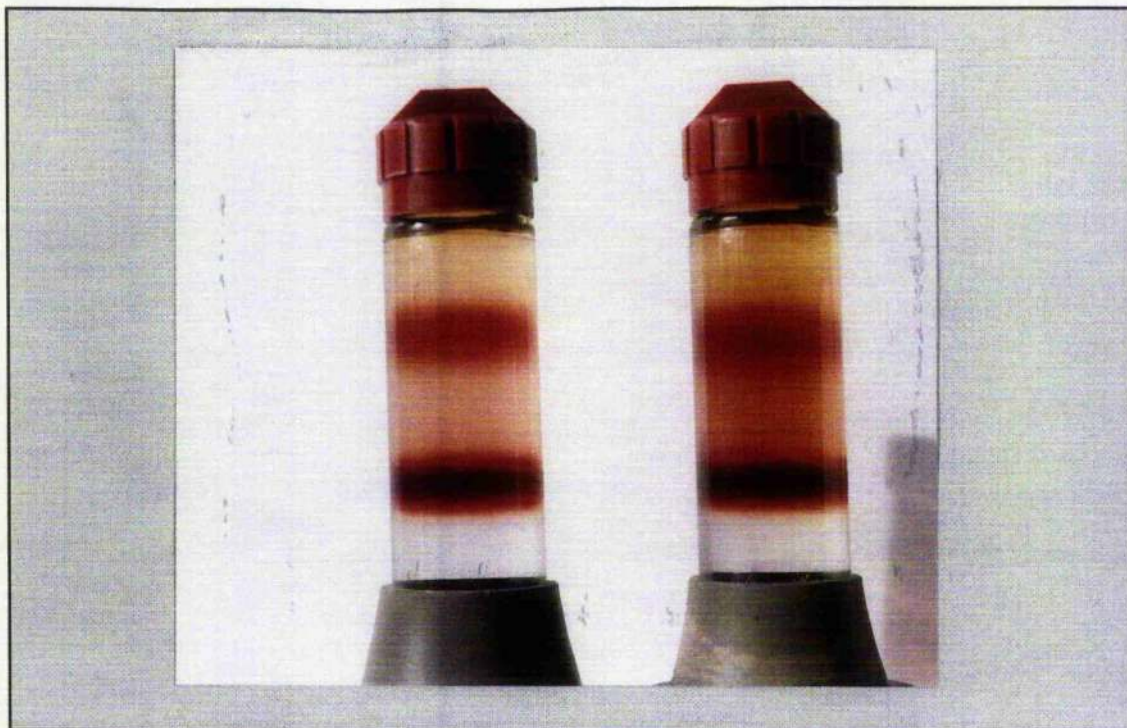


Figure 2.2. Discontinuous sucrose gradient of solubilised photosynthetic membranes from high light grown *Rps. cryptolactis* after centrifugation for 16hrs. The gradient consisted of 0.3M, 0.6M and 1.0M sucrose solubilised in 20mM Tris-HCl, pH8.0, containing 0.2% (v/v) LDAO. Two pigmented bands can be seen. The upper band contains LH2 and the lower band contains LH1-RC complex.

through the column was easily visualised due to its pigmented nature. The pigmented fractions were collected manually and analysed by absorption spectroscopy (see section 3.1). Fractions with an $A_{\lambda_{\max}}:A_{280} \geq 1.7$ were considered suitable for further purification by gel filtration chromatography.

2.4.4. Gel filtration chromatography

Prior to passage through a gel filtration column the pooled LH1-RC

fractions from the anion exchange chromatography step were concentrated using Centricon[®] 50 centrifugal concentrators (Amicon). This sped up the purification process as only small volumes of sample can be fractionated at any one time by gel filtration. 2ml of sample was placed in each concentration device and spun (5,000 x g, 4°C) in a Sigma 3K20 centrifuge until minimum volume (usually about 300µl) was achieved. The concentrated samples were then pooled. Typically, this resulted in a total volume of 2ml-5ml of concentrated sample.

Gel filtration was performed with a 1m long Superdex 200 (prep grade) XK16 column (Pharmacia) connected to a Pharmacia HPLC system fitted with a 10ml superloop. The apparatus was operated under low illumination in a cold room at 4°C. 2-5ml of concentrated sample was applied to a column equilibrated with two column volumes of 20mM Tris-HCl, pH8.0, 0.1% LDAO and eluted at a flow rate of 0.75ml min⁻¹ with the same buffer. The buffer was filtered through a 0.22µm filter (Millipore) and degassed under vacuum before use. 0.5ml fractions were collected with a Frac-100 fraction collector (Pharmacia) and their absorption spectra measured between 950nm and 250nm. Those fractions with an $A_{\lambda_{max}}:A_{280} > 2.0$ were considered pure enough for 3-D crystallisation experiments. Purified LH1-RC samples for crystallisation experiments were used immediately. Some samples required a second passage through the column before the desired degree of purity was achieved.

2.4.5. Detergent exchange

As well as LDAO, several other types of detergent were screened during 3-D crystallisation trials of the core complex (see section 2.6). Therefore, the LDAO that was used to isolate and purify the core complex had to be

exchanged for the new detergent. The purified core complex sample from the gel filtration column was concentrated to a minimum volume (usually ~ 200 μ l) by centrifugation (5,000 \times g, 4°C) using a Centricon[®] 50 centrifugal concentrator (Amicon). The sample was then diluted with detergent-free buffer (20mM Tris-HCl, pH8.0) and again centrifuged to a minimum volume. This procedure was repeated twice to ensure removal of the original detergent. The final traces of LDAO were removed by performing a third wash in which 0.5mM sodium dithionite was included in the washing buffer. Sodium dithionite degrades LDAO by reducing the amine oxide bond. To prevent precipitation of the core complex, the third wash also contained the new detergent in a concentration at, or slightly above, the critical micelle concentration (cmc). This procedure allowed a complete exchange of detergent. After the final wash the sample was diluted with 20mM Tris-HCl, pH8.0, containing the new detergent and concentrated to a volume which gave the desired OD for 3-D crystallisation trials.

2.5. Purification of *Rhodobium marinum* B880 complex

The purification protocol for *Rh. marinum* strain 2698 B880 complexes was modified from Meckenstock *et al.*, (1992). Initially, photosynthetic membranes were prepared and solubilised as described in sections 2.3 and 2.4.1. The solubilised membranes were dialysed for about 20 hours against 20mM Tris-HCl, pH8.0, containing 0.1% (v/v) LDAO, using prepared Spectra/Por[®] CE dialysis membrane (Spectrum[®]) with a molecular weight cut-off of 12-14kD. After dialysis the membranes were concentrated to an OD₆₈₀ of 100 cm⁻¹ by ultrafiltration using an Amicon[®] 8050 or 8200 stirred ultrafiltration cell operating at a nitrogen pressure of 70 p.s.i. This procedure was carried out in the dark on ice. To remove the RC from it's

surrounding LH1 ring, the concentrated sample was mixed in a volume ratio of 1:1 with a 3.5M $(\text{NH}_4)_2\text{SO}_4$ solution that was adjusted to pH8.0 immediately before use. The mixture was then stirred for 2hrs in the dark at 4°C. The mixture was poured into 8ml polycarbonate centrifuge tubes (Nalgene) and centrifuged ($197,000 \times g$, 1hr, 4°C) in a Beckman L7 ultracentrifuge. The pelleted material contained the RC and cytochromes. The supernatant, which contained B880 complex, was pipetted into prepared Spectra/Por[®] CE dialysis membrane (Spectrum[®]) with a molecular weight cut-off of 12-14kD and dialysed for 24hrs against 20mM Tris-HCl, pH8.0, containing 0.05% (v/v) LDAO. After dialysis the complex was concentrated to an OD_{880} of 10 cm^{-1} using Centricon[®] 50 centrifugal concentrators (Amicon). At this stage the B880 complex was considered pure enough for spectroscopic investigation (see Chapter 6). The complex was stored in the dark at 4°C. Under these conditions it is stable for several months (Meckenstock *et al.*, 1992).

For 3-D crystallisation trials, the B880 complex was further purified by anion exchange and gel filtration chromatography as described in sections 2.4.3 and 2.4.4, respectively. The purified B880 complex was concentrated and used immediately for crystallisation trials.

2.6. 3-D crystallisation of the LH1-RC core and B880 complexes

The strategy behind the crystallisation of macromolecules involves the gradual alteration of the characteristics of a concentrated protein solution in order to drive the system, very slowly, toward a state of limited supersaturation. Such a state favours the formation of protein crystals without inducing the phenomenon of phase separation (McPherson, 1990; Michel, 1983, 1990). The technique used to achieve supersaturation in the 3-

D crystallisation trials for this work was that of vapour diffusion using the sitting drop method (Michel, 1990; Garavito *et al.*, 1996). In such a system, a state of reduced solubility of the protein solution is achieved by modifying the properties of the solvent by osmotic equilibration, through the gas phase, with precipitating agents (McPherson, 1990). The latter are present in a reservoir of larger volume and higher osmotic pressure than the protein solution.

The search for successful crystallisation conditions requires that a systematic approach, in which a wide range of crystallisation parameters are investigated, be carried out. For each strain and species investigated the following crystallisation parameters were varied: (i) protein concentration; (ii) type and concentration of precipitant; (iii) detergent type and concentration; (iv) pH; (v) type and ionic strength of salt; (vi) effect of amphiphiles and additives; and, (vii) incubation temperature. A detailed list of the crystallisation screens performed appears in Appendix C.

Previous work performed on the crystallisation of the LH1-RC complex by Dawkins (1988), Gall (1994) and Wacker *et al.*, (1986) was used as a starting point for this study. These trials successfully used polyethylene glycol (PEG) as a precipitant. PEG is a synthetic polymer, available in a variety of molecular weights, that causes protein precipitation by chaotropic action (Arakawa & Timasheff, 1985; McPherson, 1990). The advantage of using PEG as a precipitant is that most proteins tend to crystallise within a narrow range (4%-18%) of PEG concentrations and crystals can form within about 2% to 3% of the optimal concentration (McPherson, 1990).

A wide range of PEGs (Fluka; BDH), encompassing molecular weights from 200 to 20,000, at concentrations varying from 5% - 30% (v/v or w/v), were investigated during crystallisation trials. In some cases the PEG was repurified before use (see section 2.6.1) to remove contaminants which

could prove deleterious to the protein (Jurnak, 1985). Stock PEG solutions were stored in the dark at 4°C. Initial crystallisation trials were conducted using the FASTPEG screen devised by Gall (1994) and the commercially available Membfac™ screens (Hampton Research). The latter screens were specifically designed for crystallisation of membrane proteins and, as well as PEGs, contain other precipitants such as organic solvents (see Appendix C). Some crystallisation trials were also performed using ammonium sulphate and potassium phosphate as precipitants.

Choice of detergent, although empirical, is of major importance in the crystallisation of membrane proteins. Taking this into account, over 30 types of detergent were screened for their efficacy in producing 3-D crystals of the core complex. These included the 24 detergents in the commercially available Detergent Screen Kit (Hampton Research) as well as detergents from other suppliers (Sigma Chemical Co. ; Fluka; Calbiochem). Where possible, ultrapure detergents were purchased. Refer to Appendix C for a list of all detergents screened.

To prevent phase separation occurring, a number of small amphiphiles were used during crystallisation trials (Michel & Oesterhelt, 1980; Garavito & Rosenbusch, 1980). Other small additive molecules, which may have an effect on crystal formation, were also investigated. 48 different amphiphiles and additives from the Hampton Research Additive Screen Kits I and II were screened.

Purified, detergent solubilised core complex was mixed in a volume ratio of 1:1 (or 4:5 if Hampton Research additives were to be included in the screen) with mother liquor, which contained all the required crystallisation chemicals, in a virgin 1.5ml eppendorf tube. The mother liquor solution was made up fresh and sterile filtered by passage through a 0.22µm filter (Millipore) before use. Any unsolubilised or precipitated material was

removed by centrifugation (3,000 x g, 3mins, room temperature) in a benchtop centrifuge (MSF Microcentaur). 10 μ l or 20 μ l of supernatant was pipetted into the wells of a Cryschem MVD 24 well plate (Cryschem Inc.) and 1ml of reservoir solution was pipetted into the moat which surrounded each well. The crystallisation plate was sealed with clear adhesive tape (3M) and incubated in the dark at 10°C or 15°C in thermostatically controlled incubation cabinets.

After a period of 1-2 weeks, the crystal trials were examined under a stereo-zoom light microscope. Conditions that looked promising for crystal formation were noted and then altered in subsequent trials by independently varying, over a narrow range, the factors that influence crystal formation. If crystals did form, they were examined visually for their potential suitability for X-ray diffraction studies. Characterisation and diffraction studies of crystals were performed by Dr. S. M. Prince, Dept. of Chemistry, University of Glasgow (see section 2.6.2).

2.6.1. Purification of PEG

PEG was purified according to the method described by Ducruix and Giegé (1992). A glass chromatography column was filled with 25ml of TMD8 mixed bed ion exchange resin (Sigma Chemical Co.). The column was washed firstly with 300ml of 3:7 methanol:water solution then 500ml of distilled water. A solution of 200g of PEG dissolved in 500ml of distilled water was degassed under vacuum with gentle stirring. 1.24g of sodium dithionite was added to the solution which was then left to stand for 1 hour. The solution was passed through the ion exchange column and the first 30ml of eluate was discarded. The following eluate was collected and the concentration of PEG determined by refractometry. A standard curve

was constructed using known concentrations of PEG. The purified PEG solution was stored in 10ml aliquots at -20°C. Before use, the thawed out aliquots had the antioxidant *p*-hydroxyanisole (1.3mg/ml in isopropanol) added in a ratio of 1µl per ml of PEG.

2.6.2. Crystal characterisation and X-ray diffraction studies

X-ray analysis and subsequent data evaluation of core complex crystals was performed by Dr. S.M. Prince, Dept. of Chemistry, University of Glasgow. Crystals were examined by light microscope and those thought suitable for X-ray analysis were removed from the mother liquor in which they were grown and transferred to a fresh soak solution. The crystals were mounted in 1mm Lindeman tubes. The ends of the Lindeman tubes were then sealed with beeswax. To check if the crystals were of a quality that diffracted X-rays, preliminary characterisation of them was performed on either a (i) Siemens multi-wire area detector in conjunction with a Siemens rotating anode X-ray generator, or (ii) a Nonius system with DIP1030 and DIP2020 image plate detectors. This equipment is located in the Dept. of Protein Crystallography, University of Glasgow. During this process the lifetime of the crystals in the X-ray beam was observed. In order to improve both the lifetime of the crystals and the quality of the diffraction data, crystals were taken to the synchrotron radiation source at the ESRF facility at Grenoble, France, where measurements were performed at cryogenic temperatures. In order to prevent damage to the crystals due to ice formation during flash cooling to cryogenic temperatures, the cryoprotectant glycerol (20% v/v) was added to the mother liquor solutions of the crystals. To avoid damage to the crystals the cryoprotectant was introduced slowly by dialysis. To ensure that crystals were indeed of LH1-RC

core complex, specimens from each batch to be studied were taken to the Krebs Institute, University of Sheffield, by Drs. K. McAulcy-Hecht and P.K. Fyfe, and their absorption spectra recorded on a spectrophotometer manufacture by Guided Wave.

CHAPTER THREE

MATERIALS & METHODS PART B:

SPECTROSCOPIC & ANALYTICAL TECHNIQUES

3.1. Absorption spectroscopy

Absorption spectra were measured on two different models of spectrophotometer. For routine laboratory work a Shimadzu UV160A scanning absorption spectrophotometer was used to measure absorbance in the range 250nm to 1000nm. Samples for analysis were pipetted into one of a matched pair of 3 ml or 1 ml quartz cuvettes with a pathlength of 1 cm.

For more accurate absorption measurements a Shimadzu UV-PC2101 double-beam spectrophotometer was used. This spectrophotometer enabled absorption measurements to be stored on 3.5 inch floppy disks. Data was collected from 250nm to 900nm using the Windows® based software supplied by the spectrophotometer manufacturers. Slit widths were set to 2mm and scan speed was set to very slow (50nm min⁻¹). A new baseline was recorded before each measurement. Collected data were converted into a graphical form using the spreadsheet package Microsoft® Excel v5.0. All absorption spectra were recorded at room temperature.

The Shimadzu UV-PC2101 spectrophotometer was used to investigate the effects of mild chemical oxidation on the room temperature absorption spectrum of the LH1 complex from *Rh. marinum*. 1 ml of the buffer in which the LH1 complex was solubilised (20mM Tris-HCl, pH8.0, containing 0.05% LDAO) was pipetted into the quartz reference and sample cuvettes and a baseline recorded. Isolated LH1, with an OD₈₈₀ of ~0.17 cm⁻¹, was then pipetted into the washed sample cuvette and the absorption spectrum recorded from 750nm to 900nm. The baseline was then reset and the absorption spectrum of fresh LH1 sample containing potassium ferricyanide was measured. This process was repeated for different concentrations of potassium ferricyanide ranging from 1mM to 100mM. Potassium ferricyanide was made up as either a 500mM or 100mM stock solution. All

spectra were recorded immediately, over a 2 minute period, upon addition of the ferricyanide.

3.2. Fluorescence emission spectroscopy

Room temperature fluorescence emission spectra of *Rh. marinum* LH1 complexes were measured between 800nm to 1000nm with a Spex Fluorolog 1681 spectrofluorimeter using a 1 cm pathlength quartz cuvette. Slit widths were set 10nm and 2nm on the excitation and emission sides, respectively. The excitation wavelength was 590nm and the fluorescence emission was measured at 90° to the excitation beam. For all measurements the OD₈₈₀ of the LH1 sample was adjusted to ~0.17 cm⁻¹. This helped to prevent self absorption of fluorescence. As with absorption spectra, collected data were converted into a graphical form using the spreadsheet package Microsoft® Excel v5.0. To investigate the effects of mild chemical oxidation on the fluorescence emission of LH1 from *Rh. marinum* different concentrations of potassium ferricyanide were added to the sample. All spectra were recorded over a two minute period and a fresh cell filling was used for each measurement.

3.3. Fluorescence induction spectroscopy

Fluorescence induction spectroscopy of photosynthetic membranes of the purple non-sulphur bacterium *Rps. acidophila* strain 7750 was performed in the laboratory of Dr. Hans-Wilhelm Trissl at the University of Osnabrück, Germany. The bacteria were grown under different conditions, as described in section 2.3.1, so as to alter the peripheral antenna

composition (Angerhofer *et al.*, 1986).

For fluorescence induction measurements the absorbance of each membrane sample was adjusted to <0.1 at the Bchl *a* Q_y absorption maximum. This ensured a homogeneous light distribution within the sample and limited the degree of self absorption of fluorescence. To obtain single electron transfer during measurements, terbutryn (200 μ M) was added to the sample. Addition of 0.5 μ M phenazine metosulphate (PMS) ensured that all RCs were open during the dark adaptation period of 10 minutes. A fresh sample was used for each measurement. Measurements were performed at room temperature and at 4°C, with and without the presence of divalent cations (Mg^{2+}) by employing a xenon flash technique described by Trissl (1996). The rationale behind using a xenon flash as a source of excitation energy is based on the experimental requirement for single electron transfer. To prevent secondary electron transfer the recording time window needs to be faster ($<1-2ms$) than that which mechanical shutters can provide. Four different excitation wavelengths were used ($\sim 800nm$, $\sim 820nm$, $\sim 850nm$ and $\sim 870nm$). Wavelength selections were achieved with narrow-band interference filters (Schott). The energy of the xenon flash was measured with a black body energymeter (Rm-3700; Laser-Probe Inc.).

The fluorescence induction apparatus, which was designed and built by Dr. H.-W. Trissl, is shown in Figure 3.1. The sample was contained in a 3 ml cuvette with a cross-section of 1 x 1cm which was placed in a thermostatically controlled cuvette holder. The excitation light source consisted of a photographic flash (Braun 370BVC) which delivered its light through one of four glass filters (801.3nm, 819.8nm, 848.2nm or 868.7nm) (Schott) to a cross-sectional converting light-pipe with scrambled fibres. The excitation wavelengths correspond approximately to the major Q_y absorption bands of the LL growth type of the bacterium studied. In order to

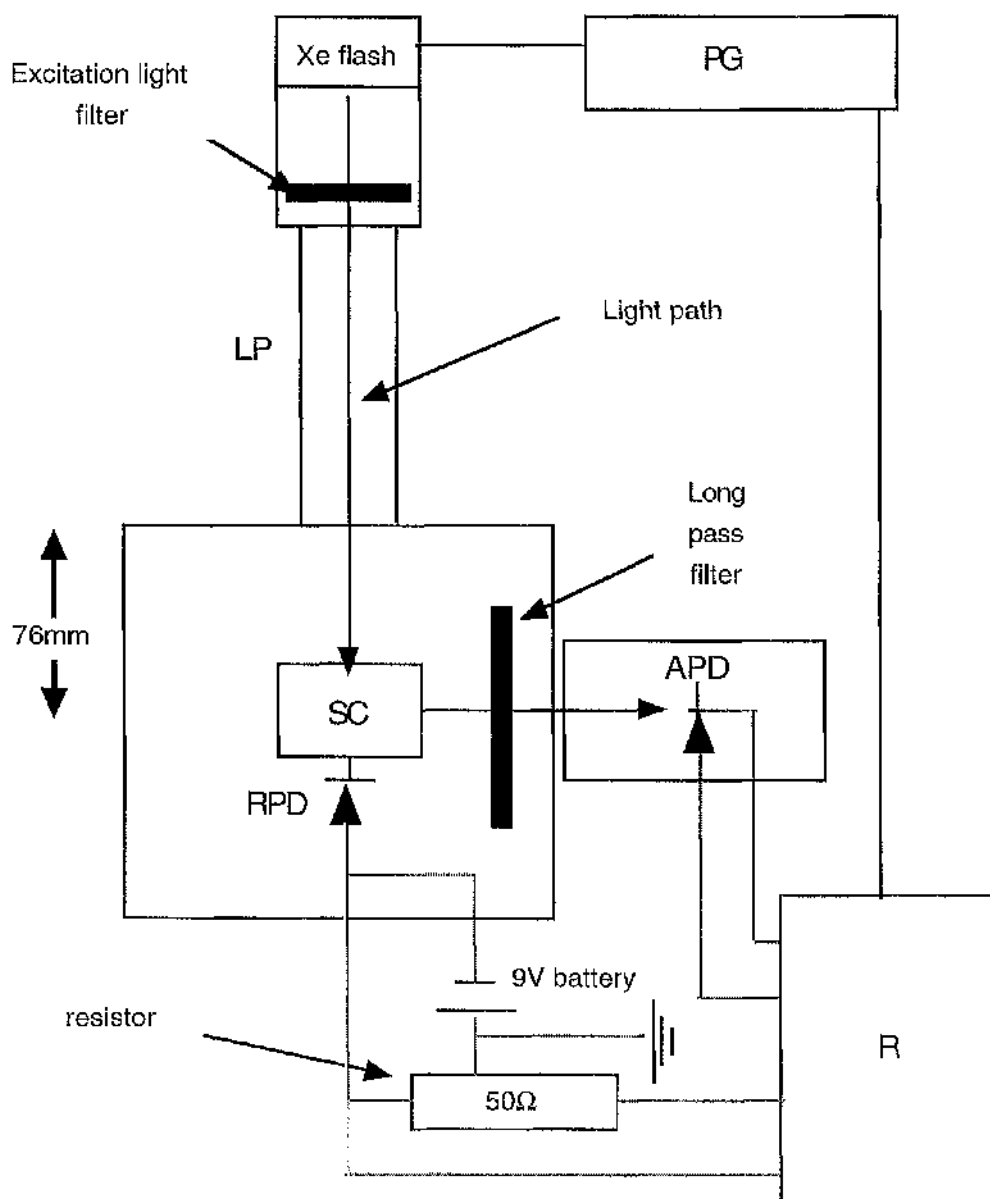


Figure 3.1. Schematic diagram of the fluorescence induction apparatus designed by Dr. H.-W. Trissl. The dotted lines represent the electrical circuitry of the apparatus. The long pass filter protected the avalanche photodiode from stray excitation light. Narrow-band interference filters (802, 819, 848 and 869nm) were used to select the desired excitation wavelength. Abbreviations: LP, light pipe; APD, avalanche photodiode; RPD, reference photodiode; PG, pulse generator; SC, sample cuvette; R, double transient recorder. Refer to the text for a full description of the apparatus.

achieve homogeneous illumination the output of the light-pipe was placed at a distance of 76mm from the centre of the cuvette holder. An Si-pin photodiode (Motorola MRD-500) with a resistance of 50Ω monitored the time course of the xenon flash. The xenon flash, which had a duration of $\sim 400\mu\text{s}$, was triggered by a pulse generator. The total energy of this flash at the middle plane of the cuvette was determined by separate measurements. For further data evaluation the average value of 5 flashes was taken, since the shot to shot energy scattered by $\sim 10\%$.

Fluorescence was detected at 90° with respect to the excitation light by a large area, high gain Si-avalanche photodiode (APD) (model 394-7071-521; Advanced Photonix Inc., U.S.A) operating at approximately 2400 V and with a working resistance of $11\text{k}\Omega$. The latter value was chosen as it gave a compromise between the highest time resolution and highest sensitivity (H.-W. Trissl, personal communication). The APD was protected from stray excitation light by a 895.8nm long pass glass filter (Schott).

Fluorescence yield measurements in the sub-millisecond time range were obtained by feeding the outputs of the photodiodes into a double-trace transient recorder (Nicolet, Pro 90). This allowed the simultaneous recording of the time course of excitation light intensity and fluorescence intensity. Both traces were set into proportion and the time-base converted into an artificially linearised one. This allowed the construction of fluorescence induction curves equivalent to those obtained by mechanical shutter opening. Details are given in Trissl (1996). The time resolution of the recording channels was tested with 30 ps flashes. Baselines measurements were made at each excitation wavelength by using a buffer filled cuvette. The slower response of the APD compared to the reference photodiode was taken into account by a $0.3\mu\text{s}$ shift in the data analysis. Data were stored on 3.5 inch floppy disks and analysed on a personal computer

using a mathematical program written by Dr. H.-W. Trissl.

3.3.1 Spectral decomposition

The contribution to the absorption cross section of each discernable pigment pool (B800, B820, B850, B880 and RC) of the *Rps. acidophila* photosynthetic membranes was ascertained by a spectral deconvolution of the absorption spectra. This was performed by sets of standard spectra, normalised to an integrated area of 1, that described the various pigment pools (Fig. 3.2). Each standard spectrum consisted of 3 Gaussian sub-bands that described a typical Bchl *a* antenna pigment pool between -100nm and +50nm from the location of the Q_y absorption maximum. The widths and relative amplitudes of the the 3 Gaussians were of the same order as those needed for the fit of the NIR absorption spectrum of *Rs. rubrum*, a purple bacterium containing only B880 as its LH complex. The Gaussian function for one band - say B800 - had the following structure:

$$G_{800}(\lambda) = \frac{1}{\sum_{i=1}^3 a_i} \left(\sum_{i=1}^3 \frac{1}{\sqrt{2\pi\Delta\lambda_i}} e^{-\left(\frac{\lambda_{\max} - \lambda}{\sqrt{2\Delta\lambda_i}}\right)^2} \right)$$

The total absorption spectrum was constructed by the sum of the bands weighted with their relative antenna sizes, N , using the equation:

$$G(\lambda) = N_{800} \cdot G_{800}(\lambda) + N_{850} \cdot G_{850}(\lambda) + N_{880} \cdot G_{880}(\lambda)$$

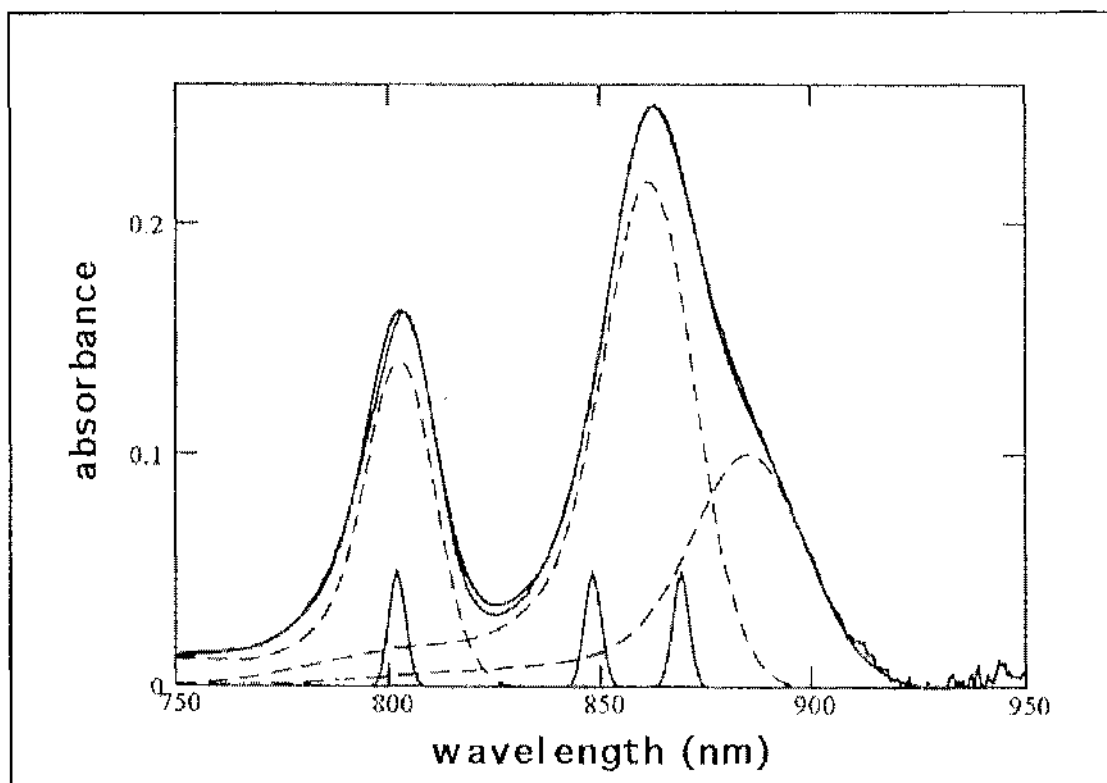


Figure 3.2. Decomposition of the absorption spectrum of photosynthetic membranes of *Rps. acidophila* strain 7750 grown under high light conditions. The spectrum was fitted with 3 Gaussian sub-bands (dashed lines) which correspond to the contributions of the B800, B850 and B880 pigment pools. The small peaks located at 802nm, 848nm and 869nm represent the transmission of the filters used for achieving excitation wavelength selection.

This decomposition accounted for the very weak absorption of the hypsochromic part of the Q_y absorption region of Bchl *a*. This detail is relevant because B880 pigments as well as B800 pigments contribute to absorption at 800nm. A molar absorption coefficient in the Q_y transition of $\epsilon=107 \text{ mM}^{-1}\text{cm}^{-1}$ (Gall, 1994) was assumed and the absorption spectrum of the membranes was fitted with the relative concentrations of each pigment pool, taking into account the absorption spectrum of the RC ($\epsilon_{880}= 130 \text{ mM}^{-1}$

1cm^{-1} at 875nm, Clayton, 1980). This allowed calculation of the absolute contribution of each pigment pool to the PSU and yielded an effective molar absorption coefficient, ϵ , at the excitation wavelength by integration with the transmission of the interference filters used to achieve that excitation wavelength (see section 3.3). The molar extinction coefficients were used in further calculations to determine the size of the PSU as described in Results (section 7.1).

3.4. Circular dichroism (CD) spectroscopy

CD spectroscopy of the LH1-RC complexes was performed with the help of Drs. N.C. Price and S.M. Kelly at the BBSRC Circular Dichroism Facility, University of Stirling, Stirling, U.K. CD was measured at room temperature on a Jasco J-600 spectropolarimeter (Japan Spectroscopic Co.), which had been calibrated with *d*-10-camphorsulphonic acid, under constant nitrogen flush. CD spectra were recorded over the wavelength range 280nm to 700nm. A red-sensitive photomultiplier tube (Hamamatsu R316) was used at wavelengths above 700nm. The scan rate was set to 20nm min^{-1} and data was collected every 0.4nm. The average of 4 scans was recorded and the curves were usually smoothed with the noise reduction programme of the J-600 system software. The CD data were expressed in terms of millidegrees (mdeg).

The optical density (OD) of the core complex solutions at the NIR maximum varied between $\sim 1.5\text{ cm}^{-1}$. Their absorption spectra were recorded on a Jasco V-550 uv/vis spectrophotometer before and immediately after the collection of the CD spectra to ensure that no denaturation had occurred during the measurements. For CD, fused silica cells with a pathlength of 0.5cm were used throughout.

3.5. Polypeptide analysis

3.5.1. Determination of protein concentration

Protein concentrations in the μg range were determined using the protein-dye binding method of Bradford (1976). 100 μl of either solubilised photosynthetic membranes, purified LH2 or LH1-RC were pipetted into labelled, disposable plastic test tubes. 3 ml of Bradford reagent was then added to each test tube. After standing for 5-30 minutes the absorbance of each solution at 595nm was measured. Protein standards, ranging from 50 $\mu\text{g}/\text{ml}$ to 1400 $\mu\text{g}/\text{ml}$, were prepared from a 2mg/ml stock solution of bovine serum albumin (BSA fraction V, Sigma Chemical Co.). 100 μl of each standard protein solution (equivalent to 5-140 μg of protein) was added to each of 7 labelled test tubes. 100 μl of dH_2O was added to the control tube. 3 ml of carefully mixed Bradford reagent was pipetted into each test tube and the absorbance of the solution at 595nm was read between 5-30 minutes after addition of the reagent. The A_{595} of the control solution was then subtracted from the recorded absorbance each of the standard solutions. This procedure was duplicated and the results used to construct a calibration curve (Fig. 3.3). The BSA calibration curve was then used to determine the concentration of the sample pigment-protein solutions. For SDS-PAGE, the pigment-protein samples were either concentrated using centrifugal concentrators or diluted with 20mM Tris-HCl, pH8.0, 0.1% (v/v) LDAO to give a protein concentration of 5 mg ml^{-1} . 20 μl (equivalent to 100 μg of protein) of this was then used for analysis.

3.5.2. SDS-PAGE

Sodium dodecyl sulphate-polyacrylamide gel electrophoresis (SDS-

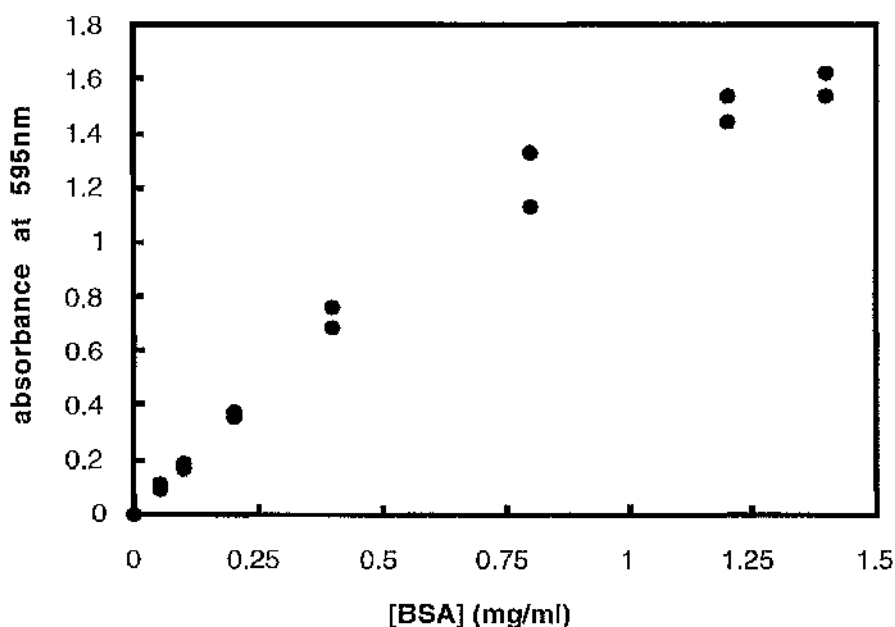


Figure 3.3. Protein concentration calibration curve. The curve was constructed using bovine serum albumin (BSA) protein standards according to the protein-dye binding method of Bradford (1976). Two separate measurements were made for each protein concentration. This curve was then used to determine the protein concentration of pigment-protein samples.

PAGE) was used to analyse the polypeptide composition of solubilised photosynthetic membranes, LH2 and LH1-RC core complexes of each of the species studied. The method used was based on that described by Laemmli (1970) as modified by Schägger and von Jagow (1987).

Polyacrylamide gels were prepared using the gel solutions described in Appendix B. The gels were cast between two clean glass plates, held apart by a 1.5mm plastic spacer, which were clamped together in a gel former. 11.5-18.5% gradient gels were formed by running 18.5% and 11.5% concentrations of acrylamide solutions between the gel plates via a gradient

mixer. The solutions were mixed in the wells of the gradient mixer by stirring with a magnetic stirring bar. A layer of 50% (v/v) methanol: H₂O was then pipetted onto the top of the resolving gel. This prevented the formation of a meniscus and also helped to prevent oxidation of the gel. Once the gel had set, usually after 30-40 minutes, the methanol: H₂O solution was decanted. A stacking gel was poured onto the top of the resolving gel and a plastic comb inserted. Once set, the gel sandwich was removed from the gel former apparatus and inserted into a Studier-type gel apparatus (Atta). Freshly prepared electrophoresis buffers (see Appendix B) were added to the cathode and anode reservoirs, taking care to ensure no air bubbles formed beneath the gel, and the well-forming comb was removed.

20 μ l of 5 mg ml⁻¹ pigment-protein sample was mixed in a 1:1 volume ratio with gel sample buffer (Appendix B) in a 1.5 ml eppendorf tube. In the case of samples which contained core complex the sample buffer used dithiothriitol as a reducing agent. In other cases mercaptoethanol was used. Both buffers contained a bromophenol blue marker dye to aid observation of loading and monitoring the sample migration. Samples containing RC protein were incubated for 30 minutes at 70°C. This was done because the RC polypeptides tend to form a viscous precipitate if heated at 100°C (R.J. Cogdell, personal communication). Other samples, such as LH2, were boiled for 2 minutes at 100°C. The samples were centrifuged at high speed for 2 minutes in a benchtop centrifuge (MSE Microcentaur) to remove any precipitated material. 20 μ l of the supernatant (equivalent to 50 μ g of protein) was pipetted into the wells of the gel using a Hamilton syringe. Protein standards (Sigma Chemical Co.) covering the range from 97.4-6.5 kDa were prepared in the same manner.

The gels were run overnight (approximately 16 hours) at 15 mA and switched off when the blue dye front had reached the bottom of the gel. The

gel was carefully removed from the glass plates and placed in staining solution which contained Coomassie blue dye (Appendix B). After staining for about 3 hours, the gel was removed and placed in a bath of destain solution (Appendix B). Several washes in destainer were usually required before the polypeptide bands could be visualised.

3.6. Electron microscopy

Electron microscopy (EM) was used to study the structure and aggregation behaviour of purified LH1-RC core complexes. EM was performed with the help of Dr. W. Kühlbrandt, Mr. H. Rogl and Mr. D. Mills at the Max Planck Institute for Biophysics, Frankfurt am Main, Germany. LH1-RC core complex samples were prepared as described previously (Chapter 2). 5 μ l of core complex sample, at a concentration of $\sim 50 \mu\text{l ml}^{-1}$, was pipetted onto a carbon coated copper support grid (Agar Scientific Ltd., U.K.) which was clamped into a pair of ant-capillary forceps (Duemont, Switzerland). The carbon coating helped to increase the hydrophobicity of the surface of the grid (W. Kühlbrandt, personal communication). The sample was left to bind to the grid for 30 seconds. Excess sample was removed by blotting with a piece of torn filter paper (Whatman No. 4). The sample was then negatively stained with a 1% (w/v) solution of uranyl acetate. 2 μ l of this solution was pipetted onto the sample and left to stain for 30 seconds. Once again, excess uranyl acetate was removed by blotting. The sample was then left to air dry. The fixed core complex sample was examined with a Philips 301 transmission electron microscope operating at ~ 80 kV at a magnifications between 30-60, 000. To prevent excessive damage, care was taken not to expose the section of the specimen to be recorded to too much preillumination. Electron

micrographs were recorded on Kodak SO163 film and developed by Mr. H. Rogl.

CHAPTER FOUR

PURIFICATION & CHARACTERISATION OF THE LH1-RC CORE COMPLEX

4.1. Purification and characterisation of the LH1-RC core complex

The isolation and purification of the LH1-RC core complex from a range of purple photosynthetic bacteria is described in Chapter 2. Cells were grown under conditions which maximised the abundance of core complex relative to other membrane protein components in the ICM. The purification protocol involved the use of sucrose gradient centrifugation, anion exchange and gel filtration chromatography. The integrity of the core complex at each purification stage was monitored spectroscopically. The ratio of the absorbance at the NIR maximum to the protein absorption peak at 280nm was used as a measure of the purity of the complex. Generally, core complex samples with an $A_{\text{NIR}}:A_{280}$ greater than 2 were considered to be fully purified. The use of a measurement of the optical density (OD) of the core complex multiplied by the sample volume gave a value (the ODV) which allowed calculation of the percentage yield of core complex from each stage of the purification process. In LH2-containing species the NIR absorption maximum is made up of contributions from both the LH2 B850 (820) Bchl's and the LH1 Bchl's. For these species it is not possible to calculate the percentage yield of LH1-RC core complex from the membrane solubilisation step of the purification process without performing a complicated spectral deconvolution. Therefore, the percentage yield values given in Tables 4.1-4.8 were calculated arbitrarily, assuming a 100% recovery of core complex from sucrose gradients. The results of the purification process for each of the species and strains investigated is presented below.

4.2. *Rhodopseudomonas acidophila* strain 10050

Rps. acidophila strains were grown in 10L flasks of Pfennig's medium

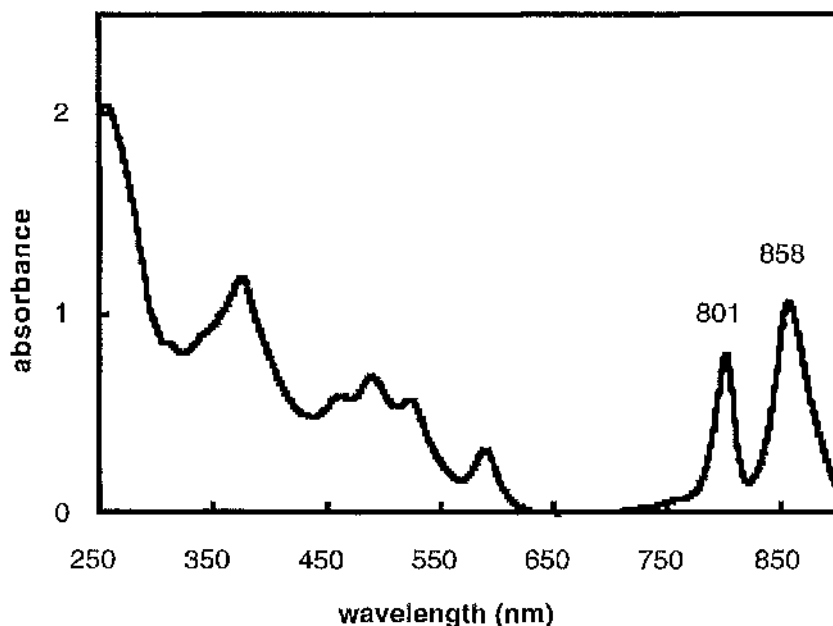


Figure 4.1. Absorption spectrum of photosynthetic membranes from *Rps. acidophila* 10050 solubilised in 1% (v/v) LDAO. The solubilised membranes possess two strong NIR absorption peaks located at 801nm and 858nm. Refer to the main body text for a full description.

(Pfennig, 1969) under the conditions described in section 2.1.1. After harvesting and disruption of the cells the resulting photosynthetic membranes (PSM's) were adjusted to an OD of 50cm^{-1} at the NIR absorption maximum. The PSM's were then solubilised by the addition of 1% (v/v) LDAO (Fluka Biochemicals), stirring for 15 mins in the dark at room temperature. The absorption spectrum of the detergent-solubilised PSM's shows two NIR absorption peaks located near 801nm and 858nm (Figure 4.1). These two peaks are mostly due to absorption by the Q_y transition of the B800 and B850 Bchl *as* of the LH2 complexes in the photosynthetic

Table 4.1. Purification table for the LH1-RC core complex of *Rps. acidophila* strain 10050. The values represent the arithmetical mean and standard deviation of measurements from a sample size of $n=26$. Cultures were grown in 10 L batches.

Purification step	Volume (ml)	OD ₈₈₃ * (cm ⁻¹)	A ₈₈₃ :A ₂₈₀ *	ODV	% yield of core
Solubilisation of photosynthetic membranes	29 ± 3	51.5 ± 3.4	0.83 ± 0.18	1493	-
Sucrose gradient centrifugation	66.6 ± 30.6	7.57 ± 1.96	1.63 ± 0.27	504	100
Anion exchange chromatography	13.25 ± 3.60	24.6 ± 8.87	1.77 ± 0.35	326	65
Gel filtration chromatography	12.0 ± 2.45	11.35 ± 4.26	2.03 ± 0.24	136	27

* The OD of photosynthetic membranes was measured at the NIR absorption maximum which was located at 858nm.

membrane. The 800nm-absorbing component of the RC is masked out by the LH2 B800 band. The 858nm band has a shoulder to the red of the maximum which represents absorption by the LH1 B880 Bchl *a*'s. The small peak near 590nm is due to the Q_x transition of Bchl *a*. The three finger-like peaks located between ~450nm to ~520nm are due to carotenoids which, in

the LH2 complex of *Rps. acidophila* strain 10050, are mainly rhodopin glucoside (McDermott *et al.*, 1995). The strong absorption band at ~390nm is the Soret band and this is due to the B_x transition of the Bchl *a* molecules in the antenna complexes (see section 1.5.1). The large peak at 280nm is ascribable to the aromatic amino acid residues of proteins present in the crude photosynthetic membrane preparation. The ratio of the NIR absorption maximum to the 280nm peak in solubilised PSM's was about 0.8:1 (Table 4.1). This ratio varied by $\pm 25\%$ between individual preparations. Typically, after the removal of unsolubilised material by centrifugation (section 2.4.1) about 30ml of solubilised PSM's with an OD of $\sim 50\text{cm}^{-1}$ were recovered per 10 L of bacteria harvested. To prevent denaturation of the antenna complexes by the relatively high concentration of detergent used in the solubilisation process the solubilised PSM's were immediately diluted 5-fold with 20mM Tris-HCl, pH8.0. This resulted in about 150ml of crude PSM's solubilised in buffer containing 0.2% (v/v) LDAO. Subsequently, the LH1-RC core complex was separated from the LH2 complex by sucrose gradient centrifugation.

Sucrose gradients were prepared as described in section 2.4.2. After centrifugation for 16 hours two well defined, pigmented bands formed (Fig. 4.2). The broad upper band, located just below the interface between the 0.3M and 0.6M sucrose, represented LH2 complex while the lower, finer band, located at the interface between 0.6M and 1.0M sucrose, represented LH1-RC (see Fig. 4.3). There was a slight orange colouration at the top of the sucrose gradient. This was due to the presence of free carotenoid and indicated that some of the protein may have become denatured. In some cases a small white pellet of cell walls formed at the bottom of the centrifuge tube.

The absorption spectra of the bands formed in the sucrose gradients are

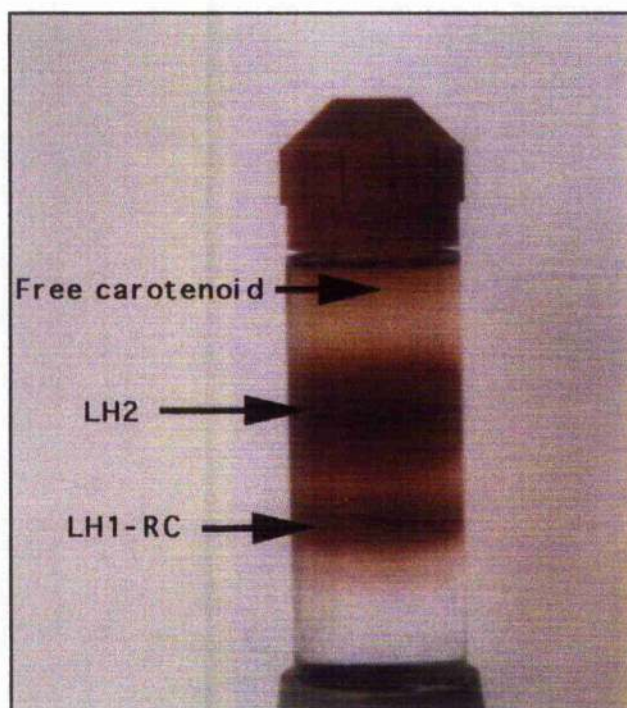


Figure 4.2. Discontinuous sucrose gradient (0.3M, 0.6M and 1.0M sucrose) of solubilised photosynthetic membranes from *Rps. acidophila* strain 10050. Two distinct pigmented bands form after 16 hours centrifugation. The upper band represents LH2 complex and the smaller, lower band represents LH1-RC core complex.

shown in Figure 4.3. The spectrum of the top, LH2-containing band displays two intense NIR peaks located at 801nm and 858nm. These peaks represent absorption due to the Q_y transition of the B800 and B850 Bchl *as* of the complex, respectively. The small peak at ~590nm arises from the Q_x Bchl *a* transition and the large band at ~380nm is the Soret band. The three peaks located between 450nm to 530nm are due to absorption by the carotenoid rhodopin glucoside. The rather flattened absorption band centred at 280nm is due to aromatic amino acid absorption.

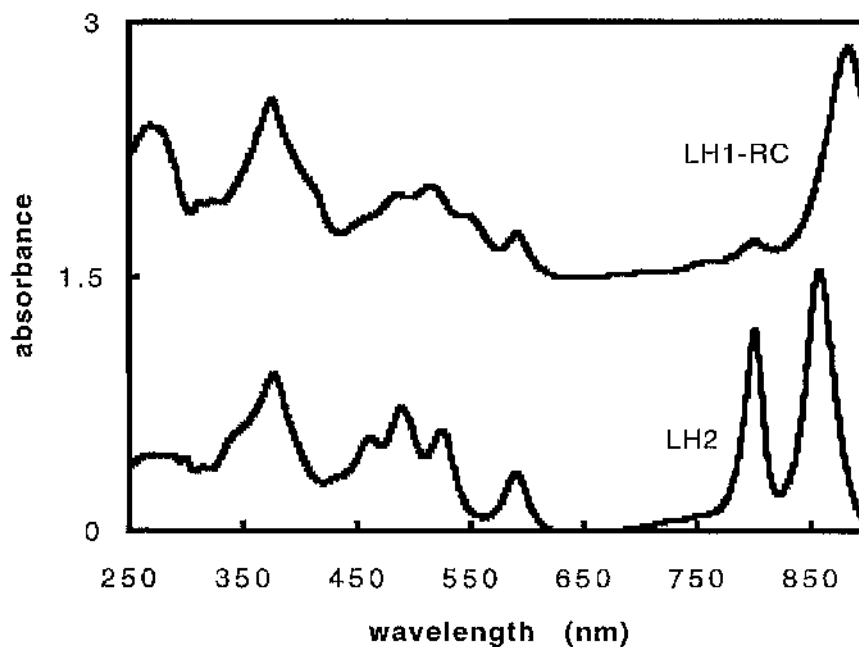


Figure 4.3. Absorption spectra of the LH1-RC and LH2 bands retrieved from the sucrose gradient illustrated in Figure 4.2. For clarity the LH1-RC spectrum has been offset by 1.5 absorbance units. Refer to the main body text for a full description of this figure.

In contrast to the LH2 absorption spectrum, the LH1-RC core complex spectrum exhibits only a single strong NIR absorption band located at 883nm. This band arises from the Q_y transition of the LH1 antenna Bchl *a* 's. The small peak at 800nm is attributable to absorption by the Bchl *a* molecules of the RC. The small shoulder to the blue of the 800nm peak is due to the RC bacteriopheophytins. The carotenoid absorption bands of the core complex, located between 480nm and 550nm, have a different profile and are shifted slightly to the red compared to those of the LH2 antenna. This is because the LH1 antenna has a different carotenoid composition to the LH2 complex. The Soret band located at 380nm possesses

an obvious shoulder to the red of the absorption maximum which is not present in the Soret band of the LH2 complex. This shoulder is probably due to a cytochrome bound to the RC. The 280nm-absorption band is much more intense relative to the NIR absorption maximum than that of the LH2 complex. It is also much sharper in profile.

0.75ml aliquots of the sucrose gradient were removed from the bottom of the centrifuge tube using a glass Pasteur pipette connected by plastic tubing to a peristaltic pump (Pharmacia P-1). The length of the tubing was made as short as possible to prevent mixing of the gradient. The absorption of each aliquot at 280nm and 883nm was measured and used to construct a profile of the sucrose gradient (Fig. 4.4). The profile of the 280nm protein absorption shows two peaks representing the LH1-RC and LH2 complexes. The LH2 protein absorption peak is considerably larger than that of LH1-RC reflecting the greater abundance of the former in the ICM. The ratio of the absorbance at 883nm, which is the absorption maximum of the LH1-RC core complex, to that at 280nm shows a single peak with a maximum value of ~2 associated with the bottom protein band of the sucrose gradient. In subsequent sucrose gradients the bottom, LH1-RC core-containing band was removed using a Pasteur pipette and the samples pooled. As can be seen in Table 4.1 about 66ml of core complex with an OD of $7.57 \pm 1.96 \text{ cm}^{-1}$ was recovered from each run of sucrose gradients produced from the solubilisation of PSM's from 10L of bacteria. The mean and standard deviation of the $A_{883}:A_{280}$ ratio from the pooled core complex samples from 26 individual sucrose gradient centrifugation runs was 1.63 ± 0.27 . The pooled samples were further purified by anion exchange chromatography.

Anion exchange chromatography was performed using a gravity flow DEAE-cellulose column as described in section 2.4.3. After the column was

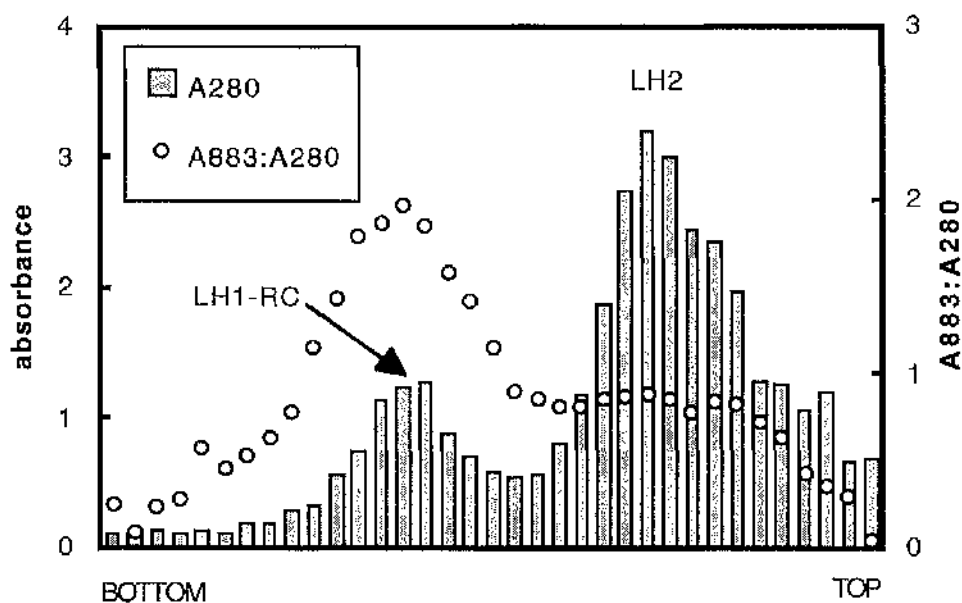


Figure 4.4. Profile of the protein distribution (as determined by the absorption at 280nm) after 16 hours centrifugation in a discontinuous sucrose gradient (0.3M, 0.6M and 1.0M sucrose) to which detergent solubilised photosynthetic membranes from *Rps. acidophila* strain 10050 were applied. The profile shows two distinct protein bands which represent the LH1-RC core complex and LH2 complex. The ratio of absorbance at the NIR absorption maximum of the core complex (883nm) to that at 280nm (general protein absorption) was used as an indicator of the purity of the core complex. Samples were diluted 4-fold with 20mM Tris-HCl, pH8.0, 0.1% LDAO prior to measurement of their absorption spectrum.

equilibrated with detergent-containing buffer, the pooled core complex sample from the sucrose gradients was applied to the top of the column and eluted stepwise using a discontinuous salt gradient ranging from 50mM to 160mM NaCl dissolved in 20mM Tris-HCl, pH8.0, containing 0.1% (v/v) LDAO. The pigmented nature of the core complex allowed the easy visualisation of its progress down the column. Once the pigmented band

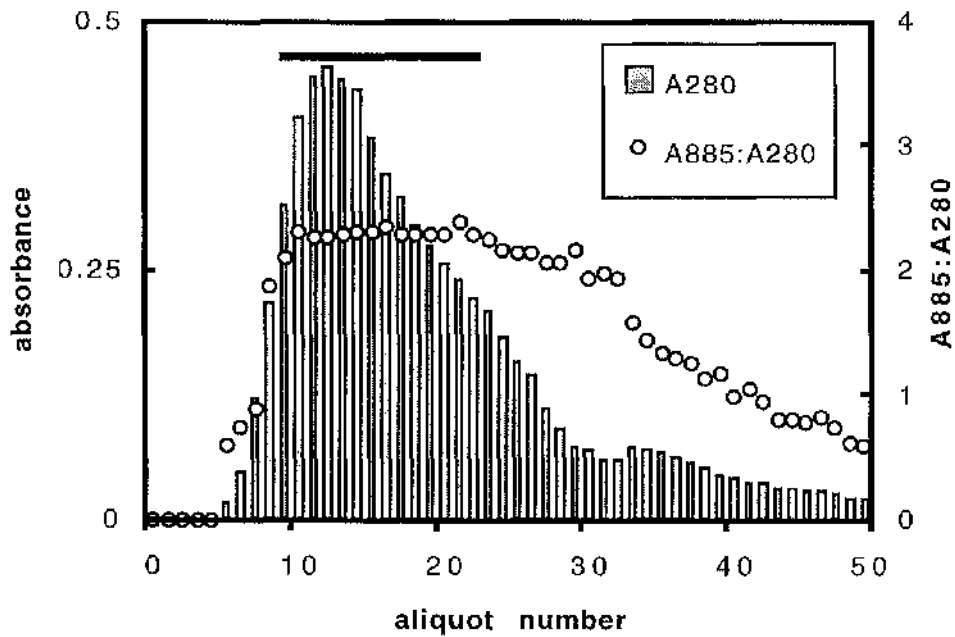


Figure 4.5. Elution profile of *Rps. acidophila* strain 10050 LH1-RC core complex from a DE52 anion exchange chromatography column. In this particular example 42.5ml of pooled core complex sample from sucrose gradients was applied to the top of the column. The complex was eluted using a salt gradient from 50mM to 160mM NaCl. 20ml of eluant was collected and discarded prior to the collection of 650 μ l aliquots of pigmented, core-containing eluant. Samples from each aliquot were diluted 20-fold with 20mM Tris-HCl, pH8.0, 0.1% LDAO prior to their absorption spectrum being measured. The thick black line represents the aliquots of intact core complex which were pooled for further purification by gel filtration chromatography.

had migrated to near the bottom of the column 650 μ l aliquots of eluant were collected until all of the pigmented band had run off the column. The absorption of each aliquot at 280nm and 885nm was measured and used to construct an elution profile (Fig. 4.5).

The protein absorption of the elution profile displayed a single peak which tails off with increasing aliquot number and, as such, with increasing

salt concentration. There was an initial steep increase in 280nm absorption until a maximum was achieved at aliquot number 13. There then followed a gradual decrease in the protein absorption until all the pigmented band had been eluted. Such an elution profile suggested the presence of a heterogeneous population of pigment-protein complex within the anion exchange column. This suggestion was supported by the absorption spectra of aliquots taken at different time points during the elution (Fig. 4.6). Examination of the NIR region of selected aliquots showed that initially RC enriched fractions, which had a relatively large absorbance at 800nm and ~770nm, were eluted (Fig. 4.6a). These fractions were represented by aliquots 6-8 inclusive in the elution profile. The $A_{885}:A_{280}$ ratio of these fractions was also low (~0.8) indicating contamination by other protein and/or degradation of the LH1 antenna. The Soret band in the absorption spectra of the initial aliquots displayed a prominent shoulder located at ~405nm which is probably due to absorption by cytochrome. This shoulder is much more pronounced than in the absorption spectrum of intact LH1-RC core complex (Fig. 4.6b). As such, it is probable that the RC bound cytochrome from some of the core complex sample has become dissociated and eluted with the initial aliquots. As the NaCl concentration was increased intact LH1-RC core complex (aliquots 9-22) was eluted. The absorption spectrum of a representative aliquot of intact core complex is shown in Figure 4.6b. The spectrum exhibits a single strong NIR absorbance band located at 885nm and a smaller peak at 801nm. The ratio of the LH1 antenna Bchl *a* absorbance at 885nm to the RC Bchl *a* absorbance at 801nm is ~4:1. This value is much greater than that of the initially eluted, RC enriched aliquots. The $A_{885}:A_{280}$ ratio was ~1.5:1. The other features of the spectrum are essentially the same as those of the fully purified LH1-RC core complex shown in Figure 4.8. The absorption spectrum of a representative aliquot of the fractions which

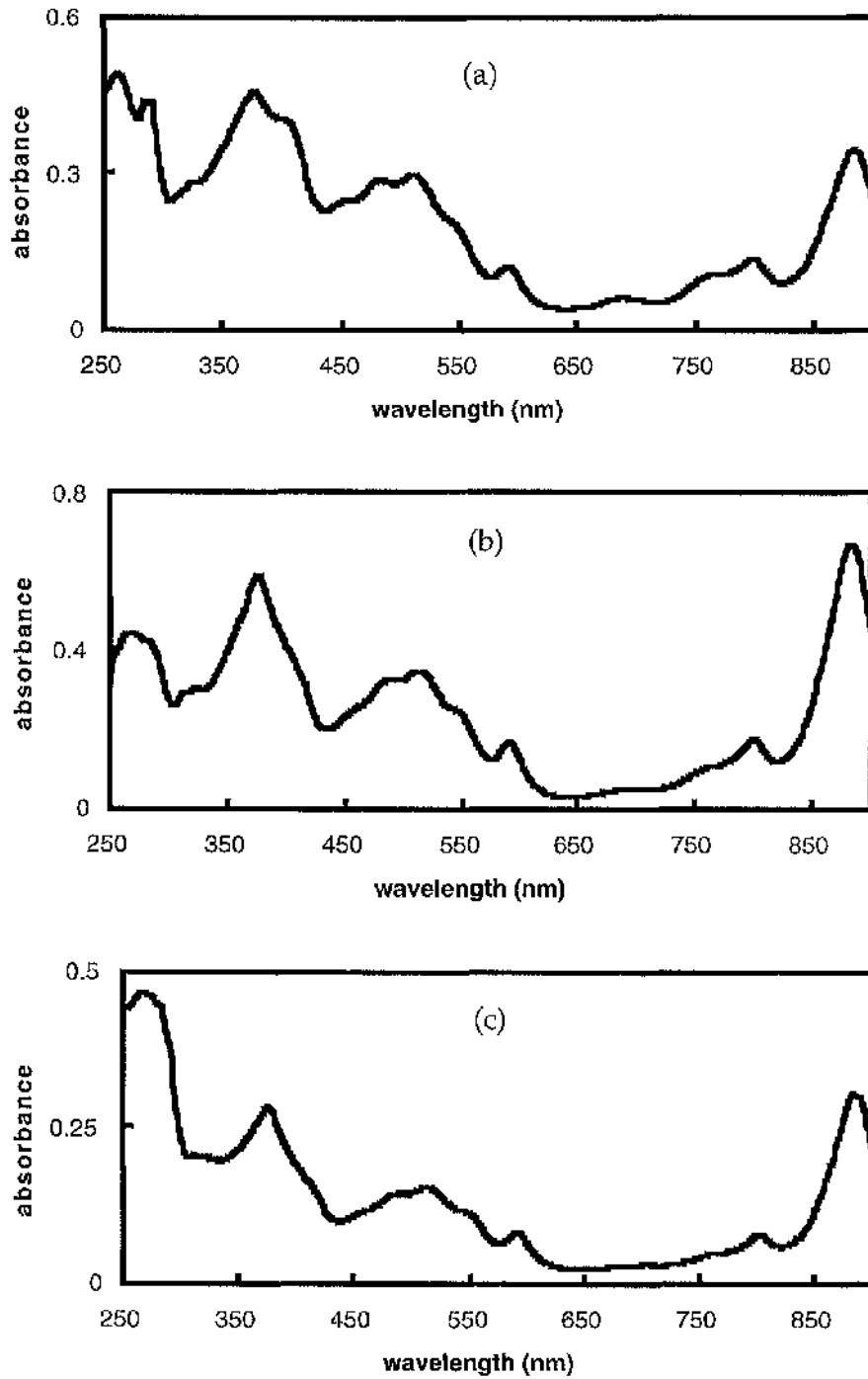


Figure 4.6. Absorption spectra of selected aliquots of LH1-RC core complex which had been removed from sucrose gradients and then eluted from a DE52 anion exchange column by a discontinuous salt gradient. Spectrum (a) is from the RC enriched, initially eluted fractions. Spectrum (b) represents intact core complex, and spectrum (c) represents core complex sample which is contaminated with other proteins.

eluted at the highest NaCl concentrations (aliquots 23-50) is shown in Figure 4.6c. The NIR region of the spectrum is similar to that of the intact core complex illustrated in Figure 4.6b. However the $A_{885}:A_{280}$ ratio is much lower (~ 0.7). This is probably due to heavy contamination of the sample with other proteins.

The spectroscopically intact core complex samples with an $A_{885}:A_{280} \geq 1.7$ were pooled. Typically, this resulted in the collection of ~ 13 ml of intact core complex sample with an OD of $\sim 25 \text{ cm}^{-1}$ (Table 4.1). The $A_{885}:A_{280}$ ratio for these samples was 1.77 ± 0.35 which represented an increase in core complex purity of $\sim 9\%$ compared to the pooled samples from the sucrose gradient purification step. As described in section 2.4.4 the pooled samples from the anion exchange chromatography purification step were then concentrated by centrifugation using Centricon[®] 50 centrifugal concentrators (Amicon). As well as concentrating the sample, the centrifugal concentrators also removed up to 99% of the NaCl present (Amicon data sheet). Typically, this resulted in 2-5ml of concentrated core complex sample suitable for further purification by gel filtration chromatography.

Gel filtration chromatography was performed using a Superdex 200 (prep grade) column connected to a Pharmacia FPLC system (refer to section 2.4.4). The core complex sample was injected onto the top of the column and eluted with 20mM Tris-HCl, pH 8.0, containing 0.1% (v/v) LDAO. 0.5ml aliquots of eluant from the column were collected. Generally, about 30ml of eluant was collected before the pigmented, core complex-containing band started to elute. The absorption spectrum of each pigmented aliquot was measured and the data contained therein was used to construct an elution profile (Fig. 4.7). The protein elution profile displays a Gaussian-like shape with a single peak located at the centre. The $A_{885}:A_{280}$ ratio increased from a

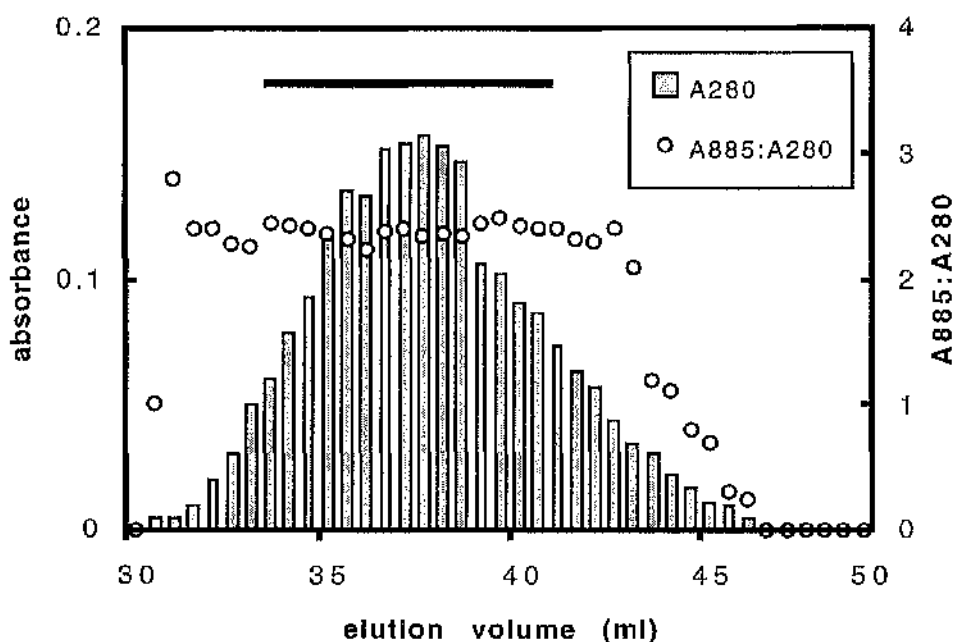


Figure 4.7. Elution profile of *Rps. acidophila* strain 10050 LH1-RC core complex from a Superdex 200 gel filtration column connected to a Pharmacia FPLC system. The core complex was eluted with 20mM Tris-HCl, pH8.0, containing 0.1% (v/v) LDAO at a rate of 0.75ml/min. 30ml of eluant was collected and discarded prior to 0.5ml aliquots of pigmented complex being collected. Samples of each aliquot were diluted 10-fold with 20mM Tris-HCl, pH8.0, 0.1% LDAO and their absorption spectra measured. The thick black line represents those aliquots of core complex which were regarded as fully purified. These aliquots were pooled and used for 3-D crystallisation or CD spectroscopy experiments.

value of zero after the elution of 0.5ml of pigmented eluant to a value of ~2.3 after the second 0.5ml fraction was collected. The ratio remained around the latter value for the next 10ml of sample collected then decreased steeply again to a value of zero. Aliquots from the protein peak with an $A_{885}:A_{280} \geq 2$ and which displayed an NIR absorption spectra consistent with that of intact core complex (Fig.4.8) were considered as fully purified

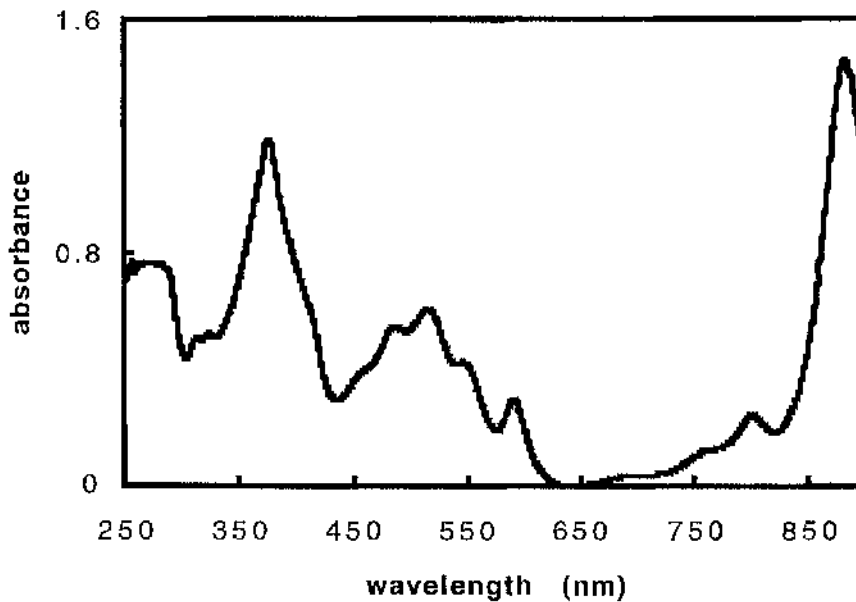


Figure 4.8. Absorption spectrum of fully purified *Rps. acidophila* strain 10050 core complex. The ratio of the LH1 antenna NIR absorption maximum located at 885nm to the 800nm RC Bchl a absorption band is about 6:1 whilst the $A_{885}:A_{280}$ ratio is about 1.9:1. The core complex sample was diluted 10-fold with 20mM Tris-HCl, pH8.0, 0.1% LDAO prior to measurement of the spectrum.

About 12ml of purified LH1-RC core complex with an OD of $\sim 11\text{cm}^{-1}$ was obtained per 10 L of bacteria (Table 4.1). This represented a final yield of core complex of 27%. Most of the loss can be attributed to the fact that, during anion exchange and gel filtration chromatography, only the spectroscopically pure core complex fractions from the elution profile peaks were retained. The mean $A_{885}:A_{280}$ ratio of the pooled core complex samples from the gel filtration column was ~ 2.3 and the $A_{885}:A_{800}$ ratio was ~ 5.6 (Table 4.9).

The purified LH1-RC core complex was concentrated to the desired OD

and either used immediately for 3-D crystallisation experiments or stored in the dark at -20°C for subsequent investigation by SDS-PAGE and electron microscopy (see below) or circular dichroism (CD) spectroscopy (see Chapter 5). For some crystallisation experiments, the LDAO used to solubilise and purify the complex was exchanged for a new detergent. The detergent exchange procedure is described in section 2.4.5.

The polypeptide composition of the antenna complexes was investigated by SDS-PAGE using 11.5-18.5% SDS-polyacrylamide gradients (Dawkins *et al.*, 1988). The polyacrylamide gradient was stabilised by a 15-70% sucrose gradient (section 3.5). In some cases the samples removed from the sucrose gradients were too dilute for analysis by gel electrophoresis and so they were concentrated using Centricon[®] centrifugal concentrators (Amicon). The fully purified LH1-RC complex contained five polypeptides in SDS-PAGE (Fig. 4.9, lanes 1, 2, 4 & 5). The H, M and L subunits of the RC had apparent molecular weights of ~ 39 , 36 and 32 kDa, respectively. As in *Chr. purpuratum* (Kerfeld *et al.*, 1994), *Rv. gelatinosus* (Agalidis & Reiss-Husson., 1992) and *Rs. salexigens* (Wacker *et al.*, 1988) the Coomassie blue staining of these subunits varied in intensity. The two low molecular weight apoproteins of the LH1 antenna are not well resolved and migrated as a single band with apparent mass of ~ 9 kDa. This was a common problem with all the species studied and was probably due to the high degree of hydrophobicity inherent in these polypeptides (Zuber & Brunisholz, 1991). The polypeptide composition of the LH2 and LH1-RC-containing bands from the sucrose density gradients is shown in lanes 7 & 8, respectively. Once again the core complex had three bands between 30-40kDa which corresponded to the RC subunits, and a diffuse band around 9kDa which corresponded to the LH1 antenna polypeptides. Some other polypeptide bands, due to contaminating proteins, were also present. The LH2 α - and β -

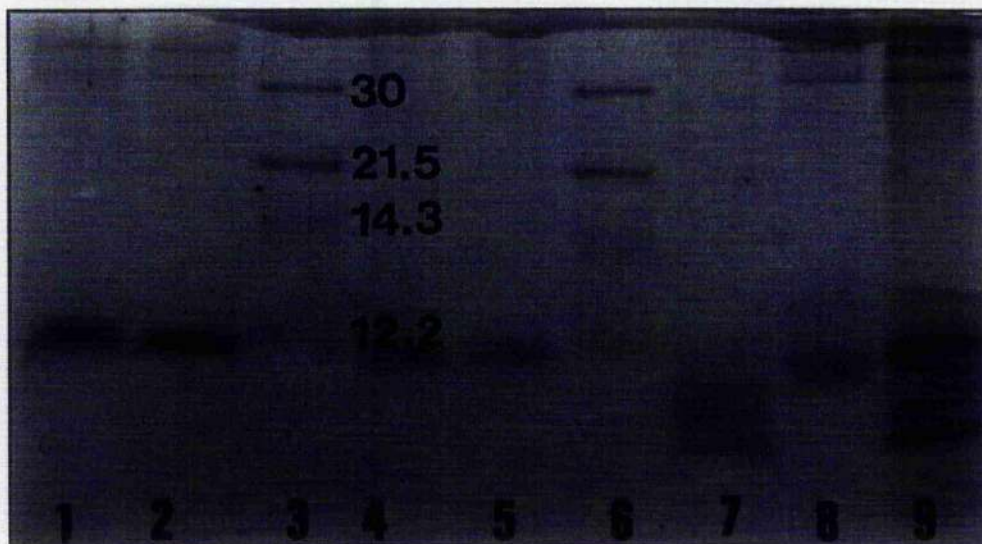


Figure 4.9. Analysis of the polypeptide composition of the antenna complexes from *Rps. acidophila* strain 10050 by an 11.5-18.5% SDS-polyacrylamide gradient gel. Lanes (1 and 2) and (4 and 5), fully purified LH1-RC core complex. Lanes (3) and (6), molecular weight marker proteins. These markers were carbonic anhydrase (30kDa), trypsin inhibitor (21.5kDa), lysozyme (14.3kDa) and cytochrome *c* (12.2kDa). Lanes (7) and (8), LH2 and LH1-RC from the pigmented bands from sucrose gradients. Lane (9), solubilised photosynthetic membrane fragments.

polypeptides were much better resolved and appeared as two stained bands with apparent masses of ~5.6 and ~5kDa, respectively. The solubilised PSM's displayed a polypeptide pattern which was consistent with the presence of both LH2 and LH1-RC complexes, with RC polypeptides between 30-40kDa and bands which corresponded to the LH1 and LH2 antenna polypeptides around 5-9kDa (lane 9). The gels from the other species investigated showed some variation in the molecular weights of both the RC subunits and the LH1 polypeptides.

The purified *Rps. acidophila* strain 10050 core complex was further investigated by electron microscopy as described in section 3. 6. An electron

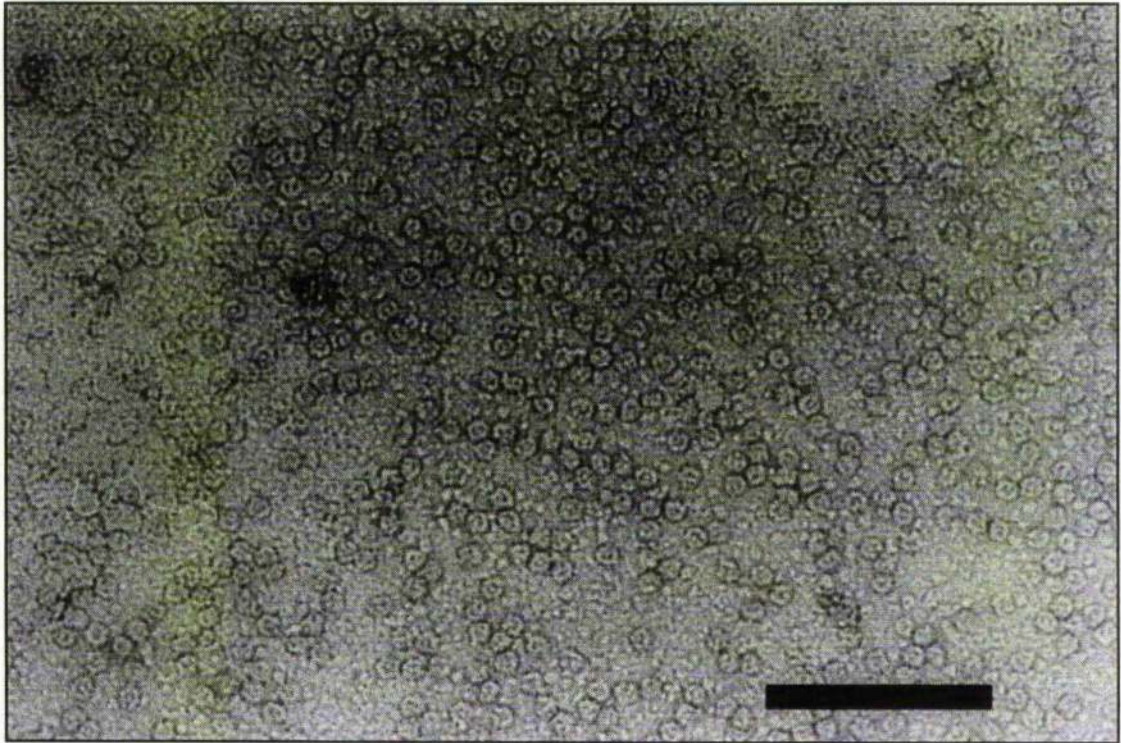


Figure 4.10. Electron micrograph of LDAO solubilised LH1-RC core complexes isolated from the photosynthetic membrane of *Rps. acidophila* strain 10050. The complexes were negatively stained with 1% (w/v) uranyl acetate. From the top view the complexes appear as ring-like structures which surround a central staining region. Bar=100nm.

micrograph of purified LH1-RC core complexes in LDAO solution, and negatively stained with 1% (w/v) uranyl acetate is shown in Figure 4.10. In the top view position the core complexes appeared as uniformly sized, ring-like particles with diameters in the range of $\sim 100\text{-}120\text{\AA}$. This measurement is consistent with measurements of the diameter of core complexes from *Rh. marinum* (Meckenstock *et al.*, 1992b), *Rs. rubrum* (Karrasch *et al.*, 1995) and *Rs. molischianum* (Boonstra *et al.*, 1994). The rings could be equated

with the LH1 antenna of the complex. The ring-like structures often presented a central region which appeared to stain differentially. This central staining region probably represents the photochemical RC. In some cases the RC may have become dissociated from its light harvesting antenna and this could explain the differential staining. Similar observations have been reported previously for the B875 complex from *Rb. sphaeroides* (Boonstra *et al.*, 1993) and the core complexes from *Rs. molischanum* (Boonstra *et al.*, 1994) and *Rv. gelatinosus* (Jiraskova *et al.*, 1996; 1997).

Rps. acidophila strain 10050 core complex was found to be one of the most stable of all the core complexes studied in this thesis. It could withstand several rounds of freezing and thawing without any apparent detrimental effects to its structural integrity as revealed by absorption spectroscopy. Indeed, several samples were stored for over two years at -20°C then thawed and their absorption spectra recorded. The spectra all maintained a $A_{885}:A_{280}$ ratio of ≥ 2 and the spectral features were very similar to that of freshly purified complex.

LH1-RC core complex from *Rps. acidophila* strains 7050 and 7750 grown under the conditions described in section 2.1.1 was solubilised and purified in the same manner as the core complex from *Rps. acidophila* strain 10050. The absorption spectra, sucrose gradients and elution profiles of strains 7050 and 7750 core complex were both qualitatively and quantitatively very similar to those obtained for strain 10050 and, therefore, are not presented here.

The absorption spectra of the PSM's (or chromatophores), LH2 and LH1-RC complexes of the other LH2-containing species studied all shared common features. These features are discussed here to avoid repetition in subsequent sections. In all LH2 species the absorption spectra of PSM's exhibited two intense NIR absorption peaks located at $\sim 800\text{nm}$ and between

~850-860nm. The 800nm peak was due mostly to the Q_y transition of the LH2 B800 Bchl a 's with a small contribution from the RC Bchl a 's. The peak around 850-860nm was due to a combination of the Q_y transitions of the LH2 B850 Bchl a 's and the LH1 antenna Bchl a 's. The Bchl a Q_x transition and Soret bands were located at ~590nm and ~370nm, respectively. The carotenoids absorbed between ~450-550nm and the aromatic amino acid absorption peak was located at 280nm. In all the species studied the absorption spectra of the LH1-RC complexes all exhibited a single, strong NIR peak at between ~875-885nm. This peak came from the Q_y transitions of the LH1 antenna Bchl a 's. A smaller peak, due to absorption by the RC, was located at ~800nm. The features in the other regions of the spectra were similar to those displayed by the PSM's.

The sucrose gradient, anion exchange and gel filtration elution profiles of the other LH2-containing species studied were also similar to those of *Rps. acidophila*. Once again, to avoid repetition of data they have not been reproduced. Instead, a brief description of the results of the purification protocol for each of these species, including representative absorption spectra from each stage of the purification process, is presented. A summary of the $A_{NIR\ max}:A_{280}$ and $A_{NIR\ max}:A_{800}$ ratios of the fully purified core complex from each species is presented in Table 4.9.

4.3. *Rhodopseudomonas palustris* strain French

This species of purple bacteria was originally a gift from Dr. B. Robert,

Saclay, France. As the strain of the *Rps. palustris* culture was unknown it was given the arbitrary name "French".

10L cultures of *Rps. palustris* French were grown under high light conditions in C-succinate medium as described in section 2.1.1. As with *Rps. acidophila*, breakage of *Rps. palustris* cells produced photosynthetic membrane (PSM) fragments which were diluted to an OD_{NIR} of 50cm^{-1} and solubilised by the addition of 0.75% (v/v) LDAO (Dawkins *et al.*, 1988). Unsolubilised material was removed by low speed centrifugation (section 2.4.1) then the sample was diluted 3-fold with 20mM Tris-HCl, pH8.0, to reduce the LDAO concentration to $\sim 0.25\%$ (v/v).

The absorption spectrum of the solubilised PSM's is shown in Figure 4.11. As was the case with *Rps. acidophila*, the spectrum showed two strong NIR absorption bands. In *Rps. palustris* strain French these bands were located at 802nm and 857nm. The Bchl *a* Q_x transition was located at $\sim 590\text{nm}$ and the Soret band at $\sim 370\text{nm}$. The carotenoids of the antenna complexes and RC were revealed by the three characteristic, finger-like peaks located between 470nm-530nm.

Sucrose gradient centrifugation of the solubilised PSM's resulted in the formation of two separate dark reddish-purple bands. The upper LH2-containing band was much broader than the lower band, which consisted of LH1-RC core complex. This reflected the greater abundance of LH2 within the ICM. The absorption spectra of each band is shown in Figure 4.12. The LH1-RC absorption spectrum shows a single strong NIR peak located at 878nm and a smaller peak at 803nm. The remainder of the spectrum is similar to that of the solubilised PSM's shown in Figure 4.11, except that the absorption peaks due to the carotenoids are not as well defined.

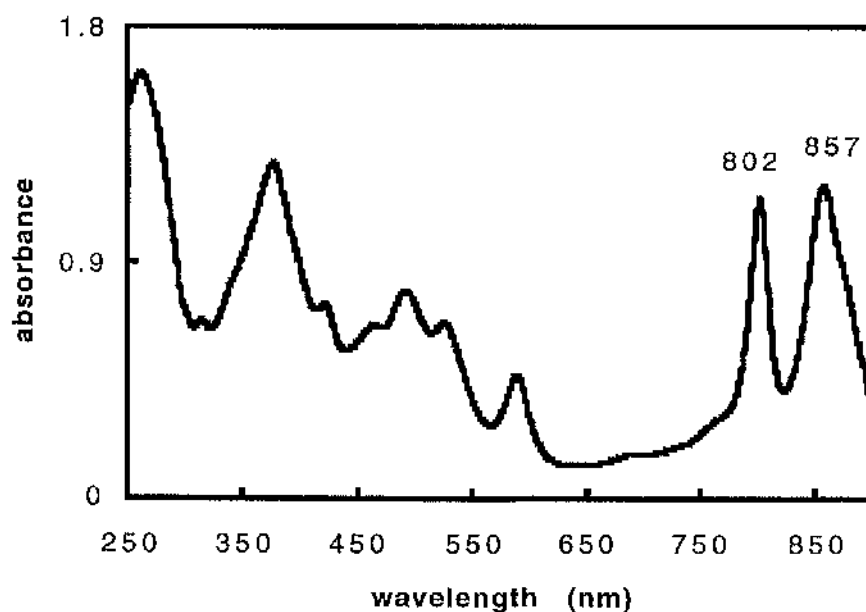


Figure 4.11. Absorption spectrum of LDAO solubilised photosynthetic membranes from *Rps. palustris* strain French. The spectrum shows two strong NIR absorption bands located at 802nm and 857nm. The $A_{857}:A_{280}$ ratio is 0.72. The sample was diluted 20-fold with 20mM Tris-HCl, pH8.0, 0.1% LDAO prior to measurement of the spectrum.

The lower, core complex-containing bands from the sucrose gradients were pooled and further purified by anion exchange chromatography (section 2.4.3). The elution profile of core complex from the anion exchange column was very similar to that of *Rps. acidophila* (Fig. 4.5). Aliquots of core complex which displayed an absorption spectrum consistent with that

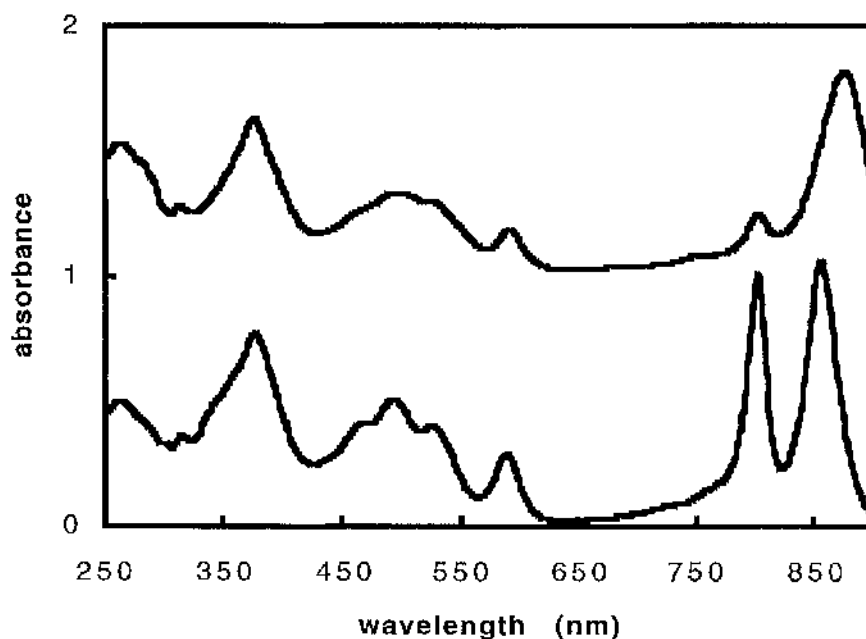


Figure 4.12. Absorption spectra of the pigmented bands formed by the density sucrose gradient centrifugation of solubilised PSM's from *Rps. palustris* strain French. The top band from the sucrose gradient (LH2) shows two strong NIR absorption peaks located at 856nm and 802nm. The lower band, (LH1-RC) shows a single strong NIR peak at 878nm. A smaller NIR peak, due to absorption by the RC Bchl *a*'s, is located at 803nm. The $A_{878}:A_{280}$ ratio in the above spectrum is 1.65. The samples were diluted 20-fold in 20mM Tris-HCl, pH8.0, 0.1% (v/v) LDAO prior to their spectra being measured. For clarity the core complex spectrum was offset by 1 absorbance unit.

of intact core complex and an $A_{878}:A_{280}$ ratio of ≥ 2 were pooled. The $A_{878}:A_{280}$ ratio of the pooled fractions was 2.08 (Table 4.2). This represented a 22% increase in purity (in terms of $A_{878}:A_{280}$ ratios) compared to the core complex samples retrieved from the sucrose gradients. Assuming a 100% recovery of core from the sucrose gradients the yield of core was 77%.

Table 4.2. Purification table for the LH1-RC core complex of *Rps. palustris* strain French. The values represent the arithmetical mean and standard deviation of measurements from a sample size of $n=8$. Cultures were grown in 10 L batches.

Purification step	Volume (ml)	OD ₈₇₈ *(cm ⁻¹)	A ₈₇₈ :A ₂₈₀ *	ODV	% yield of core
Solubilisation of photosynthetic membranes	118 ± 33	17.2 ± 4.7	0.75 ± 0.2	2006	-
Sucrose gradient centrifugation	26 ± 6	13.3 ± 8.6	1.7 ± 0.15	345	100
Anion exchange chromatography	11.8 ± 2.7	22.7 ± 6.7	2.08 ± 0.15	267	77
Gel filtration chromatography	15.0 ± 2.6	10.1 ± 2.9	2.13 ± 0.11	151.5	44

* The OD of photosynthetic membranes was measured at the NIR absorption maximum which was located at 857nm.

The elution profile of the LH1-RC core complex from the gel filtration column showed a single 280nm protein peak. The peak fractions were pooled and the absorption spectrum measured (Fig.4.13). The A₈₇₈:A₂₈₀ ratio of the purified *Rps. palustris* core was ~2.13 (Table 4.9).

The results of the purification of *Rps. palustris* strain 1a1 were very

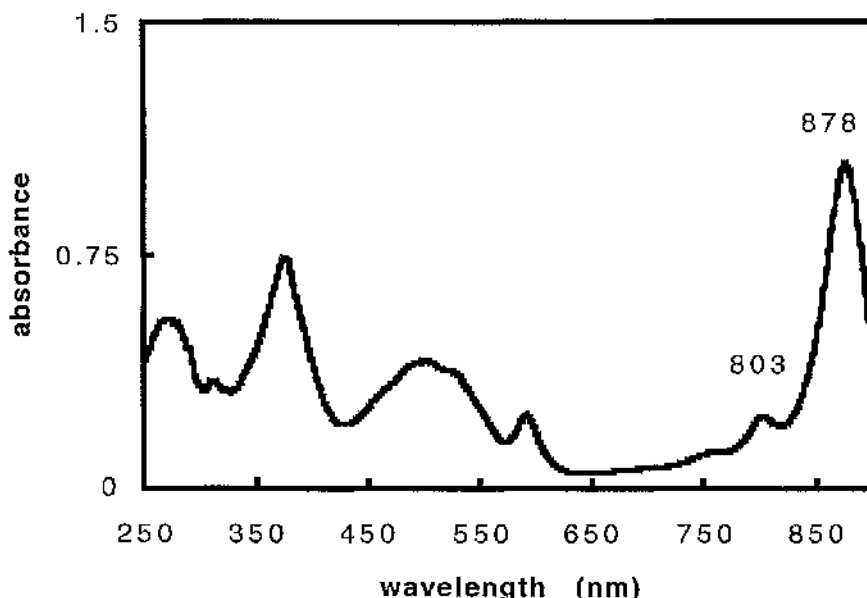


Figure 4.13. Absorption spectrum of fully purified LH1-RC core complex from *Rps. palustris* strain French. The position of the NIR absorption bands is indicated. The spectrum is similar to that of the core complex from the sucrose gradients except that in this case the $A_{878}:A_{280}$ ratio has increased to a value of 2. The sample was diluted 5-fold with 20mM Tris-HCl, pH8.0, 0.1% LDAO prior to the spectrum being measured.

similar to those of *Rps. palustris* strain French. The OD, $A_{NIR}:A_{280}$, ODV and % yield values of strain 1a1 core complex at each purification stage were within 5% of those presented in Table 4.2 for strain French. The absorption spectrum of strain 1a1 core complex was also very similar to the absorption spectrum of core complex from strain French except that the locations of the two NIR bands were shifted 1nm to the blue to 877nm and 802nm (Fig. 4.14).

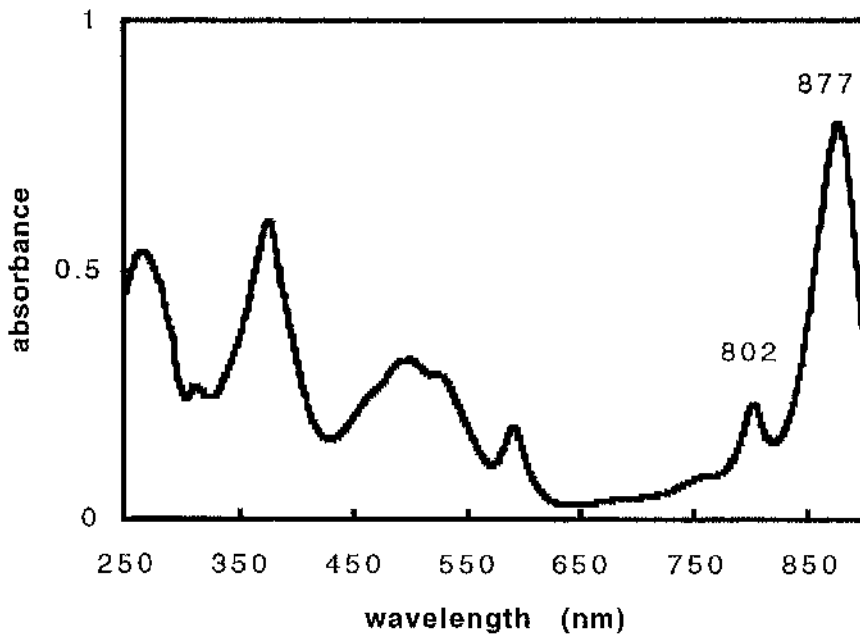


Figure 4.14. Absorption spectrum of *Rps. palustris* strain 1a1 core complex from a sucrose density gradient. The location of the NIR absorption bands is indicated. The $A_{877}:A_{280}$ ratio is 1.55. The sample was diluted 10-fold prior to the spectrum being measured.

4.4. *Rhodospseudomonas cryptolactis*

Rps. cryptolactis is a thermotolerant species of purple non-sulphur bacteria with an optimum growth temperature of $\sim 40^{\circ}\text{C}$ (Halloren *et al.*, 1995). Like *Rps. acidophila* strains 7050 and 7750 (Cogdell *et al.*, 1983; Gardiner *et al.*, 1993), *Rps. cryptolactis* can synthesise two types of peripheral antenna complex. A B800-820 type peripheral antenna complex was the major component when cells were grown at a low light intensity. At a high light intensity the B800-850 complex was the major antenna component (Halloren *et al.*, 1995). Therefore, in order to simplify the purification

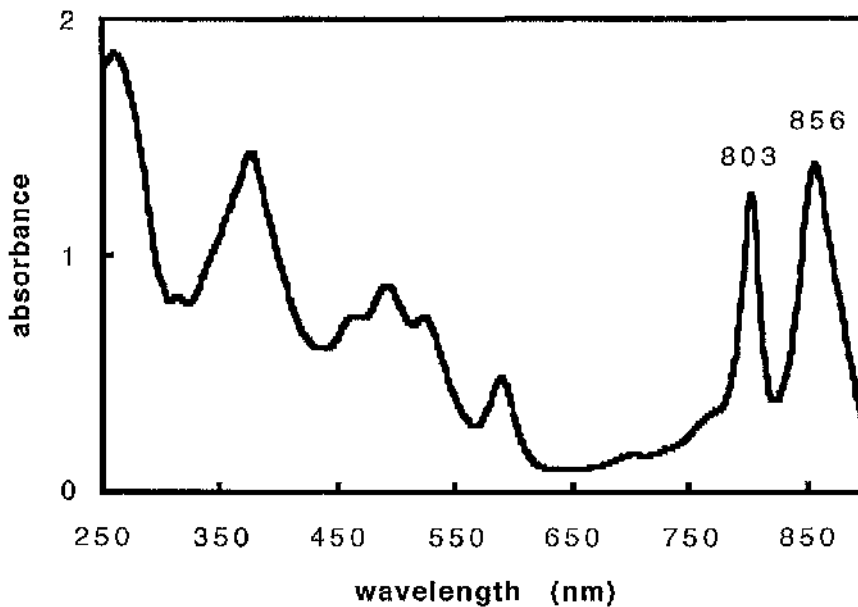


Figure 4.15. Absorption spectrum of LDAO solubilised photosynthetic membranes of high-light grown cells of *Rps. cryptolactis*. The wavelengths of the NIR absorption maxima are indicated. This sample was diluted 30-fold with 20mM Tris-HCl, pH8.0, prior to measurement of the spectrum.

process and maximise the amount of LH1-RC core complex synthesised, *Rps. cryptolactis* was grown anaerobically at 42°C under high light conditions in THERMED medium (sections 2.1 and 2.1.4). Cells of this species required ~72 hours growth before they were of a sufficient density to be harvested for isolation and purification of the core complex.

Photosynthetic membranes were isolated and solubilised as described previously (sections 2.3 and 2.4.1). The absorption spectrum of the solubilised PSM's is shown in Figure 4.15. The spectrum is qualitatively similar to those described previously for *Rps. acidophila* and *Rps. palustris*, and is characteristic of the presence of both LH2 and LH1-RC complexes

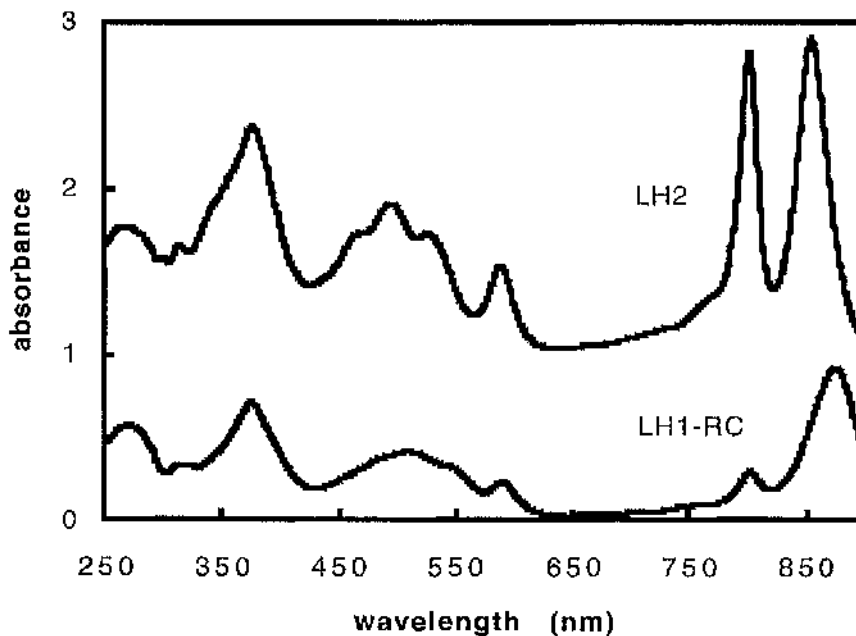


Figure 4.16. Absorption spectra of the lower (LH1-RC) and upper (LH2) pigmented bands resulting from the sucrose density gradient centrifugation of solubilised PSM's from high-light grown *Rps. cryptolactis*. For clarity the LH2 spectrum has been offset by 1 absorbance unit. Samples were diluted 5-fold with 20mM Tris-HCl, pH8.0, 0.1% LDAO.

The spectrum shows two major NIR peaks at 803nm and 856nm. The small peak at ~680nm was due to the presence of an oxidised breakdown product of Bchl *a*. The peaks between 450nm-550nm were due to carotenoids, of which spirilloxanthin is the major component in both the LH1-RC and LH2 complexes (Halloren *et al.*, 1995). The Bchl *a* Q_x and Soret band absorption peaks were located at ~590nm and ~370nm, respectively. The mean ratio of $A_{856}:A_{280}$ for the solubilised membrane preparations was 0.77 (Table 4.3).

Sucrose density gradient centrifugation (section 2.4.2) of the solubilised PSM's resulted in the formation of two pigmented bands. Measurement of

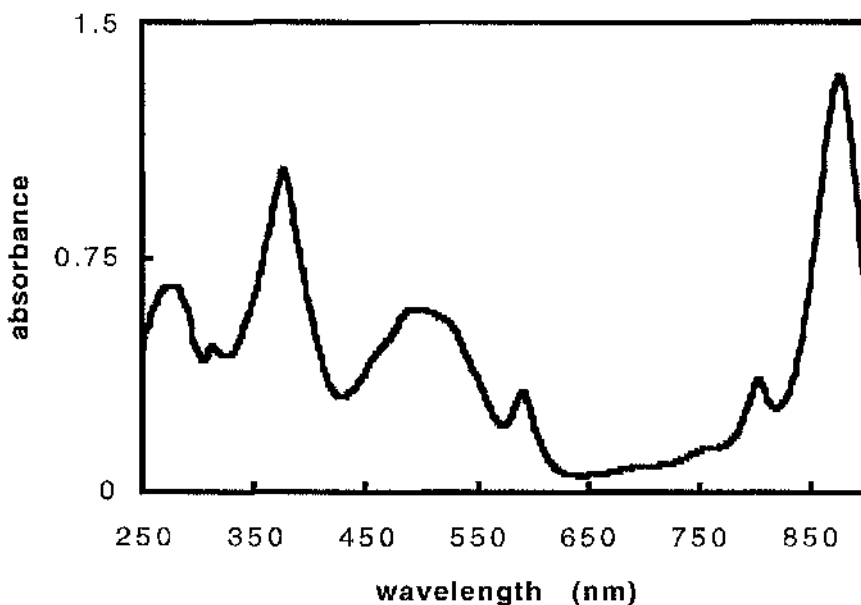


Figure 4.17. Absorption spectrum of fully purified, high-light grown *Rps. cryptolactis* LH1-RC core complex after gel filtration chromatography. This spectrum is very similar to the spectrum of core complex retrieved from sucrose density gradients (Fig. 4.13) except the ratio of absorbance at 877nm to that at 280nm is much greater (2.1:1 compared to 1.6:1). The sample was diluted 10-fold prior to the spectrum being measured.

the absorption spectra of the bands indicated the upper and lower bands consisted of LH2 and LH1-RC complex, respectively (Fig. 4.16). The LH1-RC spectrum exhibited an intense NIR peak at 877nm and a smaller one at 803nm. The LH2 absorption spectrum shows two, strong NIR peaks located at 855nm and 802nm. This spectrum is characteristic of the B800-850 type of LH2 complex. In both cases the features of the remainder of the absorption spectra closely resembled each other and the spectrum of solubilised PSM's that was described previously (Fig. 4.15). Sucrose density gradient centrifugation increased the $A_{877}:A_{280}$ ratio to 1.56 (Table 4.3).

Purity of the *Rps. cryptolactis* LH1-RC core complex was further increased by passage through anion exchange and gel filtration columns as described in sections 2.4.3 and 2.4.4, respectively. The purity of the sample, as determined spectroscopically from the $A_{877}:A_{280}$ ratio, increased from ~1.56 after sucrose density gradient centrifugation to ~2.2 after gel filtration (Fig. 4.17 and Table 4.3). The final yield of core complex was 21%. Fully purified complex was concentrated and used immediately for crystallisation experiments (sections 2.4.5 and 2.6) or stored at -20°C until required.

4.5. *Rubrivivax gelatinosus*

Two strains of *Rv. gelatinosus* were studied - DSM 149 and DSM 151. Cells were grown under high-light conditions in 10L flasks of C-succinate medium as described in section 2.1.1. In contrast to the other species of purple bacteria investigated *Rv. gelatinosus* cells produced a mucus which promoted cell aggregation and hindered the initial steps of the purification process. Generally, strain DSM 151 produced the largest quantities of mucus. After harvesting, the cells were washed thoroughly with 20mM MES, Tris-HCl, pH8.0, and disrupted by passage through a French pressure cell (section 2.3).

Rv. gelatinosus cells possess a tubular type of intracytoplasmic membrane system (Remsen, 1978) which, like the *Rhodospseudomonas* species studied here, produces photosynthetic membrane fragments when French pressed. The absorption spectrum of the PSM fragments of strain DSM 149 is shown in Figure 4.18. The spectrum closely resembled those of the other LH2-containing species studied with two strong NIR peaks at 856nm and 803nm and peaks at ~590nm (Bchl a Q_x), ~370nm (Soret band) and between ~440-520nm (carotenoids) (Jiraskova & Reiss-Husson, 1993,

Table 4.3. Purification table for the LH1-RC core complex of high-light grown *Rps. cryptolactis*. The values represent the arithmetical mean and standard deviation of measurements from a sample size of $n=5$. Cultures were grown in 10 L batches.

Purification step	Volume (ml)	OD ₈₇₇ * (cm ⁻¹)	A ₈₇₇ :A ₂₈₀ *	ODV	% yield of core
Solubilisation of photosynthetic membranes	42 ± 13	50 ± 6	0.77 ± 0.05	2100	-
Sucrose gradient centrifugation	77.5 ± 2.5	6.02 ± 0.87	1.56 ± 0.04	466	100
Anion exchange chromatography	9.5 ± 2.5	14.1 ± 5.6	2.05 ± 0.05	133	28
Gel filtration chromatography	9.5 ± 2.3	10.1 ± 4.6	2.19 ± 0.02	96	21

* The OD of photosynthetic membranes was measured at the NIR absorption maximum which was located at 856nm.

1994). The absorption spectrum of strain DSM 151 was very similar to that of strain DSM 149.

The isolated PSM's were diluted to an OD of 50 cm⁻¹ at the NIR absorption maximum and solubilised with 1% (v/v) LDAO. Due to the instability of the LH1-RC core complex from this species in the presence of

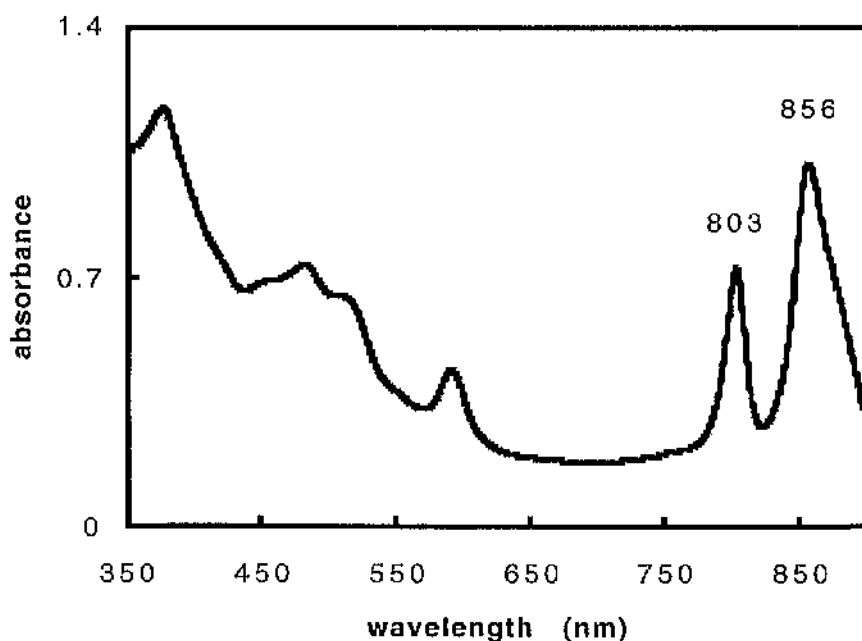


Figure 4.18. Absorption spectrum of unsolubilised PSM fragments from *Rv. gelatinosus* DSM 149, suspended in 20mM Tris-HCl, pH8.0. The increase in the intensity of the absorbance between 650nm-750nm compared to the corresponding spectra of solubilised membranes was due to light scattering. The spectrum of PSM's from *Rv. gelatinosus* strain DSM 151 was very similar. Refer to text for a full description.

relatively high concentrations of detergent, the solubilised PSM's were immediately diluted with 20mM Tris-HCl, pH8.0, to reduce the LDAO concentration to 0.2% (v/v). The mean $A_{856}:A_{280}$ ratio of the solubilised PSM's was 0.45 (Table 4.4). This ratio was ~30-40% lower than the ratios of the other species studied and was probably due to the presence of mucus in the sample.

The absorption spectra of the pigmented bands from the sucrose gradients are shown in Figure 4.19. The spectrum of the upper, LH2-

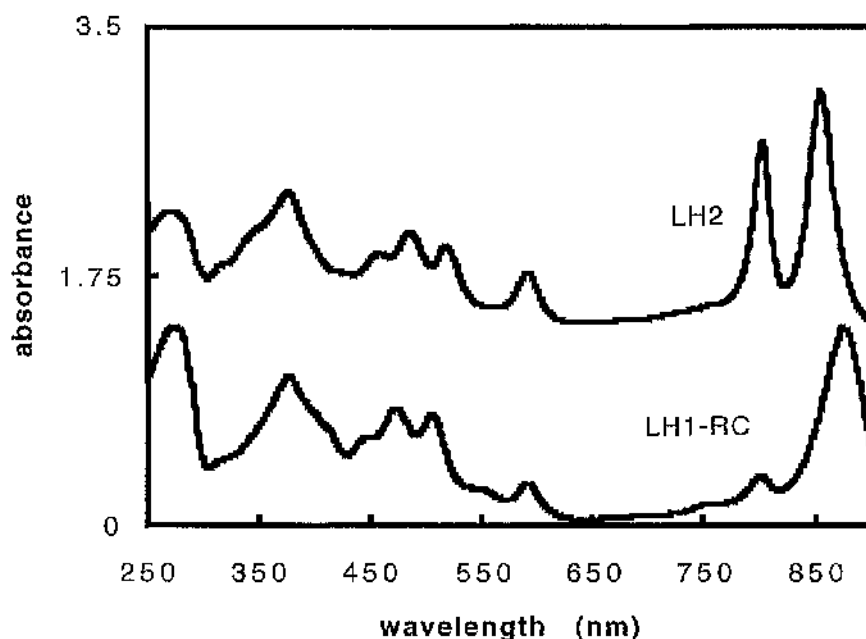


Figure 4.19. Absorption spectra of the upper (LH2) and lower (LH1-RC) pigmented bands which resulted from the sucrose density gradient centrifugation of solubilised PSM's from *Rv. gelatinosus* DSM 149. The samples were diluted 5-fold with 20mM Tris-HCl, pH8.0, 0.1%(v/v) LDAO prior to their spectra being measured. For clarity the LH2 spectrum was offset by 1.4 absorbance units.

containing band shows two, strong NIR absorption peaks, located at 854nm and 803nm. The spectrum of the lower, LH1-RC core complex-containing band revealed a single, intense NIR Bchl a Q_y transition absorption peak located at 877nm and a smaller peak at 801nm. The carotenoid absorption peaks of the LH1-RC complex, located between ~430-550nm, were blue-shifted by ~10nm and also had slightly different relative intensities compared to the LH2 carotenoid absorption peaks. This was probably due to a difference in carotenoid composition between the two complexes. The peak at 550nm in the core complex spectrum, which was not present in the

Table 4.4. Purification table for the LH1-RC core complex of *Rv. gelatinosus* strain 149. The values represent the arithmetical mean and standard deviation of measurements from a sample size of $n=4$. Cultures were grown in 10 L batches.

Purification step	Volume (ml)	OD ₈₇₇ * (cm ⁻¹)	A ₈₇₇ :A ₂₈₀ *	ODV	% yield of core
Solubilisation of photosynthetic membranes	38 ± 4	50 ± 2	0.45 ± 0.05	1900	-
Sucrose gradient centrifugation	77 ± 8	7.06 ± 1.7	1.0 ± 0.15	544	100
Anion exchange chromatography	10 ± 3.5	27.6 ± 6.4	1.28 ± 0.21	276	51
Gel filtration chromatography	17.75 ± 0.25	2.25 ± 0.42	1.55 ± 0.2	38	7

* The OD of photosynthetic membranes was measured at the NIR absorption maximum which was located at 856nm.

core spectra of the other species studied, was due to absorption by the carotenoid hydroxyspheroidene (Jiraskova and Reiss-Husson, 1993). The 405nm shoulder on the Soret band, which was not present in the spectrum of the LH2 complex, probably came from RC associated cytochrome. The absorption spectra of the pigmented LH2 and LH1-RC bands from *Rv. gelatinosus* DSM 151 were very similar to those for strain DSM 149. The

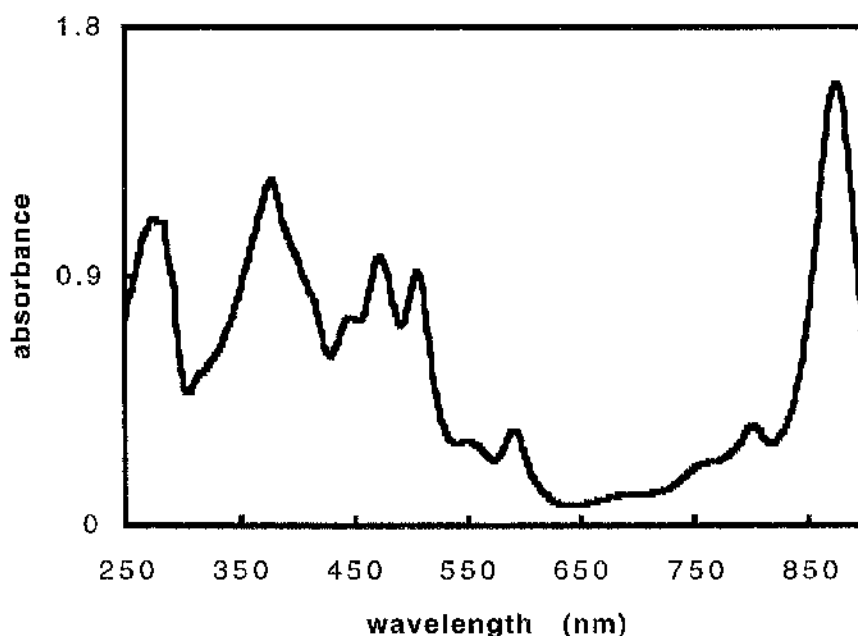


Figure 4.20. Absorption spectrum of fully purified LH1-RC core complex from *Rv. gelatinosus* strain DSM 149. This absorption spectrum closely resembles that of fully purified core complex from strain DSM 151. The NIR absorption maximum in both cases was located at 877nm, with smaller peaks located at 801nm and 760nm. The small absorption at 680nm was due to an oxidised breakdown product of Bchl *a* and the peak at 550nm came from the carotenoid hydroxyspheroidene. The $A_{877}:A_{280}$ ratio of this sample was 1.5.

$A_{877}:A_{280}$ ratio of the pooled core complex sample from sucrose gradients was ~ 1 (Table 4.4). This ratio was significantly lower than that of the other species studied and may reflect the inherent instability of the this core complex when it is isolated and solubilised in LDAO.

Anion exchange and gel filtration chromatography (sections 2.4.3 and 2.4.4, respectively) of the core complex were performed to achieve the desired degree of purity for crystallisation and CD experiments. The

absorption spectrum of fully purified *Rv. gelatinosus* DSM 149 core complex is shown in Figure 4.17. The final stage of the purification process resulted in a ~7% yield of core complex. The $A_{877}:A_{280}$ ratio was 1.55 (Table 4.4). The $A_{877}:A_{280}$ ratio of fully purified *Rv. gelatinosus* DSM 151 was only 1.34. The combination of the low yield of core complex and the low $A_{877}:A_{280}$ ratios were indicative of the instability of the core complex from this species. It appeared that much of the core complex actually degraded during purification. In an attempt to improve the stability of the complex extra care was taken to ensure that unnecessary exposure to light and temperatures above 4°C were avoided during the purification process. However, these precautions did not significantly change the values presented in Table 4.4. The instability of the isolated, LDAO solubilised *Rv. gelatinosus* core complex was underlined when samples with an $A_{877}:A_{280}$ ratio of 1.5 were stored at -20°C. When the samples were thawed, the $A_{877}:A_{280}$ ratio frequently decreased to ~1.1.

4.6. *Chromatium vinosum* strain D

In contrast to the other species of purple bacteria investigated in this thesis, *Chr. vinosum* is a sulphur bacteria which can utilise reduced sulphur compounds as electron donors for the reduction of CO₂. The light-harvesting system of *Chr. vinosum* is one of the most complex antenna systems of the purple bacteria with five different spectral forms of antenna Bchl reported (Thornber, 1970; Hayashi & Morita, 1980; Hayashi *et al.*, 1981). The type(s) of antenna complex synthesised is dependent upon light intensity, temperature and nutritional conditions (Thornber, 1970). The spectral response of *Chr. vinosum* cells to low light and/or low temperature is similar to that of *Rps. acidophila* and *Rps. palustris* (Zuber &

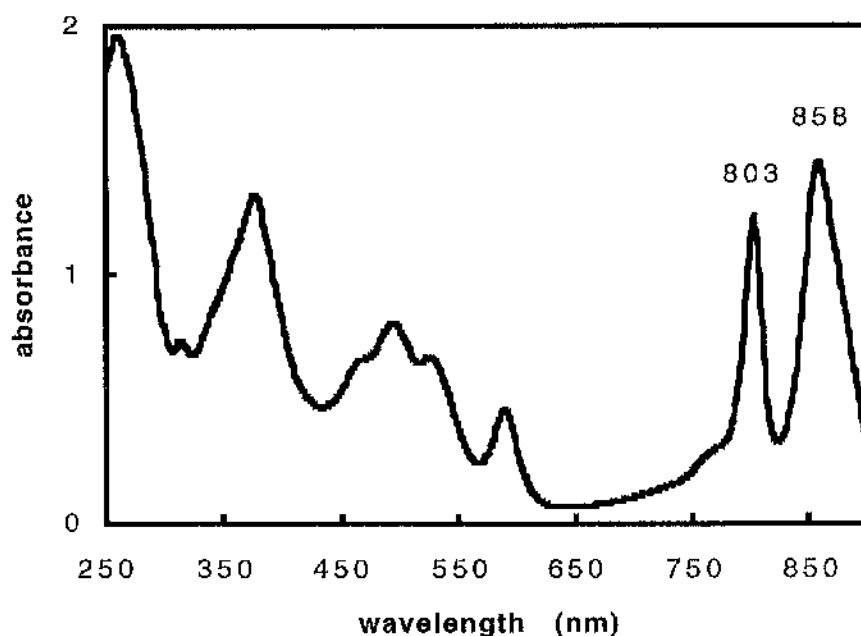


Figure 4.21. Absorption spectrum of LDAO-solubilised chromatophores of high-light grown *Chr. vinosum* strain D. The chromatophores possess two strong NIR peaks located at 803nm and 858nm. The sample was diluted 30-fold with 20mM Tris-HCl, pH8.0, prior to the recording of the spectrum.

Brunisholz, 1991).

To prevent synthesis of B800-820 type LH2 complexes *Chr. vinosum* strain D cells were grown under high light conditions ($150\mu\text{mol/s/m}^2$) at a temperature of $28\pm 2^\circ\text{C}$ in 10l. flasks of Fuller's medium (Fuller *et al.*, 1963). *Chr. vinosum* cells contain vesicular intracytoplasmic membranes which yield chromatophores when French pressed. The chromatophores were solubilised by the addition of 1% (v/v) LDAO. The absorption spectrum of the solubilised chromatophores is shown in Figure 4.21 and is similar to those described previously, with two strong NIR absorption peaks located at 803nm and 858nm. Such a spectrum is typical of bacteria that produce a

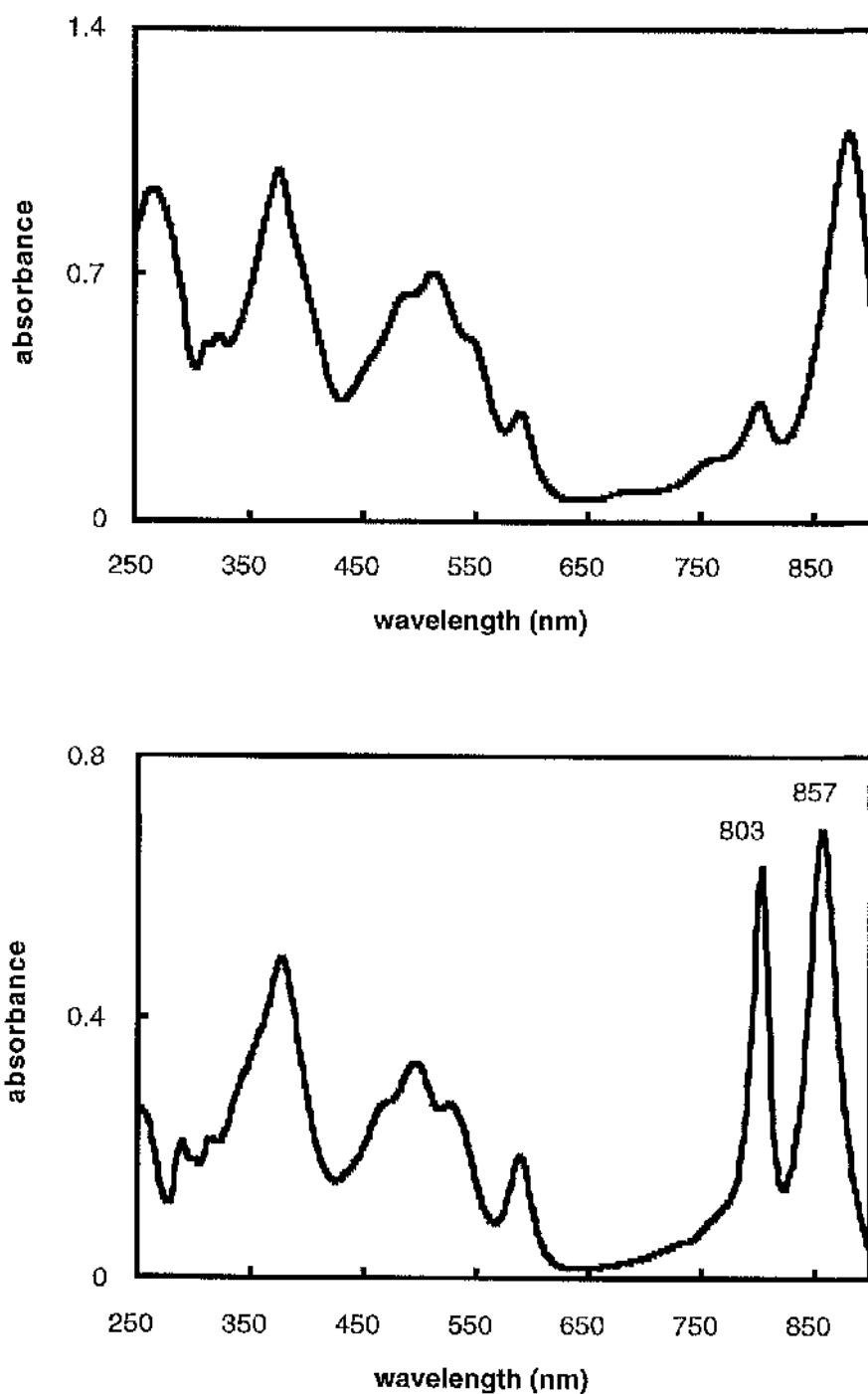


Figure 4.22. Absorption spectra of the LH1-RC (top) and LH2 (bottom) pigmented bands from the sucrose density gradient centrifugation of LDAO solubilised chromatophores of *Chr. vinosum* strain D. The LH1-RC sample was diluted 4-fold and LH2 10 fold with 20mM Tris-HCl, pH8.0, prior to measurement of the spectra.

Table 4.5. Purification table for the LH1-RC core complex of *Chr. vinosum* strain D. The values represent the arithmetical mean and standard deviation of measurements from a sample size of $n = 8$. Cultures were grown in 10 L batches.

Purification step	Volume (ml)	OD ₈₇₈ * (cm ⁻¹)	A ₈₇₈ :A ₂₈₀ *	ODV	% yield of core
Solubilisation of photosynthetic membranes	72.5 ± 2.5	50 ± 6	0.74 ± 0.09	3625	-
Sucrose gradient centrifugation	63.5 ± 1.5	9.14 ± 0.36	1.31 ± 0.17	580	100
Anion exchange chromatography	22 ± 2	21.4 ± 5.6	1.72 ± 0.25	470	87
Gel filtration chromatography	34 ± 4.7	7.49 ± 0.59	2.11 ± 0.07	255	44

* The OD of photosynthetic membranes was measured at the NIR absorption maximum which was located at 858nm.

B800-850 type of LH2 complex. The mean A₈₅₈:A₂₈₀ ratio of the solubilised chromatophores was 0.74 (Table 4.5).

As with the other LH2-containing species studied, two well defined pigmented bands formed upon sucrose gradient centrifugation of the solubilised chromatophores (section 2.4.2). The spectra of the bands are

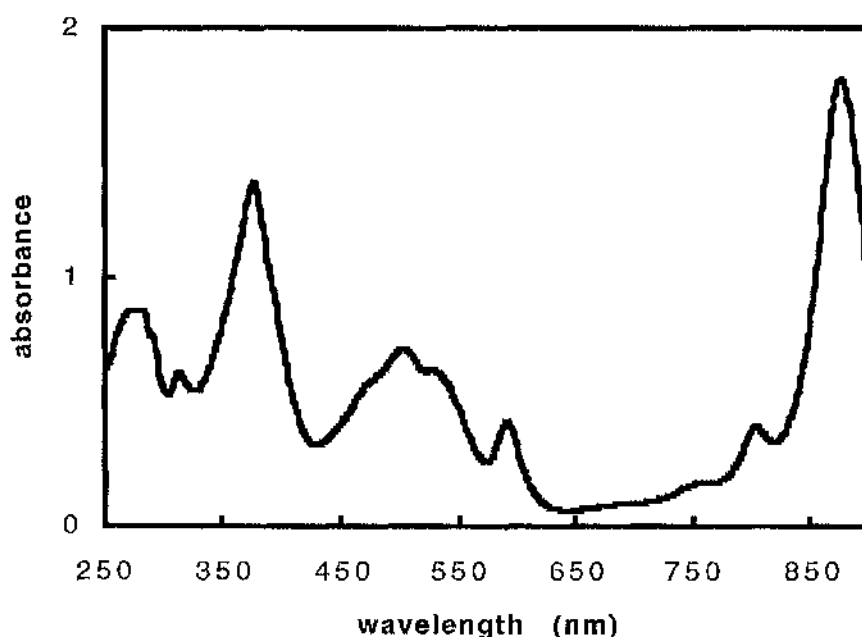


Figure 4.23. Absorption spectrum of fully purified LH1-RC core complex from *Chr. vinosum* strain D. The intense LH1 antenna Bchl *a* absorption band is located at 878nm. The small peaks at 801nm and 760nm are attributable to the RC Bchl *a* and RC bacteriopheophytin, respectively. The Bchl *a* Q_x transition gave rise to the absorption peak at 590nm. The Soret band is located at 370nm. The carotenoids, of which spirilloxanthin is the major component in the *Chr. vinosum* core complex, absorbed between 450-550nm. The lack of an obvious peak at 680nm, which is usually associated with an oxidised breakdown product of Bchl *a*, indicated the core complex was relatively stable during purification. The $A_{878}:A_{280}$ ratio of this core complex sample was 2.2. The sample was diluted 4-fold prior to recording of the spectrum.

shown in Figure 4.22. The spectrum of the lower, LH1-RC-containing band shows a single strong NIR absorption peak located at 878nm and a smaller peak at 801nm. The absorption at ~760nm came from the RC bacteriopheophytin. The absorption spectrum of the upper, LH2-containing band shows two strong peaks located at 857nm and 803nm. This confirmed

that, under the growth conditions employed, the *Chr. vinosum* cells synthesised a B800-850 type of LH2 complex. The remaining features of both spectra closely resemble each other with only slight differences in the 450-550nm region. These differences can be explained by the fact that the LH1-RC core complex has spirilloxanthin as the major carotenoid (Thornber, 1970), whereas the LH2 complex has lycopene as its major carotenoid (Schmidt *et al.*, 1965). This A₈₇₈:A₂₈₀ ratio at this stage of the purification process was ~1.3 (Table 4.5).

The 280nm elution profile of the core complex from the anion exchange chromatography column displayed a single, sharp peak. The peak fractions with a A₈₇₈:A₂₈₀ ratio ≥ 1.7 were pooled. As can be seen from Table 4.5, there was very little loss of core complex from this stage of the purification process but there was an increase in the A₈₇₈:A₂₈₀ ratio from 1.31 to 1.72.

The pooled LH1-RC complex fractions from the anion exchange column were subjected to a final purification by gel filtration chromatography, as described in section 2.4.4. The absorption spectrum of a sample of fully purified core complex from *Chr. vinosum* strain D is shown in Figure 4.23. The A₈₇₈:A₂₈₀ ratio of the complex increased to a mean of 2.11 after this purification step. This represented a ~24% increase in purity over the anion exchange chromatography stage. The final yield of core complex, assuming 100% recovery from the sucrose gradients, was ~44% (Table 4.5). The relatively large yield compared to the other LH2-containing species studied was indicative of the stability of this core complex during purification.

4.7. *Rhodospirillum rubrum* strain S1

Rs. rubrum S1 is an example of a "core only" producing species of

Table 4.6. Purification table for the LH1-RC core complex of *Rs. rubrum* strain S1. The values represent the arithmetical mean and standard deviation of measurements from a sample size of $n=5$. Cultures were grown in 10 L batches.

Purification step	Volume (ml)	OD ₆₇₅ (cm ⁻¹)	A ₈₇₅ :A ₂₈₀	ODV	% yield
Solubilisation of photosynthetic membranes	47.7 ± 13.8	50 ± 2	0.48 ± 0.13	2385	100
Anion exchange chromatography	45 ± 4	30.9 ± 6.6	1.35 ± 0.17	1390	58
Gel filtration chromatography	13 ± 2.5	28.3 ± 4.6	1.86 ± 0.15	368	15

purple non sulphur bacteria that possess LH1 as their only antenna complex (see Zuber & Cogdell, 1995). As *Rs. rubrum* does not produce LH2, the protocol for the isolation and purification of the LH1-RC core complex was simplified by the omission of the sucrose gradient step.

Rs. rubrum cells were grown under high light conditions (150 μmols/s/m²) at a temperature of 28±2°C in 10L flasks of C-succinate medium. The cells grew vigorously under these conditions and were

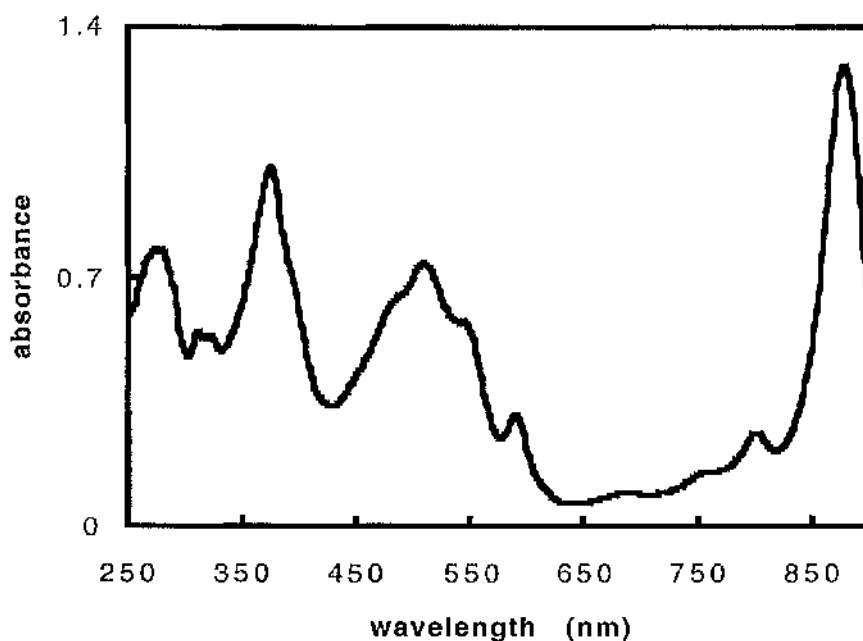


Figure 4.24. Absorption spectrum of fully purified LH1-RC core complex from *Rs. rubrum* strain S1. The spectrum shows an intense NIR absorption band located at 875nm with a smaller band located at 802nm. The $A_{875}:A_{280}$ ratio of this particular sample was 1.7. The sample was diluted 20-fold with 20mM Tris-HCl, pH8.0, 0.1% (v/v) LDAO prior to recording of the spectrum.

harvested after 24 hours (section 2.2). Like *Chr. vinosum*, *Rs. rubrum* cells contain a vesicular intracytoplasmic membrane system that yields chromatophores when the cells are disrupted by passage through a French press (Niederman & Gibson, 1978). Chromatophores were prepared as described in section 2.3 and diluted with 20mM Tris-HCl, pH8.0, to give an OD at the NIR absorption maximum of 50 cm^{-1} . The chromatophores were then solubilised by the addition of 0.5% (v/v) LDAO (Dawkins *et al.*, 1988). This stage of the purification process yielded a mean of ~47ml of chromatophores that had an $A_{875}:A_{280}$ ratio of 0.48 (Table 4.6).

Anion exchange chromatography of solubilised chromatophores produced a 58% yield of core complex (Table 4.6). The relatively low yield was due to a combination of: (i) the lability of the core in detergent (Gingras & Jolchine, 1969; Wang & Clayton, 1973), and; (ii) the fact that only the core fractions from the peak of the elution profile were pooled. The pooled fractions were subjected to further purification by gel filtration chromatography (section 2.4.4).

The absorption spectrum of spectroscopically pure core complex from the gel filtration column is shown in Figure 4.24. The spectrum is in agreement with those previously published (Garcia *et al.*, 1966; Chang *et al.*, 1990) and shows a single strong NIR peak located at 875nm. The smaller NIR peaks at 802nm and 760nm were representative of absorption by RC Bchl *a* and bacteriopheophytin, respectively. There is a small absorption band located at ~680nm which can be attributed to an oxidised breakdown product of Bchl *a*. This again indicated that some degradation of the core complex may have occurred during purification. *Rs. rubrum* strain S1 core complex contains spirilloxanthin as its major carotenoid and this absorbed between 450-550nm.

The final stage of the purification process resulted in an $A_{875}:A_{280}$ ratio of 1.86. The $A_{875}:A_{800}$ ratio was 4.9 (Table 4.9). There was a 15% yield of core complex from the solubilisation of chromatophores from 10L of bacteria (Table 4.6).

4.8. *Rhodobium marinum* strain DSM 2698

Rh. marinum DSM 2698 is another example of a "core only" purple bacterium (Meckenstock *et al.*, 1992a). This marine species, first described by

Imhoff (1983) and formerly named *Rps. marina*, was grown anaerobically under high light conditions ($150\mu\text{mol/s/m}^2$) at a temperature of $28\pm 2^\circ\text{C}$ in DSM-27 *Rhodospirillaceae* medium which was supplemented with 3% NaCl (section 2.1.2). As the cultures grew slowly in small volumes of media, a 20L flask of medium was heavily inoculated with cells and incubated for 5 days before harvesting. *Rh. marinum* was a convenient species to study as the RC can be dissociated from its B880 antenna complex. The results of the isolation and purification of the B880 complex are presented in section 4.9.

Cells were harvested and disrupted as described in sections 2.2 and 2.3. The resulting photosynthetic membrane fragments were adjusted to an OD_{880} of 50 cm^{-1} and solubilised by the addition of 1% (v/v) LDAO. The absorption spectrum of the solubilised PSM's (Fig.4.25) shows an intense NIR peak at 880nm and two smaller peaks at 796nm and 750nm. The Bchl *a* Q_x transition appears as a peak at $\sim 590\text{nm}$ and the Soret band is located at $\sim 370\text{nm}$. There is a shoulder to the red of the Soret band which belongs to cytochromes (Meckenstock *et al.*, 1992a). The carotenoids absorb between $\sim 460\text{-}560\text{nm}$. There are no traces of free Bchl *a*, which would appear as a peak at 777nm. This stage of the purification process yielded $\sim 108\text{ml}$ of solubilised PSM's with an OD_{880} of 50 cm^{-1} from 20L of culture. The mean $A_{880}:A_{280}$ ratio was 0.86 (Table 4.7).

As *Rh. marinum* is a "core only" species, it was not necessary to separate the core complex from unwanted peripheral complexes. Therefore, the sucrose density gradient step of the purification protocol was omitted and the solubilised membranes applied to an anion exchange column. The spectroscopically pure fractions eluted from the column were pooled. This purification step increased the purity of the sample, as measured by the $A_{879}:A_{280}$ ratio, to 1.65. The recovery of the complex after anion exchange

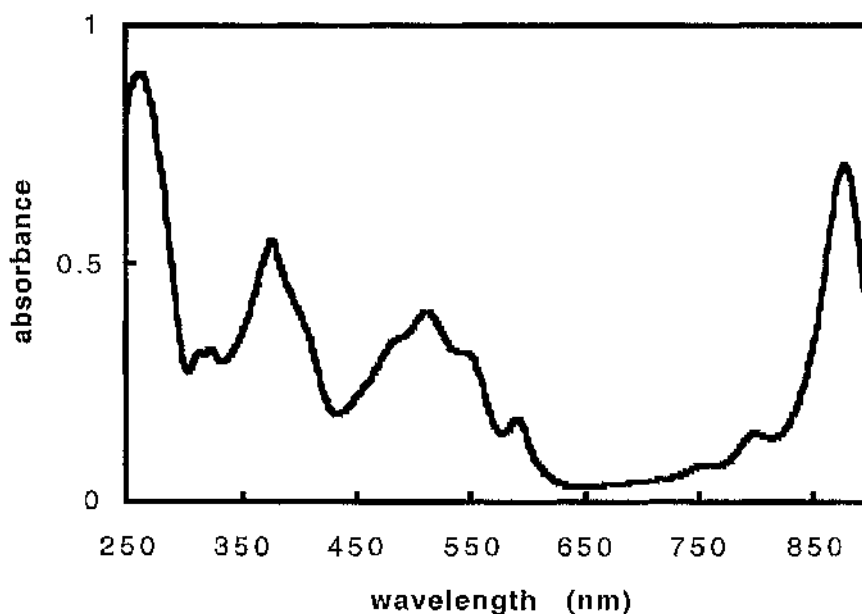


Figure 4.25. Absorption spectrum of LDAO solubilised PSM's from *Rh. marinum* DSM 2698. The spectrum shows a strong NIR absorption peak at 880nm and smaller peaks at 796nm and 750nm. The protein absorbance at 280nm is very intense. The ratio of the 880nm:280nm absorbance in this sample is 0.8. The sample was diluted about 65-fold with 20mM Tris-HCl, pH8.0 prior to recording the spectrum.

chromatography was 20% (Table 4.7). The large loss of complex from this stage of the purification process arose because only the fractions from the elution profile peak were retained for further purification.

Final purification by gel filtration chromatography (section 2.4.4) resulted in an 8.5% yield of core from the solubilised PSM's from 20L of bacterial culture. The yield of spectroscopically pure core complex was much lower than that of the other "core only" species studied, *Rs. rubrum*, and may indicate that the *Rh. marinum* core complex was less stable. The $A_{879}:A_{280}$ ratio increased to 1.86 upon gel filtration (Table 4.7). The $A_{879}:A_{796}$ ratio of the fully purified complex was ~4.9 (Table 4.9).

Table 4.7. Purification table for the LH1-RC core complex of *Rh. marinum* strain DSM 2698. The values represent the arithmetical mean and standard deviation of measurements from a sample size of $n=3$. Cultures were grown in 20 L batches.

Purification step	Volume (ml)	OD ₈₇₉ (cm ⁻¹)	$\Lambda_{879}:\Lambda_{280}$	ODV	% yield of core
Solubilisation of photosynthetic membranes	108 ± 18	50 ± 3	0.86 ± 0.19	5400	100
Anion exchange chromatography	48 ± 6	30.9 ± 4.2	1.65 ± 0.18	1483	27
Gel filtration chromatography	17.5 ± 4.8	26.1 ± 3.9	1.86 ± 0.13	457	8.5

The absorption spectrum of the fully purified core complex is shown in Figure 4.26. The spectrum closely resembled that of the solubilised membranes (Fig. 4.25), with absorption peaks at 879nm (LH1 antenna Bchl *a*'s), 797nm and ~750nm (RC Bchl *a* and bacteriopheophytin, respectively), ~590nm (Bchl *a* Q_x transition), ~370nm (Soret band) and between 450-550nm (carotenoids).

4.9. *Rhodobium marinum* DSM 2698 B880 complex

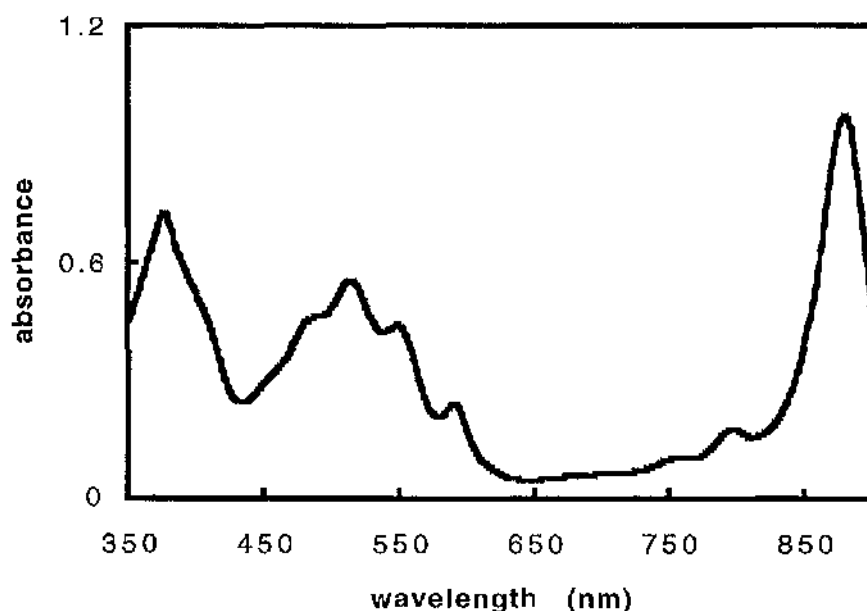


Figure 4.26. Absorption spectrum of fully purified LH1-RC core complex from *Rh. marinum* DSM 2698. The NIR absorption maximum is located at 879nm. The complex was diluted about 25-fold with 20mM Tris-HCl, pH8.0, 0.1% (v/v) LDAO prior to the spectrum being measured.

The *Rh. marinum* core complex was unique among the others investigated in this thesis in that the RC polypeptides could be totally dissociated to leave the intact LH1 (or B880) complex (Meckenstock *et al.*, 1992a).

The purification protocol for the B880 complex was based on a combination of those described by Meckenstock *et al.*, (1992a) and Dawkins *et al.*, (1988). Cells were grown, harvested and photosynthetic membranes prepared as described in sections 2.1.2, 2.2 and 2.3, respectively. The membranes were adjusted to an OD_{880} of 50 cm^{-1} and solubilised by the addition of 1% (v/v) LDAO. After undergoing dialysis against 20mM Tris-

Table 4.8. Purification table for the LH1(B880) complex of *Rh. marinum* strain DSM 2698. The values represent the arithmetical mean and standard deviation of measurements from a sample size of $n=5$. Cultures were grown in 20 L batches.

Purification step	Volume (ml)	OD ₈₈₀ * (cm ⁻¹)	A ₈₈₀ :A ₂₈₀ *	ODV	% yield of B880
Solubilisation of photosynthetic membranes	105 ± 23	49 ± 3	0.92 ± 0.22	5145	100
Ammonium sulphate precipitation	60.3 ± 7.6	18.3 ± 0.28	1.68 ± 0.40	1103	21
Anion exchange chromatography	31.5 ± 0.5	14.0 ± 2.7	1.74 ± 0.30	441	8.6
Gel filtration chromatography	15.06 ± 2.49	5.38 ± 2.09	1.84 ± 0.45	81	1.6

HCl, pH8.0, containing 0.1% (v/v) LDAO the OD₈₈₀ of the membranes was adjusted to 100 cm⁻¹. The concentrated sample was mixed in a volume ratio of 1:1 with 3.5M (NH₄)₂SO₄ solution to remove the RC from its LH1 antenna. After stirring for 2 hours the mixture was centrifuged and the supernatant, which contained the B880 complex, was dialysed for 24 hours

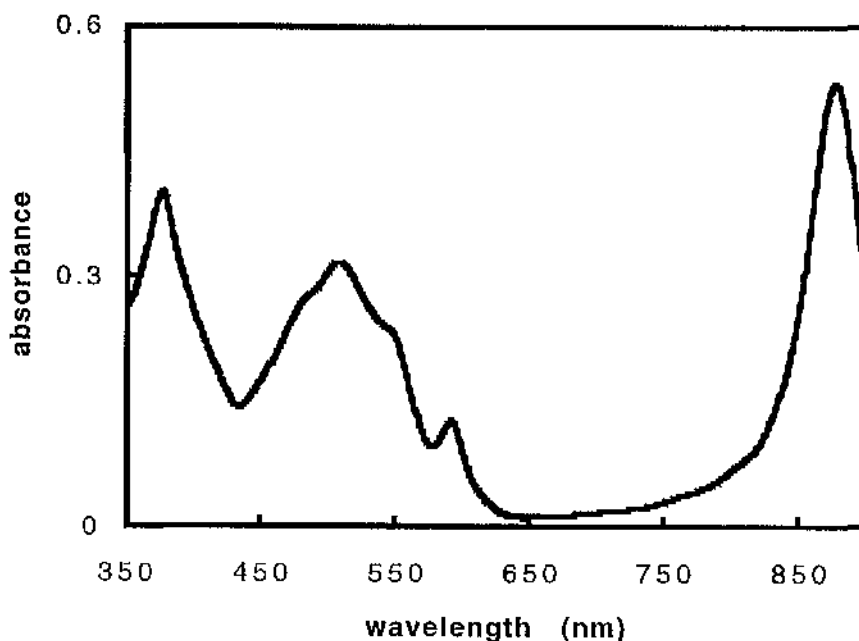


Figure 4.27. Absorption spectrum of fully purified B880 (LH1-only) complex from the purple bacterium *Rh. marinum* DSM 2698. The spectrum shows a single NIR peak located at 880nm. The presence of RC or cytochromes is not detectable from this spectrum. The sample was diluted 10-fold in 20mM Tris-HCl, pH8.0, 0.05% LDAO prior to the spectrum being measured.

against 20mM Tris-HCl, pH8.0, containing 0.05% LDAO. The success of $(\text{NH}_4)_2\text{SO}_4$ precipitation at removing the RC was monitored by absorption spectroscopy of the B880-containing supernatant. The absorption spectrum did not exhibit the $\sim 800\text{nm}$ and $\sim 760\text{nm}$ absorption peaks associated with RC (Fig. 4.27). The $A_{880}:A_{280}$ ratio at this stage of the purification process was 1.68. The yield of B880 was 21% (Table 4.8). The large loss of B880 from this stage of the purification process was probably due to a combination of general protein denaturation and the inability of the ammonium sulphate treatment to remove the RC from its associated antenna in all of the

sample.

The dialysed B880 complex was loaded onto a DEAE-cellulose anion exchange column and eluted stepwise with a 50-250mM NaCl gradient. The yield of B880 from anion exchange chromatography was 8.6% and the $A_{880}:A_{280}$ ratio was 1.74 (Table 4.8).

The isolated B880 complex was photosensitive. Photooxidation of the B880 Bchl *a*'s was revealed by a decrease in the intensity of the 880nm absorption peak when the complex was exposed to light (refer to Chapter 6). Therefore, care was taken to ensure that the anion exchange and subsequent stages of the purification process were performed under low illumination.

In Superdex 200 (prep grade) gel filtration chromatography the B880 complex eluted in a single peak. The absorption spectrum of the spectroscopically pure peak fractions is shown in Figure 4.27. The spectrum shows a single NIR absorption band, due to the B880 Bchl *a*, at 880nm. The absorption bands associated with the presence of RC (~800nm and ~760nm) or cytochromes (a shoulder at ~405nm on the Soret band) were not detectable, indicating the successful removal of the RC during purification. The other features of the spectrum resembled those of the *Rh. marinum* LH1-RC core complex with a peak at ~590nm (Bchl *a* Q_x transition), ~370nm (Soret band), and triple peaks (due to carotenoids) between ~450-550nm.

The $A_{880}:A_{280}$ ratio of B880 after gel filtration was 1.84 and the final recovery of pure B880 from 20L of bacterial culture was 1.6% (Table 4.8). The low recovery was probably due to a combination of the harshness of the ammonium sulphate precipitation, the photosensitive nature of the isolated B880 complex and protein denaturation during the latter stages of the purification. However, the fully purified complex was stable for at least two months when maintained in the dark at 4°C. This observation was

LH1-RC core

Table 4.9. Summary of the ratios of the NIR absorption maximum to the protein absorption peak at 280nm and the RC absorption peak near 800nm. The values are presented as the arithmetical mean \pm the standard deviation of the ratios from sample size, n . The ratios for the 7750 and 7050 strains of *Rps. acidophila* fell within the ranges presented for strain 10050. The ratios for the 1a1 strain of *Rps. palustris* and strain DSM 151 of *Rv. gelatinosus* fell within the range of values presented for the French and DSM 149 strains of these species.

Species	$A_{\text{NIR max}}:A_{280}$	$A_{\text{NIR max}}:A_{800}$	n
<i>Rps. acidophila</i> 10050	2.03 \pm 0.24	4.4 \pm 0.6	26
<i>Rps. palustris</i> French	2.13 \pm 0.11	4.2 \pm 0.7	8
<i>Rps. cryptolactis</i>	2.19 \pm 0.02	4.2 \pm 0.5	5
<i>Rv. gelatinosus</i> DSM 149	1.55 \pm 0.20	5.0 \pm 0.4	4
<i>Chr. vinosum</i> strain D	2.11 \pm 0.07	4.3 \pm 0.5	8
<i>Rs. rubrum</i> strain S1	1.86 \pm 0.15	4.9 \pm 0.3	5
<i>Rh. marinum</i> DSM 2698	1.84 \pm 0.45	4.9 \pm 0.4	3

consistent with that of Meckenstock *et al.*, (1992a).

The results presented in this chapter show that it is possible to isolate and purify, in the presence of the detergent LDAO, the LH1-RC core complex from a range of photosynthetic bacteria. In most of the species studied the core complex was stable enough to allow it to be used for further

spectroscopic studies and 3-D crystallisation trials. However, the core complex from species such as *Rv. gelatinosus* was found to be very unstable when isolated in LDAO. In these cases the inherent instability of the core hampered further characterisation (see the discussion in Chapter 9).

CHAPTER FIVE

CIRCULAR DICHROISM SPECTROSCOPY OF THE LH1-RC CORE COMPLEXES

5.1. Circular dichroism (CD) spectroscopy of the LH1-RC core complexes

Circular dichroism (CD) is the differential absorption of the left and right circularly polarised components of electromagnetic radiation. The CD effect is observed when chromophores are chiral, either inherently or because they are located in an asymmetric environment (reviewed in Price, 1995). As both these cases apply to the Bchl's of the purple bacterial light-harvesting complexes and RC's, CD provides a useful tool for obtaining information on both the environment around the Bchl's and Bchl-Bchl interactions (Sauer, 1972; Sauer, 1975; Gregory, 1977; Cogdell & Scheer, 1985).

Previous CD investigations have focused on the Bchl *a* containing membranes, membrane fractions, RC's or peripheral antennae from *Rb. sphaeroides* (Steffen & Calvin, 1970; Phillipson & Sauer, 1973; Bolt *et al.*, 1981; Clayton & Clayton, 1981; Kramer *et al.*, 1984; Miyazaki *et al.*, 1979; Koolhaas *et al.*, 1998), *Rps. capsulata* (Bolt *et al.*, 1981), *Rps. palustris* (Hayashi *et al.*, 1982; Miyazaki & Morita, 1981), *Chr. vinosum* (Hayashi *et al.*, 1981; Miyazaki & Morita, 1981; Cogdell & Scheer, 1985), *Rps. acidophila* (Cogdell & Scheer, 1985; Alden *et al.*, 1997) and *Rs. rubrum* (Sauer & Austin, 1978). However, little detailed CD work has been performed with the isolated LH1-RC core or B880 complexes of the purple bacteria, some exceptions being the core complexes of *Rps. palustris* (Hayashi *et al.*, 1982), *Chr. purpuratum* (Kerfeld *et al.*, 1994) and *Rps. cryptolactis* (Halloren *et al.*, 1995), the B880 (B875) complexes from *Rps. acidophila*, *Rs. rubrum* (Cogdell & Scheer, 1985), *Rh. marinum* (Meckenstock *et al.*, 1992a) and *Rv. gelatinosus* (Jiraskova & Reiss-Husson, 1993), and reconstituted LH1 from *Rb. sphaeroides* and *Rs. rubrum* (Davis *et al.*, 1995).

In general, the theory does not yet exist to allow the prediction of structure from CD spectra. However, CD spectra are sensitive to structural

changes. Therefore, CD spectroscopy can provide an indirect method by which the structural integrity and stability of isolated core complexes can be monitored. This chapter presents CD data, covering the range from 280nm to 950nm, on purified LH1-RC core complexes from nine different species and strains of purple photosynthetic bacteria.

LH1-RC core complexes were prepared and purified as described in Materials and Methods (Chapter 2). Room temperature CD spectra were measured with the help of Drs. N.C. Price and S.M. Kelly at the BBSRC Circular Dichroism Facility, University of Stirling, U.K., using a Jasco J-600 spectropolarimeter as described in section 3.4. The core complexes were solubilised in 20mM Tris-HCl, pH8.0, 0.1% (v/v) LDAO. The OD at the NIR absorption maximum was between 1-5 cm^{-1} for the measurements. The relative anisotropies and position of the CD bands related to the Bchl's and carotenoids of each core complex are summarised in Table 5.1. The relative anisotropies were defined as the ratios of the circular dichroism, ΔA (expressed as the difference in absorbance, $\Delta A = A_L - A_R$) at the wavelengths indicated in parentheses, and the absorption at the NIR maximum ($A_{\text{max, NIR}}$) multiplied by 10^3 (Cogdell & Scheer, 1985). Because the CD spectra presented here were expressed in terms of ellipticity, θ (in millidegrees), the simple numerical relationship between ΔA and θ , namely:

$$\theta = 32.98\Delta A$$

where θ is in degrees, was used to convert the ellipticity values to ΔA values (Price, 1995). The absorbance measurements were performed using 1cm pathlength cuvettes. The CD measurements were performed using 0.5cm pathlength cells. Therefore, the optical density of each core complex

sample at the NIR absorption maximum was divided by 2 to correct for the difference in pathlength.

5.2. *Rhodopseudomonas acidophila* strain 10050 core complex

The room temperature CD spectrum of *Rps. acidophila* 10050 core complex is shown in Figure 5.1. The CD spectrum is qualitatively similar to that previously reported for *Rps. acidophila* strain 7750 core (Cogdell & Scheer, 1985). In the NIR range the spectrum exhibits a pair of non-conservative double CD signals (or couplets) with peaks at 883nm and 798nm, and troughs at 818nm and 913nm. The shorter wavelength couplet, with a zero-crossing point at 808nm, corresponds to RC Bchl *a* Q_y transition (Sauer *et al.*, 1968) and is only moderately anisotropic (Table 5.1). The long wavelength couplet, which has a zero-crossing point at 896nm and corresponds to the 885nm peak in the absorption spectrum (Fig. 4.8), is attributable to the Q_y transition of the LH1 antenna Bchl *a*. The 883nm lobe has a shoulder at ~860nm which belongs to the RC special pair (Phillipson & Sauer, 1973).

In all the species investigated here the NIR CD signals were different from the CD spectrum of Bchl's in organic solvents (Sauer *et al.*, 1968). In aqueous solution, monomeric Bchl gives a weak negative CD signal, whereas dimeric or aggregated Bchl's give rise to a double CD signal (Davidov, 1971; Scherz *et al.*, 1991). Therefore, the positive and negative waves displayed by the long wavelength NIR CD band of the spectrum in Figure 5.1 indicate that the Bchl *a* molecules which contribute to this signal are strongly exciton coupled (Sauer, 1975; Cogdell & Scheer, 1985). Some of the signal is also due to the asymmetric environment in which the Bchl's are located (Gregory, 1977).

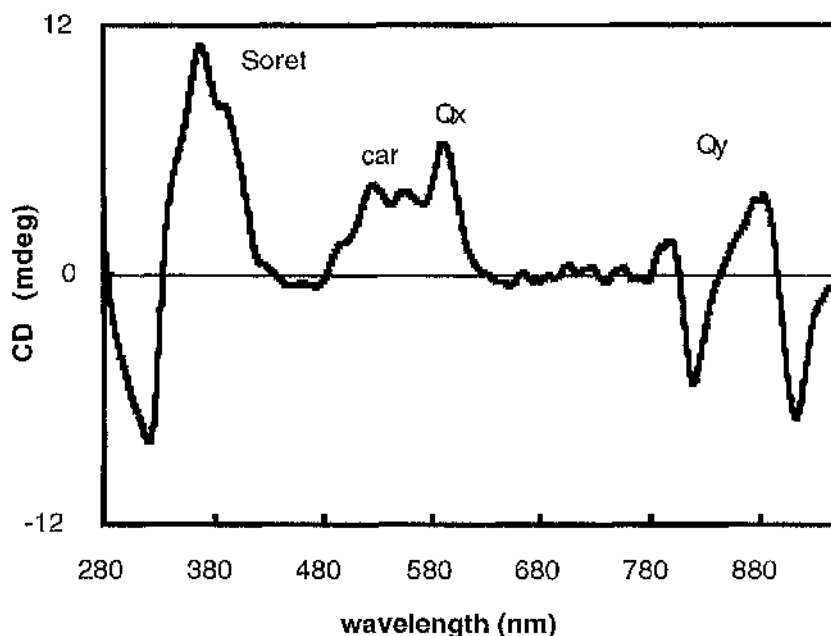


Figure 5.1. CD spectrum of the LH1-RC complex from *Rps. acidophila* strain 10050. The complex was suspended in 20mM Tris-HCl, pH8.0, 0.1% (v/v) LDAO and the OD of the sample at the NIR absorption maximum was 1.0 cm^{-1} . The spectrum was recorded in a 0.5cm pathlength cell and was baseline corrected. The CD signals due to the Bchl Q_y , Q_x and Soret transitions, and carotenoids (car) are indicated.

In the visible region of the spectrum there is a positive CD band centred at 591nm which corresponds to the Bchl a Q_x transition. The Bchl a Soret region shows an intense double CD signal, positive at 368nm and negative at 321nm. This CD signal is non-conservative with a net positive sign. There is a distinct shoulder to the red of the 368nm lobe which is probably due to RC-bound cytochrome. The amplitude of the positive lobe of the Soret band is about twice as intense as that of the 883nm Bchl a Q_y band. The carotenoid related CD signals are located between 480-570nm. These well defined, moderately intense signals are strongly non-conservative

Table 5.1. Summary of the results of the analysis of CD spectra of the LH1-RC core complex isolated from a range of purple bacteria.

Species	NIR absorption maximum (nm)	Relative anisotropies ¶ and positions (nm) of CD bands related to:	
		Bacteriochlorophylls	Carotenoids
<i>Rps. acidophila</i> 10050	885	+0.21¶¶ (898) +0.10¶¶ (808) +0.38 (591) -0.49 ¶¶(333)	+0.23 (552) +0.23 (527)
<i>Rps. palustris</i> strain French	878	+0.28¶¶ (889) +0.20¶¶ (810) +0.25 (590) -0.57¶¶ (325)	+0.22 (530)
<i>Rps. palustris</i> strain 1a1	877	+0.31¶¶ (882) +0.20¶¶ (811) +0.26 (590) -0.62¶¶ (327)	+0.12 (568) +0.21 (531)
<i>Rps. cryptolactis</i>	877	+0.32¶¶ (883) +0.18¶¶ (810) +0.30 (590) -0.63¶¶ (330)	+0.17 (554) +0.16 (536)
<i>Rv. gelatinosus</i> DSM 149	877	+0.31¶¶ (873) +0.17¶¶ (807) +0.31 (591) +0.45 (348)	+1.01 (512) +0.47 (482)
<i>Rv. gelatinosus</i> DSM 151	877	+0.15¶¶ (882) +0.19¶¶ (806) +0.31 (589) +0.44 (349)	+1.00 (512) +0.42 (484)
<i>Chr. vinosum</i> strain D	878	+0.29¶¶ (887) +0.17¶¶ (812) +0.21 (590) -0.28¶¶ (327)	+0.15 (556) +0.13 (512)

Species	NIR absorption maximum (nm)	Relative anisotropies ¶ and positions (nm) of CD bands related to:	
		Bacteriochlorophylls	Carotenoids
<i>Rs. rubrum</i> strain S1	875	+0.21 ^{¶¶} (896)	+0.22 (557)
		+0.06 ^{¶¶} (804)	+0.11 (526)
		+0.24 (589)	
		-0.57 ^{¶¶} (323)	
<i>Rh. marinum</i> DSM 2698	879	+0.12 ^{¶¶} (896)	+0.08 (560)
		+0.15 ^{¶¶} (823)	+0.03 (529)
		+0.16 (590)	
		-0.34 ^{¶¶} (393)	

¶ Relative anisotropies are defined as the ratios of the circular dichroism at the wavelength indicated in brackets and the absorption at the NIR maximum of the core complex, multiplied by 10^3 . The wavelengths in brackets correspond to the CD peaks/troughs (absorption-like CD signals), or zero crossings (S-shaped CD bands).

¶¶ S-shaped CD band. The sign is positive if the shorter wavelength lobe is positive.

with a net positive sign. The ellipticity ratio of the bands at 552 and 527nm is 1. This is in accord with the ellipticity ratio of the same bands in the corresponding CD spectrum of *Rps. acidophila* strain 7750 core (Cogdell & Scheer, 1985). Due to their intrinsic symmetry, isolated carotenoids in solution do not normally give rise to CD signals (R.J. Cogdell, personal communication). Therefore, the signals observed in the carotenoid region of the CD spectrum of the core complex must be due to the environment in which the carotenoids are situated. Examination of the 3-D structure of the LH2 complex from *Rps. acidophila* (McDermott *et al.*, 1995; Freer *et al.*, 1996) and *Rs. molischianum* (Koepke *et al.*, 1996) reveals that the carotenoids are twisted on their path through the complex. The RC of the core complex also contains carotenoid (Deisenhofer & Michel, 1989; Arnoux *et al.*, 1989). In the

RC from *Rb. sphaeroides*, the carotenoid spheroidene is bound to the M subunit in a kinked conformation perpendicular to the membrane spanning helices (Yeates *et al.*, 1988; Ermler *et al.*, 1994). A similar twisting or kinking of the carotenoid molecules in the LH1 antenna and RC of the *Rps. acidophila* core complex would therefore give rise to the CD signals exhibited between ~480-580nm in Figure 5.1. The core complexes of the other species investigated here also exhibited carotenoid related CD signals. Therefore, the carotenoids in those core complexes are also most probably twisted or kinked.

5.3. *Rhodopseudomonas palustris* strains French and 1a1 core complexes

The CD spectra of the core complexes of *Rps. palustris* strains French and 1a1 are shown in Figure 5.2. For these measurements the OD of each sample at the NIR absorption maximum was 4.7 cm^{-1} . The CD spectra of both strains are almost identical. They are also very similar to the corresponding spectrum from *Rps. acidophila*. The NIR region of the CD spectra in Figure 5.2 exhibit a pair of non-conservative CD couplets indicative of exciton coupling between Bchl's (Sauer, 1975). The origins of these signals were discussed in the previous section. In the spectrum of core complex from *Rps. palustris* strain French the CD couplets have peaks at 800nm and 867nm and troughs at 818nm and 900nm. In strain 1a1 the long wavelength peak is blue-shifted by 7nm to 860nm. In both cases the longer wavelength couplet has a broad shoulder, which is due to the RC special pair (Phillipson & Sauer, 1973), located to the red of the peak. The intensities of the 800nm peaks are about twice that of the corresponding peak in the *Rps. acidophila* CD spectrum (Table 5.1). For both the *Rps.*

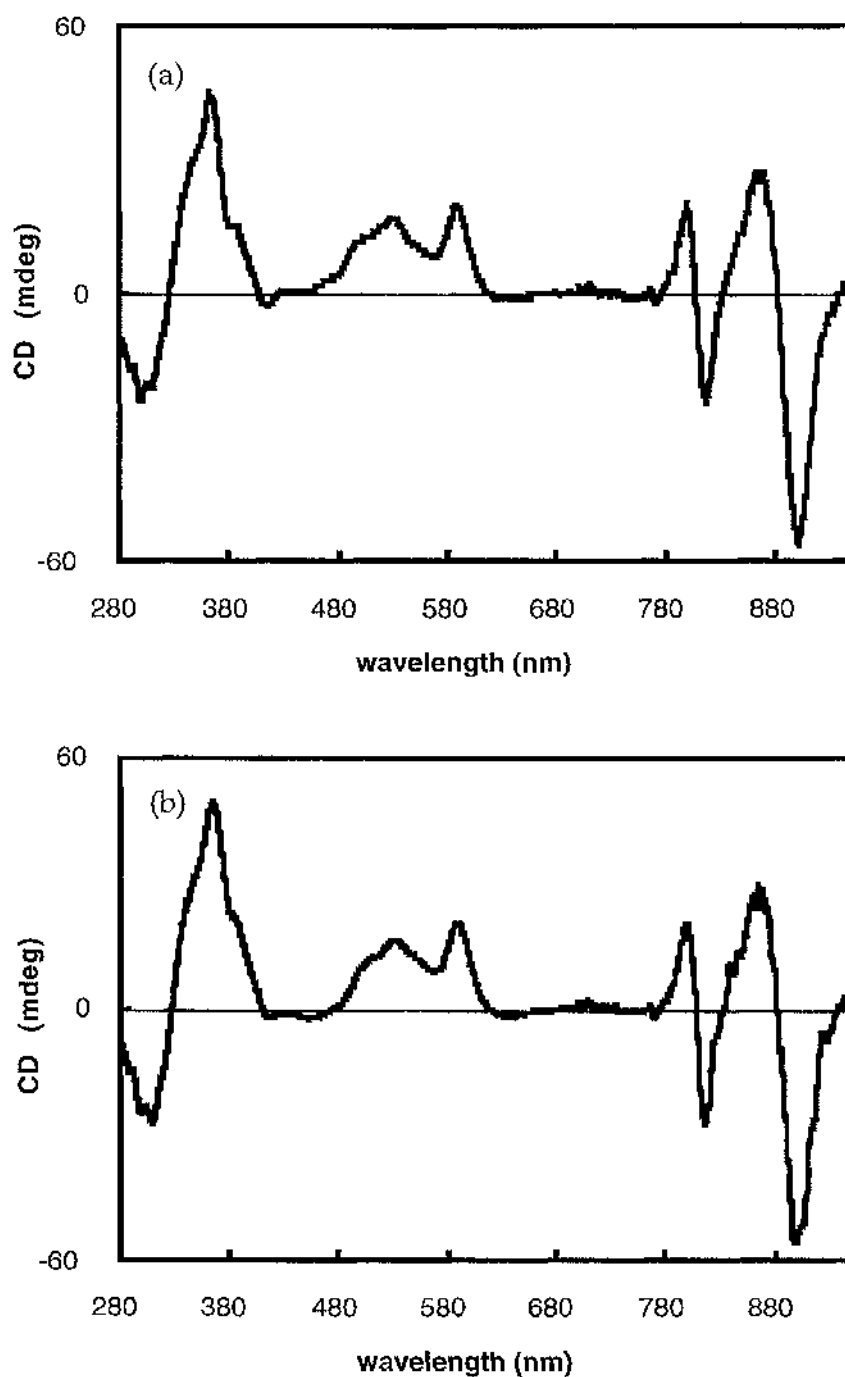


Figure 5.2. CD spectra of the LH1-RC core complex from (a) *Rps. palustris* strain French, and (b) *Rps. palustris* strain 1a1. The OD of each sample was adjusted to 4.7 cm^{-1} . Both spectra were baseline corrected.

palustris strains the ratio of the intensity of the 867 (or 860) nm peak to the 800nm peak was ~1.5 while the ratio of the intensity of the 900nm trough to its 818nm counterpart was ~2. This is at variance with a previously published NIR CD spectrum of the LH1-RC complex of an unknown strain of *Rps. palustris* in which the intensities of the peaks and troughs of both the longer and shorter wavelength NIR couplets were about the same (Hayashi *et al.*, 1982). The lower intensity of both the positive and negative waves of the longer wavelength NIR CD couplet of this spectrum compared to the same couplet of the spectra in Figure 5.2 could simply be due to the fact that different strains were investigated. However, the core complex studied by Hayashi *et al.* (1982) was solubilised in a mixture of SDS and Triton X-100 whereas the complexes investigated here were solubilised in LDAO. Therefore, the differences between the previously reported spectrum (Hayashi *et al.*, 1982) and those presented here could have arisen as a result of the different detergents used to solubilise the complexes.

The absorption spectra of the core complex samples from *Rps. palustris* strains French and 1a1 were measured prior to, and immediately after, recording of the CD spectra. The absorption spectra recorded both before and after the accumulation of CD data were in close agreement with those of the purified core complexes shown in Figures 4.13 and 4.14. This indicated that no denaturation had occurred during the CD measurements. The core complex studied by Hayashi *et al.* (1982) was also shown to be in its native state since the CD spectrum of the intact intracytoplasmic membrane could be generated by the summing of the CD spectra of the isolated core and peripheral complexes.

The visible regions of the *Rps. palustris* core complex CD spectra both show a positive, moderately intense CD band, due to the Bchl *a* Q_x transition, centred at 590nm. This band is not as anisotropic as the

corresponding band of the *Rps. acidophila* core complex CD spectrum (Table 5.1). A broader positive band between ~480-570nm is attributable to the carotenoids of the core complexes. In both strains the structure of the carotenoid CD signal is not as well defined as that of *Rps. acidophila* (Fig. 5.1). This probably reflects a difference in carotenoid composition between the species.

The Bchl *a* Soret region of both spectra show an intense, non-conservative double CD signal with a peak at ~365nm and trough at ~310nm. The zero-crossing occurs at 325nm. A well defined shoulder, probably due to cytochrome, is apparent at ~390nm. The positive lobe of the Soret CD signal is more intense and the negative lobe less intense than those of the corresponding signal in *Rps. acidophila*. The reasons for this are not clear but it may be due to discrete differences in the environment of the Bchl *a* molecules.

5.4. *Rhodopseudomonas cryptolactis* core complex

The CD spectrum of the core complex ($OD_{NIR\ max} = 2.8\ cm^{-1}$) from *Rps. cryptolactis* (Fig. 5.3) is similar to those of the other *Rhodopseudomonas* species studied here and is also in close agreement with one reported previously (Halloren *et al.*, 1995). The NIR region of the spectrum displays a pair of non-conservative CD couplets with peaks at 867nm and 802nm and troughs at 902nm and 819nm. Again, these signals arise from the LH1 antenna and RC Bchl *a*'s (Halloren *et al.*, 1995) and are characteristic of exciton coupled Bchl-Bchl interactions (Sauer, 1975). As was the case with *Rps. palustris* (Fig. 5.2) the ratio of the intensity of the 867nm peak to the 802nm peak was ~1.5 while the ratio of the intensity of the 902nm trough to its 819nm counterpart was ~2. However, in the CD spectrum reported by

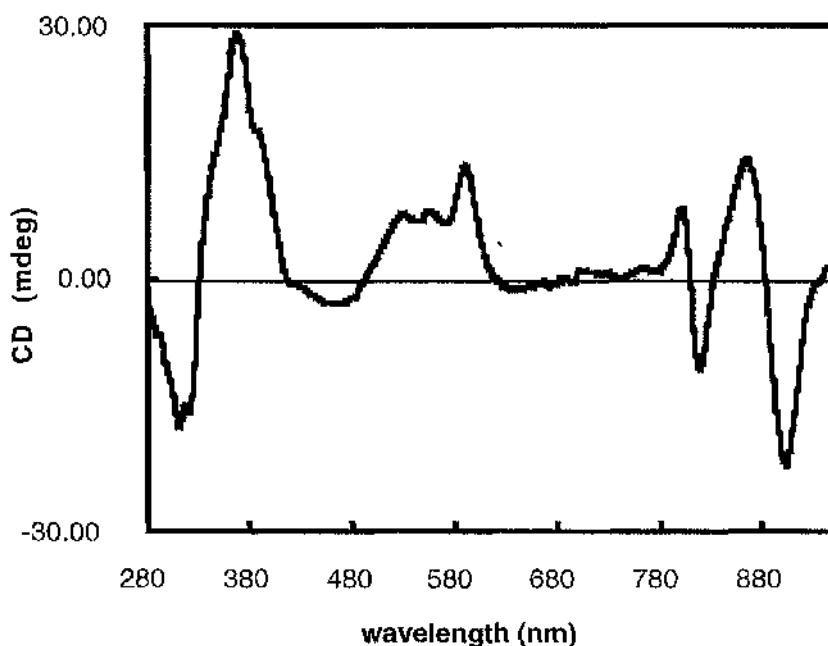


Figure 5.3. Room temperature CD spectrum of the LH1-RC core complex from *Rps. cryptolactis* grown under high-light conditions. The OD of the complex was adjusted to 2.8 cm^{-1} at the NIR absorption maximum by dilution with 20mM Tris-HCl, pH8.0, 0.1% (v/v) LDAO.

Halloren *et al.* (1995) the ratio of the intensity of the 902nm trough to the 810nm trough was ~ 4.5 . The absorption spectrum of the *Rps. cryptolactis* core complex recorded after the CD measurements was quantitatively different from the corresponding spectrum recorded before, in that the amplitude of the 877nm absorption peak (due to LH1 antenna Bchl *a*) had decreased with respect to the amplitude of the 800nm peak. This indicated that some denaturation of the complex had occurred during accumulation of the CD data. Denaturation would cause a change in environment of the Bchl's and this could explain the much lower intensity of the 902nm trough

in the CD spectrum presented here (Fig. 5.3) compared to the same trough in the previously reported CD spectrum (Halloren *et al.*, 1995).

In the visible region of the spectrum, the CD band due to the Q_x absorption of Bchl *a* appears as a well resolved, non-conservative peak centred at 590nm. This peak is equal in intensity to the longer wavelength NIR peak (Table 5.1). The bands due to the carotenoids, of which spirilloxanthin and anhydrorhodovibrin are the major components in this core complex (Halloren *et al.*, 1995), are centred at 554nm and 536nm. These bands, which have equal anisotropy, are non-conservative with a net positive sign. The double CD signal in the Soret region of the spectrum is similar to its *Rps. palustris* counterpart, with an intense positive lobe at 368nm, a negative lobe at 310nm, and a zero-crossing at 330nm. This signal is strongly non-conservative, the positive lobe being nearly twice as intense as the negative lobe. Once again, a shoulder is clearly visible on the longer wavelength side of the positive lobe.

5.5. *Rubrivivax gelatinosus* strains DSM 149 and DSM 151 core complexes

The CD spectra of the LH1-RC core complexes (with an OD at the NIR absorption maximum of 1.6 cm^{-1}) from *Rv. gelatinosus* strains DSM 149 and DSM 151 are shown in Figure 5.4. The CD spectra are similar to each other. However, they are quite different compared to the corresponding spectra of the *Rhodospseudomonas* species investigated even though their absorption spectra are similar (compare Figs. 4.13, 4.17 and 4.20). It has been noted before that Bchl's of pigment-protein complexes from different species may have similar absorption spectra without exhibiting similar CD spectra (Scherz & Parson, 1986; Scherz & Rosenbach-Belkin, 1989).

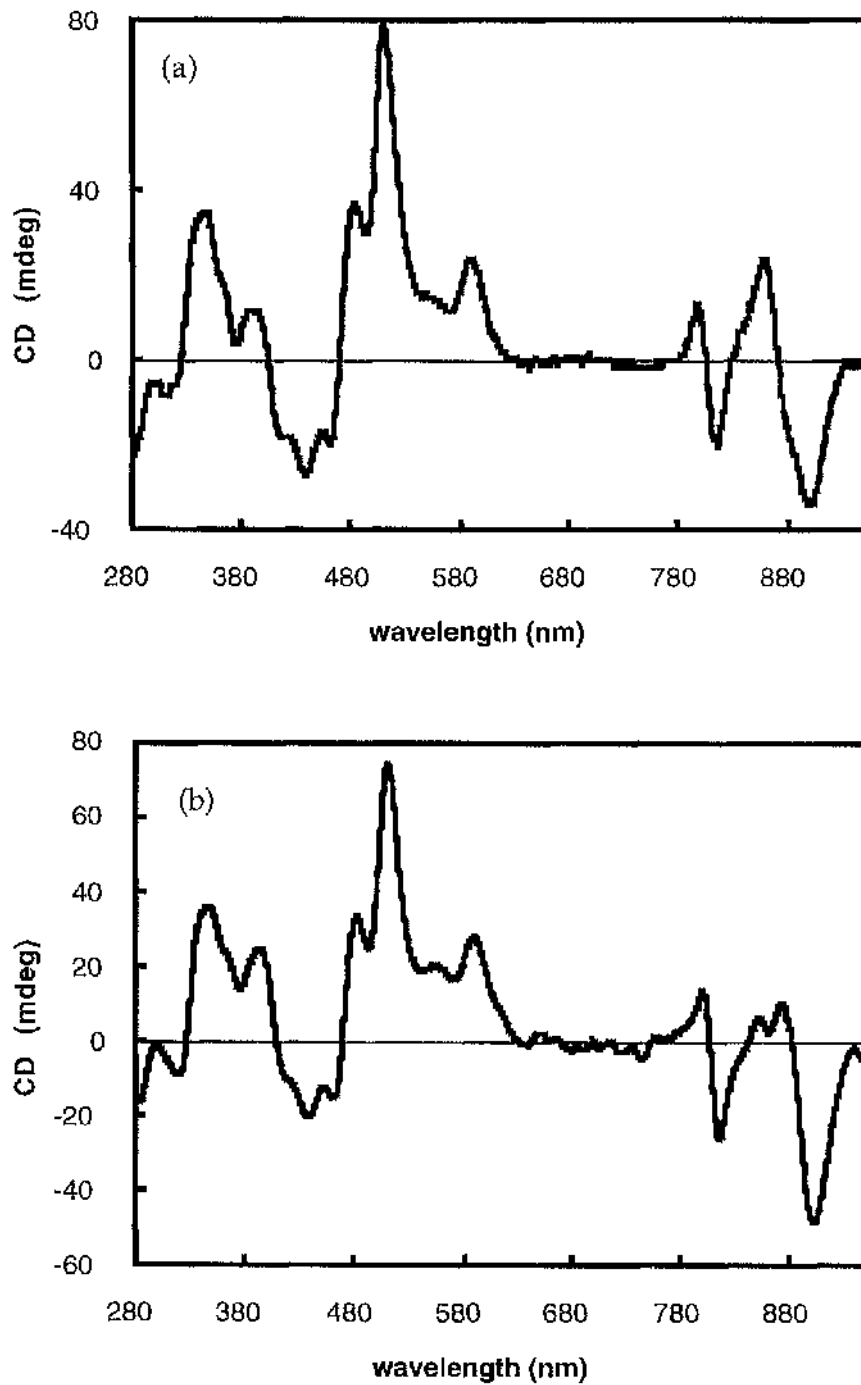


Figure 5.4. CD spectra of the LH1-RC core complex from *Rv. gelatinosus* strains (a) DSM 149, and (b) DSM 151. The CD of each core complex sample at the NIR absorption maximum was 1.6 cm^{-1} . The samples were suspended in 20mM Tris-HCl, pH8.0, 0.1% (v/v) LDAO.

The most striking feature of the *Rv. gelatinosus* core complex CD spectra are the intense, well resolved peaks, located at ~484nm, 512nm and 550nm, which are due to the carotenoid hydroxyspheroidene (Jiraskova & Reiss-Husson, 1993). These peaks are strongly non-conservative. The 512nm peak is >5 times as intense as the strongest absorbing carotenoid peak in the other species studied. This may be due to the fact that, in contrast to the LH1 antenna of the other species studied which contain only a single carotenoid per $\alpha\beta$ - dimer, the *Rv. gelatinosus* LH1 antenna complex contains two carotenoid molecules per $\alpha\beta$ - dimer (Jiraskova & Reiss-Husson, 1993; Jiraskova *et al.*, 1997). Therefore, it is possible that stronger interactions between the carotenoids of the *Rv. gelatinosus* core antenna are more likely to occur and give rise to a more intense (or modified) CD signal.

The CD signal due to the Bchl *a* Q_x transition, located at ~590nm, is also well resolved. This non-conservative signal, with a net positive sign, is about 30% as intense as the 512nm peak. In strain DSM 149 the intensity of the Q_x band is about the same as that of the longer wavelength NIR CD band, whereas in strain DSM 151 it is more than twice as intense. The relative anisotropy values of the *Rv. gelatinosus* core complex Q_x band are similar to the corresponding values for the core complexes of the *Rhodospseudomonas* species studied (Table 5.1).

The CD signals in the Bchl *a* Soret region of the *Rv. gelatinosus* core complex spectra show a complex structure which was not observed in the CD spectra of the other core complexes investigated here. The Soret band CD signal is non-conservative and is split into two positive peaks, centred at ~350nm and 396nm, and three troughs at ~416nm, 439nm and 462nm. It is possible that the 396nm peak is related to the shoulder observed on the red side of the Soret CD signal in the core complex CD spectra of the other

species investigated. In strain DSM 151 the ratio of the intensity of the 350nm peak to that at 396nm is ~1.6:1, whereas in strain DSM 149 it is 2.8:1.

The NIR region of the CD spectrum of the core complex from strain DSM 149 is similar to that of the core from the *Rhodospseudomonas* species. It exhibits a pair of non-conservative CD couplets with positive lobes at 860nm and 797nm, and negative lobes at 900nm and 815nm. The longer wavelength NIR CD peak is about twice as intense as its shorter wavelength counterpart. The core complex of strain DSM 151 displays different CD signals in the NIR region. In this case, the longer wavelength positive lobe is split into two peaks centred at 852nm and 873nm. The shorter wavelength CD peak is located at 801nm, and the troughs are at 816nm and 901nm. The ratio of the 873nm peak to that at 801nm is ~0.8:1. As mentioned in Chapter 4 (section 4.5) the core complex of this strain was very unstable when isolated and solubilised in LDAO. Examination of the absorption spectrum of the DSM 151 core complex recorded after accumulation of the CD data revealed the complex had become extensively denatured. Therefore, the differences observed in the NIR and Soret regions of the CD spectra of the two strains of *Rv. gelatinosus* can be attributed to the denaturation of the DSM 151 core complex. However, the carotenoid CD bands are essentially the same. It is therefore possible that the CD signals due to carotenoids are not as susceptible as the Bchl CD bands to structural perturbation.

5.6. *Chromatium vinosum* strain D core complex

The CD spectrum of the core complex of this species is shown in Figure 5.5. The OD of the sample at the NIR absorption maximum was 1.2 cm⁻¹. The CD spectrum is similar to that of the *Rps. palustris* core complex (Fig.

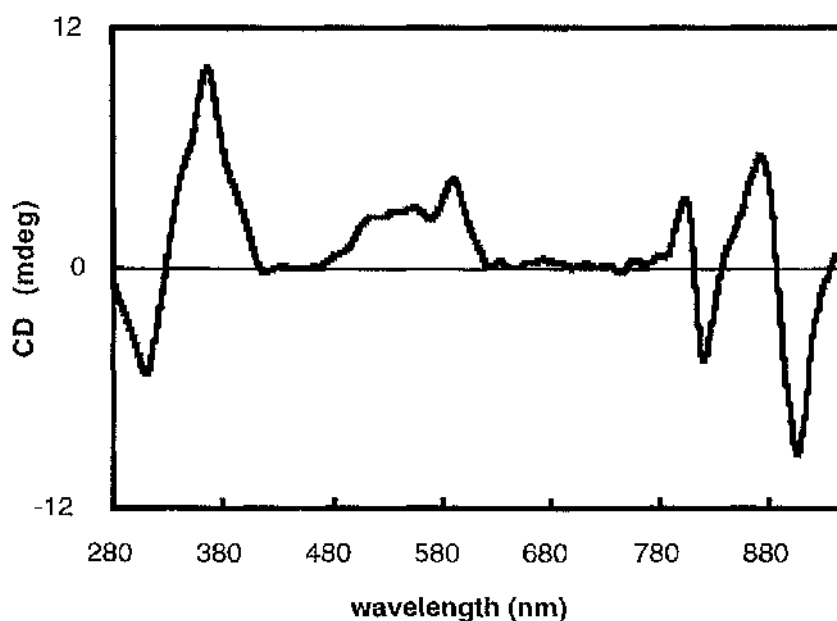


Figure 5.5. Room temperature CD spectrum of the LH1-RC core complex from *Chr. vinosum* strain D. The OD of the sample at the NIR absorption maximum was 1.2 cm^{-1} and the complex was suspended in 20mM Tris-HCl, pH8.0, 0.1% (v/v) LDAO.

5.2). The NIR region of the spectrum exhibits a pair of CD couplets. The shorter wavelength couplet, with a peak at 803nm and a trough at 820nm, is due to the RC Bchl *a* special pair (Phillipson & Sauer, 1973; Reed & Ke, 1973). The longer wavelength couplet has a peak at 871nm and a trough at 905nm, and arises from the LH1 antenna Bchl. The ratio of the intensity of the longer wavelength peak to that of the shorter wavelength one is ~2:1. The intensity of the 871nm peak is much greater than the corresponding peak in a previously reported NIR CD spectrum of a core complex-containing membrane fraction of *Chr. vinosum* (Hayashi *et al.*, 1981). As mentioned in section 5.3, the differences between the spectra could be due to the different detergents used to solubilise the complexes.

The CD signal from the Bchl Q_x transition is positive and moderately intense, with a similar anisotropy to the positive, longer wavelength Q_y signal (Table 5.1). The Soret region of the spectrum shows a double CD band, positive at 365nm and negative at 310nm. This signal is strongly non-conservative with a net positive sign. The positive, strongly non-conservative carotenoid related CD bands between ~480-560nm are poorly resolved. The poor spectral resolution of the carotenoid CD bands, which is also observed in the absorption spectrum (Fig. 4.23) has been noted before in the CD spectra of *Chr. vinosum* LH2 complexes (Cogdell & Scheer, 1985), and is thought to be a consequence of the mixture of carotenoids in these complexes.

5.7. *Rhodospirillum rubrum* and *Rhodobium marinum* core complexes

The CD spectra of the LH1-RC core complexes of the 'core only' species *Rs. rubrum* strain S1 and *Rh. marinum* strain DSM 2698 are shown in Figure 5.6. The optical density of the samples at the NIR absorption maximum was 1 cm^{-1} and 1.2 cm^{-1} , respectively. The CD spectrum of the *Rs. rubrum* core complex is in agreement with one published previously (Cogdell & Scheer, 1985) and, in the NIR region, shows the pair of CD couplets associated with the LH1 antenna and RC Bchl a 's. Both couplets are non-conservative with a net negative sign. The peaks of the couplets are located at 800nm and 886nm, and the troughs are located at 816nm and 912nm. The 886nm peak has a distinct shoulder, arising from the RC Bchl special pair, on its blue side (Phillipson & Sauer, 1973). The relative anisotropies of the NIR CD signals, which appear in Table 5.1, are less than those reported by Cogdell & Scheer (1985), indicating that there was some denaturation of the complex during the accumulation of the CD data.

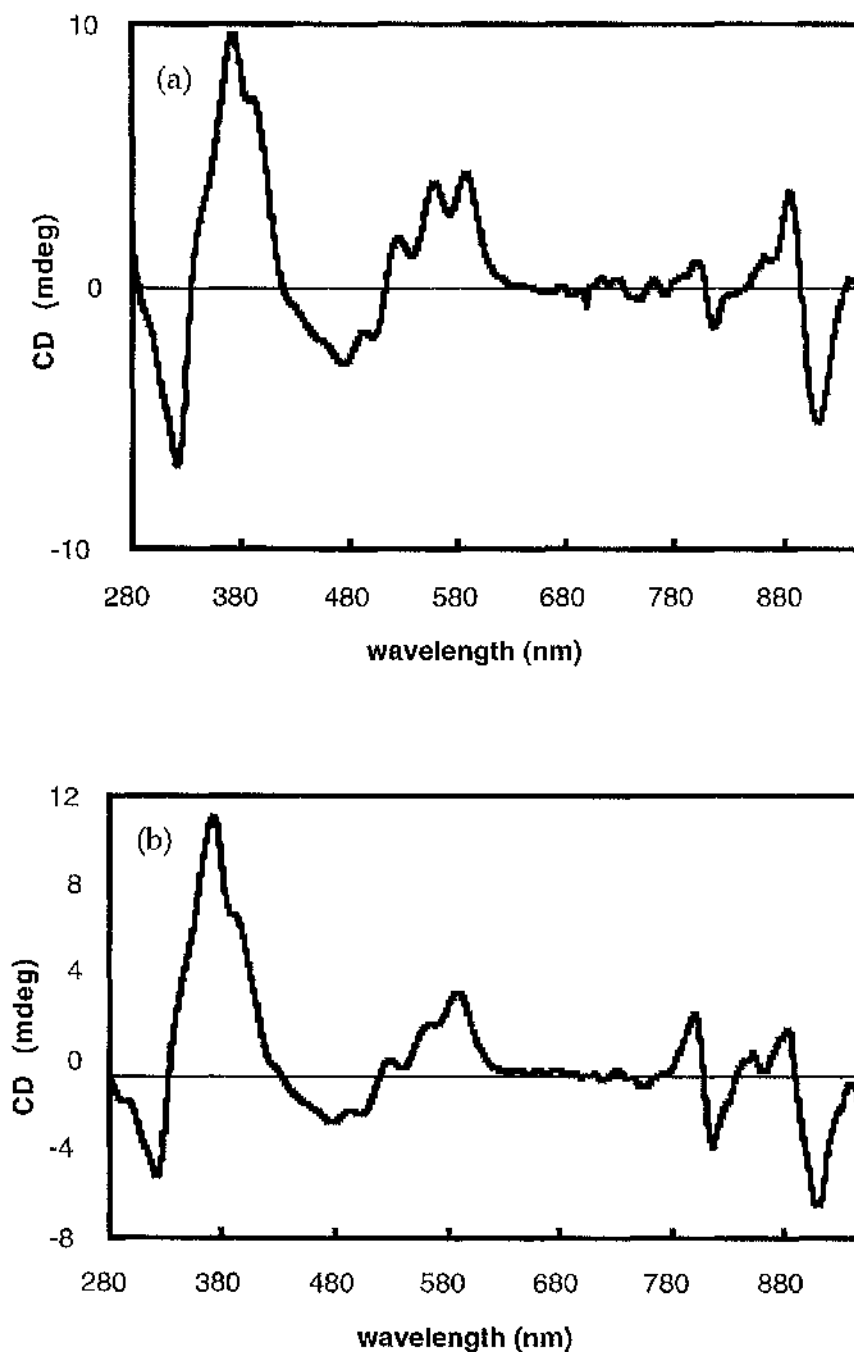


Figure 5.6. Room temperature CD spectra of the core complexes from (a) *Rh. rubrum* strain S1, and (b) *Rh. marinum* strain DSM 2698. The OD of the samples at the NIR absorption maximum was 1 cm^{-1} and 1.2 cm^{-1} , respectively.

This was confirmed by a comparison of the absorption spectra recorded before and after the CD measurements. Examination of the spectra showed that the ratio of the 875nm absorption band to that at 800nm had decreased in the spectrum recorded after the sample had been used for CD measurements.

The NIR region of the *Rh. marinum* core complex CD spectrum (Fig.5.6 b) also exhibited two non-conservative CD couplets. The intensities of the positive lobes of the couplets were much less than those of the other core complexes studied (Table 5.1). The positive lobe of the longer wavelength couplet was split into two peaks. A similar feature was observed in the CD spectrum of the core complex from *Rv. gelatinosus* strain DSM 151 (Fig. 5.4b). As CD spectra are particularly sensitive to changes in structure and inter/intra-molecular interactions the perturbation of the structure of the core complex by denaturation effects both the Bchl-Bchl interactions and interactions between the Bchl's and their protein environment. These changes are reflected by changes in the CD spectrum. The changes observed in the NIR CD spectrum of *Rh. marinum* core complex were indicative of denaturation. Examination of the absorption spectrum of the *Rh. marinum* core complex confirmed that denaturation had occurred during the CD measurements. This was due to the instability of the isolated complex in LDAO (refer to section 4.8).

The visible regions of the CD spectra are fairly similar. In both spectra the moderately intense Bchl *a* Q_x CD band, located at ~590nm, is non-conservative with a net positive sign. The CD signals arising from the carotenoid absorption bands between ~500-570nm differ between the two species. In the *Rs. rubrum* core complex spectrum the ~560nm carotenoid band has a similar intensity to the Q_x band, whereas in the *Rh. marinum* core spectrum it is half as intense. There is also a difference between the

ellipticity ratio of the bands at ~560nm and ~525nm. In *Rs. rubrum* the ratio is 2:1, whereas in *Rh. marinum* it is 2.7:1. The Soret region of both spectra are in close agreement and show an intense double CD signal with a peak at ~390nm and trough at ~322nm. The positive lobes of the ~390nm band both possess a shoulder located at ~400nm. The Soret CD signals are non-conservative with a net positive sign.

In summary, these results show that CD spectroscopy, especially in the NIR, provides a sensitive method for monitoring the structural stability of isolated LH1-RC core complexes solubilised in detergent. This is discussed further in Chapter 9.

CHAPTER SIX

THE EFFECT OF CHEMICAL OXIDATION ON THE LH1 (B880) COMPLEX FROM *Rhodobium marinum*

6.1. The effect of chemical oxidation on the fluorescence of the LH1 (B880) complex from *Rhodobium marinum*

Previous reports have shown it is possible to chemically oxidise the Bchl components of the LH1 antenna complex from purple bacteria (Goedheer, 1958; Loach *et al.*, 1963; Gomez *et al.*, 1982a & 1982b; Picorel *et al.*, 1984). Such treatment results in changes in the absorption, circular dichroism (CD) and electron spin resonance (ESR) spectral signals of the complex. Chemical oxidation of the LH1 Bchl *a* in photosynthetic membrane fragments of *Rs. rubrum* resulted in absorbance changes in the NIR (Goedheer, 1958; Loach *et al.*, 1963; Gomez *et al.*, 1982b). The spectral changes varied depending on the type of oxidation, but generally a decrease in absorbance around 880nm was accompanied by the appearance of a new absorption band at 1230nm (Gomez *et al.*, 1982b). These changes were very similar to those observed upon oxidation (both in the light and by exogenous chemical agents in the dark) of the RC 'special pair' Bchl's in which a bleaching of the absorption at 865nm was concomitant with an increase in the absorbance at 1245nm (Clayton, 1962; Dutton *et al.*, 1975). The latter was assigned to a dimeric cation radical of Bchl (Cogdell & Parson, 1975; Fajer *et al.*, 1976). The ESR signal of the oxidised primary donor of the RC exhibited a Gaussian lineshape with a *g*-value of 2.0025 and a linewidth of 9.5 G (McElroy *et al.*, 1969). The *g*-value was attributed to the extensive delocalisation over a Bchl cation radical (Picorel *et al.*, 1984). The narrow linewidth was thought to be due to a free electron spin over the special pair Bchl's (Norris & Katz, 1978). The existence of cationic Bchl upon oxidation of the LH1 antenna was also supported by ESR spectroscopy (Gomez *et al.*, 1982a; Picorel *et al.*, 1984). The room temperature ESR signal from oxidised LH1 Bchl showed a nearly Gaussian signal with a *g*-value of 2.0025 and a very narrow linewidth of 3.8 G (Gomez *et al.*, 1982a). The much narrower linewidth of this signal was

interpreted as being due to the extensive delocalisation of the cation over an aggregate of 10-12 Bchl molecules in the LH1 antenna (Picorel *et al.*, 1984).

Changes in the absorption and CD spectra of the LH2 complex in chromatophores from a carotenoidless mutant of *Rb. sphaeroides* were also observed upon photo-oxidation (Rafferty *et al.*, 1979). In this case the progressive loss and concomitant blue-shift of the NIR absorption band around 860nm were accompanied by a decrease in the intensity of the NIR CD signal. These results were attributed to the conversion of Bchl dimers to monomers upon photo-oxidation. More recently, single molecule spectroscopy suggested that fluorescence emission from the isolated LH2 complex from *Rps. acidophila*, which is structurally similar to the LH1 complex, is very strongly quenched by the presence of photo-oxidised B850 Bchl in the antenna (Bopp *et al.*, 1997). However, it was not known how extensive the oxidation in the LH1 or LH2 'ring' must be in order to produce the dramatic quenching of the fluorescence emission observed. This chapter describes the results of experiments designed to investigate this by studying the effect of mild chemical oxidation (using potassium ferricyanide) on the fluorescence emission and absorption spectra of the LH1 complex from the purple bacterium *Rhodobium marinum*. This species was chosen for this study because its RC can easily be dissociated from the LH1 ring during the purification process (Meckenstock *et al.*, 1992a). This resulted in a homogeneous population of reaction centreless LH1 complexes which were particularly amenable to spectroscopic investigation.

The isolation of the LH1 (B880) complex from *Rh. marinum* was performed as described in section 2.5. The absorption and fluorescence emission spectra were recorded as described in sections 3.1 and 3.2, respectively. For quantitative measurements, the OD₈₈₀ of the LH1 sample

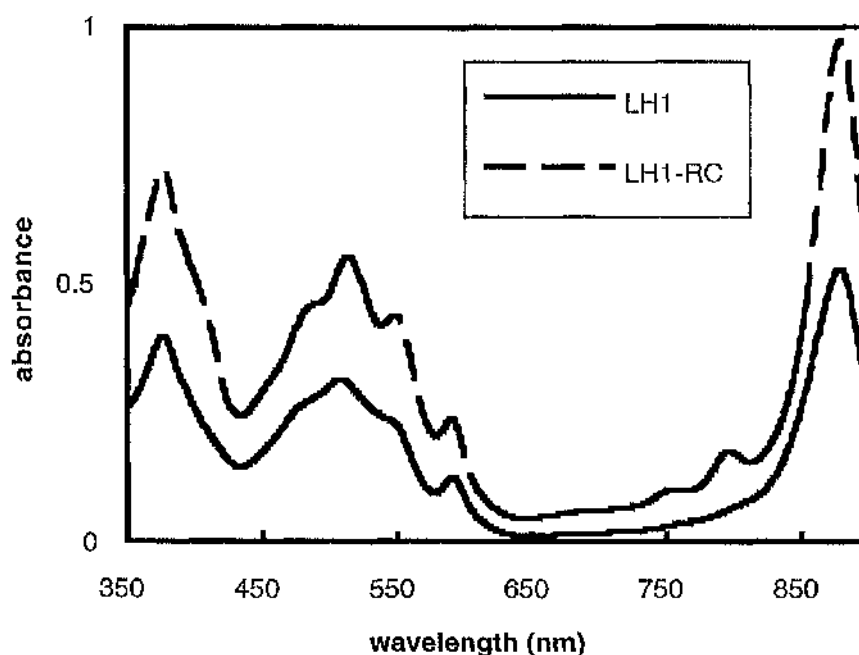


Figure 6.1. Room temperature absorption spectra of the LH1-RC core and LH1-only complexes of *Rh. maritimum*. For clarity the OD_{380} of the core complex sample was adjusted to 1 cm^{-1} and that of the LH1 complex to 0.5 cm^{-1} . The LH1 complex was suspended in 20mM Tris-HCl, pH8.0, 0.05% (v/v) LDAO.

was adjusted to $\sim 0.17 \text{ cm}^{-1}$. Potassium ferricyanide was made up as either a 500mM or 100mM stock solution in 20mM Tris-HCl, pH8.0 containing 0.05% (v/v) LDAO. The effects of different concentrations of potassium ferricyanide, ranging from 1mM to 100mM, on the absorption and fluorescence emission spectra were investigated.

The absorption spectra of the purified LH1-RC core and isolated LH1 complexes are shown in Figure 6.1 (refer also to sections 4.8 and 4.9). The spectrum of the core complex shows an NIR absorption maximum at 880nm with two smaller peaks at 800nm and 760nm. The former is attributable to the LH1 Bchl *a* Q_y transition and the latter two peaks to the

Bchl *a* and bacteriopheophytin components of the RC, respectively. The small peak at 590nm represents the Bchl *a* Q_x transition and the large absorption peak at 380nm the Soret band (Meckenstock *et al.*, 1992a). The three peaks located between 470nm and 570nm are due to the carotenoid component of the complex. The LH1-only complex also has a NIR absorption maximum at 880nm. However, the two NIR peaks at 800nm and 760nm that are associated with the presence of RC are absent, indicating successful dissociation of the RC from the LH1 antenna during the purification process (section 4.9). In the rest of the spectrum the absorption of the LH1 complex is similar to that of the full core complex.

The effect of chemical oxidation on the NIR absorption spectrum of the LH1 complex is shown in Figure 6.2. Because the absorbance changes observed were small, even at a potassium ferricyanide concentration of 100mM, for this figure a ferricyanide concentration of 250mM was employed to illustrate the bleaching effect. Also for illustrative purposes, the OD₈₈₀ of the sample in this figure was adjusted to ~0.53 cm⁻¹. Addition of potassium ferricyanide to the LH1 complex caused a bleaching of the 880nm absorption band. The extent of this bleaching increased as the concentration of potassium ferricyanide increased. The measurements were performed immediately after addition of potassium ferricyanide and took two minutes to record. There was no observable shift in the absorption maximum associated with the bleaching effect during the time course of the measurements, and the band width at the half-maximal amplitude remained constant. Bleaching of the 880nm absorption band was irreversible and could not be recovered by addition of the reducing agents sodium ascorbate or sodium dithionite. The extent of the ferricyanide induced bleaching was not very extensive even at relatively high concentrations of potassium ferricyanide. At 250mM ferricyanide there was

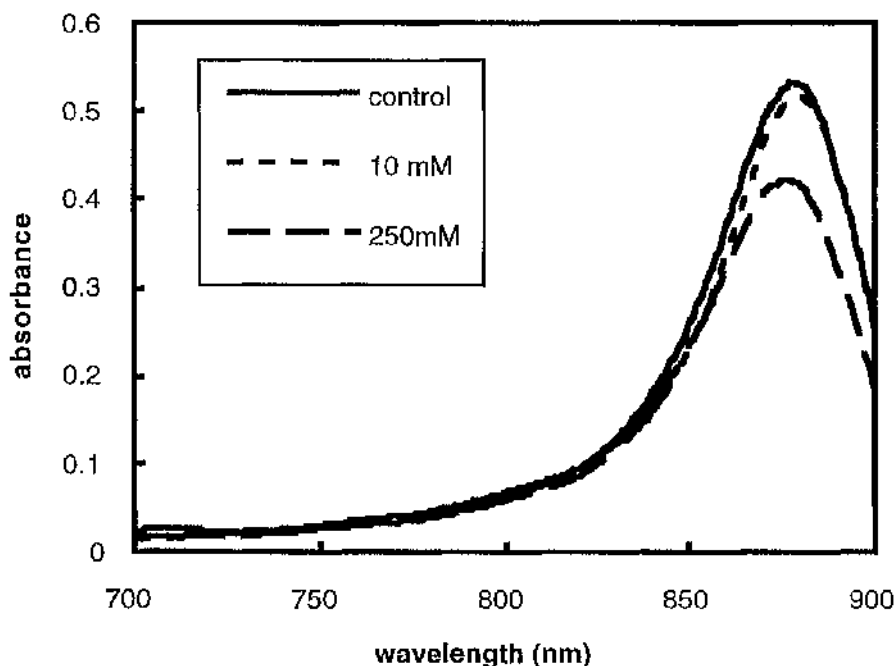


Figure 6.2. The effect of chemical oxidation on the NIR absorption spectrum of the LH1 complex from *Rh. marinum*. The concentrations of potassium ferricyanide used to achieve the oxidation were 0mM (control), 10mM and 250mM. For illustrative purposes the OD_{880} of the LH1 sample used for this figure was adjusted to 0.53 cm^{-1} compared to an OD_{880} of 0.17 cm^{-1} for the quantitative measurements. The bleaching effect is very small at low concentrations of ferricyanide. Addition of 250mM ferricyanide resulted in a 20% loss of absorbance at 880nm. The sample was suspended in 20mM Tris-HCl, pH8.0, 0.05% (v/v) LDAO.

~20% loss of the original absorbance.

The chemical oxidation of the LH1 complex was found to be time dependent and required about 40 minutes to go to completion. After 10 minutes in the presence of 100mM potassium ferricyanide, the 880nm absorption band of the LH1 complex (with an original OD_{880} of $\sim 0.53 \text{ cm}^{-1}$) had decreased to 65% of its original value (Fig. 6.3). After 40 minutes the

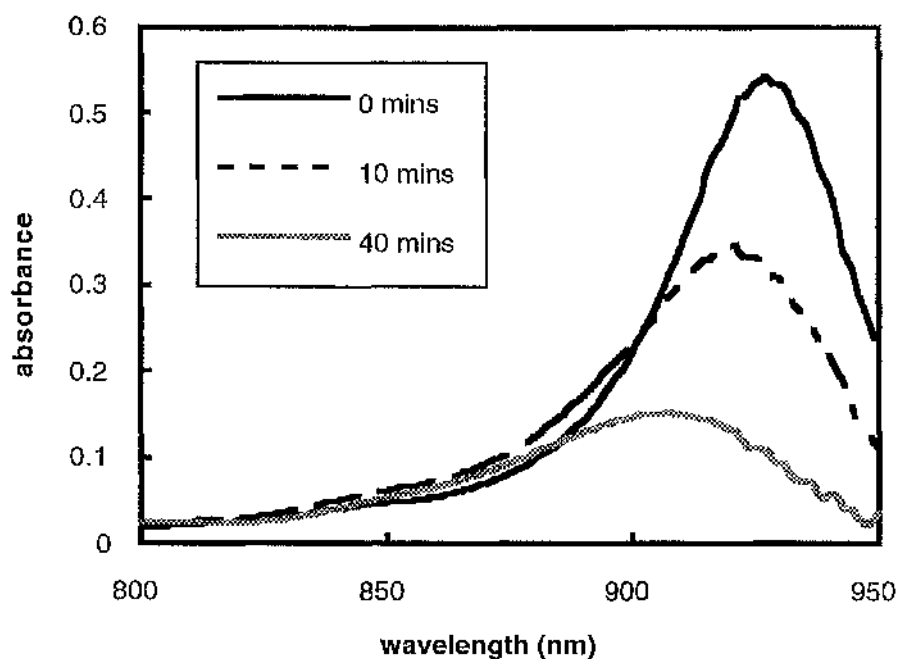


Figure 6.3. The evolution with time of the NIR absorption spectrum of the LH1 complex from *Rh. marinum* after addition of 100mM potassium ferricyanide. The oxidation reaction took about 40 minutes to go to completion. After this time only 28% of the original absorbance at 880nm remained. The decrease in absorbance was accompanied by a blue-shift of the absorption maximum. The OD_{880} of the LH1 sample before addition of ferricyanide was 0.53 cm^{-1} . The sample was suspended in 20mM Tris-HCl, pH8.0, 0.05%(v/v) LDAO.

absorbance at 880nm had decreased to 28% of its original value. Additionally, in contrast to measurements performed over a 2 minute period, there was a concomitant 22nm blue-shift of the absorption maximum from 880nm at 0 minutes to 858nm after 40 minutes.

A slow photobleaching of the LH1 complex, in the absence of potassium ferricyanide, was also observed. This photobleaching was caused by the measuring beam of the spectrophotometer. The spectra of an LH1 sample

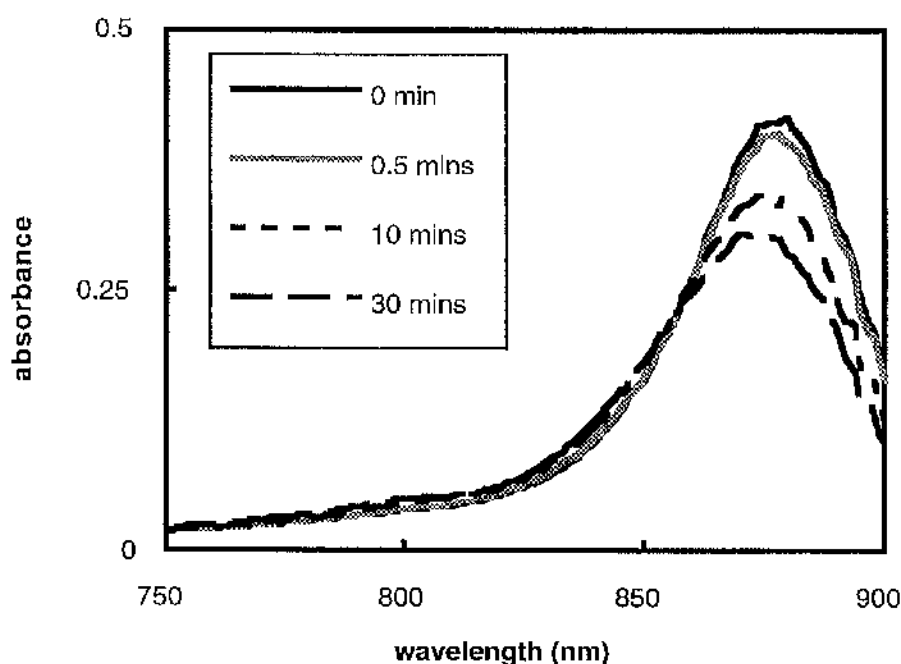


Figure 6.4. The effect of illumination, in the absence of potassium ferricyanide, on the NIR absorption spectrum of the LH1-only complex ($OD_{880} = 0.41 \text{ cm}^{-1}$) from *Rh. marinum*. The intensity of the absorption band at 880nm decreased with time. This was accompanied by a small blue-shift in the absorption maximum. The sample was suspended in 20mM Tris-HCl, pH8.0, 0.05%(v/v) LDAO.

($OD_{880} = \sim 0.4 \text{ cm}^{-1}$) taken after different periods of exposure to the spectrophotometer measuring beam showed a progressive loss in the absorption at 880nm (Fig. 6.4). After 30 secs exposure to the light beam $\sim 2\%$ of the original absorbance at 880nm was lost. This loss increased to 16% after 10 minutes, and 26% after 30 minutes exposure. The absorption loss was accompanied by a small blue shift ($\sim 3\text{-}4\text{nm}$) in the absorption maximum. Again, the original absorbance could not be regained by addition of reducing agents to the sample, indicating an irreversible photooxidation of the antenna Bchl's (Rafferty *et al.*, 1979).

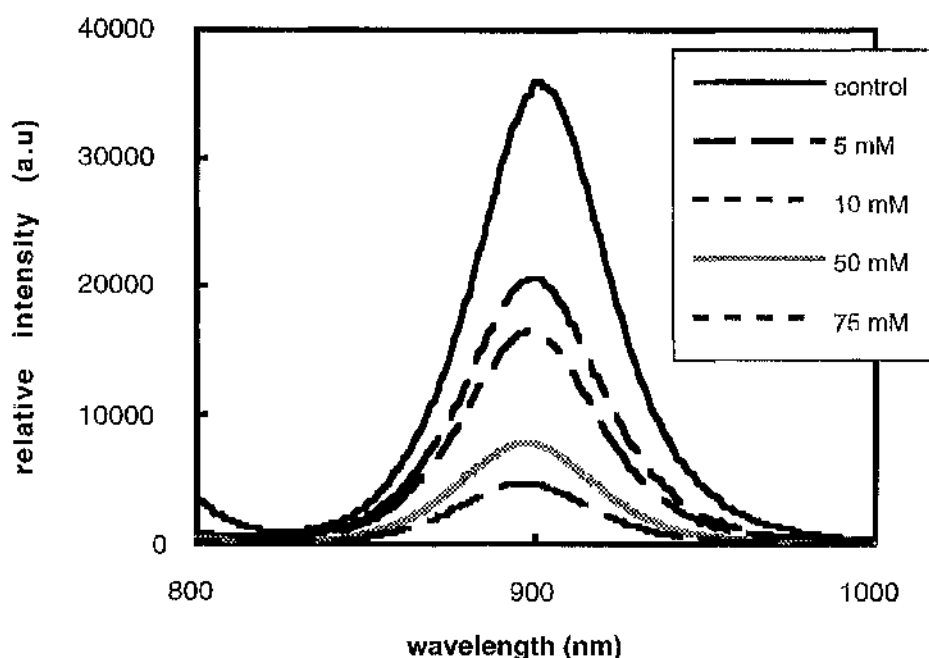


Figure 6.5. The effect of chemical oxidation on the fluorescence emission spectrum of the LH1 complex from *Rh. marinum*. The OD_{880} of the sample was 0.17 cm^{-1} . The fluorescence intensity decreased to 50% of its original value upon addition of 10mM potassium ferricyanide. Addition of 75mM ferricyanide reduced the fluorescence intensity to about 13% of the original value. The sample was suspended in 20mM Tris-HCl, pH8.0, 0.05%(v/v) LDAO.

As photobleaching of the LH1 complex could interfere with the quantitative measurements of the effects of chemical oxidation on the antenna Bchl's of the LH1 complex, both the absorption and fluorescence emission spectra were recorded under identical conditions over the same time period of 2 minutes immediately after the addition of potassium ferricyanide. A fresh sample was used for each individual measurement.

The effect of chemical oxidation on the fluorescence emission intensity of the LH1 complex is shown in Figure 6.5. A significant quenching of the

fluorescence intensity could be observed even in the presence of relatively low concentrations of potassium ferricyanide. The quenching increased as the concentration of ferricyanide in the sample increased. In contrast to the absorption of the LH1 complex (Fig. 6.2), its fluorescence was very sensitive to chemical oxidation. As little as 10mM potassium ferricyanide caused a loss of about 50% of the original fluorescence intensity. In the presence of 75mM potassium ferricyanide, the fluorescence intensity decreased to only ~13% of the original. A progressive blue-shift of the the fluorescence λ_{\max} accompanied the quenching effect. The λ_{\max} shifted by 6nm, from 901nm in the absence of potassium ferricyanide to 895nm in the presence of 75mM potassium ferricyanide.

The concentration dependence of chemical oxidation by potassium ferricyanide on the transmission and fluorescence emission intensity of the isolated LH1 complex is shown in Figure 6.6. Because absorbance is measured on a logarithmic scale and fluorescence intensity on a linear one, the transmission spectra of the LH1 complex in the presence of varying concentrations of potassium ferricyanide (ranging from 1mM -100mM) were measured. These values were then transformed into 1-transmission values, expressed as a percentage. This allowed the direct comparison of two linear scales. There was very little change in the transmission of the LH1 complex, even at concentrations of ferricyanide which caused a dramatic quenching of fluorescence. 50% of the fluorescence was quenched at a ferricyanide concentration of 10mM, while at the same concentration only 2-3% of the original transmission was lost. Addition of 100mM potassium ferricyanide resulted in a ~10% loss of the original transmission whereas the same concentration of ferricyanide caused a ~87% loss of fluorescence intensity. The shape of the curve relating to the change in fluorescence intensity upon chemical oxidation was biphasic in shape. This indicated the

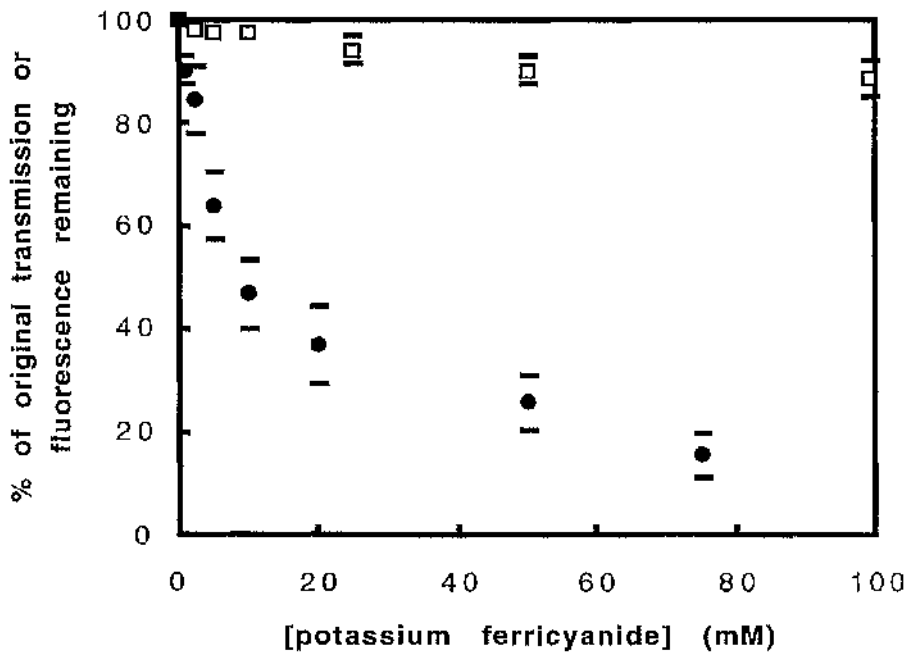


Figure 6.6. Comparison of the effect of chemical oxidation on the transmission (open squares) and fluorescence emission intensity (filled circles) of the LH1 complex from *Rh. marinum*. The change in the transmission is very small compared to the dramatic effect chemical oxidation has on the fluorescence intensity of the complex. For all the measurements the OD_{880} of the LH1 complex was 0.17 cm^{-1} . The data represent the mean \pm standard deviation of at least 5 separate measurements.

presence of complicated kinetics during oxidation of the LH1 antenna Bchl's. Assuming that a single *Rh. marinum* LH1 ring consists of 16 $\alpha\beta$ -dimers which bind a total of 32 Bchl a 's (Gall, 1994; Karrasch *et al.*, 1995; Walz & Ghosh, 1997), and that the Bchl's contribute equally to the 880nm absorption band, then oxidation of about one Bchl a molecule of the LH1 'ring' is sufficient to produce a 50% quenching of the fluorescence intensity. This value decreases to ~0.6-0.8 if the LH1 'ring' is assumed to consist of 12 $\alpha\beta$ -dimers which bind only 24 Bchl's (Zuber & Brunisholz, 1991; Meckenstock *et al.*, 1992a; Meckenstock *et al.*, 1994; Boonstra *et al.*, 1993;

Boonstra *et al.*, 1994; Franke & Amesz, 1995). However, due to the very small changes in absorbance which were observed at the concentrations of ferricyanide used during these studies, a more exact quantitation of how many Bchl *a* molecules that must be oxidised to produce complete fluorescence quenching is not possible. Nevertheless, the data clearly show that the fluorescence properties of the LH1 antenna are shut down by the chemical oxidation of a very small fraction of the total number of Bchl's in the LH1 'ring'. The significance of these observations is discussed in Chapter 9.

CHAPTER SEVEN

**ANTENNA ORGANISATION IN THE PURPLE BACTERIUM
Rhodospseudomonas acidophila STRAIN 7750 STUDIED BY
FLUORESCENCE INDUCTION**

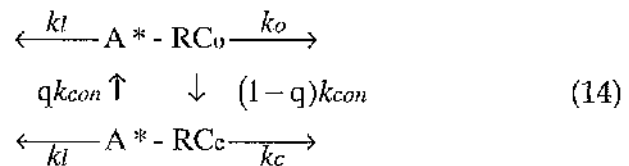
7.1. Fluorescence induction spectroscopy as a probe of PSU structure

To date, all assays applied to the study of antenna organisation within the photosynthetic membrane of purple bacteria have suffered from certain disadvantages. For example, molecular modelling may not reflect the actual antenna arrangement *in vivo*. Annihilation studies of chromatophores, used successfully in the past, require complex data analysis and sophisticated (and expensive) equipment (Deinum *et al.*, 1991). Finally, imaging techniques do not yet have sufficient resolution to allow unambiguous interpretation. An alternative to the use of the above methods to probe antenna organisation is represented by fluorescence induction measurements. These provide a powerful method of quantifying energy transfer between light-harvesting complexes and, as such, their packing density (Trissl, 1995; 1996).

Fluorescence yield is dependent upon the redox state of the RC (Duysens & Sweers, 1963). In purple bacteria three redox states of the RC are known to cause substantially different fluorescence yields: (i) the 'open' RC in the photochemically fully active state (P870 H Q_A) fluoresces little; (ii) the 'closed' RC which carries a reduced quinone (Q_A⁻) fluoresces two times as much, and; (iii) the 'closed' RC which carries an oxidised primary donor (P870⁺) fluoresces approximately three times as much as the open RC (Kingma *et al.*, 1983; van Grondelle, 1985). Fluorescence induction can be defined as 'the kinetics of the fluorescence rise observed when RCs switch from the dark adapted open state (minimal fluorescence, F_o) to the closed state (maximal fluorescence, F_m) during sudden exposure to illumination by actinic light of constant intensity.' Such measurements are usually made under single turnover conditions. These are achieved by blocking electron transfer behind Q_A by use of an appropriate inhibitor. Under such

conditions the high fluorescence closed state is attained when a single electron transfer has occurred in all RCs.

Fluorescence induction curves are usually sigmoidal. The degree of sigmoidicity is a measure of the excitonic connectivity and, hence, the spatial separation between neighbouring PSUs. Until recently, this technique had been applied mostly to PSII (Lavorel *et al.*, 1986; van Gorkom, 1986; Trissl & Lavergne, 1995). The fluorescence induction curves of this system display the typical sigmoidal shape indicating efficient exchange of energy between PSUs (Dau, 1994). A mathematical analysis of these fluorescence induction curves was first published by Joliot & Joliot (1964). In purple bacterial photosynthetic systems the exciton-radical pair equilibrium model which applies to PSII (Lavergne & Trissl, 1995) can effectively be ignored because trapping in these bacteria is rate limited by exciton transfer from LHI to the RC (Otte *et al.*, 1993; Xiao *et al.*, 1994). This leads to a simplified reaction scheme for the connected units model (Trissl, 1996):



where A^* is the antenna in the excited state; k_{con} is the inter-unit exciton transfer rate constant; k_l is deactivation of the excited state in the antenna; k_o and k_c are deactivation of the excited state in the RC in the open and closed state, respectively, and; q is the fraction of open RCs.

The basic equations necessary for a quantification of the sigmoidicity of the fluorescence induction curve have been derived independently by

several investigators (Paillotin, 1976; Strasser, 1978; Butler, 1980). A convenient re-formulation of the basic equation- by introducing the sigmoidicity parameter, J - was derived by Lavergne & Trissl (1995) and Trissl (1996). The equation:

$$J = \left(\frac{F_m}{F_o} - 1 \right) \frac{k_{con}}{k_{con} + k_f} \quad (15)$$

which contains the experimentally accessible parameters J , F_m / F_o and k_f can easily be solved for the rate constant of inter-unit exciton exchange, k_{con} . The rate constant k_f corresponds to the fluorescence decay kinetics.

In the classical fluorescence induction experiments (mostly performed with PSII) the transition from the open state to one of the closed states is evoked by dc-light switched on by a mechanical shutter. In the case of PSII the fluorescence rise occurs typically in the 10 - 100 ms range. A corresponding experiment with purple bacteria is hampered firstly by the smaller fluorescence yield which leads to a poor signal to noise ratio and secondly by the inappropriate time range in which all three redox states occur. This makes analysis of the induction curve non-transparent. The currently available theories to describe such kinetics are based on a single electron transfer (i.e. two fluorescent states only and a prerequisite for the validity of Equation 15). Therefore, when working with purple bacteria there is a requirement to find experimental conditions for a single turn-over transition as well as an increase in the signal to noise ratio. Both requirements are met by applying an experimental technique described by Trissl (1996). Briefly, the excitation light intensity is increased by using a Xenon flash which shifts the transition from the open to the closed state in the 100 μ s range (where only the redox couple P870/P870⁺ is involved) and

also increases the signal to noise ratio enormously. For a full description of this technique refer to section 3.3.

7.2. Antenna organisation in the purple bacterium *Rhodospseudomonas acidophila* strain 7750 studied by fluorescence induction

Fluorescence induction measurements of photosynthetic membranes of the purple non-sulphur bacterium *Rps. acidophila* strain 7750 were performed to probe the excitonic connectivity of RCs and thereby gain information on the morphological arrangement of antenna complexes within the PSU of this species. *Rps. acidophila* strain 7750 was chosen for study because both the spectral properties and relative abundance of the peripheral LH2 can be modified by altering the growth conditions as described in Materials & Methods (Angerhofer *et al.*, 1986). Besides LH1-RC core complexes the photosynthetic membranes contained either B800-850, both B800-850 and B800-820, or B800-820 only as peripheral complexes.

The different antenna compositions of each growth type of *Rps. acidophila* strain 7750 are demonstrated by the NIR absorption spectra in Figure 7.1a. The membranes of high light (HL) grown cells contain the usual B800-850 peripheral complexes with Bchl *a* Q_y absorption maxima located at ~863nm and ~803nm. Low light (LL) grown cells have two strong absorption bands located near 800nm and 820nm that represent the B800-820 complex. A weaker band located at ~860nm indicates the presence of some B800-850 complex. Cells grown under conditions of low light and low temperature (LL/LT) contain only B800-820 complex, the presence of which is indicated by the two absorption bands near 800nm and 820nm. All the growth types contained LH1-RC complexes. The shoulder to the red of the 863nm absorption band of the HL and LL cells, and the small absorption

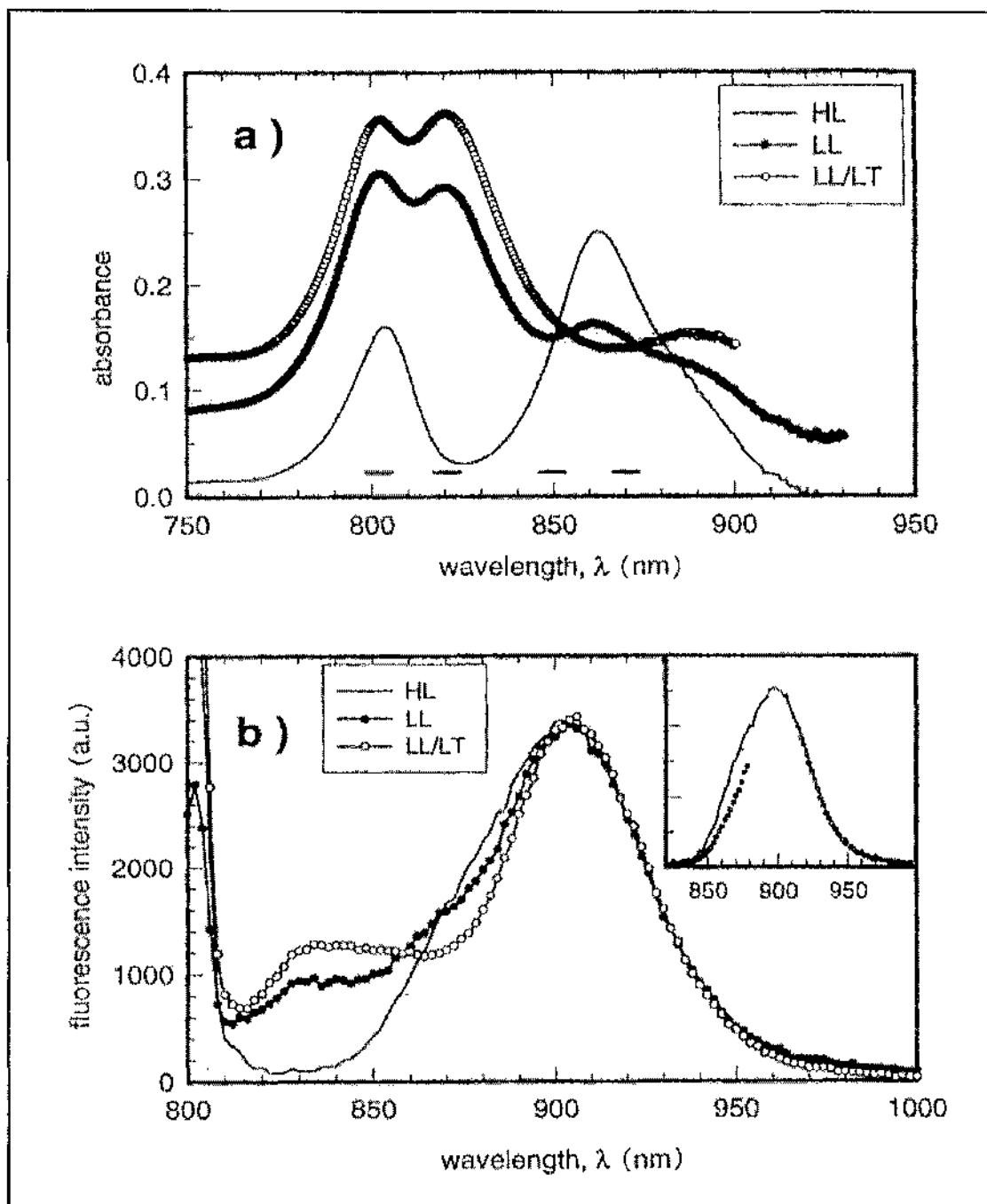


Figure 7.1. (a) NIR absorption spectra of photosynthetic membranes of HL, LL and LL/LT grown *Rps. acidophila* strain 7750. The baselines of the LL and LL/LT are shifted upwards by $A=0.05$ and $A=0.10$, respectively. (b) Quantum corrected fluorescence emission spectra of HL, LL and LL/LT photosynthetic membranes upon excitation at 802nm. Inset: Fluorescence spectrum of HL membranes excited at 802nm (solid line) and 896nm (open circles).

band located at ~883nm in the LL/LT cells is due to the Q_y transition of the LH1 Bchl *a* s. The NIR absorption spectra are very similar to those reported previously (Angerhofer *et al.*, 1986; Deinum *et al.*, 1991).

The fluorescence emission spectra of the photosynthetic membranes upon excitation of the B800 component at 802nm are shown in Figure 7.1b. They agree qualitatively with those reported previously (Deinum *et al.*, 1991). The membranes from all three growth types have the fluorescence intensity maximum located at ~903nm. Membranes from the LL and LL/LT grown bacteria also show a small fluorescence peak at ~830nm. The peaks located at 802nm are due to Rayleigh scattering. The small fluorescence amplitudes between ~820-860nm in all three cases indicate an efficient energy transfer from the peripheral antenna complexes to the RC. The inset in Figure 7.1b shows the fluorescence spectrum of membranes from HL grown bacteria excited at 802nm and 896nm. The spectrum of the 802nm-excited membranes has a shoulder located to the blue of the fluorescence maximum which is not present in the 896nm-excited membranes. All these fluorescence spectra were recorded under F_0 -conditions due to the very low flash energy of ~1 $\mu\text{J cm}^{-2}$. This can be compared to the flash energy of 56 $\mu\text{J cm}^{-2}$ used for the induction experiments. F_0 -conditions were confirmed by the observation, as expected, of an approximately 2-fold increase in the fluorescence amplitude of the spectra when the RCs were closed by the use of terbutryn and exposure to background illumination. Further confirmation that a true F_0 state was present came from the calibration of the z -axis of the fluorescence induction curve. This allowed the excitation energy to be correlated with the number of hits per PSU, z . In the case of the flash fluorimeter apparatus used for the above measurements, z was estimated as 0.1 for a single flash. The spacing of 1 s between flashes provided ample time for the small fraction of closed RCs to relax back into

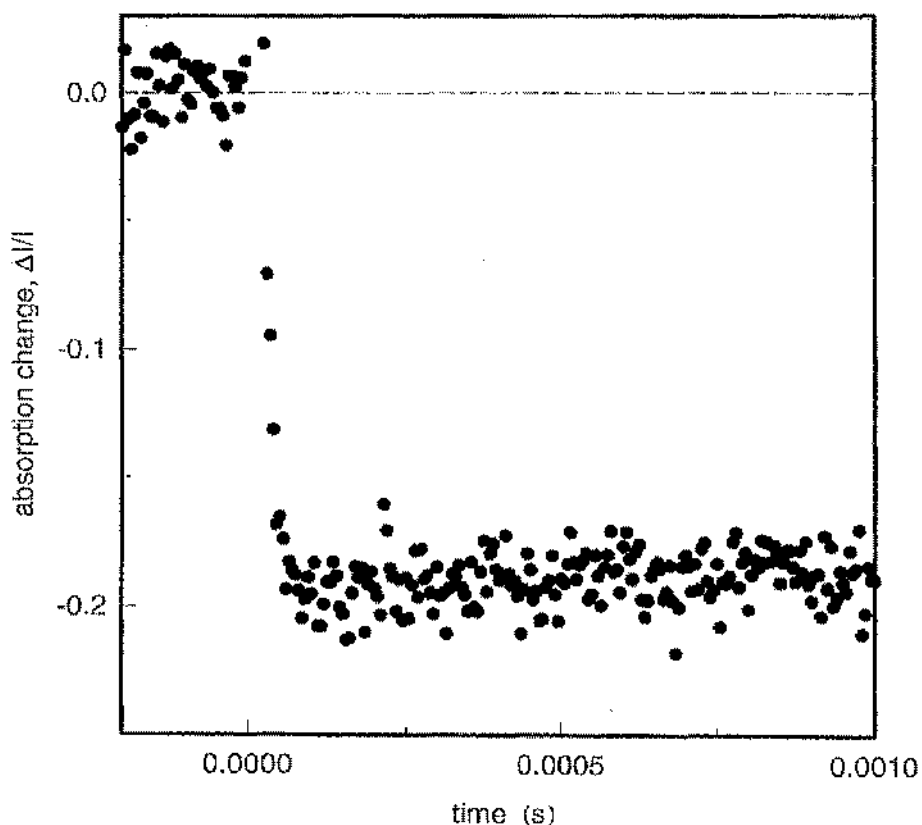


Figure 7.2. Absorption change of the primary donor, P870, of *Rps. acidophila* strain 7750 membranes measured at 871nm. The average of 10 events collected after dark adaptation periods of 2 minutes. The measuring beam was switched on 2 ms before the excitation flash was applied.

the open state. The flash induced absorbance change of P^+ at 871nm was measured with a time resolution of 20 μ s. The absorption change was step function-like (Fig. 7.2). These data are comparable to those obtained for chromatophores of *Rs. rubrum* (Trissl, 1996). Therefore, interference with the fluorescence induction curve by the re-reduction of P^+ by bound cyt c_2 appears to be negligible.

A typical single shot double-trace from HL grown photosynthetic membranes upon excitation into the B800 absorption band ($\lambda_{ex} = 802$ nm) is shown in Figure 7.3. The spikes observed near the tails of the traces are a

result of the abrupt switching off of the flash discharge capacitor by a thyristor circuit. The data are normalised to each other at the onset of the flash to illustrate the different time courses of the excitation light and fluorescence. When the data were processed as described in section 3.3 and Trissl (1996) to transform them into a time scale that corresponds to a shutter-switched dc-light source, the slightly sigmoidal fluorescence induction curve depicted in Figure 7.4a was obtained. Only these data were used for further analysis.

Fluorescence induction curves were fitted with 3 parameters, F_m / F_o , J , and an ordinate scaling factor that allowed the determination of the number of pigments belonging to a PSU (see sections 7.1 and 3.3). Briefly, the time base of an experimental fluorescence induction curve was shifted to a theoretical one (scaled in hits per RC) with a factor that is the product of an average number of the pigments coupled to the RC (i.e. antenna sizes, N) and the mean absorption cross section of an antenna pigment, σ , (experimentally accessible from the absorption spectra). For an antenna with only a single pigment type (i.e., one absorption band), the antenna size, N , is related to the total flash energy, E_o in $J\ cm^{-2}$, and the total hits per PSU, z_o , by:

$$z_o = \frac{E_o}{E_{hv}} \cdot N \cdot \sigma \quad (16a)$$

where E_{hv} is the photon energy and σ the absorption cross section (in cm^2) of an antenna pigment at the excitation wavelength. At any given wavelength the latter follows from the molar absorption coefficient according to:

$$\sigma = \frac{\epsilon \cdot \ln 10}{6 \cdot 10^{20}} \quad (17)$$

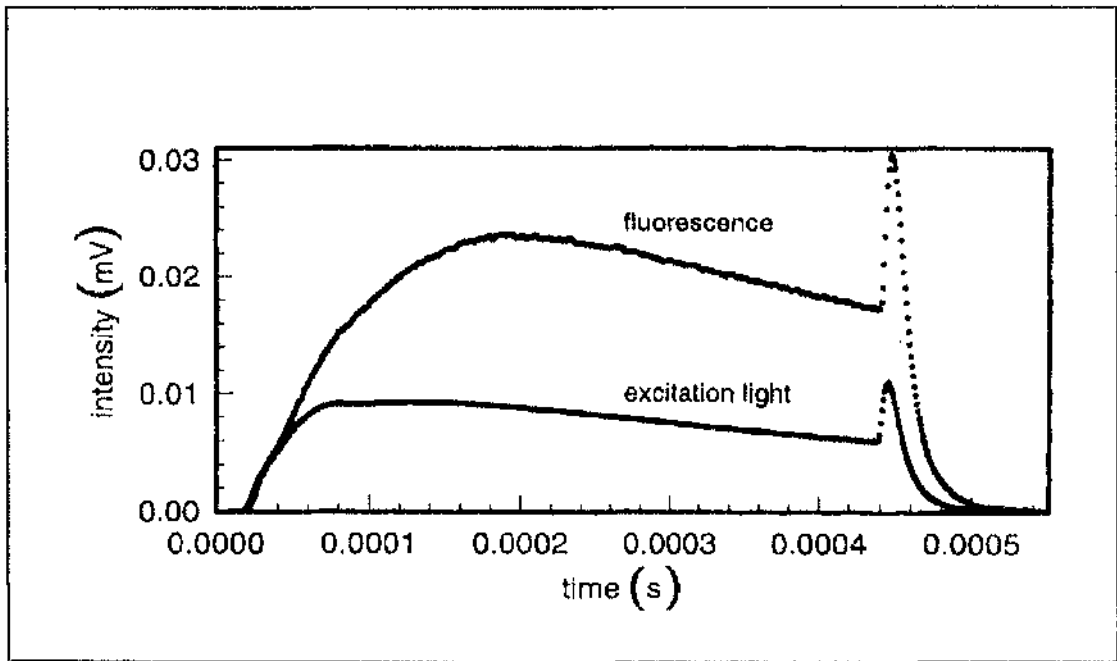


Figure 7.3. Time courses of the excitation flash and fluorescence emission from photosynthetic membranes of HL grown *Rps. acidophila* 7750 excited at a wavelength of 802nm. The total flash energy was $E = 56 \mu\text{J cm}^{-2}$.

In a heterogeneous antenna system such as that of *Rps. acidophila* where different absorption bands overlap (Fig. 7.1a) the contribution of all bands must be considered according to:

$$z_0 = \frac{E_0}{E_{hv}} \cdot (N_{B800} \cdot \sigma_{B800} + N_{B820} \cdot \sigma_{B820} + N_{B850} \cdot \sigma_{B850} + N_{B880} \cdot \sigma_{B880} + \sigma_{RC}) \quad (16b)$$

It should be noted that Equations (16a) and (16b) apply for the limiting case of optically thin samples. The factor $N \sigma$ in Equation (16a) represents an experimental fit parameter. The absorption cross sections were calculated

with Equation (17) from the molar extinction coefficients, ϵ , resulting from the spectral decomposition of the absorption spectra as described in section 3.3.1. Furthermore, the invariance of the individual antenna sizes was used as a constraint. To evaluate the size of the antenna pool per PSU in HL grown membranes Equation (16b) was solved for N_{B800} or N_{B850} - depending on the excitation wavelength - under the constraints $N_{B880} = 32$ (Karrasch *et al.*, 1995), $N_{B820} = 0$ and $N_{B850}/N_{B800} = 2$ (McDermott *et al.*, 1995). To evaluate the antenna size in membranes of LL and LL/LT grown bacteria a linear combination of Equation (16b) valid for two excitation wavelengths (802nm and 820nm, respectively) was solved for N_{B800} and N_{B820} under the constraints $N_{B880} = 32$ and $(N_{B820} + N_{B850})/N_{B800} = 2$. In all the above cases altering the constraint $N_{B880} = 32$ to $N_{B880} = 24$, to take into account an LH1 ring consisting of 12 $\alpha\beta$ -apoproteins, did not affect the fit of the fluorescence induction curve.

In the case of HL grown membranes, the best fit parameter for the horizontal axes was $N \sigma = 2.35 \times 10^{-14} \text{ cm}^2$ at an excitation wavelength of 802nm. When this number was decomposed to reveal the contributions of each pigment pool according to the procedure described above, the following antenna sizes were obtained: $N_{B800} = 46$, $N_{B850} = 95$ and $N_{B880} = 32$. Excitation of the membranes at 848nm and analogous data treatment gave slightly different numbers which were within the errors quoted in Table 7.1. The number of pigments in a pigment pool per PSU of membranes of LL and LL/LT grown bacteria were calculated in the same manner. The PSUs of both these growth types contained a similar number of B850 pigments (~30) but differed in the number of B800 and B820 pigments (Table 7.1). LL/LT membranes possessed nearly twice as much Bchl per PSU as HL membranes (348 Bchls *versus* 182 Bchls) whereas LL membranes contained a total of 227

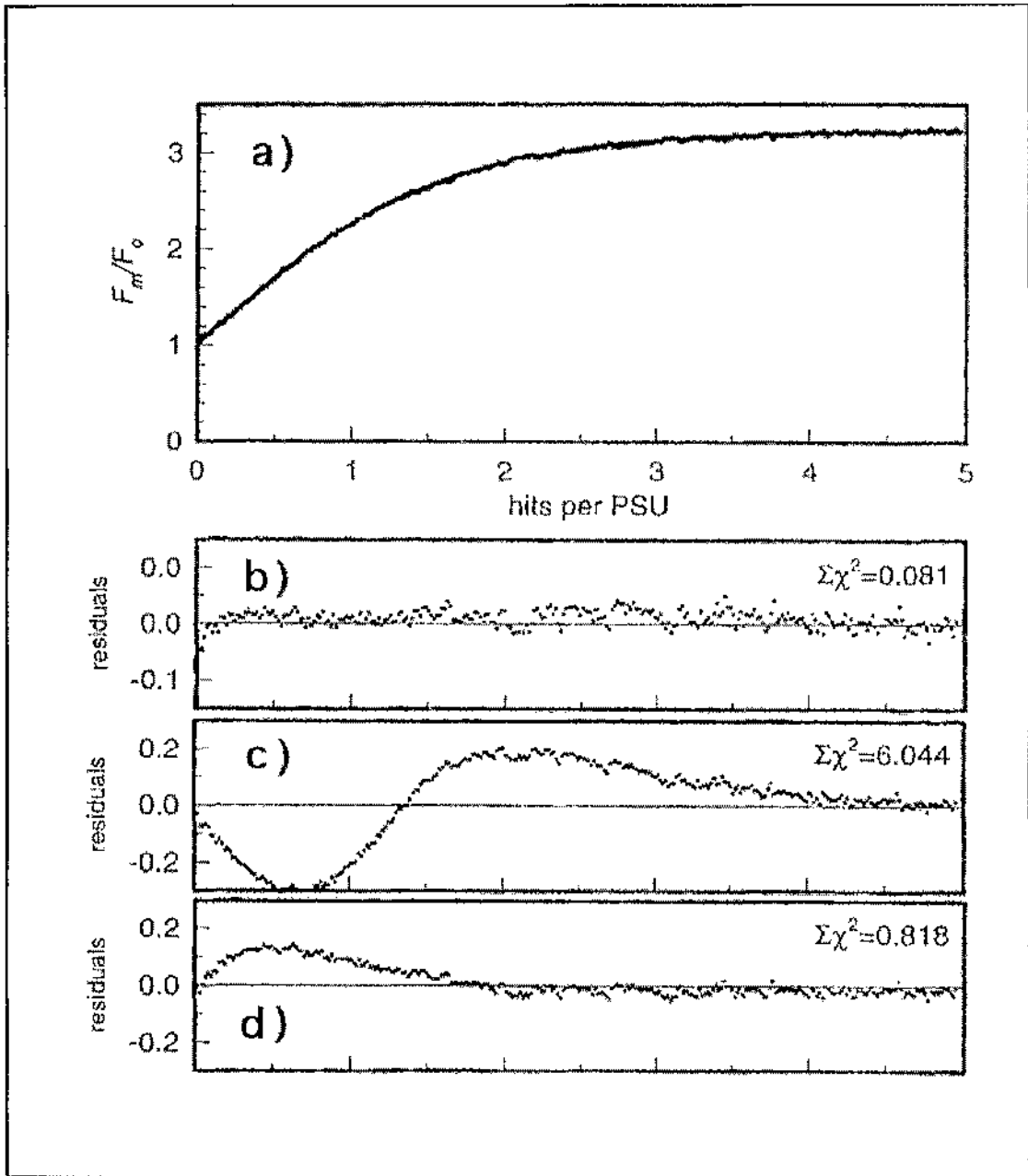


Figure 7.4. (a) Normalised fluorescence induction curve of photosynthetic membranes of *Rps. acidophila* 7750 grown under HL conditions. This curve was obtained by processing the data contained in Fig.7.3 according to the procedure described in the text and Trissl (1996). Three parameters were used to fit the curve: F_m/F_o , J , and an ordinate scaling parameter, $N\sigma$, which relates flash energy to the number of hits per PSU. Best fit data were $F_m/F_o = 3.23$ and $J = 0.34$. (b) Residuals of the best fit data. (c) Residuals when J was arbitrarily set to a value of 2.23 to represent the lake model of the PSU. (d) Residuals when J was arbitrarily set to a value of zero to represent a separate units model of antenna organisation.

Bchl per PSU. The idealised model of Papiz *et al.*, (1996), which predicts a PSU consisting of 8 LH2 complexes surrounding each LH1-RC core complex, contains a total of 248 Bchl molecules.

For the particular example of membranes from HL grown bacteria (Fig. 7.4a), the best fit of Equation (15) (section 7.1) to the processed data yielded $F_m/F_o = 3.23$ and a sigmoidicity parameter of $J = 0.34$. The significance of this method in determining the J parameter was demonstrated by assuming the lake model of antenna organisation (Monger & Parson, 1977) and setting the sigmoidicity parameter to $J_{\text{lake}} = 2.23$ (corresponding to $J_{\text{lake}} = F_m/F_o - 1$) (Lavergne & Trissl, 1995). Figure 7.4d shows the corresponding residuals for this model are 75-fold larger than those of the best fit in Figure 7.4b. Similarly, when a separate units model was assumed by setting the sigmoidicity parameter, J , to zero the residuals were about 10-fold worse than the best fit residuals (Fig. 7.4c).

Changing the excitation wavelength to 820nm, 848nm or 869nm did not effect the sigmoidicity parameter. This demonstrates that exciton transfer from the peripheral to the core complexes is a fast and efficient process. Excitation at different wavelengths also allowed the determination of the absolute antenna size of a PSU. It is conceivable that the excitonic connectivity of PSUs may be controlled by the packing density and this, in turn, by the concentration of divalent cations and temperature. This was investigated by adding 20mM $MgCl_2$ to the membrane samples and performing the fluorescence induction measurements at 4°C. Such treatment did not have an effect on the sigmoidicity parameter of any of the preparations tested.

Fluorescence induction experiments were repeated several times to ensure reproducibility. In each case fresh cell fillings were used and only one flash was given to each sample. Photosynthetic membranes from LL

Table 7.1. Number of Bchl *a* pigments in a pigment pool (i.e. antenna size) belonging to one RC. These values were determined by the fit method described in the text. The total number of Bchl *a* pigments per PSU ($N_{total} = N_{B800} + N_{B820} + N_{B850} + N_{B880}$) are listed in the last column. The Papiz model represents an idealised case in which 8 LH2 complexes surround a LH1-RC core complex (Papiz *et al.*, 1996).

Growth type	N_{B800}	N_{B820}	N_{B850}	N_{B880}	N_{total}
HL	46 ± 3	-	104 ± 14	32	182
LL	65 ± 3	124 ± 3	30 ± 8	32	227
LL/LT	105 ± 6	180 ± 6	31 ± 3	32	348
Papiz model	72	-	144	32	248

Table 7.2. Summary of the averaged fit parameters F_m/F_o and J as determined from fluorescence induction experiments of photosynthetic membranes from three different growth types of *Rps. acidophila* strain 7750. The rate constant of inter-unit energy transfer, k_{con} , was calculated with Equation (14) assuming $k_f = (60\text{ps})^{-1}$ (or, if expressed in more conventional terms, $1.67 \times 10^{10} \text{ s}^{-1}$).

Growth type	F_m/F_o	J	k_{con}	# of expts.
HL	2.89 ± 0.34	0.37 ± 0.07	$3.58 \times 10^9 \text{ s}^{-1}$	12
LL	2.66 ± 0.11	< 0.02	$< 10^8 \text{ s}^{-1}$	24
LL/LT	2.75 ± 0.12	< 0.01	$< 10^8 \text{ s}^{-1}$	16

and LL/LT grown cells were treated in the same manner as those of HL grown cells. However, in contrast to the HL membranes the fluorescence induction curves from the LL and LL/LT membranes did not display any significant sigmoidicity. The corresponding fit parameters averaged over several experiments are listed in Table 7.2. LL and LL/LT membranes showed F_m/F_o values of 2.66 and 2.75, respectively. All three growth types displayed rather high F_m/F_o ratios compared to the F_m/F_o value of 2 measured by Deinum *et al.*, (1991).

The continuum theory (Lavergne & Trissl, 1995) applied to the data evaluation places all energy transfer processes into a single rate constant k_{con} . This rate constant allowed a useful quantification of the excitonic connectivity of RCs. The relationship between the experimental fit parameter, J , and k_{con} is described by Equation (15) in section 7.1. To solve this equation for k_{con} the numerical value of k_f , which is given by the fluorescence decay kinetics, is required. This rate constant was assumed to be $k_f = (60 \text{ ps})^{-1}$ which is in agreement with time-resolved data from *Rb. sphaeroides* (Sundström *et al.*, 1986). Using this assumption the J parameter was converted into the inter-unit energy transfer rate constant, k_{con} , listed in Table 7.2. In HL grown membranes $k_{con} = 3.58 \times 10^9 \text{ s}^{-1}$, whereas in LL and LL/LT membranes k_{con} is smaller than the detection level.

The results presented in this chapter allowed the construction of models of the PSU of different growth types of the bacterium *Rps. acidophila* strain 7750. These are discussed in detail in Chapter 9.

CHAPTER EIGHT

3-D CRYSTALLISATION OF THE LH1-RC CORE COMPLEX

8.1. 3-D crystallisation of the LH1-RC core complex

Although the crystal structures of the purple bacterial LH2 complex (McDermott *et al.*, 1995; Koepke *et al.*, 1996) and the photochemical RC (Allen *et al.*, 1987a, 1987b; Buchanan *et al.*, 1993; Chang *et al.*, 1986, 1991; Deisenhofer *et al.* 1984; Yeates *et al.*, 1988) are known, no detailed structure of either the purple bacterial LH1 antenna or the complete LH1-RC core complex yet exists. In an attempt to address this problem it was decided to investigate the possibility of crystallising, in three dimensions, the LH1-RC core complex in the hope that crystals suitable for analysis by classical X-ray crystallographic techniques could be grown. To increase the probability of obtaining crystals, more than one source of the core complex was investigated. To this end, the LH1-RC core complexes from eleven different species and strains of purple bacteria, along with the LH1-only antenna complex from *Rh. marinum*, were isolated and purified as described in Chapter 2, then screened for their suitability for producing 3-D crystals.

Protein crystals can take anything from days to weeks, or even months, to form and grow. Therefore, it is a prerequisite that the protein is stable over this timescale. The core complexes from most of the species studied were stable over this time period and produced crystals. The isolated, LDAO solubilised core complex from *Rv. gelatinosus*, however, was found to be unstable (section 4.4) and denatured within a few days when used in crystallisation trials. Several attempts were made to improve the stability of this core complex by exchanging the LDAO for different detergents. These attempts failed to increase stability. Therefore, it was decided not to pursue the 3-D crystallisation of core complex from this species.

Crystallisation of the LH1-RC core complex was achieved by vapour diffusion using the sitting drop method (see sections 1.11.3 and 2.6).

Initially, a broad screen of crystallisation conditions, in which parameters such as precipitant type and concentration, protein concentration, pH, detergent type and concentration, incubation temperature, and the effect of additives were varied, was performed to determine the conditions best suited to 3-D crystal formation. These crystallisation trials were based on previous reports of the growth of 3-D crystals of core complex (Dawkins, 1988; Gall, 1994; Wacker *et al.*, 1986) and LH2 complexes (Cogdell *et al.*, 1991; Cogdell & Hawthornthwaite, 1993; Papiz *et al.*, 1989). Two broad screens were investigated in the initial crystallisation trials - Membfac™ and the Magic 46 screen (refer to Appendix C). Membfac™ (Hampton Research) is a commercially available screening kit specifically designed for the crystallisation of membrane proteins. This kit has been reported as a highly effective sparse matrix screen for finding initial crystallisation conditions for membrane proteins (UCLA Crystallisation Workshop, June 21, 1993). It allows one to perform a sparse matrix screen while changing the detergent dimension. However, using this screen with the detergents LDAO, cholate or β -OG failed to produce crystals of the core complex from any of the species studied. The Magic 46 screening protocol was established by the University of California, Berkeley, U.S.A. and utilises a range of PEG's, organic solvents and salts as precipitants (Gall, 1994). The Magic 46 trials numbered 14, 23, 45 and 46 (see Appendix C) that used PEG 400 and PEG 8000 as precipitants were successful for the crystallisation of the core complex from *Rps. palustris* 2.6.1 in β -OG (Gall, 1994). These results, however, could not be duplicated and the Magic 46 screen failed to produce crystals of core complex from any of the species and strains studied in this thesis.

Crystallisation trials in which ammonium sulphate and potassium phosphate were used as precipitants also did not produce core complex

crystals. Such a system caused denaturation of the complex within 1-2 days of setting up the experiment. Therefore, use of these precipitants for the crystallisation of core complexes was discontinued. However, the LH1-only antenna complex from *Rh. marinum* did produce crystals when ammonium sulphate and potassium phosphate were used as precipitants (section 8.8). From these observations it seems that the presence of a RC within the LH1 ring has a dramatic effect on the ability of the core complex to crystallise. The use of organic solvents as precipitants also caused a rapid denaturation of the core complexes. Denaturation was visible by a change of colour of the complexes. Upon denaturation they changed from a reddish-purple colour to a brownish-green colour as the Bchl *a* molecules became dissociated from their protein scaffold. In most cases the use of buffers with pH values below ~7.0 also resulted in denaturation of the complexes. However, the core complexes appeared to be stable in some of the Magic 46 incubations which used PEG as a precipitant at acidic pH. Taking all these observations into account it was decided to use the FASTPEG screen devised by Gall (1994) to search for favourable crystallisation conditions. This screen used various molecular weight PEG's as precipitants at mostly alkaline pH values and is described in Appendix C. This screen did not produce any core complex crystals when used with the detergents LDAO, DDAO, UDAO or β -OG. Phase separation, denaturation or a clear droplet resulted in most of the trials. However, some of the trials resulted in formation of an amorphous precipitate. Therefore, a wide range screen using PEG's with molecular weights from 200-20,000 buffered with Tris-HCl, pH 8.5-10.5, was devised. When this screen was used amorphous precipitate formed in the trials that used PEG's with molecular weights of 400-4000 in the presence of LDAO or β -OG. Encouraged by these results further crystallisation screens, using PEG's 400-4000 as precipitants, were performed

in the search for conditions that would produce core complex crystals. A previous report by Wacker *et al.* (1986) on the successful crystallisation of the LDAO solubilised core complex from *Rps. palustris* also used PEG as a precipitant. In this case PEG 2000 was used in the presence of $MgCl_2$ at pH 8.0. Therefore, these reagents were used as the starting point for the optimisation of the crystallisation conditions. The breakthrough in the crystallisation trials came when the LDAO used to solubilise the core complex was exchanged for cholate, and PEG 2000 in the presence of $MgCl_2$ was used as a precipitant (see following sections). Subsequently, crystals were grown using the detergents HECAMEG, heptyl- β -D-thioglucoiside, sucrose monocholate, taurocholate and C-HEGA-10 (see Table 8.1).

Over 5000 individual crystallisation experiments were performed. In the course of these experiments over 30 different detergents were investigated for their efficacy in producing core complex crystals. The effects of ~50 different additives were also investigated (see Appendix C). All the crystallisation trials were incubated at 15°C unless otherwise stated. This chapter will describe the conditions that were successful in producing core complex crystals.

8.2. *Rhodopseudomonas acidophila* strain 10050 core complex

The core complex of this species of purple bacteria was one of the most stable when it was isolated and purified in LDAO (see section 4.2). Therefore, it was a good candidate for producing 3-D crystals. Also, as the structure of the LH2 complex from the 10050 strain of *Rps. acidophila* has been solved (McDermott *et al.*, 1995), the elucidation of the structure of the LH1-RC core complex would allow a complete picture of the PSU of this species to be constructed. For these reasons crystallisation studies were

concentrated on this strain of bacteria.

Initial crystallisation trials were based on those described by Wacker *et al.* (1986). These trials used PEG 2000 as a precipitant and $MgCl_2$ as a salt. The crystallisation solutions were buffered to pH 8.0 with 20mM Tris-HCl and the trials were incubated in the dark at 15°C. Several small molecule additives were also screened for their efficacy at influencing crystallisation of the core complex during these trials (see Appendix C). Core complex crystals did not grow when LDAO (0.04% or 0.1% v/v) was used as detergent, even in the presence of small amphiphiles. Therefore, the LDAO was exchanged for 1% (w/v) cholate (section 2.4.5). Once again crystals did not form. However, when the small molecule L-cysteine was used as an additive in the presence of 1% (w/v) cholate, dark red, cubic crystals with dimensions of 0.1mm x 0.1mm x 0.1mm formed within about 7 days (Fig. 8.1). At the time of writing this thesis these crystals were too small to be used for X-ray diffraction analysis (S.M. Prince, personal communication). However, the analysis of small crystals has very recently been made possible now that a micro-focus X-ray beam has come on stream at the ESRF facility at Grenoble, France. The exact crystallisation conditions that produced these crystals are described below. It should be noted that the concentrations given for the protein droplet solution represent the final concentrations of each component after the core complex solution was mixed with the crystallisation reagents (see section 2.6).

Protein droplet solution: *Rps. acidophila* 10050 core complex OD = $55cm^{-1}$
10% (w/v) PEG 2000
10mM $MgCl_2$
1% (w/v) cholate
20mM Tris-HCl, pH 8.0
10mM L-cysteine

Reservoir solution: 20% (w/v) PEG 2000
 20mM MgCl₂
 1% (w/v) cholate
 20mM Tris-HCl, pH 8.0

Using the same conditions but substituting the polyamine additive spermidine (10mM) for L-cysteine resulted in the growth of cubic crystals with dimensions of ~0.15mm x 0.15mm x 0.15mm (Fig. 8.2). Spermidine, traditionally used as an effective additive for the crystallisation of nucleic acids, proved to be one of the most efficacious additives for promoting the formation of core complex crystals. The use of the additives betaine monohydrate and taurine also produced crystals of *Rps. acidophilu* strain 10050 core complex (Figs. 8.3 & 8.4, respectively). However, when these additives were used the crystals were very small and irregular in shape. From these observations it appears that additive molecules have a critical effect, both on the ability of the protein-detergent complex to form crystals and on the crystal morphology. Thus, the choice of additive, although empirical, may be an important factor in the growth of core complex crystals of sufficient quality for X-ray analysis. As such, several other additives were investigated, both alone and in combination. Using the crystallisation conditions described above, the L-cysteine was replaced with a combination of 10mM spermidine and 10mM heptane-1,2,3-triol (high m.p. isomer). Once again, dark red, cubic crystals with dimensions of ~0.15mm x 0.15mm x 0.15mm (Fig. 8.5) formed within 7-14 days of setting up the experiment. Fewer of these crystals formed compared to the number of crystals formed when other additives were used. There was also evidence of some red coloured precipitation in the crystallisation well of this trial indicating that not all of the core complex protein was utilised for crystal growth. Using the same conditions but exchanging the spermidine for 3% (v/v) dioxane also

resulted in the formation of crystals. These crystals varied in shape and were not of a uniform size (Fig. 8.6). Some looked beautiful under the microscope and had sharp edges while others had a trapezoid shape with rounded edges. There was also a lot of amorphous precipitate in the bottom of the well, again indicating that not all the core complex protein was taken up by crystal formation. X-ray analysis of these crystals indicated that they were of a poor quality. They diffracted only to 20-25Å (S.M. Prince, personal communication). A further crystallisation trial used barium chloride (10mM) as an additive in combination with heptane-1,2,3-triol. In this case, only two large, disordered plate-like crystals with dimensions of ~0.3mm x 0.5mm formed (Fig. 8.7). However, due to their poor shape and ill-defined edges none of these crystals was suitable for X-ray analysis.

The conditions for the growth of *Rps. acidophila* 10050 core complex crystals were further investigated by varying the concentration of PEG 2000 used in the trials. The concentration of core complex and additives was also varied. The conditions listed below produced the disordered, lozenge-shaped crystals shown in Figure 8.8:

Protein droplet solution: *Rps. acidophila* 10050 core complex OD = 70cm⁻¹
8.5% (w/v) PEG 2000
10mM MgCl₂
1% (w/v) cholate
20mM Tris-HCl, pH 8.0
2% (w/v) spermidine
2% (v/v) dioxane

Reservoir solution: 20% (w/v) PEG 2000
20mM MgCl₂
1% (w/v) cholate
20mM Tris-HCl, pH 8.0

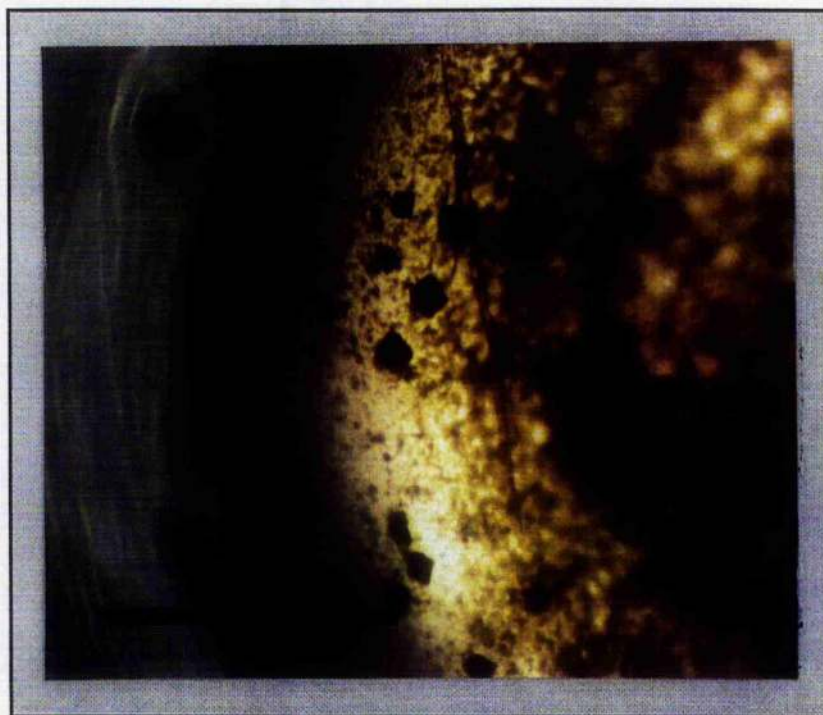


Figure 8.1. Crystals of *Rps. acidophila* 10050 core complex grown by vapour diffusion in the presence of PEG 2000 and $MgCl_2$ with L-cysteine as an additive. The LDAO was exchanged for 1% (w/v) cholate. Refer to text for a full description of the crystallisation conditions. Bar= 1mm.

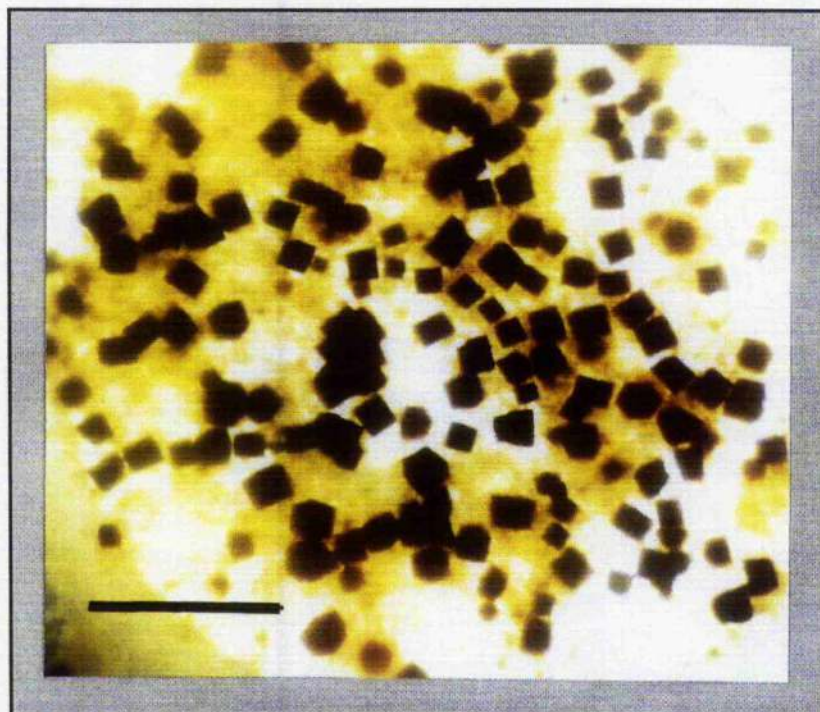


Figure 8.2. Cubic crystals of *Rps. acidophila* 10050 core complex grown using the same conditions as the crystals in the figure above, but with spermidine as an additive. Bar= 1mm.

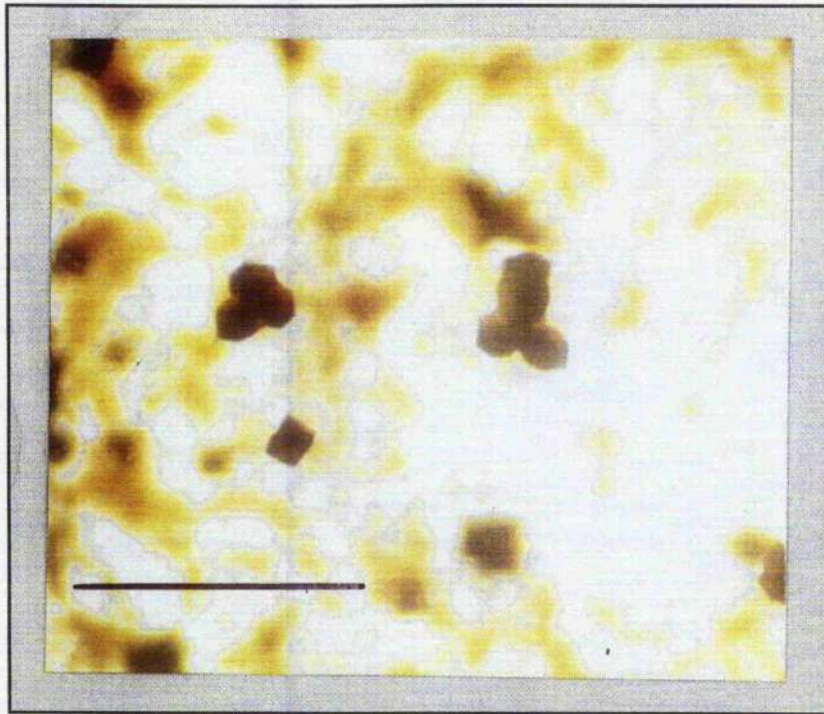


Figure 8.3. Crystals of *Rps. acidophila* 10050 core complex grown by vapour diffusion in the presence of PEG 2000 and $MgCl_2$ with betaine monohydrate as an additive. The detergent used was 1% (w/v) cholate. Refer to text for a full description of the crystallisation conditions. Bar= 1mm.

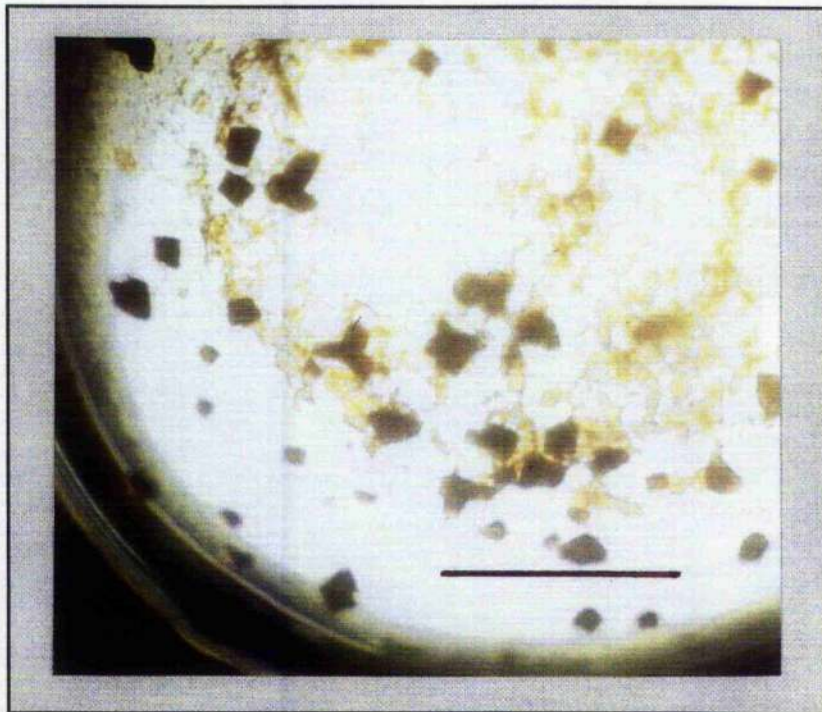


Figure 8.4. Cubic crystals of *Rps. acidophila* 10050 core complex grown using the same conditions as the crystals in the figure above, but with taurine as an additive. Bar= 1mm.

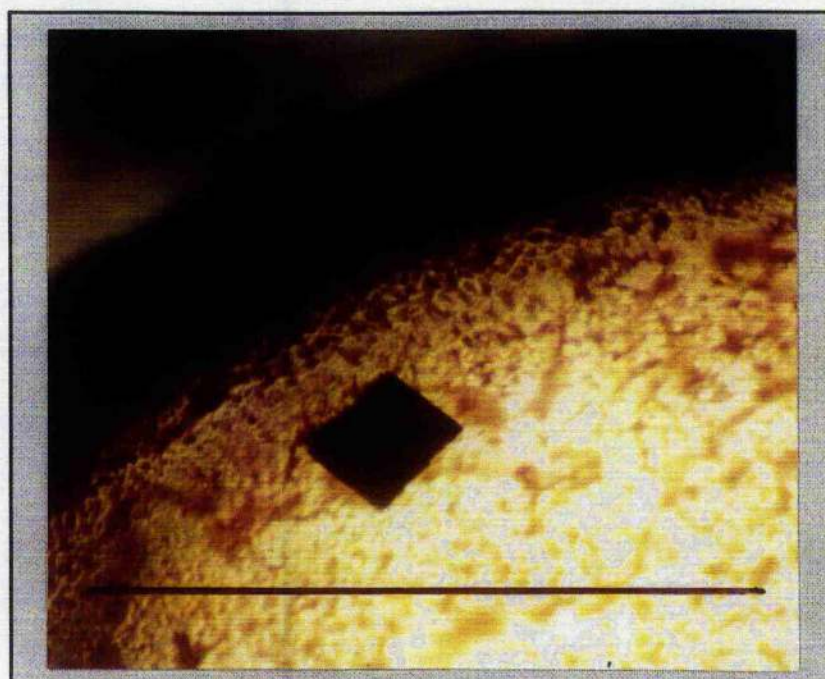


Figure 8.5. Cubic crystals of *Rps. acidophila* 10050 core complex grown in PEG 2000 with 10mM spermidine and heptane-1,2,3-triol as additives and 1% (w/v) cholate as detergent. Bar= 1mm.

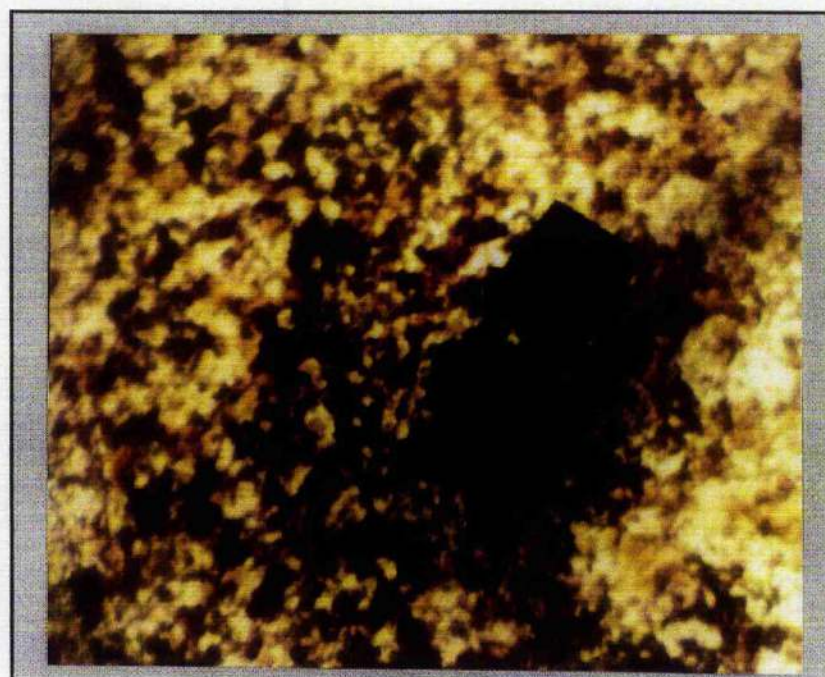


Figure 8.6. Cubic crystals of *Rps. acidophila* 10050 core complex grown under the same conditions as above but substituting 3% (v/v) dioxane for the spermidine. The crystals are not of a uniform size and some coloured precipitate can be seen in the bottom of the well.

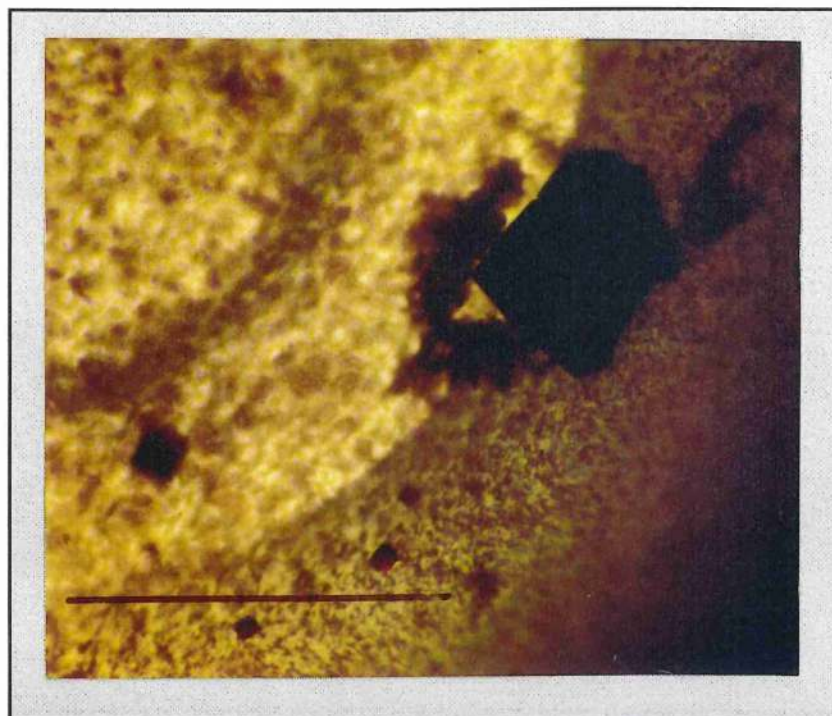


Figure 8.7. Large plate-like crystals of *Rps. acidophila* 10050 core complex formed when grown in PEG 2000 with 10mM barium chloride and heptane-1,2,3-triol as additives and 1% (w/v) cholate as detergent. Crystals are 0.3mm x 0.5mm.

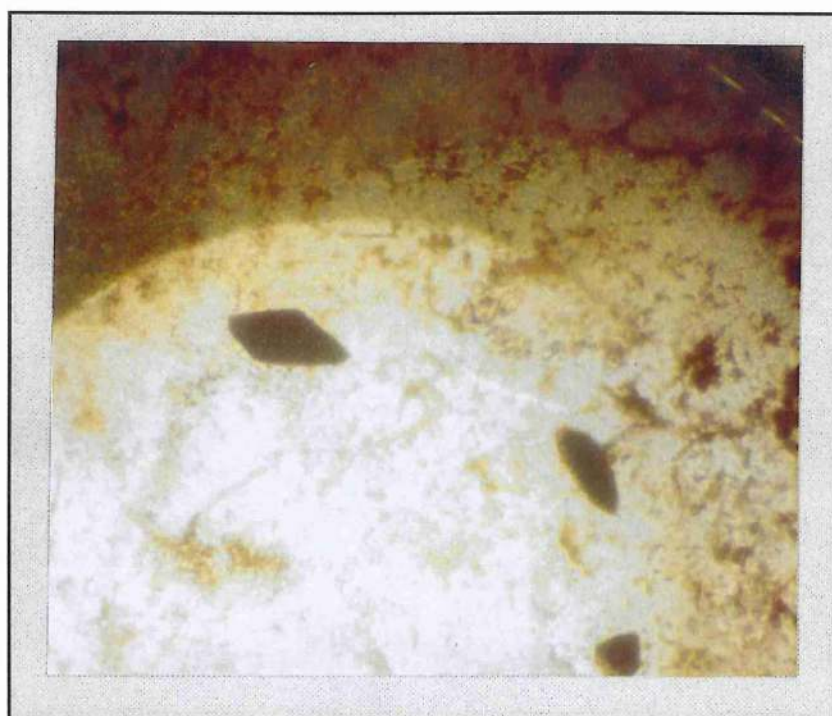


Figure 8.8. Lozenge-shaped crystals of *Rps. acidophila* 10050 core complex grown using 8.5% (w/v) PEG 2000 in the well and 20% (w/v) PEG 2000 in the reservoir. 2 % (v/v) dioxane and 2% (w/v) spermidine were used as additives and 1% (w/v) cholate as a detergent.

As some amorphous precipitation was visible in the bottom of the well of this trial, crystallisation conditions were further altered by decreasing the concentration of core complex and increasing the concentration of PEG in both the well and reservoir. This gave the following conditions:

- Protein droplet solution: *Rps. acidophila* 10050 core complex OD = 60cm⁻¹
12% (w/v) PEG 2000
10mM MgCl₂
1% (w/v) cholate
20mM Tris-HCl, pH 8.0
2% (w/v) spermidine
- Reservoir solution: 22.5% (w/v) PEG 2000
20mM MgCl₂
20mM Tris-HCl, pH 8.0

Within 4-5 days this trial yielded a shower of microcrystals which were unordered and of different sizes (Fig. 8.9). In order to slow down the rate of crystal growth the PEG concentration gradient between the well and reservoir was decreased. A reductant, in the form of ascorbic acid, was also added to the core complex solution in an attempt to keep it reduced during crystallisation. The modified crystallisation conditions consisted of:

- Protein droplet solution: *Rps. acidophila* 10050 core complex OD = 55cm⁻¹
9.5% (w/v) PEG 2000
10mM MgCl₂
1% (w/v) cholate
20mM Tris-HCl, pH 8.0
2% (w/v) spermidine
2.5mM ascorbic acid
- Reservoir solution: 15% (w/v) PEG 2000
20mM MgCl₂

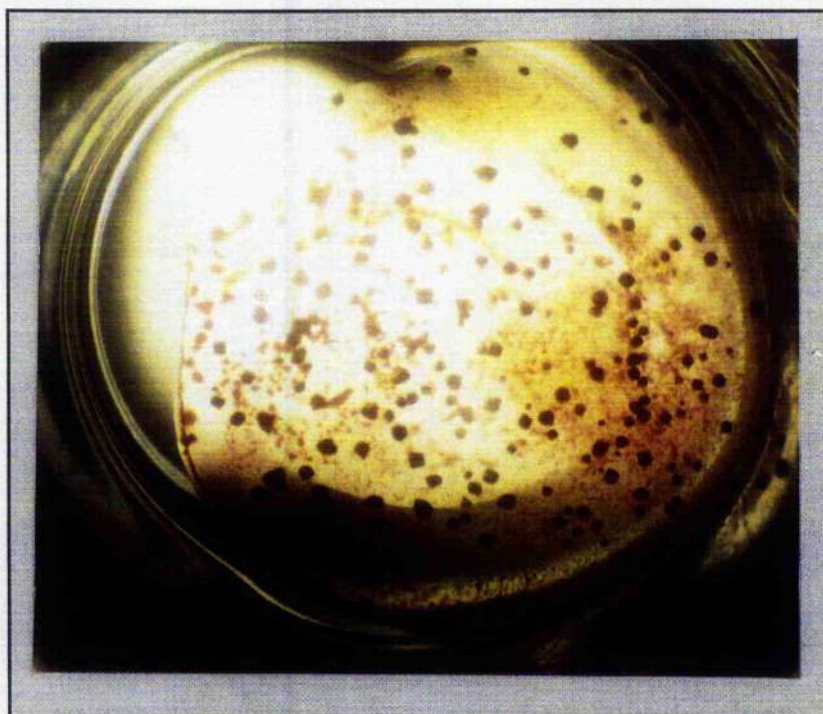


Figure 8.9. A shower of microcrystals of *Rps. acidophila* 10050 core complex formed when the concentration of PEG 2000 in the protein droplet was adjusted to 12.5% (w/v) and that in the reservoir to 22.5% (w/v). 2% (w/v) spermidine was used as an additive in the presence of 1% (w/v) cholate.

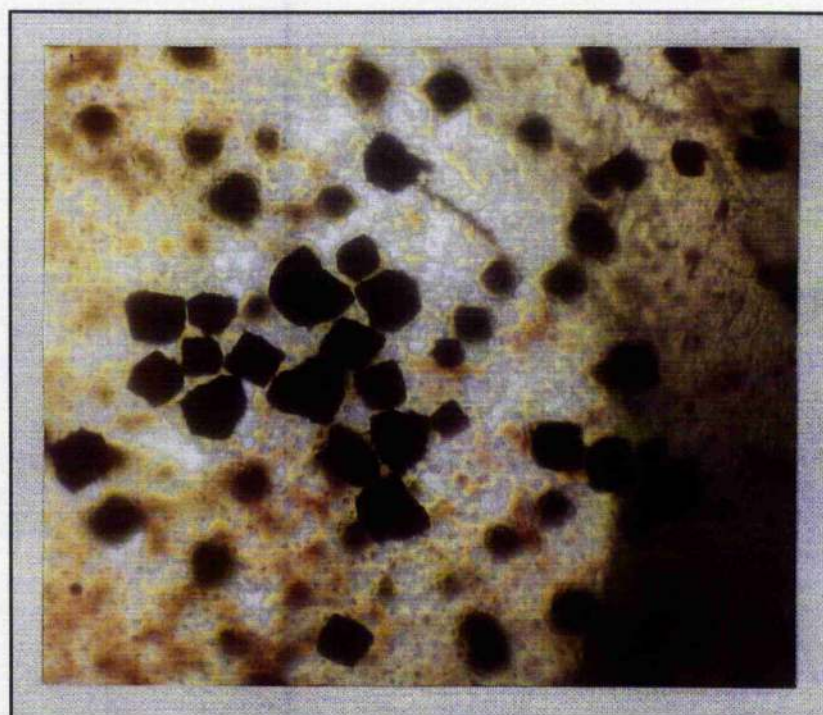


Figure 8.10. A shower of irregularly shaped crystals of *Rps. acidophila* 10050 core complex grown in PEG 2000 (see text for details). 2.5mM ascorbate was added to the protein solution droplet in an attempt to maintain the RC in a reduced state. However, it did not improve crystal quality.

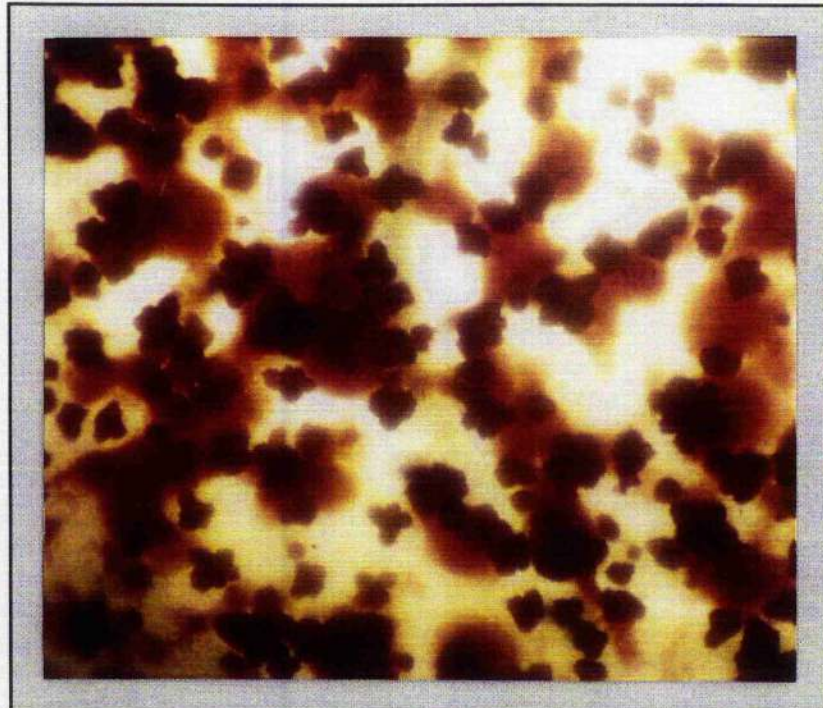


Figure 8.11. Altering the PEG concentrations to 8.5% (w/v) and 20.5 (w/v) in the protein droplet and reservoir, respectively, produced twinned crystals of *Rps. acidophila* 10050 core complex. There is also some evidence of phase separation in the well.

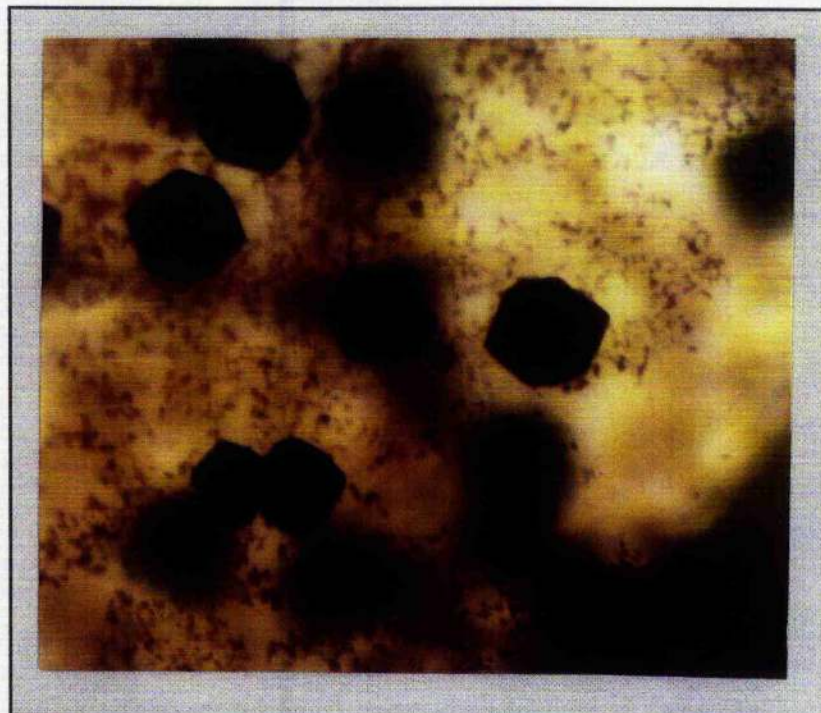


Figure 8.12. Well ordered cubic crystals of *Rps. acidophila* 10050 core complex, with dimensions of 0.1mm x0.1mm, grew when PEG concentrations were reduced to 11.5 (w/v) and 17% (w/v) in the protein droplet and reservoir, respectively.

1% (w/v) cholate
5mM ascorbic acid
20mM Tris-HCl, pH 8.0

Once again a shower of unordered, irregularly shaped crystals formed (Fig. 8.10) that were unsuitable for X-ray analysis. Using the same conditions as above but altering the PEG 2000 concentrations to 8.5% (w/v) and 20% (w/v) in the protein droplet and reservoir solutions, respectively, produced the crystals shown in Figure 8.11. These crystals were of a very poor quality with many of them twinned. Some phase separation can be seen in the background of the crystallisation well. However, a different trial in which the concentrations of PEG 2000 were altered to 11% (w/v) in the protein droplet and 17% (w/v) in the reservoir produced well ordered cubic crystals with dimensions of 0.1mm x 0.1mm x 0.1mm (Fig. 8.12). These crystals diffracted X-rays to $\sim 15\text{-}20\text{\AA}$ (S.M. Prince, personal communication). In an attempt to improve crystal quality, conditions were optimised by again changing the concentrations of PEG used in the crystallisation trials. This was performed by adjusting the PEG 2000 concentrations to 7.5% (w/v) and 18% (w/v) in the droplet and reservoir solutions, respectively. The star-shaped crystals produced, however, were very irregular and badly twinned (Fig. 8.13).

The crystals shown in Figure 8.14 grew within 1-2 weeks at 15°C when the following conditions were employed:

Protein droplet solution: *Rps. acidophila* 10050 core complex OD = 70cm^{-1}
8.5% (w/v) PEG 2000
10mM MgCl₂
1% (w/v) cholate
25mM Tris-HCl, pH 8.0

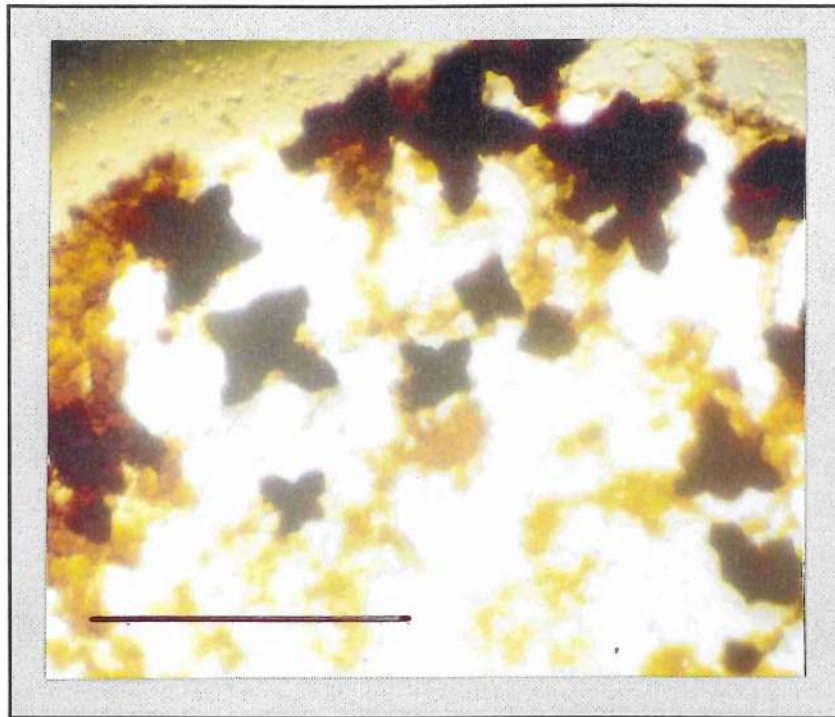


Figure 8.13. Irregular, badly twinned, star-shaped crystals of *Rps. acidophila* 10050 core complex formed using 7.5% (w/v) and 18% (w/v) PEG 2000 in the protein droplet and reservoir solutions, respectively. 1% (w/v) cholate was the detergent. Bar = 1mm.

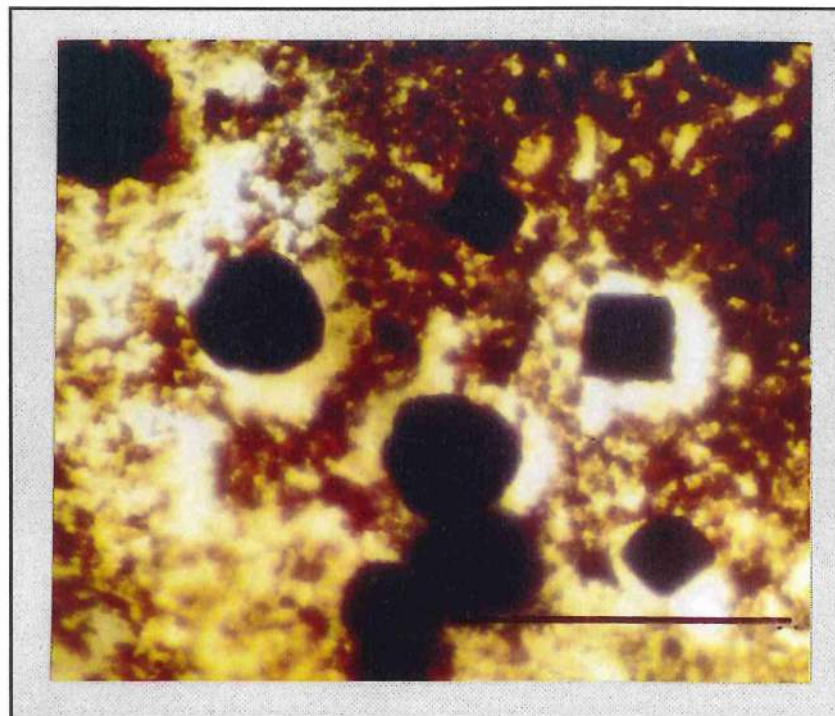


Figure 8.14. Rounded crystals of *Rps. acidophila* 10050 core complex grown in PEG 2000 with 10mM spermidine and 2% (v/v) dioxane as additives and 1% (w/v) cholate as detergent. Bar= 1mm.

	10mM spermidine
	2% (v/v) dioxane
Reservoir solution:	20% (w/v) PEG 2000
	20mM MgCl ₂
	1% (w/v) cholate
	25mM Tris-HCl, pH 8.0

Some of the crystals are poorly ordered with rounded edges. These crystals were very soft and broke easily when handled. However, others were cubic in shape with sharp, well defined edges and dimensions of ~0.12mm x 0.12mm x 0.12mm. Unfortunately they did not diffract when placed in the X-ray beam. Employing the same conditions but substituting the additive polyvinylpyrrolidone K15 (5% w/v) for dioxane and decreasing the incubation temperature to 4°C resulted in the growth of flake-like crystals shown in Figure 8.15. The crystals were irregular and of different shapes and sizes. However, the mother liquor in the well is clear and no precipitation is present, indicating that all the core complex has been utilised for crystal formation.

Over 30 detergents were screened (see Appendix C) during optimisation of the core complex crystallisation trials. When the LDAO used to solubilise the *Rps. acidophila* 10050 core complex was exchanged for sucrose monocholate and spermidine was used as an additive, flat triangular crystals with dimensions of ~0.05mm x 0.08mm x 0.08mm grew when the trial was incubated at 15°C (Fig. 8.16). The crystallisation conditions employed during this trial were:

Protein droplet solution:	<i>Rps. acidophila</i> 10050 core complex OD = 55cm ⁻¹
	10% (w/v) PEG 2000
	10mM MgCl ₂



Figure 8.15. Flake-like crystals of *Rps. acidophila* 10050 core complex. These crystals were grown using the same conditions described in Figure 8.14 but substituting 5% (w/v) polyvinylpyrrolidone for dioxane and decreasing the incubation temperature to 4°C. Bar= 1mm.

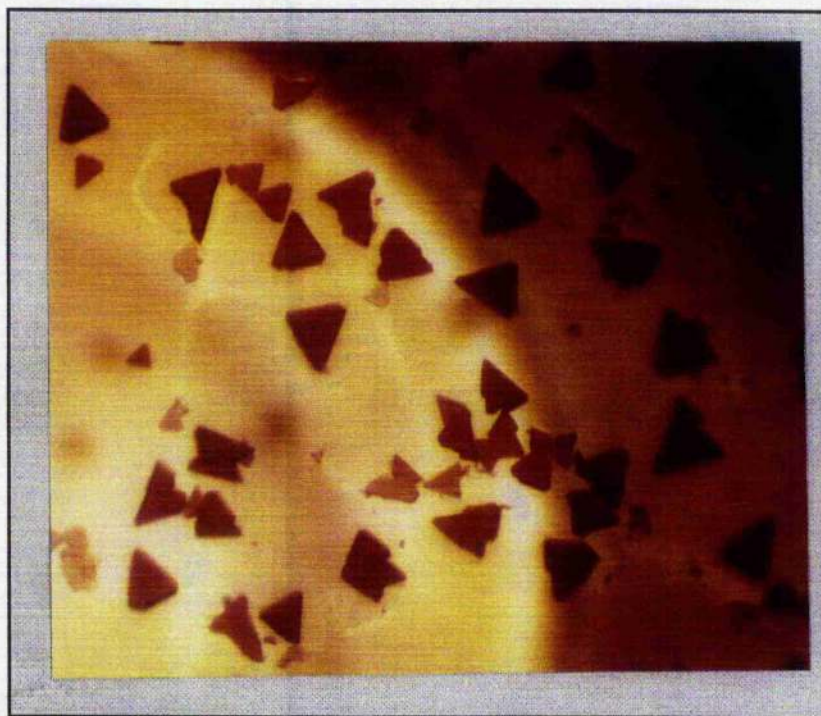


Figure 8.16. Flat, triangular crystals of *Rps. acidophila* 10050 core complex, with dimensions of 0.05mm x 0.08mm x 0.08mm, formed using sucrose monocholate as a detergent in the presence of 10mM spermidine.

5mM sucrose monocholate
40mM Tris-HCl, pH 8.0
10mM spermidine
Reservoir solution: 20% (w/v) PEG 2000
20mM MgCl₂
40mM Tris-HCl, pH 8.0

Substituting 10mM taurine as an additive in place of 10mM spermidine produced the small, irregular twinned crystals shown in Figure 8.17. This result underlines the effectiveness of spermidine as an additive for enhancing the growth of ordered core complex crystals in sucrose monocholate. Heptyl- β -D-thioglucoiside also proved effective as a detergent during crystallisation trials. Using the conditions:

Protein droplet solution: *Rps. acidophila* 10050 core complex OD = 55cm⁻¹
10% (w/v) PEG 2000
10mM MgCl₂
24.5mM heptyl- β -D-thioglucoiside
40mM Tris-HCl, pH 8.0
10mM spermidine
Reservoir solution: 20% (w/v) PEG 2000
20mM MgCl₂
40mM Tris-HCl, pH 8.0

resulted in the growth of irregularly shaped, flake-like crystals of various sizes and shapes (Fig. 8.18). Substitution of spermidine by 10mM taurine produced fewer, better ordered, rectangular crystals (Fig. 8.19). However, a lot of amorphous precipitate and some evidence of phase separation was apparent in the bottom of the crystallisation well. Using the same conditions but exchanging LDAO for HECAMEG (19.5mM) produced the

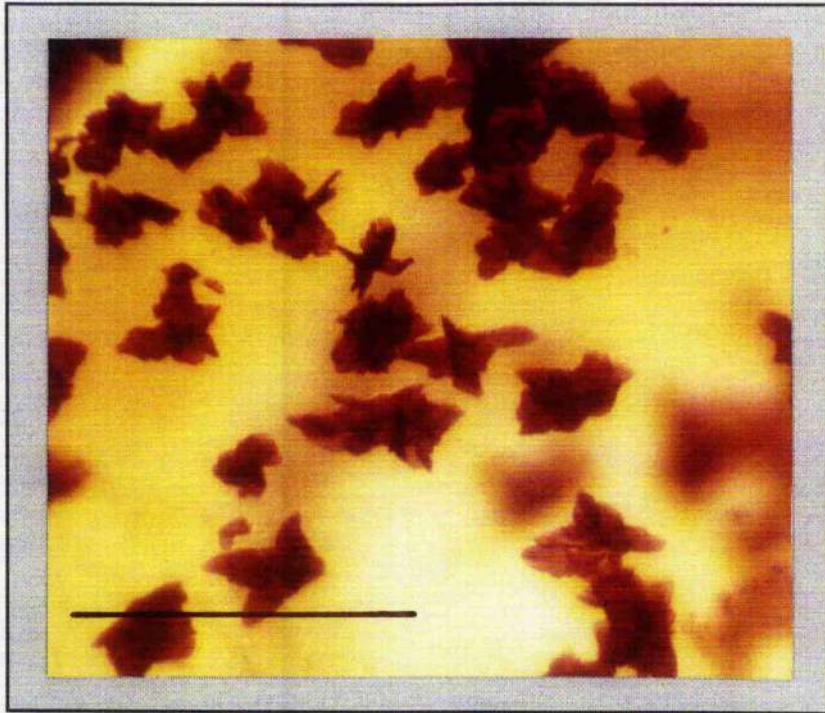


Figure 8.17. Using the crystallisation conditions which produced the crystals in Figure 8.16, but substituting 10mM taurine for spermidine, produced small, irregularly shaped and twinned crystals of *Rps. acidophila* 10050 core complex. Bar = 1mm.

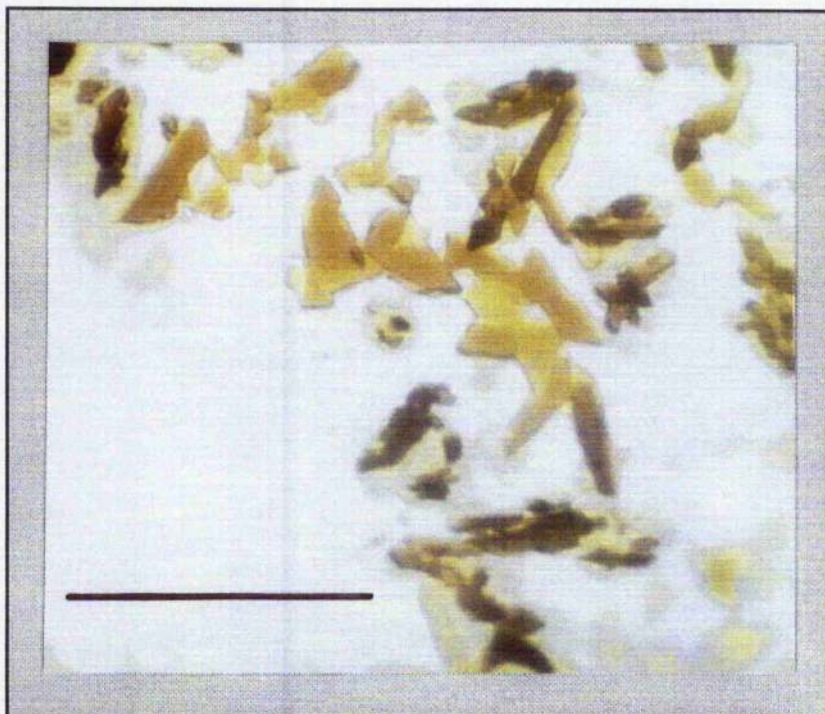


Figure 8.18. Irregular, flake-like crystals of *Rps. acidophila* 10050 core complex, formed when heptyl thioglucoside was used as a detergent in the presence of 10mM spermidine and PEG 2000 as a precipitant. Bar = 1mm.



Figure 8.19. Using heptyl thioglucoside as a detergent in the presence of the additive taurine produced rectangular crystals of *Rps. acidophila* 10050 core complex. There is evidence of amorphous precipitation and phase separation in the crystallisation well. Bar = 1mm.



Figure 8.20. Poorly ordered crystals of *Rps. acidophila* 10050 core complex grew when the heptyl thioglucoside was exchanged for HECAMEG. The crystals appear to be badly flawed and twinned. Bar = 1mm.

crystals in Figure 8.20. These crystals were very irregular in shape and poorly ordered. Most of these crystals appeared to be twinned and badly flawed. Thus, they were not of the quality required for X-ray diffraction studies.

The detergents taurocholate and C-HEGA-10 were also effective in the crystallisation of the *Rps. acidophila* 10050 core complex. The crystallisation conditions listed below produced thin, needle-like crystals with dimensions of $\sim 0.5\text{mm} \times 0.05\text{mm}$ (Fig. 8.21):

Protein droplet solution: *Rps. acidophila* 10050 core complex OD = 60cm^{-1}
12% (w/v) PEG 2000
10mM MgCl_2
1% (w/v) taurocholate
20mM Tris-HCl, pH 8.0
2% (w/v) putrescine

Reservoir solution: 20% (w/v) PEG 2000
20mM MgCl_2
20mM Tris-HCl, pH 8.0

A shower of roughly cubic, dark reddish-brown microcrystals formed (Fig. 8.22) when the conditions were modified slightly and the chaotropic agent urea was used as an additive:

Protein droplet solution: *Rps. acidophila* 10050 core complex OD = 58cm^{-1}
10% (w/v) PEG 2000
10mM MgCl_2
1% (w/v) taurocholate
20mM Tris-HCl, pH 8.0
10mM spermidine
10mM urea



Figure 8.21. Exchanging LDAO for 1% (w/v) taurocholate and including the polyamine additive putrescine produced needle-like crystals of *Rps. acidophila* 10050 core complex. The crystal dimensions are about 0.5mm x 0.05mm.

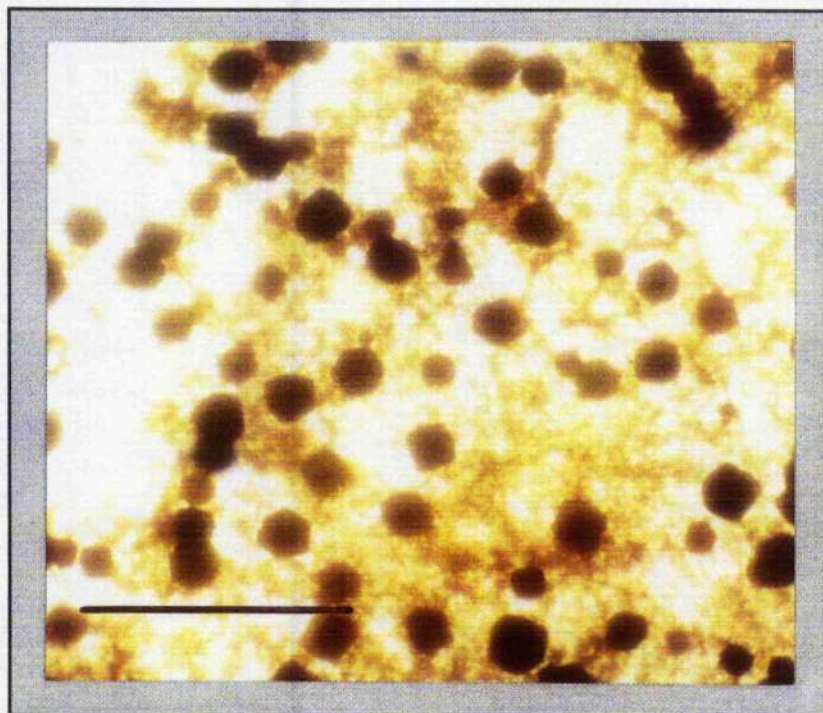


Figure 8.22. A shower of roughly cubic, dark red microcrystals of *Rps. acidophila* 10050 core complex formed when the conditions described above were modified slightly and spermidine and urea were used as additives (refer to text for details). Bar = 1mm.

Reservoir solution: 22.5% (w/v) PEG 2000
20mM MgCl₂
20mM Tris-HCl, pH 8.0

As shown in Figure 8.23, crystals of a similar size and morphology grew when the above conditions were modified by increasing the PEG 2000 concentration in the protein droplet to 12.5% (w/v) and substituting the urea with another chaotropic agent, trimethylamine HCl (10mM).

The largest crystals grew when LDAO was exchanged for the detergent C-HEGA-10. This resulted in the following crystallisation conditions:

Protein droplet solution: *Rps. acidophila* 10050 core complex OD = 55cm⁻¹
9.5% (w/v) PEG 2000
10mM MgCl₂
35mM C-HEGA-10
20mM Tris-HCl, pH 8.0
10mM taurine
10mM putrescine

Reservoir solution: 20% (w/v) PEG 2000
20mM MgCl₂
20mM Tris-HCl, pH 8.0

The flake-like crystals which formed are shown in Figure 8.24. Although the crystals were large enough for X-ray analysis they were not of a uniform shape or size and appeared to be of a poor quality. As such they were not used for X-ray diffraction studies.

During optimisation of the crystallisation trials various other molecular weight PEG's were investigated for use as precipitants. Results were achieved when using PEG 1450 (Hampton Research) and PEG 400 (Fluka Bichemicals). When the following crystallisation conditions were used:

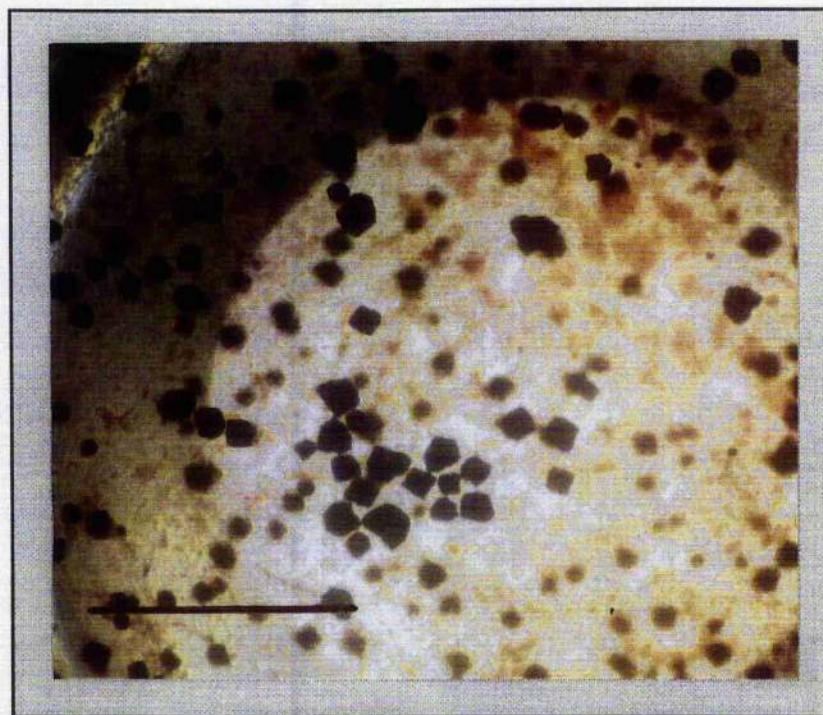


Figure 8.23. Crystals of *Rps. acidophila* 10050 core complex of a similar size and morphology to those in Figure 8.23 grew when the PEG 2000 concentration in the protein droplet was increased to 12.5% (w/v) and urea was substituted with trimethylamine HCl. Bar = 1mm.

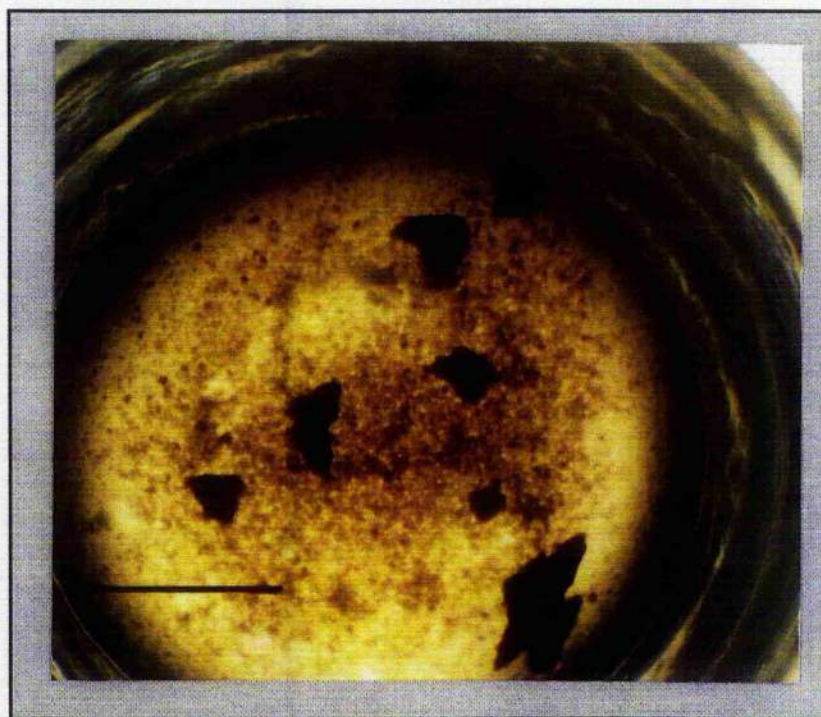


Figure 8.24. When LDAO was exchanged for C-HEGA-10, large flake-like crystals of *Rps. acidophila* 10050 core complex formed. Although large they were of poor quality. Refer to text for crystallisation conditions. Bar = 1mm.

Protein droplet solution: *Rps. acidophila* 10050 core complex OD = 55cm⁻¹
8.5% (w/v) PEG 1450
10mM MgCl₂
19.5mM HECAMEG
40mM Tris-HCl, pH 8.0
10mM spermidine or 10mM taurine

Reservoir solution: 17% (w/v) PEG 1450
20mM MgCl₂
40mM Tris-HCl, pH 8.0

small, flat triangular crystals formed (Fig. 8.25). These crystals varied in size and had rough edges. Yet others were twinned. In contrast to previous observations the type of additive (spermidine or taurine) did not appear to have an effect on the crystal morphology. Alteration of the PEG 1450 concentrations and detergent type gave rise, within 7 days, to an extensive shower of arrowhead-shaped microcrystals which formed around the edge of the crystallisation well (Fig. 8.26). The conditions employed in this trial were:

Protein droplet solution: *Rps. acidophila* 10050 core complex OD = 55cm⁻¹
9% (w/v) PEG 1450
10mM MgCl₂
24.5mM heptyl-β-D-thiogluconate
40mM Tris-HCl, pH 8.0
10mM spermidine

Reservoir solution: 18% (w/v) PEG 1450
20mM MgCl₂
40mM Tris-HCl, pH 8.0

Similar conditions, but decreasing the PEG 1450 concentrations in the protein droplet and reservoir to 7.5% (w/v) and 15% (w/v), respectively,

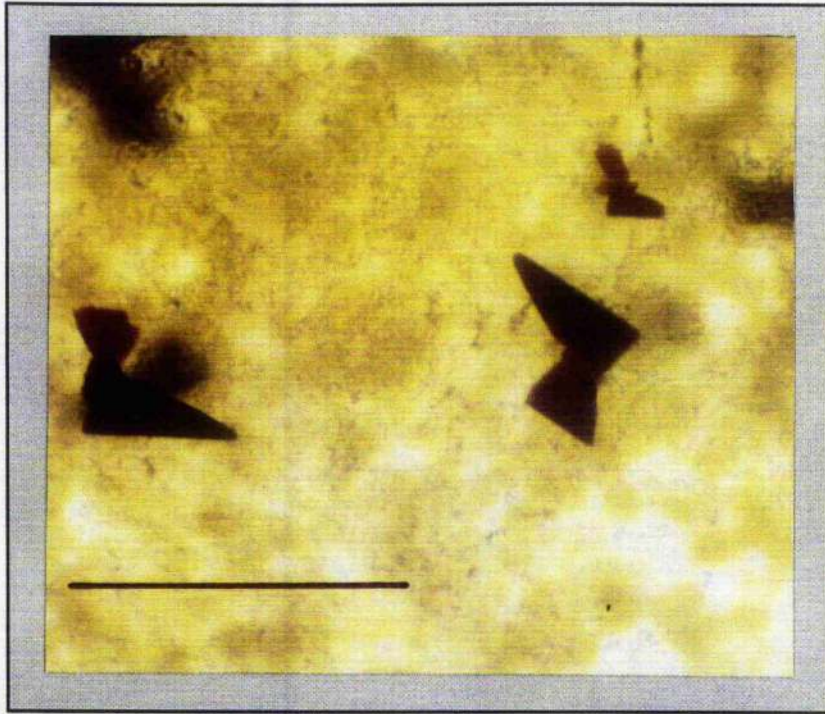


Figure 8.25. Small, flat triangular crystals of *Rps. acidophila* 10050 core complex, formed using PEG 1450 as a precipitant, HECAMEG as detergent and spermidine or taurine as additives. Some of the crystals appear twinned. Bar = 1mm.



Figure 8.26. Alteration of the PEG 1450 concentrations and using heptyl thioglucoside as a detergent in the presence of 10mM spermidine caused a shower of arrowhead-shaped microcrystals of *Rps. acidophila* core complex to form around the edge of the crystallisation well. Bar = 1mm.



Figure 8.27. Using similar conditions to those which produced the crystals in Figure 8.26 but using sucrose monocholate as a detergent produced poor quality, irregularly shaped crystals of *Rps. acidophila* 10050 core complex. These crystals were unsuitable for diffraction studies. Bar = 1mm.

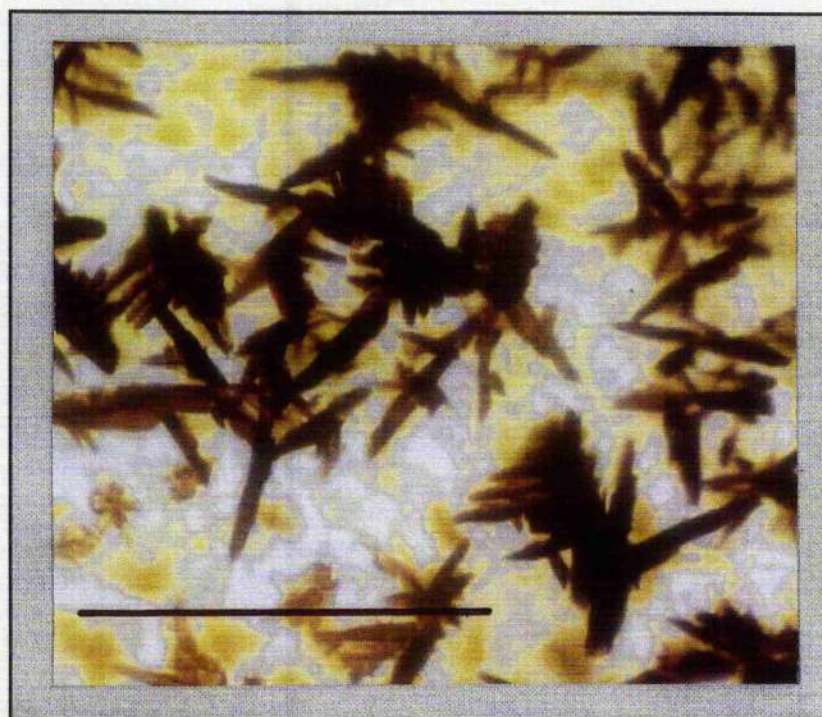


Figure 8.28. Using PEG 400 as a precipitant and heptyl thioglucoside as a detergent in the presence of the additive spermidine resulted in the growth of feather-like crystals of *Rps. acidophila* core complex. Bar = 1mm.

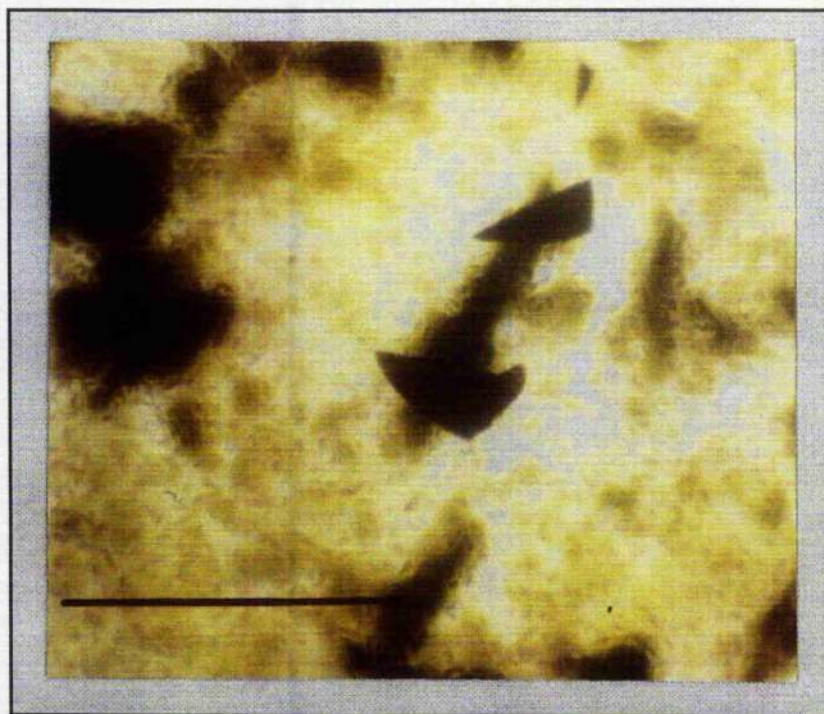


Figure 8.29. Roughly triangular crystals of *Rps. acidophila* 10050 core complex grew using the same conditions as produced the crystals in Figure 8.28 but using HECAMEG as a detergent. Bar = 1mm.

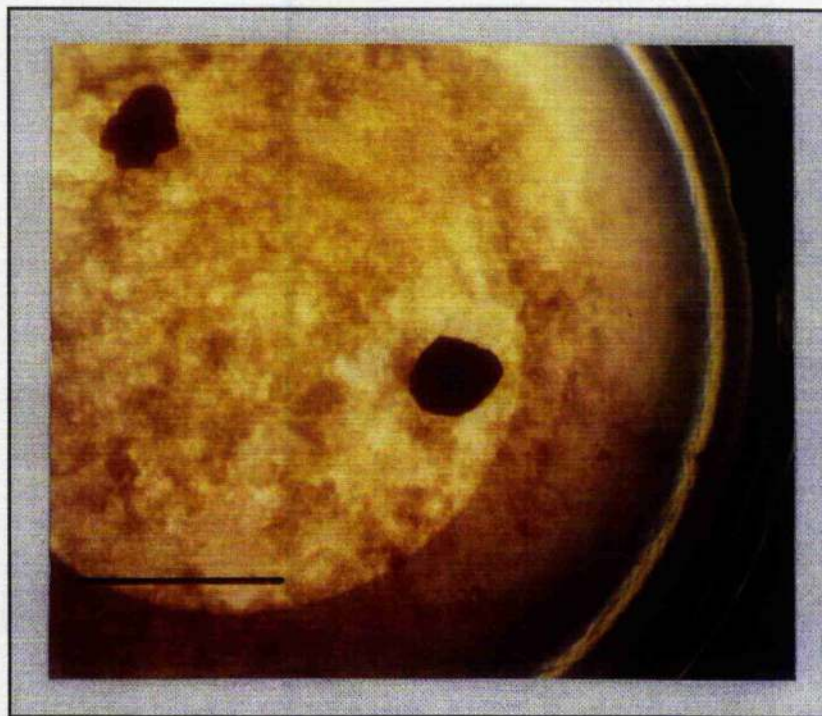


Figure 8.30. Using the same conditions as above but using sucrose monocholate as a detergent resulted in the formation of two large, but poorly shaped crystals of *Rps. acidophila* core complex. Refer to text for exact crystallisation conditions. Bar = 1mm.

and solubilising the core complex with 4.7mM sucrose monocholate also produced crystals (Fig.8.27). These crystals, however, were of a very poor quality with no regular shape. Substituting 10mM taurine for spermidine did result in fewer crystals being formed but visual inspection suggested they were still unsuitable for X-ray analysis.

The crystals formed when PEG 400 was used as a precipitant are shown in Figures 8.28 to 8.30, inclusive. The feather-like crystals shown in Figure 8.28 formed under the following conditions:

Protein droplet solution: *Rps. acidophila* 10050 core complex OD = 55cm⁻¹
10% (w/v) PEG 400
10mM MgCl₂
24.5mM heptyl-β-D-thiogluconate
20mM Tris-HCl, pH 8.0
10mM spermidine

Reservoir solution: 20% (w/v) PEG 400
20mM MgCl₂
20mM Tris-HCl, pH 8.0

Changing the detergent to 19.5mM HECAMEG altered the crystal morphology (Fig. 8.29). In this case fewer, roughly triangular crystals grew. When 4.7mM sucrose monocholate was used as a detergent, two large but poorly defined crystals formed (Fig. 8.30). Due to their poor quality these crystals proved unsuitable for X-ray analysis (S.M. Prince, personal communication).

The best result from all the crystallisation trials, including those using core complex from different species, was achieved using the conditions listed below:



Figure 8.31. A cubic crystal of *Rps. acidophila* 10050 core complex similar to the one which diffracted X-rays to a resolution of 7.6Å. This crystal was grown using PEG 2000 as a precipitant, cholate as detergent and spermine-tetraHCl as an additive. The crystal dimensions are 0.1mm x 0.1mm.

Protein droplet solution: *Rps. acidophila* 10050 core complex OD = 70 cm⁻¹

8.5% (w/v) PEG 2000

10mM MgCl₂

1% (w/v) cholate

20mM Tris-HCl, pH 8.0

3% spermine-tetraHCl

Reservoir solution: 20% (w/v) PEG 2000

20mM MgCl₂

1% (w/v) cholate

20mM Tris-HCl, pH 8.0

Over a period of about 25 weeks at an incubation temperature of 15°C, a

single dark red (almost black) tetragonal crystal with dimensions of 0.1mm x 0.1mm x 0.1mm formed. A very brief examination of this crystal under the microscope showed it to be without any flaws. This made it a good candidate for X-ray diffraction studies. As only a single crystal grew, it was decided not to photograph it, thereby preventing any unnecessary damage by exposure to the heat and light from the microscope. The crystal was taken for further investigation to the ESRF high brilliance beamline at Grenoble, France, where facilities are available for collection of diffraction data at cryogenic temperatures. In order to prevent damage to the crystal (due to ice formation) during flash cooling to cryogenic temperatures, a cryoprotectant (in this case 20% v/v glycerol) was added to the crystal's mother liquor. The cryoprotectant was introduced slowly by dialysis. Unfortunately, the crystal was broken during handling and only a fragment of it was used for the data collection (S.M. Prince, personal communication). Nevertheless, this LH1-RC crystal fragment was found to diffract to 7.6Å. Data analysis suggested the crystal space group was tetragonal P4 with unit cell dimensions of $a=b=156.56\text{Å}$ and $c=181.11\text{Å}$, and $\alpha=\beta=\gamma=90.0^\circ$ (S.M. Prince, personal communication). This result was very promising but further crystallisation trials using the same conditions failed to reproduce this quality of crystal. Although similar looking crystals formed (Fig. 8.31) they only diffracted X-rays to ~15-20Å. The irreproducibility of the experiment could be due to a number of reasons, such as: (i) small differences in the growth conditions between each batch of bacteria; (ii) small differences between the purification protocols; (iii) differences, due to pipetting error, in the composition of the crystallisation buffers, to name but a few possibilities. This underlined the fickle nature of crystallising membrane proteins.

To ensure that the crystals grown during the trials were of the LH1-RC

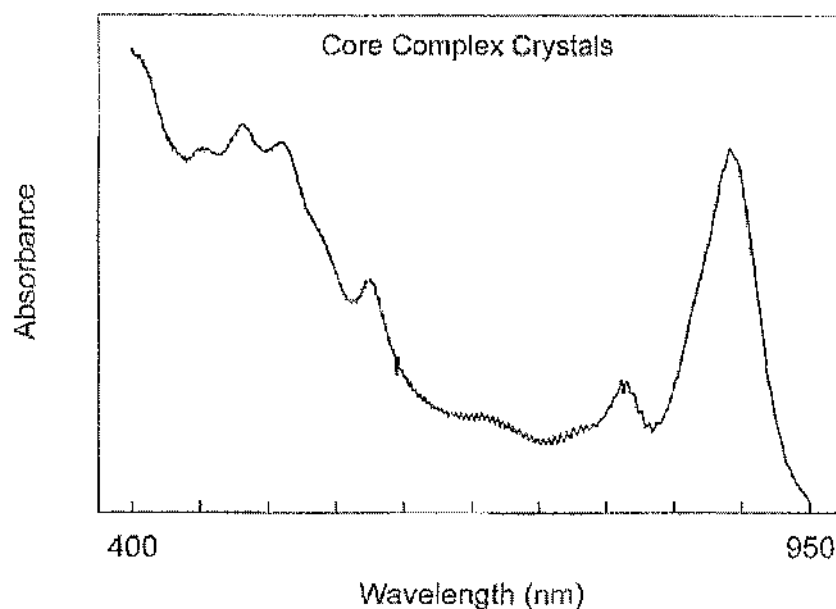


Figure 8.32. Absorption spectrum of a typical crystal of the *Rps. acidophila* strain 10050 LH1-RC core complex. The spectrum is similar to that of the purified, LDAO solubilised core complex shown in Figure 4.8, with a strong absorption peak at 885nm due to the LH1 Bchl *a*'s, and a smaller peak, due to the RC, located at 803nm. The carotenoid peaks are located between 500-580nm. The strong absorption at 400nm is due to the effect of light scattering.

core complex, their absorption spectra were measured (see section 2.6.2). A typical absorption spectrum of a crystal is shown in Figure 8.32. The spectrum is very similar to that of the purified *Rps. acidophila* core complex shown in Figure 4.8.

Due to constraints of both time and material (purified core complex), and the fact that much of the effort was concentrated on crystallising the core complex from *Rps. acidophila* strain 10050, only a limited number of crystallisation trials were performed using the core complex from other species. As such, the trials described hereafter are far from exhaustive and

only reflect experiments which investigated the efficacy of a small number of the detergents listed in Appendix C.

8.3. *Rhodopseudomonas acidophila* strains 7750 and 7050 core complexes

The core complex from the 7750 and 7050 strains of *Rps. acidophila* also yielded 3-D crystals under broadly the same conditions used for crystallisation of the 10050 strain core complex. However, none of these crystals were of a sufficient quality for X-ray diffraction studies. Cubic crystals of 7750 core complex, with dimensions of $\sim 0.1\text{mm} \times 0.1\text{mm} \times 0.1\text{mm}$ (Fig. 8.33), grew when the following conditions were employed:

Protein droplet solution: *Rps. acidophila* 7750 core complex OD = 50cm^{-1}
8% (w/v) PEG 2000
10mM MgCl_2
1% (w/v) cholate
20mM Tris-HCl, pH 8.0
1.5% (w/v) spermidine

Reservoir solution: 22.5% (w/v) PEG 2000
20mM MgCl_2
20mM Tris-HCl, pH 8.0

The red precipitate in the bottom of the crystallisation well indicates that not all of the protein was used for crystal growth.

Showers of brownish, flake-like crystals of strain 7050 core complex (Fig. 8.34) grew under the following conditions:

Protein droplet solution: *Rps. acidophila* 7050 core complex OD = 50cm^{-1}
10% (w/v) PEG 2000

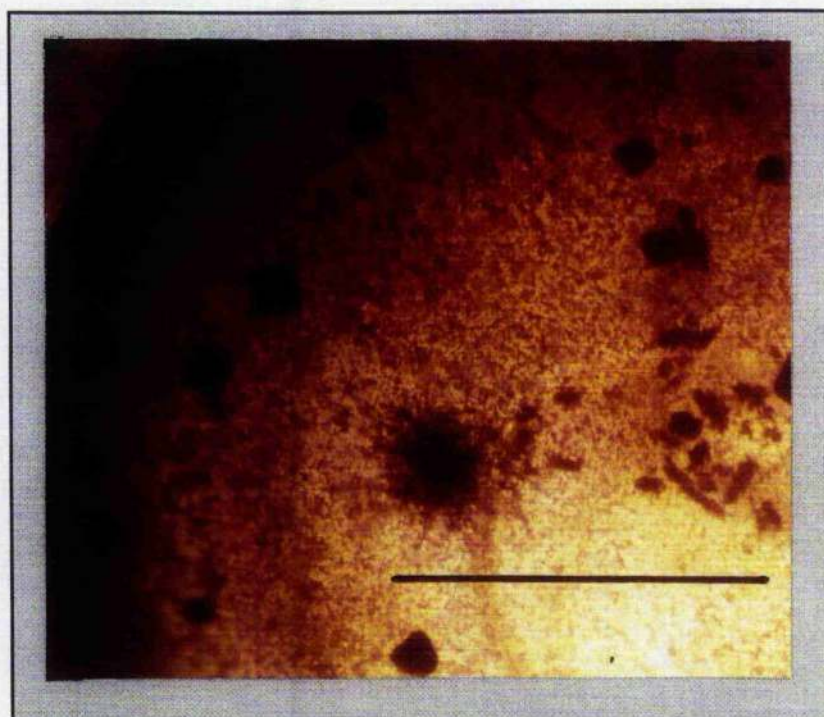


Figure 8.33. Cubic crystals of *Rps. acidophila* 7750 core complex grown in PEG 2000 with 1.5% (w/v) spermidine as an additive and 1% (w/v) cholate as detergent. The red precipitate in the bottom of the crystallisation well indicates not all the protein has been utilised for crystal formation. Bar= 1mm.

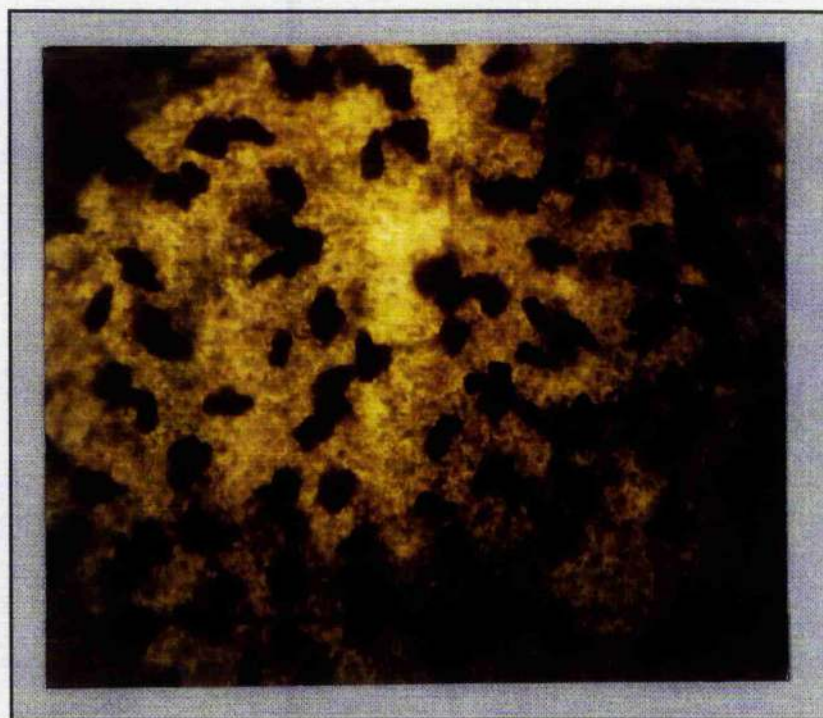


Figure 8.34. A shower of brownish coloured, flake-like crystals of *Rps. acidophila* 7050 core complex formed using PEG 2000 as a precipitant, 1% (w/v) cholate as detergent and taurine and spermidine as additives. Refer to text for exact crystallisation conditions. Bar = 1mm.

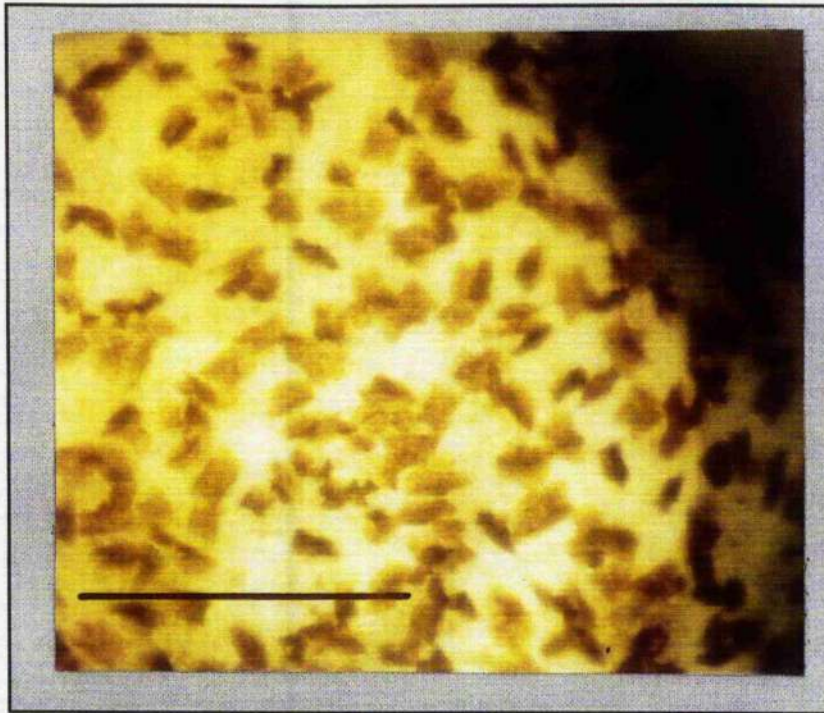


Figure 8.35. Using the same conditions which formed the crystals in Figure 8.34 but replacing taurine with betaine monohydrate produced flake-like crystals of *Rps. acidophila* strain 7050 core. Bar= 1mm.



Figure 8.36. A different crystal form of the *Rps. acidophila* 7050 core complex grew when the conditions that produced the crystals in Figure 8.35, above, were modified to include phenol as an additive instead of betaine monohydrate. Bar = 1mm..

	10mM MgCl ₂
	1% (w/v) cholate
	25mM Tris-HCl, pH 8.0
	10mM taurine
	1.7% (w/v) spermidine
Reservoir solution:	20% (w/v) PEG 2000
	20mM MgCl ₂
	25mM Tris-HCl, pH 8.0

Similar looking crystals grew when the additive taurine was replaced with 10mM betaine monohydrate (Fig. 8.35). However, when phenol (10mM) was used as an additive a different crystal form grew (Fig. 8.36).

8.4. *Rhodopseudomonas palustris* strains 1a1 and French core complexes

The core complex from these strains of *Rps. palustris* were, like those of *Rps. acidophila*, very stable when purified in LDAO (see section 4.3). As such, they were good candidates for crystallisation experiments. Previous reports by Wacker *et al.* (1986) and Gall (1994) have shown it is possible to grow 3-D crystals of core complex from strains 1e5 and 2.6.1 of this species. Crystallisation trials using the conditions described in these reports failed to produce crystals of core complex from strains French or 1a1. This could be due to differences between the core complexes from each strain or differences in the purification protocol. Modification of the conditions, however, did produce core complex crystals from both the 1a1 and French strains. The crystals produced were whisker-like needles about 1.5mm long (Fig. 8.37). The conditions that produced these crystals were:

Protein droplet solution:	<i>Rps. palustris</i> 1a1 <u>or</u> French core complex OD = 60cm ⁻¹ 10% (w/v) PEG 2000 10mM MgCl ₂ 1% (w/v) cholate 20mM Tris-HCl, pH 8.0 10mM spermidine
Reservoir solution:	20% (w/v) PEG 2000 20mM MgCl ₂ 1% (w/v) cholate 40mM Tris-HCl, pH 8.0

It should be noted that only the detergents LDAO, β -OG and cholate, and PEG 2000 as a precipitant, were investigated during crystallisation trials with *Rps. palustris* core complex. Therefore, it is possible that this complex will also crystallise with the other detergents and molecular weight PEG's listed in Table 8.1.

8.5. *Rhodopseudomonas cryptolactis* core complex

The core complex from this species was also relatively stable when purified in LDAO (section 4.4). Although there have been previous reports on the crystallisation of the B800-850 (Hällören *et al.*, 1995) and the B800-820 (Cogdell & Hawthornthwaite, 1993) complexes from *Rps. cryptolactis*, no 3-D crystals of the LH1-RC core complex have been reported. Core complex crystals from high light grown cells of this species did not form in LDAO. However, when the LDAO was exchanged for heptyl- β -D-thioglucoside, small flake-like crystals did form (Fig. 8.38). The conditions under which these crystals grew were:

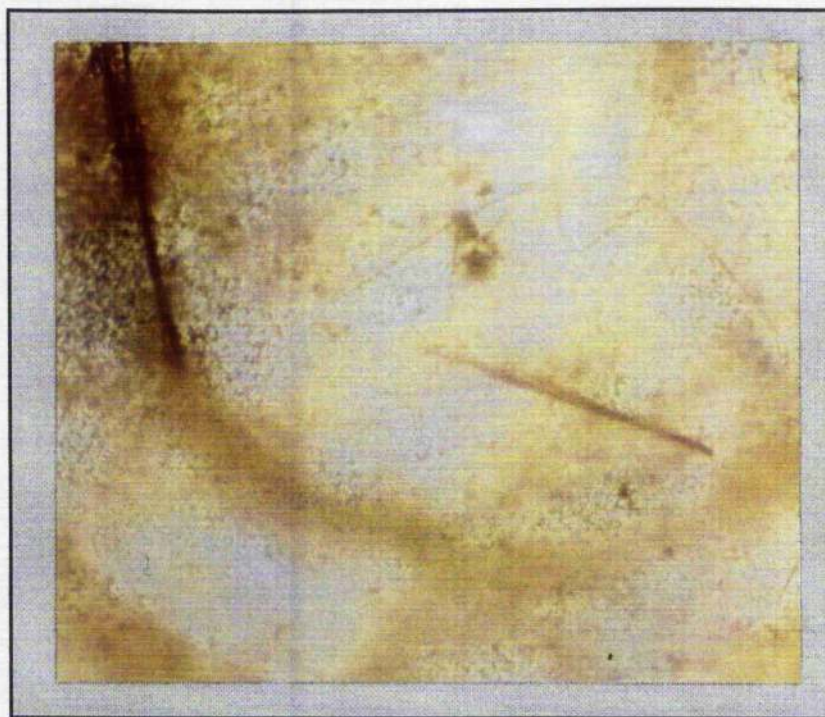


Figure 8.37. Whisker-like crystals of *Rps. palustris* core complex. The crystals are about 1.5mm long. They were grown in PEG 2000 with 10mM spermidine as an additive and 1% (w/v) cholate as detergent.

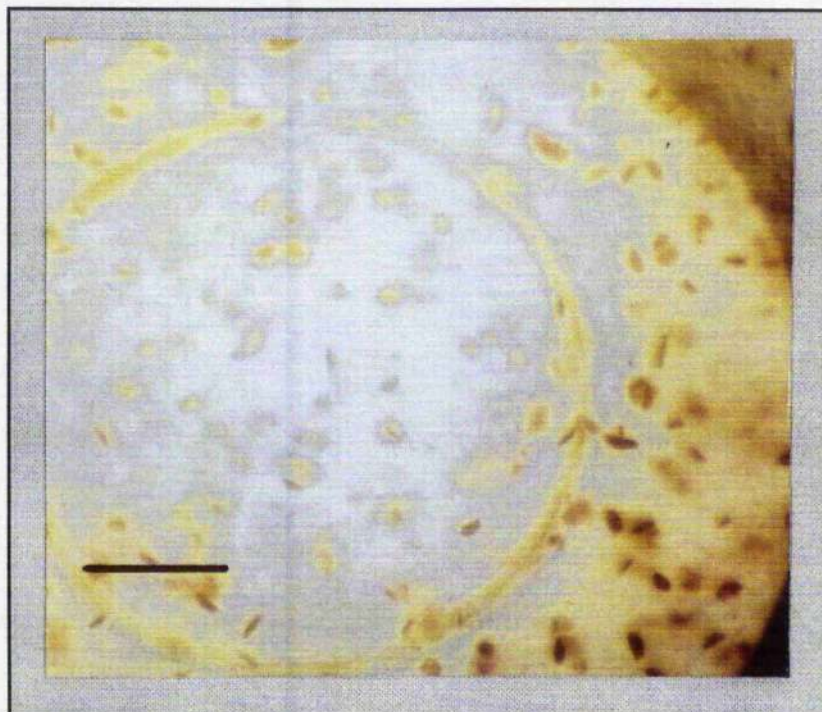


Figure 8.38. Flake-like crystals of high light grown *Rps. cryptolactis* core complex. These crystals grew using PEG 2000 as a precipitant, heptyl thioglucoside as detergent and a mixture of benzamidine hydrochloride and spermidine as additives. Refer to text for full details of the crystallisation conditions. Bar = 1mm.

Protein droplet solution:	<i>Rps. cryptolactis</i> HL core complex OD = 40cm ⁻¹ 9% (w/v) PEG 2000 10mM MgCl ₂ 24.5mM heptyl-β-D-thiogluco-side 20mM Tris-HCl, pH 8.0 0.75% (w/v) spermidine 2.5% (w/v) benzamidine hydrochloride
Reservoir solution:	22% (w/v) PEG 2000 20mM MgCl ₂ 20mM Tris-HCl, pH 8.0

8.6. *Chromatium vinosum* strain D core complex

The LH1-RC core complex from this species was the only one to crystallise in the presence of LDAO. However, in this case the use of a mixed detergent system was investigated and cholate was also present. The crystals produced in this system were large and feather-like (Fig. 8.39) but unsuitable for X-ray analysis. The conditions used to produce these crystals were:

Protein droplet solution:	<i>Chr. vinosum</i> strain D core complex OD = 55cm ⁻¹ 11% (w/v) PEG 2000 10mM MgCl ₂ 0.05% (v/v) LDAO and 1% (w/v) cholate 20mM Tris-HCl, pH 8.0 10mM spermidine 5mM ascorbate
Reservoir solution:	17% (w/v) PEG 2000 20mM MgCl ₂ 10mM ascorbate

1% (w/v) cholate
20mM Tris-HCl, pH 8.0

Crystals of similar size and morphology were produced using similar conditions (Fig. 8.40) but decreasing the concentration of PEG 2000 in the protein droplet to 9.5% (w/v). Thin needle-like crystals of better quality formed (Fig. 8.41) when the following crystallisation conditions were employed:

Protein droplet solution: *Chr. vinosum* strain D core complex OD = 25cm⁻¹
12% (w/v) PEG 2000
10mM MgCl₂
1% (w/v) cholate
20mM Tris-HCl, pH 8.0
10mM glycyl glycyl glycine
10mM spermidine

Reservoir solution: 22.5% (w/v) PEG 2000
20mM MgCl₂
20mM Tris-HCl, pH 8.0

8.7. *Rhodospirillum rubrum* S1 core complex

The LH1-RC complex from this core-only producing species of purple bacteria was not very stable when purified (see section 4.7). Nevertheless, crystallisation of the LDAO solubilised *Rs. rubrum* core complex, using PEG 2000 as a precipitant, has been reported previously (Dawkins *et al.*, 1988). The results of this published crystallisation trial could not be reproduced. The origins of the irreproducibility still remain to be clarified. However, modifying the published crystallisation conditions by exchanging the LDAO

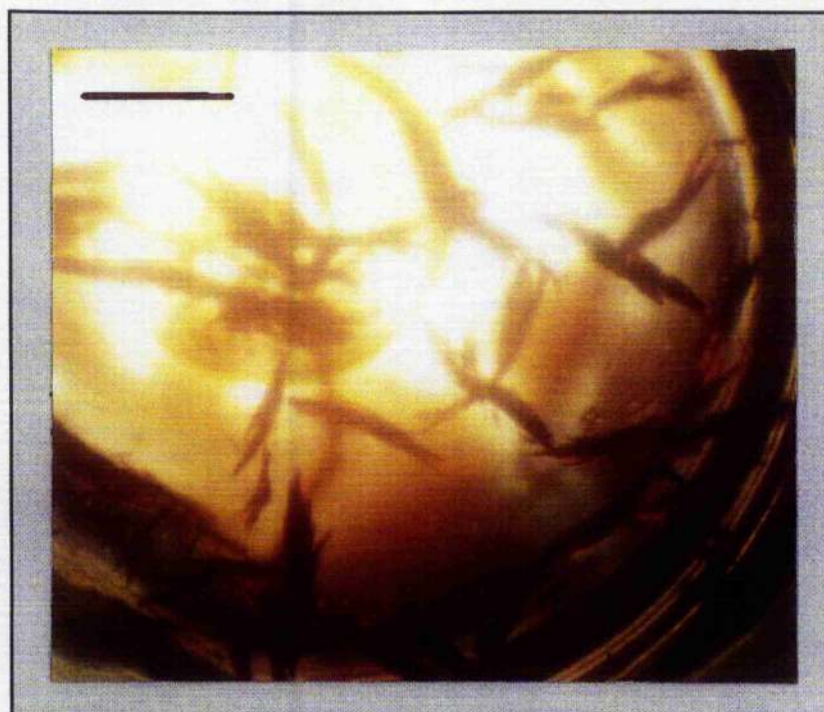


Figure 8.39. Large feather-like crystals of *Chr. vinosum* strain D core complex. These crystals grew in PEG 2000 and a mixed detergent system consisting of 0.05% (v/v) LDAO and 1% (w/v) cholate. Spermidine and ascorbate were used as additives. Bar = 1mm.



Figure 8.40. Altering the conditions which produced the crystals in Figure 8.39 by decreasing the concentration of PEG 2000 in the protein droplet to 9.5% (w/v) resulted in the formation of these *Chr. vinosum* strain D core complex crystals. Bar = 1mm.

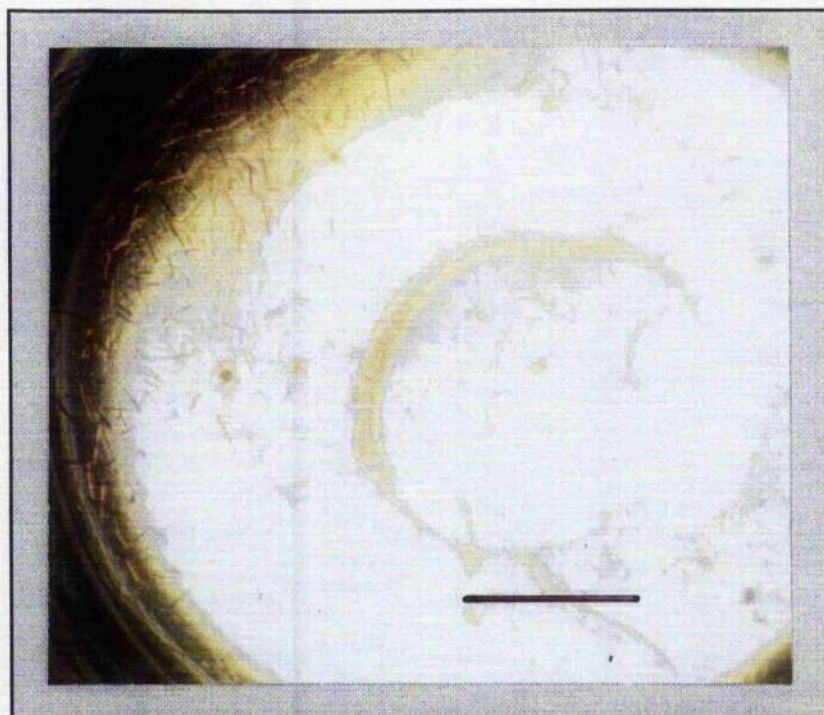


Figure 8.41. Using PEG 2000 as a precipitant, cholate as a detergent and a mixture of glycyl glycyl glycine and spermidine as additives resulted in the growth of thin needle-like crystals of *Chr. vinosum* core complex. Refer to text for a full description of the crystallisation conditions. Bar = 1mm.

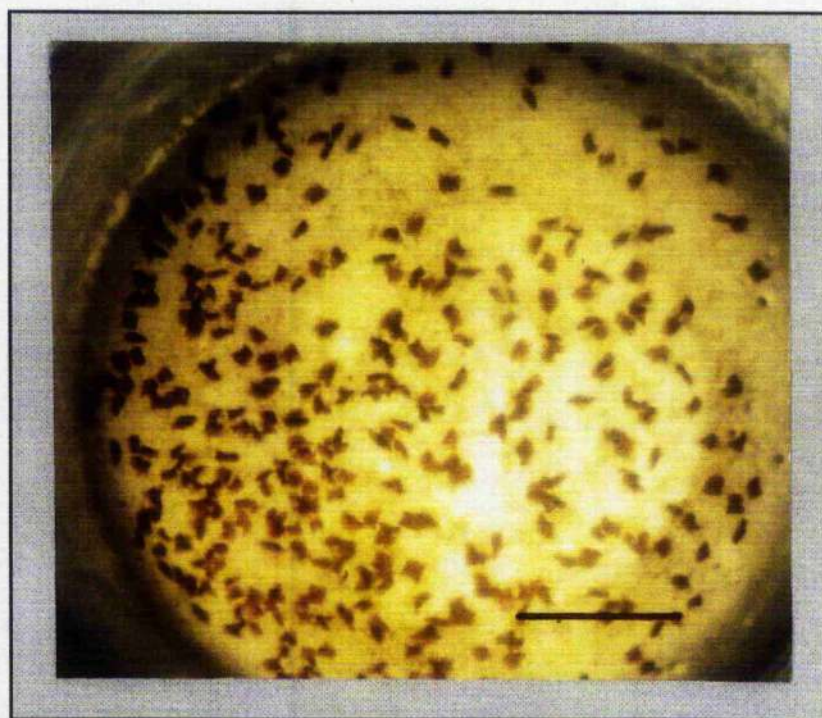


Figure 8.42. Reddish-brown flake-like crystals of *Rs. rubrum* core complex formed in about 2 weeks when PEG 2000 was used as a precipitant and LDAO was exchanged for lauryl maltoside. 10mM spermidine was included in the protein droplet solution as an additive. The crystals are of poor quality and unsuitable for X-ray diffraction studies. Bar = 1mm.

for lauryl maltoside, altering the concentrations of precipitant, adding spermidine, and incubating the trial at 15°C did result in crystal growth (Fig. 8.42). The crystals were reddish-brown flakes of various shapes and sizes that took about 2 weeks to grow. The conditions that produced these crystals were:

Protein droplet solution: *Rs. rubrum* strain S1 core complex OD = 60cm⁻¹
9% (w/v) PEG 2000
10mM MgCl₂
1% (w/v) lauryl maltoside
20mM Tris-HCl, pH 8.0
10mM spermidine

Reservoir solution: 19% (w/v) PEG 2000
20mM MgCl₂
20mM Tris-HCl, pH 8.0

8.8. *Rhodobium marinum* core and LH1-only complexes

CD spectroscopy revealed that the *Rh. marinum* core complex was one of the less stable complexes investigated (see section 5.7). In contrast the isolated LH1 (B880) complex from this species was stable over a period of months (section 4.9). Both complexes formed crystals. The LH1-RC core complex crystals grew over a period of 1-2 weeks. The crystals were dark red, well defined needles about 0.2mm long (Fig. 8.43). The conditions which produced these crystals were:

Protein droplet solution: *Rh. marinum* core complex OD = 55cm⁻¹
9.5% (w/v) PEG 1450

	10mM MgCl ₂
	4.7mM sucrose monocholate
	40mM Tris-HCl, pH 8.0
	10mM ATP di-sodium salt
	10mM spermidine
Reservoir solution:	15% (w/v) PEG 1450
	20mM MgCl ₂
	40mM Tris-HCl, pH 8.0

The LH1 (B880) complex crystals also grew over a period of 1-2 weeks. This complex was the only one to form crystals in a system which used ammonium sulphate and di-potassium phosphate as precipitants. The crystals which formed were dark red needles about 0.25mm long (Fig. 8.44). The crystallisation conditions employed were as follows:

Protein droplet solution:	<i>Rh. marinum</i> B880 complex OD = 50cm ⁻¹
	1M di-potassium phosphate, pH 8.0
	0.85% (w/v) β -octyl glucoside
	2.5% (w/v) heptane-1,2,3-triol (high m.p. isomer)
Reservoir solution:	2.8M ammonium sulphate, pH 8.0

The volume of the protein droplet solution was 10 μ l, and 1 μ l of the reservoir solution was added to this. The trial was incubated at 15°C. At the time of writing no X-ray diffraction analysis has been performed using these crystals. Due to limitations of time crystallisation trials using PEG as a precipitant were not performed.

In summary, the results presented in this chapter show it is possible to crystallise, in three dimensions, the LH1-RC core complex from a variety of species of the purple bacteria. The most favourable crystallisation



Figure 8.43. Dark red, well defined needles (about 0.2mm long) of *Rh. marinum* core complex. These crystals grew when LDAO was exchanged for sucrose monocholate and PEG 1450 was used as a precipitant in the presence of the additives ATP di-sodium salt and spermidine.



Figure 8.44. Needles of the LH1 (B880) complex of *Rh. marinum* grown using β -OG as a detergent. The crystals are about 0.25mm long. These were the only crystals to grow in a system which used di-potassium phosphate and ammonium sulphate as precipitants. The large, clear crystal in the photograph is a crystal phosphate salt.

Table 8.1. List of the precipitants, detergents and small additives and amphiphiles which were effective for the crystallisation of the LH1-RC core complex from a range of species of purple bacteria.

Precipitants	Detergents	Additives
PEG 2000	β -octyl glucoside	L-cysteine
PEG 1450	cholate	spermidine
PEG 400	sucrose monocholate	glycyl glycyl glycine
	C-IEGA-10	betaine monohydrate
	HECAMEG	taurine
	heptyl- β -D-thioglucoside	heptane-1,2,3-triol
	lauryl maltoside	benzamidine HCl
	taurocholate	dioxane
		polyvinylpyrrolidone K15
		putrescine
		barium chloride
		urea
		phenol
		trimethylamine HCl
		spermine tetraHCl
		ATP di-sodium salt
		ascorbate

conditions are those that utilise PEG 2000 or PEG 1450 as precipitants (see

Table 8.1). It appears that the presence of $MgCl_2$ and other small additives, such as spermidine, is an absolute requirement for crystallisation of the core complex. This observation is in contrast to that made by Gall (1994) who suggested that the presence of small amphiphiles was not a requirement for core complex crystal formation. However, those crystallisation trials contained the anti-microbial agent, sodium azide, in the protein solution droplets and this could have influenced crystal growth.

Unfortunately, none of the crystals described in this chapter were of a sufficient quality to allow the elucidation of the structure of the LFI1-RC core complex by classical X-ray crystallographic methods. Michel *et al.* (1993) have shown that the resolution of X-ray diffraction is directly related to the number and duration of protein purification methods. Bearing this in mind a revision of the core complex purification protocol, in which the number of purification steps was decreased and the speed of the process increased, could increase the likelihood that the crystals will diffract X-rays to a higher resolution. The availability of automated protein purification workstations and improved chromatography media may now make this feasible. Crystal quality may also be improved by the use of automated robotic crystallisation workstations. This would allow for a faster, more efficient and reproducible screening of a very wide range of crystallisation conditions.

CHAPTER NINE

DISCUSSION

9.1. Discussion

The photosynthetic membranes of most of the species of purple bacteria studied here, such as *Rps. acidophila* and *Rps. palustris*, contained peripheral LH2 as well as LH1-RC core complexes. However, two of the species studied, *Rs. rubrum* and *Rh. marinum*, contained LH1-RC as their only complex. The absorption spectra of all the isolated LH1-RC complexes were very similar to the absorption spectra of the whole cells and photosynthetic membranes of the 'core only' species (Chapter 4). Thus, it appears that the LH1-RC core complex from each of the species studied has been isolated in an intact form. The stability of the isolated complex, however, varied between species. The LDAO solubilised core complexes from *Rps. acidophila*, *Rps. palustris*, *Rps. cryptolactis* and *Chr. vinosum* were stable both during the purification process and for up to several months when stored at -20°C . Generally, these complexes could withstand several rounds of freezing and thawing without denaturing. In contrast, the core complexes from *Rv. gelatinosus*, *Rs. rubrum* and *Rh. marinum* were generally unstable when isolated.

The stability of the complexes was monitored, both during and after purification, by absorption spectroscopy. The core complexes were considered to be intact if the $A_{\text{NIR max}}:A_{280}$ ratio was $\sim 2:1$ and $A_{\text{NIR max}}:A_{800}$ ratio was $\sim 4.3:1$ (Table 4.9). Denaturation of the LH1 ring would be apparent as a decrease in the $A_{\text{NIR max}}:A_{280}$ ratio. Alternatively, loss and denaturation of the RC alone would be apparent as an increase in the $A_{\text{NIR max}}:A_{800}$ ratio with a concomitant decrease in the $A_{\text{NIR max}}:A_{280}$ ratio. Total denaturation of the LH1-RC complex could usually be monitored visually as it resulted in the core complex solution changing from a purple-red colour to a brownish-green colour as the Bchl *a* molecules dissociated from their protein scaffold.

Although the core complexes from *Rs. rubrum* and *Rh. marinum* appeared to be rather unstable according to the data in Table 4.9 (mean $A_{\text{NIR max}}:A_{280}$ ratios of $\sim 1.85:1$, and mean $A_{\text{NIR max}}:A_{800}$ ratios of $4.9:1$) and CD spectroscopy (section 5.7) they did produce crystals during crystallisation experiments (sections 8.7 and 8.8). This observation may seem contradictory as stability of the core complex is a requirement for crystal growth. However, it should be noted that the mean values for the $A_{\text{NIR max}}:A_{280}$ and $A_{\text{NIR max}}:A_{800}$ ratios given in Table 4.9 for the core of these species did fall within the lower and upper limits, respectively, of the values presented for the stable cores of the other species studied. Therefore, the core complex samples from *Rs. rubrum* and *Rh. marinum* that were used in the successful crystallisation trials may simply have originated from a batch which exhibited higher and lower $A_{\text{NIR max}}:A_{280}$ and $A_{\text{NIR max}}:A_{800}$ ratios, respectively. If this is the case it indicates a problem in the consistency of the solubilisation and purification process in these species.

The origin of the instability of some of the LH1-RC core complexes probably lies in their sensitivity to the detergent LDAO. Sensitivity to LDAO has been noted before for the core complex from *Rps. blastica* (Dawkins *et al.*, 1988). However, a previous report has shown that it is possible to isolate the *Rs. rubrum* core complex in a stable form using the phospholipid detergent diheptylphosphatidylcholine (Walz & Ghosh, 1997). This suggests that in certain cases LDAO cannot satisfy the stipulation made by Michel (1991) that, in order for membrane complexes to be solubilised in a stable form, the detergent must completely replace the lipids of the membrane without affecting the structure or stability of the protein. Therefore, isolation of the core complexes from *Rv. gelatinosus*, *Rs. rubrum* and *Rh. marinum* in a more stable state may require that they are solubilised in a different detergent.

Although analysis of absorption spectra provides a quick method of monitoring the intactness and stability of the core complexes a much more sensitive spectral test is represented by CD measurements. The NIR CD spectra of the stable, intact LH1-RC cores from *Rps. acidophila*, *Rps. palustris*, *Rps. cryptolactis* and *Chr. vinosum* are all similar, consisting of a pair of non-conservative CD couplets with their positive peaks located between ~800nm-900nm (Chapter 5). In these spectra both the positive and negative lobes of the longer wavelength NIR CD signal are more intense than those of the shorter wavelength NIR CD signal. Strongly anisotropic and complex double CD signals such as these are indicative of strong exciton coupling among several Bchl *a* molecules (Gottstein & Scheer, 1983). On the other hand the NIR CD signals of the LH1-RC core complexes from *Rs. rubrum*, *Rh. marinum* and *Rv. gelatinosus* DSM 151 appear very different to those of the stable core complexes. In these cases the relative anisotropy values of the longer wavelength NIR CD signals are generally lower than those calculated for the stable core complexes (Table 5.1). In the *Rh. marinum* and *Rv. gelatinosus* DSM 151 core CD spectra (Figs. 5.6b & 5.4b, respectively) both the positive and negative lobes of the longer wavelength NIR CD couplet are much less intense relative to those of the shorter wavelength couplet. The positive lobes of the longer wavelength CD couplets are also split into two peaks. Because this couplet is composed of contributions from both the LH1 Bchl *a*'s and the RC special pair (with the contribution from the RC special pair represented by the shoulder on the blue side of the couplet) denaturation of the LH1 ring alone, with the resultant loss of dimerisation between the B875 Bchl's, would cause such a splitting. Some of the decrease in the intensity of the longer wavelength couplet can also be attributed to loss of the asymmetric environment of the Bchl's as they dissociate from the LH1 ring. Therefore, it seems that in the

case of the core complexes from *Rh. marinum* and *Rv. gelatinosus* DSM 151, it is the LH1 ring of the core complex and not the RC which is susceptible to denaturation upon exposure to LDAO. Although this would cause a dissociation of the RC from its LH1 ring it may not necessarily result in denaturation of the RC. However, in the case of *Rs. rubrum* the relative intensity of the shorter wavelength NIR CD signal is much weaker than that of the longer wavelength NIR CD signal (Fig. 5.6a and Table 5.1). The loss of intensity of this CD signal could be attributed to the denaturation of the RC. This would result in a loss of dimerisation, and therefore coupling, between the RC special pair. The dissociation of the RC Bchl *a*'s from their asymmetric environment could also contribute to a weakening of this signal (Gregory, 1977). These observations suggest that the RC of the *Rs. rubrum* core complex may be more susceptible to denaturation by LDAO than the RC's from the cores of the other species studied.

The efficacy of the purification process was confirmed by SDS polyacrylamide gel electrophoresis. For all the species studied the purified LH1-RC core complex could usually be resolved into five, differentially staining bands representing the α - and β - polypeptides of the LH1 antenna and the H, M and L subunits of the RC (Fig.4.9). The LH1 α - and β - polypeptides were, in most cases, poorly resolved and migrated as a diffuse band with an apparent molecular mass of between ~6-9kDa. The H, M and L subunits of the RC could be much more clearly resolved. The RC subunits of *Rps. acidophila*, *Rps. cryptolactis* and *Rh. marinum* had apparent molecular masses of between 30-40kDa, whereas those from *Rps. palustris*, *Rv. gelatinosus*, *Chr. vinosum* and *Rs. rubrum* displayed masses of between ~26-31kDa. These observations are similar to some reported previously (Agalidis & Reiss-Husson, 1992; Dawkins *et al.*, 1988; Gall, 1994; Halloren *et*

al., 1995). Therefore, it appears that the size of the RC can vary considerably between species, even those in the same genus. However, it should be noted that the apparent molecular masses of the polypeptides derived from SDS-PAGE cannot be taken at face value. This is because the proteins used as calibration markers were hydrophilic, globular proteins which may behave differently in the gel compared to the hydrophobic polypeptides of the LH1-RC complex.

In the case of the *Chr. vinosum* core complex an additional diffuse staining band with an apparent mass of ~40-45kDa could be resolved. The RC of this species, like that of other *Chromatium* species and *Rps. viridis*, possesses a tightly bound cytochrome (Kerfeld *et al.*, 1994). This band, therefore, is presumably due to the cytochrome. Although there is evidence for a tightly bound cytochrome associated with the RC of some of the other species studied, such as *Rps. acidophila* (Matsuura & Shimada, 1986), *Rv. gelatinosus* (Agalidis & Reiss-Husson, 1992) and *Rh. marinum* (Meyer *et al.*, 1990), a band corresponding to this cytochrome could not be resolved in the gel lanes containing fully purified LH1-RC core complex from any of these species. However, a band with an apparent molecular mass of ~40-45kDa could be resolved in the gel lanes which contained solubilised photosynthetic membranes from these species. This band could be a possible candidate for the cytochrome although it is impossible to assign it as such without further investigation. This suggests that the RC-bound cytochrome may dissociate during purification. The use of a procedure in which the polypeptide bands in the gel are stained for peroxidase activity (Thomas *et al.*, 1976) or haem may clarify this.

Investigation of the purified LH1-RC core preparations by SDS-PAGE gave no evidence of a *puf X* or *puf X*-like gene product, a 9kDa protein which has been found associated with the LH1-RC of *Rb. sphaeroides* and

Rb. capsulatus (Farchaus *et al.*, 1992; Recchia *et al.*, 1998), in any of the species studied. Nevertheless, it is possible that the presence of a *pufX* component of the core complex could be masked out in the SDS polyacrylamide gels by the α - and β -polypeptides of the LH1 antenna. It should be noted, however, that there is no evidence to suggest that any of the species investigated in this thesis contain such a protein. Further investigations, perhaps involving the systematic screening for possible *pufX* encoding genes in these species, are required before this issue can be satisfactorily resolved.

Electron microscopy studies clearly show that the purified, LDAO solubilised *Rps. acidophila* strain 10050 LH1-RC core consists of a uniform ring-like structure that surrounds a central staining region (Fig. 4.10). This supports a structure of the core complex in which the LH1 antenna completely surrounds the RC as suggested by the studies of Karrasch *et al.* (1995), Walz & Ghosh (1997) and Walz *et al.* (1998).

The purified LH1-RC core complexes were investigated for their ability to form 3-D crystals. The core complexes from all the species studied, except those from *Rv. gelatinosus*, produced crystals, but only when PEG was used as a precipitant in the presence of $MgCl_2$ and some other small additive molecules (see Table 8.1). The fact that crystals formed is indicative of the purity of the isolated core complexes. It also suggests a homogeneous ring size for the LH1 antenna. The reason for the absolute requirement of $MgCl_2$ for crystal formation is not understood but it is known that divalent ions can influence the aggregation of membrane proteins and this, in turn, could promote the packing of the core complexes in the crystal lattice. Alternatively, small crystals of $MgCl_2$ could act as nucleation sites for the growth of core complex crystals. No core complex crystals formed when ammonium sulphate or potassium phosphate were used as precipitants.

However, crystals of isolated B880 from *Rh. marinum* did form in such a system (see section 8.8). This suggests that the presence of a RC is a major barrier when attempting to crystallise the core complex using ammonium sulphate and phosphate as precipitants. The reasons for this are not understood but may be related to the fact that because of its insolubility in potassium phosphate, $MgCl_2$ cannot be used as an additive in this system.

Crystals did not form under any of the crystallisation conditions investigated when the core complexes were solubilised in LDAO. Exchanging LDAO for other detergents, such as cholate or heptyl thioglucoside for example, did result in crystal formation. For a list of detergents used in successful crystallisation trials refer to Table 8.1. These detergents may be more successful at promoting crystal growth because they allow more contact to be made between the hydrophilic surface domains of the core complex proteins which, in turn, would allow a better packing of the crystal lattice.

Although in many cases the core complex crystals looked beautiful under the microscope they generally diffracted X-rays poorly, to a resolution of 20-25Å. Only in one case did a crystal of *Rps. acidophila* strain 10050 core complex diffract X-rays to a resolution (7.6Å) sufficient for performing an initial characterisation of the crystal space group and unit cell dimensions (see section 8.2). However, the results of this crystallisation trial could not be reproduced. There are several possible reasons for the generally poor degree of order and irreproducibility of the crystals. Firstly, variation in the lipid content of the core complex preparations is often a source of heterogeneity that can disorder crystals of this type (Hawthornthwaite & Cogdell, 1993). Previous reports have shown that growth conditions can effect the lipid composition and content of membranes of *Rps. viridis* (Pucheu et al., 1974) and *Rps. capsulata* (Kaufmann et al., 1982). Therefore, slight differences in

culture conditions between batches of bacteria may have a dramatic effect on the final lipid composition of the core complex preparations. This may offer an explanation for the irreproducibility of some of the crystallisation experiments. A second possible cause of crystal disorder may be due to differing redox states in the RC of the core complex. A change in redox state could cause a conformational change in the protein which could affect the crystallographic contacts and crystal packing. This potential problem was addressed by adding a reducing agent, ascorbate, to the crystallisation solutions in order to maintain the RC in a reduced state. Its presence, however, did not improve the resolution of diffraction of the crystals. Therefore, it seems that differing RC redox states are not the main cause of crystal disorder. A final, and more probable source of crystal disorder is protein heterogeneity within the purified core complex samples. As mentioned before, the RC's of some of the purple bacteria studied here possess a tightly bound cytochrome. In other species the cytochrome is much more loosely associated with the RC. SDS-PAGE analysis of the polypeptide composition of the fully purified LH1-RC core complex preparations from all the species studied, except *Chr. vinosum*, seemed to suggest that the cytochrome was removed during the purification process. However, Coomassie blue staining may not be sensitive enough to detect the presence of small amounts of cytochrome. Therefore, the purified core preparations could still contain some RC associated cytochrome. This would be a major source of heterogeneity within the preparation and would have a dramatic effect on crystallographic contacts and thus the ability of the cores to form into a regular lattice. This may be the main stumbling block in the production of core complex crystals that diffract X-rays to a resolution suitable for structural studies and it certainly warrants further investigation. Nevertheless, the crystallisation trials reported in this thesis were

promising and they lay the groundwork for future studies which, hopefully, will lead to the structural elucidation of the LH1-RC core complex.

The isolated LHI (B880)-only complex from *Rh. marinum* was used as the focus for functional studies in this thesis. The purification process described in section 2.5 resulted in an isolated LH1 complex that was free of RC and other contaminants such as cytochrome (see section 4.9). The isolated LH1 ring was particularly amenable to investigation of the effect of chemical oxidation on its absorbance and fluorescence properties (Chapter 6). As shown in Figure 6.6, the mild chemical oxidation of the LH1 antenna with potassium ferricyanide dramatically quenches its fluorescence at concentrations of added ferricyanide that only bleach its Q_y absorption band by 2-3%. Therefore, if an LHI ring is considered to bind either 24 or 32 Bchl *a*'s, then oxidation of about less than or equal to one Bchl *a* molecule of the LH1 ring results in a 50% quenching of the fluorescence emission intensity. These data suggest that fluorescence emission from the LH1 ring is shut down by the oxidation of only a very small fraction of the total Bchl's in the ring. This observation is consistent with the results of single molecule spectroscopy experiments performed in LH2 complexes from *Rps. acidophila* which suggested that photobleaching of Bchl *a* in LH2 caused fluorescence to switch off completely (Bopp *et al.*, 1997). It appears, therefore, that the presence of a single oxidised Bchl molecule in either the LH1 or LH2 ring (a single quencher) can effectively quench the fluorescence of the complete ring. These results open up the intriguing possibility of redox control of energy transfer (for a review refer to Blankenship *et al.*, 1995). It is not clear whether this occurs in purple bacteria. However, measurements in chlorosomes of the green sulphur bacterium *Chlorobium tepidum* have shown that their fluorescence lifetime is redox dependent and that this effect may be due to a few oxidised Bchl *c* molecules (van Noort *et al.*, 1997).

Control of the fluorescence lifetime (and therefore energy transfer efficiency) by redox potential is a very effective mechanism for switching on and off energy transfer. Indeed, the formation of quenchers at high redox potentials could provide a rapid nonradiative decay pathway that competes with energy transfer. This would prevent photochemistry in an RC which may already be oxidised and can therefore be damaged by an excess of excitation energy (Blankenship *et al.*, 1993; 1995).

The relationship between the LH1-RC core and the LH2 complexes in the natural photosynthetic membrane of *Rps. acidophila* were studied by fluorescence induction spectroscopy (Chapter 7). This technique offers a powerful method of quantifying energy transfer between antenna complexes, and allowed the construction of several models of the PSU in *Rps. acidophila* strain 7750 to be proposed. This species was chosen for study because the spectral properties and relative amounts of LH2 can be modified by altering the growth conditions (Angerhofer *et al.*, 1986; Gardiner *et al.*, 1993).

The analysis of the data presented in Chapter 7 is based on the concept of the PSU, which can conveniently be defined as the stoichiometric ratio of antenna pigments to RC's. Although this neglects a possible distribution of antenna sizes, it is the commonly accepted approach. In favourable cases, such as in the LH1-RC only purple bacteria where the RC is surrounded by the LH1 ring (Karrasch *et al.*, 1995; Walz & Ghosh, 1997), the PSU has a structural correlate which simply consists of the LH1-RC complex. In other cases, such as in *Rps. acidophila* which belongs to the LH2-LH1-RC type of purple bacteria, it is conceivable that - depending on the in-plane organisation of the LH2 complexes - a photon absorbed by an LH2 complex may be supplied (eventually via another LH2 complex) to one or another LH1-RC core (Fig. 9.1). Thus, LH2 complexes may be shared between

different RC's and the PSU does not have a structural correlate. The continuum theory applied to the data evaluation does not account for these structural details but places all energy transfer processes between RC's into a single rate constant, k_{con} . Nevertheless, this rate constant allowed a useful quantification of the excitonic connectivity of RC's.

A tight structural coupling between the peripheral LH2 and core complexes in all the growth types of *Rps. acidophila* investigated in the study was supported by the following experimental observations: (i) the lack of significant fluorescence in the range between 820 and 860nm upon excitation into the B800 band of the LH2 complexes (Fig. 7.1b); (ii) invariance of the sigmoidicity parameter, J , on the excitation wavelength; (iii) invariance of the sigmoidicity parameter, J , on divalent ions, and; (iv) invariance of the sigmoidicity parameter, J , on the temperature. One can conclude from this that in all the membranes unconnected LH2 complexes are absent, which due to the nanosecond lifetime of the excited state are highly fluorescent. Thus, a model of the PSU in which the LH rings diffuse laterally as isolated units in a fluid mosaic membrane can be discarded because higher excitonic connectivity could not be achieved by experimental conditions that favour protein aggregation (*e.g.* divalent ions and low temperature). If the complexes did diffuse one would expect the existence of some free, highly fluorescent antenna complexes. Such a scenario would result in a much larger fluorescence intensity around 820nm-860nm than the one observed in Figure 7.1b. For this reason any structural model of the antenna organisation must consist of clustered, closely attached elements.

The value of $k_{\text{con}} = 3.58 \times 10^9 \text{ s}^{-1}$ found for high light (HL) grown membranes is more than six times slower than the one reported previously for *Rb. capsulatus*, another LH2-containing purple bacterium (Trissl, 1996). This inter-unit energy transfer is also significantly smaller than in *Rs.*

rubrum, an organism containing only LH1-RC complexes (Trissl, 1996). This seems to support the conclusion in Trissl (1996) that LH2 complexes of the B800-850 type bring about an excitonic barrier between RC's, although the extent may vary in different species. Whether this barrier is a consequence of larger average distances between the complexes involved or whether it is due to the uphill energy transfer required for a B880→B850→B880 transfer in the more densely packed arrangement, or both, cannot be distinguished by fluorescence induction alone and is still open to debate.

Four possible different organisational forms for the antenna arrangement in *Rps. acidophila* are depicted in Figure 9.1. Initially, these will be discussed in the light of the data obtained from experiments with photosynthetic membranes the low light (LL) and low light/low temperature (LL/LT) grown bacteria (Chapter 7). Model (a) is analogous to the one favoured by Pullerits and Sundström (1996) and Papiz *et al.* (1996) for LL grown cells. As an essential feature, the PSU consists of 8 densely packed rings of LH2 completely surrounding a single LH1-RC core complex. This model predicts an absolute antenna size of $N_{B800} = 72$, $N_{B850} = 144$ and $N_{B880} = 32$, giving a total of 248 Bchl a's (Table 7.1). The number of pigments per RC, $N_{tot} = 230$, that was calculated for LL membranes by fluorescence induction measurements is close to this ideal case. In the model suggested by Papiz *et al.* (1996) for LL membranes, several of the PSU's are in contact with each other. In this model inter-unit energy transfer can only occur via LH2 complexes and direct LH1-LH1 transfer is excluded. As such, the apparent excitonic barrier following from the experiments described in Chapter 7 (lack of sigmoidicity in the fluorescence induction curves of LL and also LL/LT membranes) could very well result from the unfavourable uphill energy transfer from the B880 to the B850 pigments of the LH2. However, more studies are required in this area

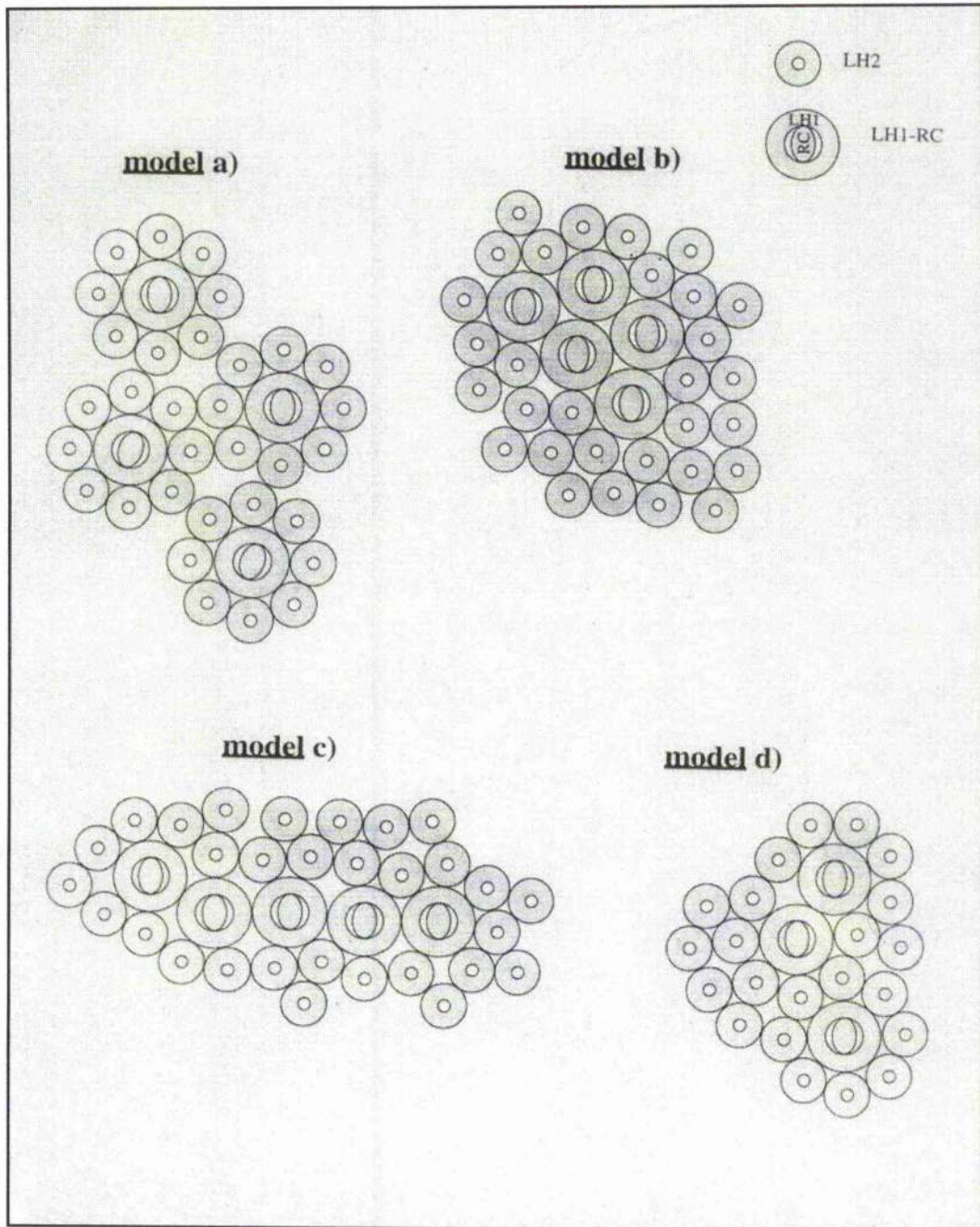


Figure 9.1. Different models for the antenna organisation of the LH2-containing purple bacterium *Rps. acidophila* strain 7750. (a) Model that reproduces the one published by Papiz *et al.* (1996). (b) Cluster model proposed by Monger and Parson (1977). (c) Linear chain model in which several LH1-RC complexes are in intimate contact with each other. (d) Model that reproduces the one published by Papiz *et al.* (1996) but adapted to the case of high-light grown membranes.

to clarify if this really is the case.

Model (b) in Figure 9.1 assumes several clustered or aggregated LH1-RC cores and these clusters are surrounded by LH2, as suggested by Monger and Parson (1977). On the one hand the value of k_{con} for the HL membranes (Table 7.2) could be compatible with this model, since a small number of well connected LH1-RC units - as supported by the high value of $k_{\text{con}} = 5 \times 10^{10} \text{ s}^{-1}$ in *Rs. rubrum* (Trissl, 1996) - can lead to a similar sigmoidicity as the actually measured one (Trissl & Lavergne, 1995). However, the data on the LL and LL/LT membranes which support rather separate units ($k_{\text{con}} \rightarrow 0 \text{ s}^{-1}$) are totally inconsistent with this model. Therefore, the structural arrangement in Figure 9.1b can be excluded to apply (at least) to low light grown *Rps. acidophila* cells. Model (c) in Figure 9.1, which assumes a linear chain of LH1-RC complexes can be excluded for the same reasons.

Therefore only model (a), in which inter-unit exciton transfer in *Rps. acidophila* can only occur via LH2 complexes, is consistent with the present experimental data for LL and LL/LT membranes. In this model, with fixed and short chromophore distances between neighbouring rings, the weak inter-unit energy exchange (large barrier for inter-unit energy transfer) could be explained by a very small probability for B880→B820→B880 and B880→B850→B880 transfer.

Finally, it has to be concluded that the densely packed ring model (Fig. 9.1a) cannot apply to HL membranes since the too low stoichiometric ratio of LH2 complexes (Table 7.1) does not allow for a complete circumferential occupation of an LH1-RC core complex. In this case the connectivity observed (Table 7.2) could be due to some degree of direct LH1-RC to LH1-RC contact in a small fraction of PSU's as depicted in model (d). In another fraction of PSU's the LH2-free sites could be occupied by other membrane proteins such as cytochromes and ATP-synthases. When there is less LH2

than needed for a dense circumferential packing of LH1, some LH2 could be shared by other LH1 rings.

In the case of LL/LT membranes the antenna size is significantly larger than that predicted by the densely packed ring model (Table 7.1 and Fig. 9.1a) and therefore further LH2 rings are implanted in the photosynthetic membrane as depicted by Papiz *et al.* (1996). These more distant LH2 can transfer excitation energy to LH1 with a similar high efficiency as those LH2 located closest to LH1. This is apparent from the small amplitude of the fluorescence spectrum at 830-840nm (Fig. 7.1b).

In summary, the work presented in this thesis shows it is possible to isolate the LH1-RC complex from several species of the purple photosynthetic bacteria in a pure and, in most cases, stable form. The purified complexes can be successfully crystallised in three dimensions. Although these crystals did not diffract X-rays very well it is conceivable that slight modification of the purification protocol and optimisation of the crystallisation conditions could produce 3-D crystals of a quality which would allow the elucidation of the structure of the LH1-RC core complex.

APPENDICES

APPENDIX A: COMPOSITION OF GROWTH MEDIA

Rps. acidophila was grown in Pfennig's medium (Pfennig, 1969). *Rps. cryptolactis* was grown in THERMED medium (Stadtwald-Demchick *et al.*, 1990), and *Chr. vinosum* in Fuller's medium (Fuller, 1963). *Rh. marinum* was grown in modified DSM-27 Rhodospirillaceae medium (Imhoff, 1983). All the other species studied were grown in C-succinate medium (Bose, 1969). This appendix lists all the solutions required to make up each medium. All media were sterilised by autoclaving before use.

A1. C-succinate medium (Bose, 1969)	<u>per litre</u>
concentrated base (see A1.1)	20ml
di-potassium hydrogen orthophosphate (1M)	10ml
potassium di-hydrogen orthophosphate (1M)	10ml
ammonium sulphate (10%)	5ml
sodium or potassium succinate pH6.8 (1M)	10ml
Growth factors (see A1.2)	1ml
Casamino acids	1g

Make up with tap water then autoclave at 15 lb/in² for 30 mins.

<u>A1.1. Concentrated base</u>	<u>per litre</u>
nitrioloacetic acid	10.0g
magnesium sulphate	14.45g
calcium chloride.2H ₂ O	3.4g
ammonium molybdate	9.25mg
ferrous sulphate.7H ₂ O	99.0mg
nicotinic acid	50.0mg
aneurine hydrochloride	25.0mg
biotin	
Metos 44 (see A1.3)	50.0ml

Add 500ml of dH₂O and pH to 6.8 with 5N KOH. Then make up to final volume.

<u>A1.2. Growth factors</u>	<u>per 100ml</u>
Biotin	2mg
sodium hydrogen carbonate	50mg
Add water and dissolve, then add;	
nicotinic acid	100mg

aneurine hydrochloride	50mg
4-aminobenzoic acid	100mg
Boil to dissolve.	

A1.3. Metos 44 per 250ml

disodium EDTA	2.5g
zinc sulphate	10.95g
manganous sulphate.4H ₂ O	1.54g
copper sulphate.5H ₂ O	0.39g
cobaltous nitrate.6H ₂ O	0.25g
ferrous sulphate.7H ₂ O	5.0g
disodium tetraborate.10H ₂ O	0.18g
concentrated H ₂ SO ₄	~20 drops

A2. Pfennig's medium (Pfennig, 1969) per litre

potassium dihydrogen orthophosphate	1.0g
magnesium sulphate.7H ₂ O	0.4g
sodium chloride	0.4g
sodium succinate	1.5g
or	
succinic acid	0.65g
calcium chloride.2H ₂ O	0.05g
ammonium chloride	0.5g
ferric citrate solution (see A2.1)	5.0ml
Trace element solution (see A2.2)	10.0ml

Make up with tap water then adjust pH to 5.2 with HCl. Autoclave.

A2.1. Ferric citrate solution per 100ml

Add 100mg of ferric citrate to 100ml of dH₂O and boil until completely dissolved. Store at 4°C.

A2.2. Trace element solution per litre

disodium EDTA	0.5g
ferrous sulphate.7H ₂ O	10.0mg
manganous chloride.4H ₂ O	3.0mg
boric acid	30.0mg
cobalt chloride.2H ₂ O	20.0mg

calcium chloride.2H ₂ O	1.0mg
nickel chloride	2.0mg
sodium molybdate.2H ₂ O	3.0mg

Adjust pH to 3-4 and store at 4°C.

A3. THERMED medium (Stadtwald-Demchick *et al.*, 1990) per litre

To 500 ml of dH₂O, add:

0.64M potassium phosphate buffer (see A3.1)	5.0ml
10% ammonium chloride solution	10.0ml
1% disodium EDTA	0.5ml
20% magnesium sulphate.7H ₂ O	1.0ml
TBTE (see A3.2)	1.0ml
7.5% calcium chloride.2H ₂ O	1.0ml
chelated iron solution (see A3.3)	2.0ml
vitamin B12 (20µg/ml) solution	1.0ml
niacin (10mg/ml) solution	1.0ml
PABA (3mg/ml) solution	1.0ml
sodium thiosulphate.5H ₂ O	0.5g
sodium pyruvate	2.2g

Adjust pH to 6.8 and bring final volume to 1 litre with dH₂O. Autoclave.

A3.1. 0.64M potassium phosphate buffer per litre

To 900ml of dH₂O, add:

potassium dihydrogen orthophosphate	40.0g
dipotassium hydrogen orthophosphate	60.0g

pH to 6.8 and bring final volume to 1L with dH₂O.

A3.2. True Blue Trace Elements (TBTE) per 250ml

To 200ml dH₂O add:

disodium EDTA	2.5g
manganous chloride.4H ₂ O	0.2g
boric acid	0.1g
sodium molybdate.2H ₂ O	0.1g
zinc chloride	0.05g

nickel (II) chloride.6H ₂ O	0.05g
cobalt (II) chloride. 6H ₂ O	0.02g
copper (II) chloride.2H ₂ O	0.01g
sodium selenite	5.0mg
sodium metavanadate	5.0mg

Adjust volume to 250ml.

A3.3. Chelated iron solution

per litre

To 900ml dH₂O, add:

disodium EDTA	2.0g
iron (II) chloride.4H ₂ O	1.0g
concentrated HCl	3.0ml

Adjust volume to 1L.

A4. Chromatium medium (Fuller, 1963)

per litre

Solution 1

sodium chloride	60.0g
dipotassium hydrogen orthophosphate	1.0g
potassium dihydrogen orthophosphate	1.0g
ammonium chloride	2.0g
calcium chloride	0.25g
magnesium chloride	1.0g

Make up with dH₂O then adjust pH to 7-8.

Solution 2

sodium thiosulphate.5H ₂ O	6.0g
sodium hydrogen carbonate	8.0g

Make up with dH₂O then adjust pH to 7-8.

Solution 3

ferrous sulphate.7H ₂ O	1.6g
EDTA	3.0g

Add solutions together as follows:

	<u>per 2 litres</u>
Solution 1	1L
Solution 2	1L
Solution 3	8ml

A5. Modified Rhodospirillaceae medium	<u>per litre</u>
yeast extract	0.3g
ethanol	0.5ml
disodium succinate	1.0g
ammonium acetate	0.5g
ferric citrate solution (see A2.1)	5.0ml
potassium dihydrogen orthophosphate	0.5g
magnesium sulphate.7H ₂ O	0.4g
sodium chloride	30.0g
ammonium chloride	0.4g
calcium chloride.2H ₂ O	0.05g
vitamin B12 (1mg/ml) solution	0.4ml
trace element solution SL-6 (see A5.1)	1.0ml

Adjust pH to 6.8 and autoclave.

<u>A5.1. Trace element solution SL-6</u>	<u>per litre</u>
zinc sulphate.7H ₂ O	0.1g
manganous chloride.4H ₂ O	0.03g
boric acid	0.3g
cobaltous chloride.6H ₂ O	0.2g
copper chloride.2H ₂ O	0.01g
nickel chloride.6H ₂ O	0.02g
sodium molybdate.2H ₂ O	0.03g

APPENDIX B: SDS-PAGE STOCK SOLUTIONS

Acrylamide solutions were purchased ready made and consisted of 30% (w/v) acrylamide, 1.579% (w/v) bis-acrylamide (EASIGel, Scotlab).

B1. Resolving gels

SDS-PAGE resolving gels from 7.5% to 18.5% were made up from stock solutions according to the table below.

solution	concentration (%)				
	7.5	10.0	11.5	15	18.5
running gel buffer (see B1.1)	10ml	10ml	10ml	10ml	10ml
30% acrylamide solution	10ml	13.4ml	15.4ml	20ml	24.8ml
dH ₂ O	20ml	16.6ml	14.6ml	10ml	5.2ml
10% ammonium persulphate (fresh)	200µl	200µl	200µl	200µl	200µl
TEMED	25µl	25µl	25µl	25µl	25µl

B1.1. Running gel bufferper litre

Tris
SDS

181.2g
4.0g

Make up with dH₂O then pH to 8.8 with HCl. Check pH before each use. Store at 4°C.

B2. Stacking gelper 20ml

stacking gel buffer (see B2.1)
30% acrylamide solution
dH₂O
10% (w/v) ammonium persulphate (fresh)
TEMED

5ml
3ml
12ml
60µl
20µl

<u>B2.1. Stacking gel buffer</u>	<u>per 250ml</u>
0.5M Tris	15.1g
0.4% SDS solution	1.0g
B3. Anode buffer	<u>per litre</u>
Tris	24.4g
Adjust pH to 8.45 with HCl.	
B4. Cathode buffer	<u>per litre</u>
Tris	3.0g
SDS	1.0g
glycine	14.56g
B5. Protein sample buffer	<u>per 10ml</u>
50mM Tris-HCl	0.06g
2% (w/v) SDS	0.02g
10% (v/v) glycerol	1.0ml
2% (v/v) mercaptoethanol	0.2ml
0.1% (w/v) bromophenol blue	0.01g
Adjust pH to 6.8 with HCl.	
The above sample buffer is for use with samples that do not contain RC. When RC proteins are present (as in the LH1-RC core complex) the mercaptoethanol is replaced with 10mM dithiothreitol.	
B6. Stain and destain solutions	
<u>B6.1. Adel's fast staining solution</u>	<u>per litre</u>
dH ₂ O	500ml
methanol	500ml
glacial acetic acid	200ml
Coomassie blue	1.2g
<u>B6.2. Adel's destain solution</u>	<u>per litre</u>
propan-2-ol	125ml
glacial acetic acid	100ml
dH ₂ O	775ml

APPENDIX C: CRYSTALLISATION SCREENS, DETERGENTS AND ADDITIVES.

C1. The FASTPEG screen devised by Gall (1994) based on salts and PEG as precipitants.

FASTPEG NUMBER	SALT	BUFFER	PRECIPITANT
1	0.1M NH ₄ ⁺ acetate	50mM MES pH6.0	5% PEG 8000
2	0.1M K phosphate	50mM TRIS pH8.5	25% PEG 300
3	0.1M Na citrate	50mM CHES pH9.5	10% PEG 6000
4	0.1M Zn acetate	50mM TRIS pH8.5	2.5% PEG 1000
5	0.1M Na acetate	50mM MES pH6.5	12.5% PEG 1000
6	0.1M Zn chloride	50mM MES pH 6.0	10% PEG 600
7	0.1M Mg acetate	50mM MES pH 6.0	2.5% PEG 6000
8	0.1M Na citrate	50mM HEPES pH7.5	10% PEG 6000
9	0.1M Mg chloride	50mM CHES pH9.0	15% PEG 400
10	0.1M NH ₄ ⁺ sulphate	50mM CHES pH 9.5	2.5% PEG 6000
11	0.1M Ca chloride	50mM TRIS pH8.0	15% PEG 300
12	0.1M NH ₄ ⁺ sulphate	50mM MES pH6.5	5% PEG 600
13	0.1M Na acetate	50mM HEPES pH7.5	10% PEG 400
14	0.1M NH ₄ ⁺ sulphate	50mM TRIS pH 8.0	7.5% PEG 4000
15	0.1M Li sulphate	50mM TRIS pH8.5	10% PEG 400
16	0.1M Mg chloride	50mM MES pH6.0	15% PEG 400
17	0.1M Na acetate	50mM CHES pH 9.5	10% PEG 400
18	0.1M K phosphate	50mM MES pH6.0	10% PEG 200
19	0.1M Ca acetate	50mM HEPES pH7.5	2.5% PEG 4000
20	0.1M Ca acetate	50mM TRIS pH 8.5	25% PEG 600
21	0.1M Ca acetate	50mM CHES pH9.5	12.5% PEG 8000
22	0.1M Mg acetate	50mM TRIS pH 8.0	2.5% PEG 2000
23	0.1M Na citrate	50mM MES pH 6.5	12.5% PEG 6000
24	0.1M Na acetate	50mM MES pH 6.0	5% PEG 1000
25	0.1M Zn chloride	50mM MES pH 6.0	15% PEG 300
26	0.1M Na citrate	50mM HEPES pH7.0	10% PEG 1000
27	0.1M Zn chloride	50mM TRIS pH 8.5	12.5% PEG 4000
28	0.1M Na citrate	50mM HEPES pH7.5	12.5% PEG 6000
29	0.1M Li sulphate	50mM TRIS pH 8.0	25% PEG 300
30	0.1M NH ₄ ⁺ sulphate	50mM HEPES pH7.0	7.5% PEG 4000
31	0.1M Ca chloride	50mM CHES pH 9.0	15% PEG 200
32	0.1M NH ₄ ⁺ acetate	50mM CHES pH 9.5	20% PEG 600
33	0.1M Ca acetate	50mM MES pH 6.0	10% PEG 1000
34	0.1M K phosphate	50mM HEPES pH7.0	20% PEG 200
35	0.1M Mg acetate	50mM TRIS pH 8.5	15% PEG 200
36	0.1M NH ₄ ⁺ acetate	50mM TRIS pH 8.0	5% PEG 2000
37	0.1M Mg acetate	50mM MES pH 6.5	20% PEG 6000
38	0.1M Mg chloride	50mM CHES pH 9.0	2.5% PEG 2000
39	0.1M Zn acetate	50mM HEPES pH7.0	2.5% PEG 8000
40	0.1M Ca chloride	50mM HEPES pH7.5	10% PEG 2000
41	0.1M Ca acetate	50mM HEPES pH7.0	5% PEG 8000
42	0.1M Li sulphate	50mM MES pH 6.5	25% PEG 200
43	0.1M Ca chloride	50mM TRIS pH 8.0	10% PEG 8000

FASTPEG NUMBER	SALT	BUFFER	PRECIPITANT
44	0.1M NH ₄ ⁺ acetate	50mM CHES pH 9.0	2.5% PEG 400
45	0.1M Mg chloride	50mM CHES pH 9.0	12.5% PEG 1000
46	0.1M K phosphate	50mM CHES pH 9.5	15% PEG 200
47	0.1M Li sulphate	50mM MES pH 6.0	15% PEG 300
48	0.1M Zn acetate	50mM HEPES pH7.0	5% PEG 2000

C2. The Magic 46 crystallisation screen developed at the University of California, Berkeley, U.S.A. This wide ranging screen uses salts, organic solvents and PEG as precipitants, and covers a pH range from ~4 to ~8.5.

MAGIC 46 NO.	SALT	BUFFER	PRECIPITANT (w/v or v/v)
1	0.1M Ca chloride	50mM Na acetate pH4	15% MPD
2			0.2M KNa tartrate
3			0.2M NH ₄ ⁺ phosphate
4		50mM TRIS pH8.5	1.0M NH ₄ ⁺ sulphate
5	0.1M Na citrate	50mM HEPES pH7.5	20% MPD
6	0.1M Mg chloride	50mM TRIS pH8.5	30% PEG 4000
7		50mM Na cacodylate	0.7M Na acetate
8	0.1M Na citrate		15% propan-2-ol
9	0.1M NH ₄ ⁺ acetate	50mM Na citrate	15% PEG 4000
10	0.1M NH ₄ ⁺ acetate	50mM Na acetate	15% PEG 4000
11		50mM Na citrate	0.5M NH ₄ ⁺ phosphate
12	0.1M Mg chloride	50mM HEPES pH7.5	15% propa-2-ol
13	0.1M Na citrate	50mM TRIS pH8.5	15% PEG 400
14	0.1M Ca chloride	50mM HEPES pH7.5	14% PEG 400
15	0.1M NH ₄ ⁺ sulphate	50mM Na cacodylate	15% PEG 8000
16		50mM HEPES pH7.5	0.75M Li sulphate
17	0.1M Li sulphate	50mM TRIS pH8.5	15% PEG 4000
18	0.1M Mg acetate	50mM Na caodylate	10% PEG 8000
19	0.1M NH ₄ ⁺ acetate	50mM TRIS pH8.5	15% propan-2-ol
20	0.1M NH ₄ ⁺ sulphate	50mM Na acetate	12.5% PEG 4000
21	0.1M Mg acetate	50mM Na cacodylate	15% MPD
22	0.1M Na acetate	50mM TRIS pH 8.5	15% PEG 4000
23	0.1M Mg chloride	50mM HEPES pH7.5	15% PEG 400
24	0.1M Ca chloride	50mM Na acetate	10% propan-2-ol
25		50mM imidazole	0.5M Na acetate
26	0.1M NH ₄ ⁺ acetate	50mM Na acetate	15% MPD
27	0.1M Na citrate	50mM HEPES pH7.5	10% propan-2-ol
28	0.1M Na acetate	50mM Na cacodylate	30% PEG 8000
29		50mM HEPES pH7.5	0.4M KCa tartrate
30	0.1M NH ₄ ⁺ sulphate		15% PEG 8000
31	0.1M NH ₄ ⁺ sulphate		15% PEG 4000
32			1.0M NH ₄ ⁺ sulphate
33			2.0M Na formate
34		50mM Na acetate	1.0M Na formate
35		50mM HEPES pH7.5	0.9M K phosphate

MAGIC 46 NO.	SALT	BUFFER	PRECIPITANT (w/v or v/v)
36		50mM TRIS pH 8.5	4% PEG 8000
37		50mM Na acetate	4% PEG 4000
38		50mM HEPES pH7.5	0.7M Na citrate
39		50mM HEPES pH7.5	1% PEG400; 1.0M NH ₄ ⁺ sulphate
40		50mM Na citrate	10% Propan-2-ol; 10% PEG 4000
41		50mM HEPES pH7.5	5% propan-2-ol; 10% PEG 4000
42	25mM K phosphate		10% PEG 8000
43			15% PEG 2000
44			0.1M Na formate
45	0.1M Zn acetate	50mM Na cacodylate	9% PEG 8000
46	0.1M Ca acetate	50mM Na cacodylate	9% PEG 8000

C3. The commercially available Membfac sparse matrix screen (Hampton Research) for the crystallisation of membrane proteins.

MEMBFAC NO.	SALT	BUFFER	PRECIPITANT (w/v or v/v)
1	0.1M Na chloride	0.1M Na acetate pH4.6	12% MPD
2	0.1M zinc acetate	0.1M Na acetate pH4.6	12% PEG 4000
3	0.2M ammonium sulphate	0.1M Na acetate pH4.6	10% PEG 4000
4	0.1M Na chloride	0.1M Na acetate pH4.6	12% isopropanol
5		0.1M Na acetate pH4.6	12% PEG 4000
6		0.1M Na acetate pH4.6	1.0M ammonium sulphate
7	1.0M magnesium sulphate	0.1M Na acetate pH4.6	
8	0.1M magnesium chloride	0.1M Na acetate pH4.6	18% PEG 400
9	0.1M lithium sulphate	0.1M Na acetate pH4.6	1.0M ammonium sulphate
10	0.1M Na chloride	0.1M Na acetate pH4.6	12% PEG 6000
11	0.1M magnesium chloride	0.1M Na acetate pH4.6	12% PEG 6000
12	0.1M Na chloride	0.1M Na citrate pH 5.6	18% PEG 400
13	0.1M lithium sulphate	0.1M Na citrate pH 5.6	12% PEG 4000
14	0.1M Na citrate	0.1M Na citrate pH 5.6	10% isopropanol
15	0.1M Na chloride	0.1M Na citrate pH 5.6	12% MPD
16		0.1M Na citrate pH 5.6	1.0M Mg sulphate
17	0.1M Na chloride	0.1M Na citrate pH 5.6	12% PEG 4000
18	0.1M lithium sulphate	0.1M Na citrate pH 5.6	12% PEG 6000
19	0.1M Mg chloride	0.1M Na citrate pH 5.6	4% MPD

MEMBFAC NO.	SALT	BUFFER	PRECIPITANT (w/v or v/v)
20	0.1M Na chloride	0.1M Na citrate pH 5.6	
21	0.1M lithium sulphate	0.1M Na citrate pH 5.6	4% PEG 400
22		0.1M ADA pH 6.5	1.0M ammonium sulphate
23	0.1M lithium sulphate	0.1M ADA pH 6.5	12% PEG 4000 and 2% isopropanol
24		0.1M ADA pH 6.5	1.0M di-ammonium phosphate
25	0.1M magnesium chloride	0.1M ADA pH 6.5	12% PEG 6000
26		0.1M ADA pH 6.5	12% MPD
27	0.1M lithium sulphate	0.1M ADA pH 6.5	1.0M magnesium sulphate
28	0.3M lithium sulphate	0.1M ADA pH 6.5	4% PEG 400
29	0.1M ammonium sulphate	0.1M ADA pH 6.5	1.0M di-Na/K phosphate
30	0.1M Na chloride	0.1M Na HEPES pH 7.5	10% PEG 4000
31	0.1M magnesium chloride	0.1M Na HEPES pH 7.5	18% PEG 400
32		0.1M Na HEPES pH 7.5	1.0M K/Na tartrate
33	0.1M ammonium sulphate	0.1M Na HEPES pH 7.5	18% PEG 400
34	0.1M ammonium sulphate	0.1M Na HEPES pH 7.5	10% PEG 4000
35	0.1M Na citrate	0.1M Na HEPES pH 7.5	12% MPD
36		0.1M Na HEPES pH 7.5	1.0M Na citrate
37	0.6M magnesium sulphate	0.1M Na HEPES pH 7.5	4% PEG 400
38	0.6M magnesium sulphate	0.1M Na HEPES pH 7.5	4% MPD
39	0.1M lithium sulphate	0.1M Na HEPES pH 7.5	0.1M K/Na tartrate
40	0.1M lithium sulphate	0.1M Tris HCl pH 8.5	12% MPD
41	1.0M di-Na/K phosphate	0.1M Tris HCl pH 8.5	1.0M di-ammonium phosphate
42		0.1M Tris HCl pH 8.5	0.1M Na acetate
43	0.1M Na chloride	0.1M Tris HCl pH 8.5	
44	0.1M di-ammonium phosphate	0.1M Tris HCl pH 8.5	12% PEG 6000
45	0.1M K/Na tartrate	0.1M Tris HCl pH 8.5	0.4M magnesium sulphate
46		0.1M Tris HCl pH 8.5	0.2M lithium sulphate
47		0.1M Tris HCl pH 8.5	0.5M ammonium sulphate
48	0.1M Na citrate	0.1M Tris HCl pH 8.5	5% PEG 400

C4. List of detergents screened for their effectiveness for producing crystals of the LH1-RC core complex. Some of the detergents formed part of the Hampton Research Detergent Screen kit while others were purchased from alternative sources.

1. C₁₂E₉
2. C₁₂ E₈
3. n-dodecyl-β-D-maltoside
4. sucrose monolaurate
5. CYMAL[®]-6
6. TRITON X-100
7. CTAB
8. deoxy-BigChap
9. n-decyl-β-D-maltoside
10. LDAO
11. CYMAL[®]-5
12. ZWITTERGENT[®]3-12
13. nonyl-β-D-glucoside
14. 1-s-octyl-β-D-thioglucoside
15. DDAO
16. UDAO
17. HFCAMEG
18. heptyl-β-D-thioglucoside
19. n-octanoylsucrose
20. n-octyl-β-D-glucoside
21. CYMAL[®]-3
22. C-HEGA-10
23. ZWITTERGENT[®] 3-10
24. MEGA-8
25. n-hexyl-β-D-glucoside
26. cholate
27. sucrose monocholate
28. CHAPS
29. deoxy-cholate
30. taurocholate

C5. List of additives and small amphiphiles screened for their effectiveness for producing crystals of the LH1-RC core complex.

1. barium chloride dihydrate
2. cadmium chloride dihydrate
3. calcium chloride dihydrate
4. cobaltous chloride dihydrate
5. cupric chloride dihydrate
6. magnesium chloride hexahydrate

7. magnesium chloride tetrahydrate
8. strontium chloride hexahydrate
9. yttrium chloride hexahydrate
10. zinc chloride
11. ethylene glycol
12. glycerol
13. 1,6-hexanediol
14. 2-methyl-2,4-pentane diol
15. PEG 400
16. trimethylamine HCl
17. guanidine HCl
18. urea
19. 1,2,3-heptane triol
20. benzamidine HCl
21. dioxane
22. ethanol
23. iso-propanol
24. methanol
25. sodium iodide
26. L-cysteine
27. EDTA sodium salt
28. NAD
29. ATP disodium salt
30. D (+)-glucose
31. D (+)-sucrose
32. xylitol
33. spermidine
34. spermine tetraHCl
35. 6-aminocaproic acid
36. 1,5-diaminopentane di-HCl
37. 1,6-diaminohexane
38. 1,8-diaminooctane
39. glycine
40. glycyl-glycyl-glycine
41. hexaminecobalt trichloride
42. taurine
43. betaine monohydrate
44. polyvinylpyrrolidone K15
45. non-detergent sulfo-betaine 195
46. non-detergent sulfo-betaine 201
47. phenol
48. dimethyl sulfoxide

REFERENCES

* denotes references not available in the main library

Aagard, J. & Sistrom, W.R. (1972) Control of synthesis of reaction centre bacteriochlorophyll in photosynthetic bacteria. *Photochem. Photobiol.* **15**, 209-225.

Agalidis, I. & Reiss-Husson, F. (1983). Several properties of the LM unit extracted with sodium dodecyl sulphate from *Rhodospseudomonas sphaeroides* purified reaction centres. *Biochim. Biophys. Acta* **724**, 340-351.

Agalidis, I. & Reiss-Husson, F. (1992). Purification and characterization of *Rhodocyclus gelatinosus* photochemical reaction center. *Biochim. Biophys. Acta* **1098**, 201-208.

Alden, R.G., Johnson, E., Nagarajan, V., Parson, W.W., Law, C.J. & Cogdell, R.J. (1997) Calculations of the spectroscopic properties of the LH2 bacteriochlorophyll-protein antenna complex from *Rhodospseudomonas acidophila*. *J. Phys. Chem. B*, **101**, 4667-4680.

Allen, J.P., Fehrer, G., Yeates, T.O., Rees, D.C., Eisenberg, D.S., Deisenhofer, J., Michel, H. & Huber, R. (1986) Preliminary electron-density mapping of the reaction centers from *Rhodospseudomonas sphaeroides* using the molecular replacement method. *Biophys. J.* **49**, 583a.

Allen, J.P., Fehrer, G., Yeates, T.O., Komiyama, H. & Rees, D.C. (1987a) Structure of the reaction center from *Rhodobacter sphaeroides* R-26; the cofactors. *Proc. Natl. Acad. Sci. USA.* **84**, 5730-5734.

Allen, J.P., Fehrer, G., Yeates, T.O., Komiyama, H. & Rees, D.C. (1987b) Structure of the reaction center from *Rhodobacter sphaeroides* R-26; the protein subunits. *Proc. Natl. Acad. Sci. USA.* **84**, 6162-6166.

Allen, J.P., Fehrer, G., Yeates, T.O., Komiyama, H. & Rees, D.C. (1988a) In: *The Photosynthetic Reaction Center*. NATO ASI Series A: Life Sciences (Breton, J. & Vermaglio, A., eds.), pp5-72. Plenum Press, New York.

Allen, J.P., Fehrer, G., Yeates, T.O., Komiyama, H. & Rees, D.C. (1988b) Structure of the reaction center from *Rhodobacter sphaeroides* R-26: Protein-cofactor (quinones and Fe²⁺) interactions. *Proc. Natl. Acad. Sci. USA.* **85**, 8487-8491.

Allen, J.P., Fehrer, G., Yeates, T.O., Rees, D.C., Deisenhofer, J., Michel, H. & Huber, R. (1986b) Structural homology of reaction centers from *Rhodobacter sphaeroides* and *Rhodospseudomonas viridis* as determined by x-ray diffraction. *Proc. Natl. Acad. Sci. USA.* **83**, 8589-8593.

Andersson, P.O., Cogdell, R.J. & Gillbro, T. (1996) Femtosecond dynamics of carotenoid-to-bacteriochlorophyll *a* energy transfer in the light-harvesting antenna complexes from the purple bacterium *Chromatium purpuratum*. *Chem. Physics* **210**, 195-217.

Angerhofer, A., Cogdell, R.J. & Hipkins, M. F. (1986) A spectral characterisation of the light-harvesting pigment-protein complexes from *Rhodospseudomonas acidophila*. *Biochim. Biophys. Acta* **848**, 333-341.

Angerhofer, A., Bornhäuser, F., Gall, A. & Cogdell, R.J. (1995) Optical and optically detected magnetic resonance investigation on purple photosynthetic bacterial antenna complexes. *Chem. Phys.* **194**, 259-274.

- Arakawa, T. & Timasheff, S. N. (1985a) Mechanism of poly (ethylene glycol) interaction with proteins. *Biochemistry* **24**, 6756-6762.
- Arakawa, T. & Timasheff, S. N. (1985b) In: *Methods in Enzymology. Diffraction Methods for Biological Macromolecules*. **114**, 49.
- Arnoux, B., Ducruix, A., Reiss-Husson, F., Lutz, M., Norris, J., Schiffer, M. & Chang, C.-H. (1989) Structure of spheroidene in the photosynthetic reaction center from *Y Rhodobacter sphaeroides*. *FEBS Lett.* **258**, 47-50.
- Arnoux, B., Gaucher, J-F., Ducruix, A. & Reiss-Husson, F. (1995) Structure of the photochemical reaction center of a spheroidene-containing purple bacterium, *Rhodobacter sphaeroides* Y, at 3Å resolution. *Acta. Cryst.* **D51**, 368-379.
- Babst, M., Albrecht, H., Wegmann, I., Brunisholz, R.A. & Zuber, H. (1991) Single amino acid substitutions in the α - and β -870 light-harvesting polypeptides of *Rhodobacter capsulatus*: Structural and spectral effects. *Eur. J. Biochem.* **282**, 277-284.
- Bartley, G.E. & Scolnik, P.A. (1989) Carotenoid biosynthesis in photosynthetic bacteria - genetic characterization of the *Rhodobacter capsulatus* crt1 protein. *J. Biol. Chem.* **264**, 13109-13113.
- Bartsch, R.G. (1978) In: *The Photosynthetic Bacteria* (Clayton, R.K. & Sistrom, W.R., eds.), pp249-279. Plenum Press, New York.
- Barz, W.P., Francia, F., Venturoli, G., Melandri, B.A., Vermeglio, A. & Oesterheld, D. (1995a) Role of the pufX protein in photosynthetic growth of *Rhodobacter sphaeroides*. 1. PufX is required for efficient light-driven electron transfer and photophosphorylation under anaerobic conditions. *Biochemistry* **34**, 15235-15247.
- Barz, W.P., Vermeglio, A., Francia, F., Venturoli, G., Melandri, B.A. & Oesterheld, D. (1995b) Role of the pufX protein in photosynthetic growth of *Rhodobacter sphaeroides*. 2. PufX is required for efficient ubiquinone/ubiquinol exchange between the reaction center Q_B site and the cytochrome bc₁ complex. *Biochemistry* **34**, 15248-15258.
- Bauer, C.E., Young, D.A. & Marrs, B.L. (1988) Analysis of the *Rhodobacter capsulatus* puf operon, location of the oxygen promoter region and the identification of an additional puf encoded gene. *J. Biol. Chem.* **263**, 4820-4827.
- *Bavendamm, W. (1924) *Die farblosen und roten Schwefelbakterien des Süß-und Salzwassers*. Fischer Verlag, Jena.
- Beddard, G.S. & Cogdell, R.J. (1982) Structure and excitation dynamics of light-harvesting protein complexes. In *Molecular Biology, Biochemistry and Photophysics, Vol.35. Light Reaction Path of Photosynthesis* (Fong, F.K., ed.), pp46-79. Springer-Verlag, Berlin.
- Bélanger, G., Bérard, J., Corriveau, P. & Gingras, G. (1988) Genes coding for the L and M subunits of the *Rhodospirillum rubrum* photoreaction center. *Biochemistry* **263**, 7632-7638.
- Bergstrom, H., van Grondelle, R. & Sundström, V. (1989) Characterization of excitation energy trapping in photosynthetic bacteria at 77K. *FEBS Lett.* **250**, 503-508.
- Bergstrom, H., Sundström, V., van Grondelle, R., Gillbro, T. & Cogdell, R.J. (1988) Energy transfer dynamics of isolated B800-850 and B800-820 pigment-protein

- complexes of *Rhodobacter sphaeroides* and *Rhodospseudomonas acidophila*. *Biochim. Biophys. Acta* **936**, 90-98.
- Bissig, I., Wagner-Huber, R., Brunisholz, R.A., Frank, G. & Zuber, H. (1989) Multiple forms of light-harvesting polypeptides in *Chromatium vinosum*. In: *Molecular Biology of Membrane-Bound Complexes of Phototrophic Bacteria* (Drews, G. & Davies, E.A., eds.), pp199-210. Plenum Press, New York.
- Blankenship, R.E., Cheng, P.E., Causgrove, T.P., Brune, D.C., Wang, S.H., Choh, J. & Wang, J. (1993) Redox regulation of energy transfer efficiency in antennas of green photosynthetic bacteria. *Photochem. Photobiol.* **57**, 103-107.
- Blankenship, R.E., Olson, J.M. & Miller, M. (1995) Antenna complexes from green photosynthetic bacteria. In: *Anoxygenic photosynthetic bacteria* (Blankenship, R.E., Madigan, M.T. & Bauer, C.E., eds.), pp399-435. Kluwer Academic Publishers, Dordrecht.
- Bolt, J.D., Sauer, K., Shiozawa, J. A. & Drews, G. (1981) Linear and circular dichroism of membranes from *Rhodospseudomonas capsulata*. *Biochim. Biophys. Acta* **635**, 535-541.
- Bondarev, S.L. & Knyukshto, V.N. (1994) Fluorescence from the S₁ (2¹Ag) state of all-trans- β -carotene. *Chem. Phys. Lett.* **225**, 346-350.
- Boonstra, A.F., Germeroth, L. & Boekma, E.J. (1994) Structure of the light-harvesting antenna from *Rhodospirillum rubrum* studied by electron microscopy. *Biochim. Biophys. Acta* **1184**, 227-234.
- Boonstra, A.F., Visschers, R.W., Calkoen, F., van Grondelle, R., van Bruggen, E.F.J. & Boekma, E.J. (1993) Structural characterisation of the B800-850 and B875 light-harvesting antenna complexes from *Rhodobacter sphaeroides* by electron microscopy. *Biochim. Biophys. Acta* **1142**, 181-188.
- Bopp, M.A., Jia, Y., Li, L., Cogdell, R.J. & Hochstrasser, R.M. (1997) Fluorescence and photobleaching dynamics of single light-harvesting complexes. *Proc. Natl. Acad. Sci. USA* **94**, 10630-10635.
- Borisov, A.Y. (1978) Energy migration mechanisms in antenna chlorophylls. In: *The Photosynthetic Bacteria* (Clayton, R.K. & Sistrom, W.R., eds.), pp323-332. Plenum Press, New York.
- Bose, S.K. (1963) In: *Bacterial Photosynthesis* (Gest, H., San Pietro, A. & Vernon, L.F., eds.), Antioch Press, Yellow Springs, Ohio.
- Bradford, M.M. (1976) A refined and sensitive method for the quantitation of microgram quantities of protein utilizing the principle of protein-dye binding. *Anal. Biochem.* **72**, 248.
- Breton, J. & Navedryk, E. (1984) Transmembrane orientation of α -helices and the organization of chlorophyll in photosynthetic pigment-protein complexes. *FEBS Lett.* **176**, 355-359.
- Brunisholz, R.A. & Zuber, H. (1988) Primary structure analyses of bacterial antenna polypeptides: Correlation of aromatic amino acids with spectral properties. Structural similarities with reaction center polypeptides. In: *Photosynthetic Light-Harvesting Systems* (Scheer, H. & Schneider, S., eds.), pp103. Walter de Gruyter, Berlin.

- Brunisholz, R.A. & Zuber, H. (1993) Spectral modifications of bacterial antenna complexes by limited proteolysis. *Photochem. Photobiol.* **57**, 6-12.
- Brunisholz, R.A., Wiemken, V., Suter, F., Bachofen, R. & Zuber, H. (1984) The light-harvesting polypeptides of *Rhodospirillum rubrum*: II. Localization of amino terminal regions of the light-harvesting polypeptides B870- α and B870- β and the reaction center subunit L at the cytoplasmic side of the photosynthetic membrane of *RS. rubrum* G-9⁺. *Hoppe-Seyler's Z Physiol. Chem.* **365**, 689-701.
- Brunisholz, R.A., Jay, F., Suter, F. & Zuber, H. (1985) The light-harvesting polypeptides of *Rhodospseudomonas viridis*: The complete amino acid sequences of B1015- α , B1015- β and B1015- γ . *Biol. Chem. Hoppe-Seyler* **366**, 87-89.
- Brunisholz, R.A., Zuber, H., Valentine, J., Lindsay, J.G., Wooley, K.J. & Cogdell, R.J. (1986) The membrane location of the B890-complex from *Rs. rubrum* and the effect of carotenoid on the conformation of its two apoproteins at the cytoplasmic surface. *Biochim. Biophys. Acta* **849**, 295-303.
- Buchanan, S.K., Fritsch, G., Ermler, U. & Michel, H. (1993) New crystal form of the photosynthetic reaction center from *Rhodobacter sphaeroides* of improved diffraction quality. *J. Mol. Biol.* **230**, 1311-1314.
- Bustamante, P.L. & Loach, P.A. (1994) Reconstitution of a functional photosynthetic receptor complex with isolated subunits of core light-harvesting complex and reaction centers. *Biochemistry* **33**, 13329-13339.
- Butler, W.L. (1980) Energy transfer between Photosystem II units in a connected package model of the photochemical apparatus of photosynthesis. *Proc. Natl. Acad. Sci. U.S.A.* **77**, 4697-4701.
- Caffrey, M.S., Bartsch, R.G. & Cusanovich, M.A. (1992) Study of cytochrome *c*₂-reaction center interaction by site-directed mutagenesis. *J. Biol. Chem.* **267**, 6317-6321.
- Carter, C.W. Jr. (1992) Design of crystallization experiments and protocols. In: *Crystallization of Nucleic Acids and Proteins* (Ducruix, A. & Giegé, R. eds.), pp47-70. Oxford University Press, Oxford.
- Chachisvilis, M., Kühn, O., Pullerits, T. & Sundström, V. (1997) Exciton delocalisation length in the B850 antenna of *Rhodobacter sphaeroides*. *J. Phys. Chem B.* **101**, 7275-7283.
- Chadwick, B.W. & Frank, H.A. (1986) Electron spin resonance studies of carotenoids incorporated into reaction centers of *Rhodobacter sphaeroides* R26.1. *Biochim. Biophys. Acta* **851**, 257-266.
- Chang, C.H., Tiede, D., Tang, J., Smith, U., Norris, J. & Schiffer, M. (1986) Structure of the reaction centre from *Rhodobacter sphaeroides* R-26. *FEBS Lett.* **205**, 82-86.
- Chang, C.H., El-Kabbani, O., Tiede, D., Tang, J., Norris, J. & Schiffer, M. (1991) Structure of the membrane bound protein photosynthetic reaction centre from *Rhodobacter sphaeroides*. *Biochemistry* **30**, 5352-5360.
- Chang, M.C., Callahan, P.M., Parkes-Loach, P.S., Cotton, T.M. and Loach, P.A. (1990) Spectroscopic characterization of the light-harvesting complex of *Rhodospirillum*

rubrum and its structural subunit. *Biochemistry* **29**, 421-429.

Chothia, C. (1984) Principles that determine the structure of proteins. *Ann. Rev. Biochem.* **53**, 537-572.

Chory, J.T., Donohue, J., Varga, A.R., Staehlin, L.A. & Kaplan, S. (1984) Induction of the photosynthetic membranes of *Rhodospseudomonas sphaeroides*: biochemical and morphological studies. *J. Bacteriol.* **159**, 540-544.

Chynwat, V. & Frank, H.A. The application of the energy gap law to the S₁ energies and dynamics of carotenoids. *Chem. Phys.* **194**, 237-244.

Clayton, R.K. (1980) *Photosynthesis. Physical mechanisms and chemical patterns*. Cambridge University Press.

Clayton, R.K. & Clayton, B.J. (1981) B850 pigment-protein complex of *Rhodospseudomonas sphaeroides*: Extinction coefficients, circular dichroism, and the reversible binding of bacteriochlorophyll. *Proc. Natl. Acad. Sci. U.S.A.* **78**, 5583-5587.

Cogdell, R.J. (1983) Photosynthetic reaction centers. *Ann. Rev. Plant Physiol.* **34**, 21-45.

Cogdell, R.J. (1986) Light-harvesting complexes in the purple photosynthetic bacteria. In: *Encyclopedia of Plant Physiology New Series, Vol 19, Photosynthesis III* (Staehlin, L.A. & Arntzen, C.J., eds.), pp 252-259. Springer-Verlag, Berlin.

Cogdell, R.J. (1988) The biochemistry of light-harvesting complexes. In *Photosynthetic Light-Harvesting Systems* (Scheer, H. & Schneider, eds.), pp1-10. Walter de Gruyter & Co. Berlin, New York.

Cogdell, R.J. & Frank, H.A. (1987) How carotenoids function in photosynthetic bacteria. *Biochim. Biophys. Acta* **895**, 63-79.

Cogdell, R.J. & Scheer, H. (1985) Circular dichroism of light-harvesting complexes from purple photosynthetic bacteria. *Photochem. Photobiol.* **42**, 669-678.

Cogdell, R.J. & Thornber, J.P. (1979) The preparation and characterization of different types of light-harvesting pigment-protein complexes from some purple bacteria. In: *Ciba Foundation Symposium 61 (new series)*, pp 61-79. Elsevier, Amsterdam.

Cogdell, R.J., Parson, W.W. & Kerr, M.A. (1976) The type, amount and location of carotenoids within reaction centres from *Rps. sphaeroides* and *R. rubrum*. *Biochim. Biophys. Acta* **408**, 189-199.

Cogdell, R.J., Durant, I., Valentine, J., Lindsay, J.G. & Schmidt, K. (1983) The isolation and partial characterisation of the light-harvesting pigment protein complement from *Rhodospseudomonas acidophila*. *Biochim. Biophys. Acta* **722**, 427-455.

Cogdell, R.J., Fyfe, P.K., Barrett, S.J., Prince, S.M., Freer, A.A., Isaacs, N.W., McGlynn, P. & Hunter, N.C. (1996) The purple bacterial photosynthetic unit. *Photosyn. Res.* **48**, 55-63.

Cogdell, R.J., Gillbro, T., Andersson, P.O., Liu, R.S.H. & Asato, A.E. (1994) Carotenoids as light-harvesting pigments. *Pure & Appl. Chem.* **66**, 1041-1046.

Cogdell, R.J., Isaacs, N.W., Freer, A.A., Arrelano, J., Howard, T.D., Papiz, M.Z.,

- Hawthornthwaite-Lawless, A.M. & Prince, S.M. (1997) The structure and function of the LH2 (B800-850) complex from the purple photosynthetic bacterium *Rhodospseudomonas acidophila* strain 10050. *Prog. Biophys. Molec. Biol.* **68**, 1-27.
- Cogdell, R.J., Monger, T.G. & Parson, W.W. (1975) Carotenoid triplet states in reaction centres from *Rhodospseudomonas sphaeroides* and *Rhodospirillum rubrum*. *Biochim. Biophys. Acta* **430**, 89-93.
- Cogdell, R.J., Wooley, K.J., Ferguson, L.A. & Dawkins, D.J. (1991) Crystallization of purple bacterial antenna complexes. In: *Crystallization of Membrane Proteins* (Michel, H., ed.), pp125-136. CRC Press, Boca Raton, Florida.
- Cogdell, R.J., Zuber, H., Thornber, P.J., Drews, G., Gingras, G., Niederman, R.A., Parson, W.W. & Feher, G. (1985) Recommendations for the naming of photochemical reaction centres and light-harvesting pigment-protein complexes from purple photosynthetic bacteria. *Biochim. Biophys. Acta* **806**, 185-186.
- Cohen-Bazire, G., Sistrom, W.R. & Stanier, R.Y. (1957) Kinetic studies of pigment synthesis by non-sulfur purple bacteria. *J. Cell. Comp. Physiol.* **49**, 25-51, 58-68.
- Cohn, E.J., Hughes, W.L. & Weare, J.H. (1947) *J. Am. Chem. Soc.* **69**, 1753.*
- Dau, H. (1994) Molecular mechanisms and quantitative models of variable Photosystem II fluorescence. *Photochem. Photobiol.* **60**, 1-23.
- Davydov, A.S. (1962) *Theory of Molecular Excitons* (translated by Kasa, M. & Oppenheimer, M. Jnr.). McGraw-Hill, New York.
- Davydov, A.S. (1971) In: *Theory of Molecular Excitons*. pp31, 91, 128. Plenum Press, New York.
- Davis, C.M., Bustamante, P.L. & Loach, P.A. (1995) Reconstitution of the bacterial core light-harvesting complexes of *Rhodobacter sphaeroides* and *Rhodospirillum rubrum* with isolated α - and β -polypeptides, bacteriochlorophyll *a*, and carotenoid. *J. Biol. Chem.* **270**, 5793-5804.
- Dawkins, D.J. (1988) PhD Thesis, University of Glasgow.
- Dawkins, D.J., Ferguson, L.A. & Cogdell, R. (1988) The structure of the 'core' of the purple bacterial photosynthetic unit. In: *Photosynthetic Light-Harvesting Systems*, pp115-127. Walter de Gruyter & Co., Berlin.
- Debus, R.J., Feher, G. & Okamura, M.Y. (1985) LM complex of reaction centers from *Rhodospseudomonas sphaeroides* R-26: characterization and reconstitution with the H-subunit. *Biochemistry* **24**, 2488-2500.
- Debus, R.J., Feher, G. & Okamura, M.Y. (1986) Iron-depleted reaction centers from *Rhodospseudomonas sphaeroides* R-26.1.-characterization and reconstitution with Fe^{2+} , Mn^{2+} , Co^{2+} , Ni^{2+} , Cu^{2+} , and Zn^{2+} . *Biochemistry* **25**, 2276-2287.
- Deinum, G., Otte, S.C.M., Gardiner, A.T., Aartsmaa, T.J., Cogdell, R.J. & Ames, J. (1991) Antenna organization of *Rhodospseudomonas acidophila*: A study of the excitation migration. *Biochim. Biophys. Acta* **1060**, 125-131.
- Deisenhofer, J. & Michel, H. (1989) Nobel Lecture. The photosynthetic reaction centre from the purple bacterium *Rhodospseudomonas viridis*. *EMBO J.* **8**, 2149-2170.

- Deisenhofer, J., Epp, O., Miki, F., Huber, R. & Michel, H. (1984) X-ray structure analysis of a membrane protein complex: electron density map at 3Å resolution and a model of the chromophores of the photosynthetic reaction center from *Rhodospseudomonas viridis*. *J. Mol. Biol.* **180**, 385-398.
- Deisenhofer, J., Epp, O., Miki, F., Huber, R. & Michel, H. (1985) Structure of the protein subunits in the photosynthetic reaction centre of *Rhodospseudomonas viridis* at 3Å resolution. *Nature* **318**, 618-624.
- Dexter, D.L. (1953) A theory of sensitised luminescence in solids. *J. Chem. Phys.* **21**, 836-860.
- Dickerson, R.E. (1980) Evolution and gene transfer in purple photosynthetic bacteria. *Nature* **283**, 210-212
- Drews, G. (1985) Structure and functional organization of light-harvesting complexes and photochemical reaction centers in membranes of phototrophic bacteria. *Microbiol. Revs.* **49**, 59-70.
- Ducruix, A. & Giegé, R. (1992) Methods of crystallization. In: *Crystallization of nucleic acids and proteins* (Ducruix, A. & Giegé, R., eds.) p75. Oxford University Press, New York.
- Dutton, P.L. & Prince, R.C. (1978) In: *The Photosynthetic Bacteria* (Clayton, R.K. & Sistrom, W.R., eds.), pp525-570. Plenum Press, New York.
- Dutton, P.L., Kaufmann, K.J., Chance, B. & Rentzepis, P.M. (1975) Picosecond kinetics of the 1250nm band of the *Rhodospseudomonas sphaeroides* reaction center: the nature of the primary photochemical intermediary state. *FEBS Lett.* **60**, 275-280.
- Dutton, P.L., Petty, K.M., Bonner, H.S. & Morse, S.D. (1975) Cytochrome *c*₂ and reaction center of *Rhodospseudomonas sphaeroides* Ga membranes. Extinction coefficients, content, half-reduction potentials, kinetics and electric field alterations. *Biochim. Biophys. Acta* **387**, 536-556.
- Duysens, L.N.M. & Sweers, H.E. (1963) Mechanisms of two photochemical reactions in algae as studied by means of fluorescence. In: *Studies on Microalgae and Photosynthetic Bacteria* (Japanese Society of Plant Physiologists, ed.) pp 353-372. University of Tokyo Press, Tokyo.
- Eisenberg, D. (1984) Three-dimensional structure of membrane and surface proteins. *Ann. Rev. Biochem.* **53**, 595-623.
- El-Kabbani, O., Chang, C.-H., Tiede, D., Norris, J. & Schiffer, M. (1991) Comparison of reaction centers from *Rhodobacter sphaeroides* and *Rhodospseudomonas viridis*: overall architecture and protein-pigment interactions. *Biochemistry* **30**, 5361-5369.
- Emerson, R. & Arnold, W.A. (1932) The photochemical reaction in photosynthesis. *J. Gen. Physiol.* **16**, 191-205.
- Engelhardt, H., Engel, A. & Baumcister, W. (1986) Stoichiometric model of the photosynthetic unit of *Ectothiorhodospira halochloris*. *Proc. Natl. Acad. Sci. U.S.A.* **83**, 8972-8976.
- Ermler, U., Michel, H. & Schiffer, M. (1994) Structure and function of the

- photosynthetic reaction center from *Rhodobacter sphaeroides*. *J. Bioenerg. Biomemb.* **26**, 5-15.
- Evans, M.B., Hawthornthwaite, A.M. & Cogdell, R.J. (1990) Isolation and characterisation of the different B800-850 light-harvesting complexes from low- and high-light grown cells of *Rhodospseudomonas palustris*, strain 2.1.6. *Biochim. Biophys. Acta* **1016**, 71-76.
- Fajer, J., Davis, M.S., Brune, D.C., Spaulding, L.D., Borg, D.C. & Forman, A. (1976) *Brookhaven Symp. Biol.* **28**, 74-104.
- Farchaus, J.W. & Oesterhelt, D. (1989) A *Rhodobacter sphaeroides* *pufL*, *M*, and *X* deletion mutant and its complementation *intrans* with a 5.3 kb *puf* operon shuttle fragment. *EMBO J.* **8**, 47-54.
- Farchaus, J.W., Gruenberg, H. & Oesterhelt, D. (1990a) Complementation of a reaction center-deficient *Rhodobacter sphaeroides* *pufLMX* deletion strain *intrans* with *pufBALM* does not restore the photosynthesis-positive phenotype. *J. Bacteriol.* **172**, 977-985.
- Farchaus, J.W., Gruenberg, H., Gray, K.A., Wachveitl, J., DeHoff, B., Kaplan, S. & Oesterhelt, D. (1990b) In: *Molecular Biology of Membrane-Bound Complexes in Phototropic Bacteria* (Drews, G. & Dawes, E.A., eds.), pp65-76, Plenum Press, New York.
- Farchaus, J.W., Barz, W.P., Gruenberg, H. & Oesterhelt, D. (1992) Studies on the expression of the *puf X* polypeptide and its requirement for photoheterotrophic growth in *Rhodobacter sphaeroides*. *EMBO J.* **11**, 2779-2788.
- Feher, G. & Okamura, M.Y. (1978) Chemical composition and properties of reaction centres. In: *The photosynthetic bacteria* (Clayton, R.E. & Sistrom, W.R., eds.), pp349-386. Plenum Press, New York.
- Feher, G. & Okamura, M.Y. (1984) Structure and function of the reaction center from *Rhodospseudomonas sphaeroides*. In: *Advances in Photosynthesis Research. Volume II*. (Sybesma, C. ed.), pp155-164. Nijkoff/Junk Publishers, The Hague.
- Feher, G., Allen, J.P., Okamura, M.Y. & Rees, D.C. (1989) Structure and function of bacterial photosynthetic reaction centers. *Nature* **339**, 111-116.
- Feick, R., Ertlmaier, A. & Ermler, U. (1996) Crystallization and X-ray analysis of the reaction center from the thermophilic green bacterium *Chloroflexus aurantiacus*. *FEBS Lett.* **396**, 161-164.
- Fleming, G.R. & van Grondelle, R. (1997) Femtosecond spectroscopy of photosynthetic light-harvesting systems. *Curr. Op. Struct. Biol.* **7**, 738-748.
- Foote, C.S. & Denny, R.W. (1968) *J. Am. Chem. Soc.* **90**, 6233-6235.*
- Foote, C.S., Chang, Y.C. & Denny, R.W. (1970) *J. Am. Chem. Soc.* **92**, 5216-5218.*
- Förster, T. (1948) Intermolecular energy transfer and fluorescence. *Ann. Rev. Phys.* **2**, 55-75.
- Fowler, G.J.S., Visschers, R.W., Grief, G.G., van Grondelle, R. & Hunter, C.N. (1992) Genetically modified photosynthetic antenna complexes with blue shifted

absorbance bands. *Nature* **355**, 848-850.

Fowler, G.J.S., Sockalingum, G.D., Robert, B., Grief, G.G. & Hunter, C.N. (1994) Blue shifts in bacteriochlorophyll absorbance correlate with changed hydrogen bonding patterns in light-harvesting LH2 mutants of *Rhodobacter sphaeroides* with alterations at α Tyr44 and α Tyr45. *Biochem. J.* **299**, 695-700.

Fowler, V.J., Pfennig, N., Schubert, W. & Stackebrandt, E. (1984) Towards a phylogeny of phototrophic sulfur bacteria - 16S rRNA oligonucleotide cataloguing of 11 species of Chromatiaceae. *Arch. Microbiol.* **139**, 382-387.

Frank, H.A. & Christensen, R.L. (1995) Singlet energy transfer from carotenoids to bacteriochlorophylls. In: *Anoxygenic photosynthetic bacteria* (Blankenship, R.E., Madigan, M.T. & Bauer, C.E., eds.), pp373-384. Kluwer Academic Publishers, Dordrecht.

Frank, H.A. & Cogdell, R.J. (1996) Carotenoids in photosynthesis. *Photochem. Photobiol.* **63**, 257-264.

Freer, A., Prince, S., Sauer, K., Papiz, M., Hawthornthwaite-Lawless, A., McDermott, G., Cogdell, R. & Isaacs, N.W. (1996) Pigment-pigment interactions and energy transfer in the antenna complex of the photosynthetic bacterium *Rhodospseudomonas acidophila*. *Structure* **4**, 449-462.

Freiberg, A. (1995) Coupling of antennas to reaction centers. In: *Anoxygenic photosynthetic bacteria* (Blankenship, R.E., Madigan, M.T. & Bauer, C.E., eds.), pp385-398. Kluwer Academic Publishers, Dordrecht.

Fujii, R., Onaka, K., Kuki, M., Koyama, Y. & Watanabe, Y. (1998) The $2A_g^-$ energies of all-trans-neurosporene and spheroidene as determined by fluorescence spectroscopy. *Chem. Phys. Lett.* **288**, 847-853.

Fuller, R.C., Conti, S.F. & Mellin, D.B. (1963) In: *Bacterial Photosynthesis* (Gest, H., san Pietro, A. & Vernon, L.F., eds.), p71. Antioch Press, Yellow Springs, Ohio.

Fyfe, P.K. & Cogdell, R.J. (1996) Purple bacterial antenna complexes. *Curr. Opin. Struct. Biol.* **6**, 467-472.

Gall, A. (1994) *Purification, characterisation and crystallisation from a range of Rhodospirillineae pigment-protein complexes*. PhD Thesis, University of Glasgow.

Garavito, R.M. (1991) Crystallizing membrane proteins: Experiments on different systems. In: *Crystallization of Membrane Proteins* (Michel, H., ed.), pp89-105. CRC Press, Boca Raton.

Garavito, R.M. & Rosenbusch, J.P. (1980) Three dimensional crystals of an integral membrane protein: An initial X-ray analysis. *J. Cell Biol.* **86**, 327-329.

Garavito, R.M., Jenkins, J.A., Jansonius, J.N., Karlsson, R. & Rosenbusch, J.P. (1983) X-ray diffraction analysis of matrix porin, an integral membrane protein from *Escherichia coli* outer membrane. *J. Mol. Biol.* **164**, 313-327.

Garavito, M.R., Picot, D. & Loll, P.J. (1996) Strategies for crystallizing membrane proteins. *Int. Bioenergetics and Biomembranes* **28**, 13-27.

Garcia, A., Vernon, L.P. & Mollenhauer, H. (1966) Properties of *Rhodospirillum*

- rubrum* subchromatophore particles obtained by treatment with Triton X-100. *Biochemistry* **7**, 319.
- Garcia, A., Vernon, L.P., Bacon, K. & Mollenhauer, H. (1968) Some structural and photochemical properties of *Rhodospseudomonas palustris* subchromatophore particles obtained by treatment with Triton X-100. *Biochemistry* **7**, 319-332.
- Gardiner, A.T., Cogdell, R.J. & Takaichi, S. (1993) The effect of growth conditions on the light-harvesting apparatus in *Rhodospseudomonas acidophila*. *Photosyn. Res.* **38**, 159-167.
- Gest, H. (1988) Sun-beams, cucumbers, and purple bacteria: historical milestones in early studies of photosynthesis revisited. *Photosynth. Res.* **19**, 287-308.
- Gest, H. (1997) A "misplaced chapter" in the history of photosynthesis research; the second publication (1796) on plant processes by Dr Jan Ingen-Housz, MD, discoverer of photosynthesis. *Photosynth. Res.* **53**, 65-72.
- Ghosh, R., Ghosh-Eicher, S., DiBerardino, M. & Bachofen, R. (1994a) Protein phosphorylation in *Rhodospirillum rubrum*: purification and characterisation of a water-soluble B873 protein kinase and a new component of the B873 complex, Ω , which can be phosphorylated. *Biochim. Biophys. Acta* **1184**, 28-36.
- Ghosh, R., Tschopp, P., Ghosh-Eicher, S. & Bachofen, R. (1994b) Protein phosphorylation in *Rhodospirillum rubrum*: further characterisation of kinase activity. *Biochim. Biophys. Acta* **1184**, 37-44.
- Giegé, R., Dock, A.C., Kern, D., Lorber, B., Thierry, J.C. & Moras, D. (1986) The role of purification in the crystallisation of proteins and nucleic acids. *J. Cryst. Growth* **76**, 554-561.
- Gillbro, T. & Cogdell, R.J. (1989) Carotenoid fluorescence. *Chem. Phys. Lett.* **128**, 238-243.
- *Gilliland, G. (1988) *J. Crystal Growth* **90**, 51.
- Gingras, G. & Jolchine, G. (1969) Isolation of a P870⁻ enriched particle from *Rhodospirillum rubrum*. *Prog. Photosyn. Res. Proc. Int. Congr. 1968*, 1:209.
- Giuliano, G., Pollock, D. & Scolnik, P.A. (1986) The gene *crtI* mediates the conversion of phytoene into colored carotenoids in *Rhodospseudomonas capsulata*. *J. Biol. Chem.* **261**, 12925-12929.
- Goedheer, J.C. (1958) Reversible oxidations of pigments in bacterial chromophores. *Brookhaven Symp. Biol.* **11**, 325-331.
- Goedheer, J.C. (1959) Energy transfer between carotenoids and bacteriochlorophyll in chromatophores of purple bacteria. *Biochim. Biophys. Acta* **35**, 1-8.
- Gomez, I., Sieiro, C., Ramirez, J.M., Gomez-Amores, S. & del Campo, F.F. (1982a) The antenna system of *Rhodospirillum rubrum*: Radical formation upon dark oxidation of bulk bacteriochlorophyll. *FEBS Lett.* **144**, 117-120.
- Gomez, I., Picorel, R., Ramirez, J.M. & del Campo, F.F. (1982b) Reversible oxidation of antenna bacteriochlorophyll in two photoreaction centerless mutants of *Rhodospirillum rubrum*. *Photochem. Photobiol.* **35**, 399-403.

Biochemistry **7**, 319.

Garcia, A., Vernon, L.P., Bacon, K. & Mollenhauer, H. (1968) Some structural and photochemical properties of *Rhodospseudomonas palustris* subchromatophore particles obtained by treatment with Triton X-100. *Biochemistry* **7**, 319-332.

Gardiner, A.T., Cogdell, R.J. & Takaichi, S. (1993) The effect of growth conditions on the light-harvesting apparatus in *Rhodospseudomonas acidophila*. *Photosyn. Res.* **38**, 159-167.

Gest, H. (1988) Sun-beams, cucumbers, and purple bacteria: historical milestones in early studies of photosynthesis revisited. *Photosynth. Res.* **19**, 287-308.

Gest, H. (1997) A "misplaced chapter" in the history of photosynthesis research; the second publication (1796) on plant processes by Dr Jan Ingen-Housz, MD, discoverer of photosynthesis. *Photosynth. Res.* **53**, 65-72.

Ghosh, R., Ghosh-Eicher, S., DiBerardino, M. & Bachofen, R. (1994a) Protein phosphorylation in *Rhodospirillum rubrum*: purification and characterisation of a water-soluble B873 protein kinase and a new component of the B873 complex, Ω , which can be phosphorylated. *Biochim. Biophys. Acta* **1184**, 28-36.

Ghosh, R., Tschopp, P., Ghosh-Eicher, S. & Bachofen, R. (1994b) Protein phosphorylation in *Rhodospirillum rubrum*: further characterisation of kinase activity. *Biochim. Biophys. Acta* **1184**, 37-44.

Giegé, R., Dock, A.C., Kern, D., Lorber, B., Thierry, J.C. & Moras, D. (1986) The role of purification in the crystallisation of proteins and nucleic acids. *J. Cryst. Growth* **76**, 554-561.

Gillbro, T. & Cogdell, R.J. (1989) Carotenoid fluorescence. *Chem. Phys. Lett.* **128**, 238-243.

Gilliland, G. (1988) *J. Crystal Growth* **90**, 51.*

Gingras, G. & Jolchine, G. (1969) Isolation of a P870⁻ enriched particle from *Rhodospirillum rubrum*. *Prog. Photosyn. Res. Proc. Int. Congr. 1968*, **1**:209.

Giuliano, G., Pollock, D. & Scolnik, P.A. (1986) The gene *ctl1* mediates the conversion of phytoene into colored carotenoids in *Rhodospseudomonas capsulata*. *J. Biol. Chem.* **261**, 12925-12929.

Goedheer, J.C. (1958) Reversible oxidations of pigments in bacterial chromophores. *Brookhaven Symp. Biol.* **11**, 325-331.

Goedheer, J.C. (1959) Energy transfer between carotenoids and bacteriochlorophyll in chromatophores of purple bacteria. *Biochim. Biophys. Acta* **35**, 1-8.

Gomez, I., Sieiro, C., Ramirez, J.M., Gomez-Amores, S. & del Campo, F.F. (1982a) The antenna system of *Rhodospirillum rubrum*: Radical formation upon dark oxidation of bulk bacteriochlorophyll. *FEBS Lett.* **144**, 117-120.

Gomez, I., Picorel, R., Ramirez, J.M. & del Campo, F.F. (1982b) Reversible oxidation of antenna bacteriochlorophyll in two photoreaction centerless mutants of *Rhodospirillum rubrum*. *Photochem. Photobiol.* **35**, 399-403.

- Gorrell, T.E. & Uffen, R.L. (1977) Fermentative metabolism of pyruvate by *Rhodospirillum rubrum* after anaerobic growth in darkness. *J. Bacteriol.* **131**, 533-543.
- Gottstein, J. & Scheer, H. (1983) *Proc. Natl. Acad. Sci. U.S.A.* **80**, 2231-2234.
- Gregory, R.P.F. (1977) In: *Topics in Photosynthesis* (Barber, J., ed.) Vol 2, pp.465-492. Elsevier, Amsterdam.
- Gregory, R.P.F. (1989) *Biochemistry of photosynthesis*. J. Wiley & Sons, New York.
- Green, D.W., Ingram, V.M. & Perutz, M.F. (1954) The structure of haemoglobin. *Proc. Roy. Soc.* **A225**, 287-295.
- Griffiths, M., Sistrom, W.R., Cohen-Bazire, G. & Stanier, R.Y. (1955) Functions of carotenoids in photosynthesis. *Nature* **176**, 1211-1214.
- Griffiths, M. & Stanier, R.Y. (1956) Some mutational changes in the photosynthetic pigment system of *Rhodospseudomonas sphaeroides*. *J. Gen. Microbiol.* **14**, 698-715.
- Halloren, E., McDermott, G., Lindsay, J.G., Miller, C., Freer, A.A., Isaacs, N.W. & Cogdell, R.J. (1995) Studies on the light-harvesting complexes from the thermotolerant purple bacterium *Rhodospseudomonas cryptolactis*. *Photosynth. Res.* **44**, 149-155.
- Halsey, Y.D. & Byers, B. (1975) A large photoreactive particle from *Chromatium vinosum* chromatophores. *Biochim. Biophys. Acta* **387**, 349-367
- Hampel, A., Labanaskas, M., Connors, P.G., Kirkegard, L., RajBahandary, U.L., Sigler, P.B. & Bock, R.M. (1968) Single crystals of transfer RNA from formylmethionine and phenylalanine transfer RNA's. *Science*, **162**, 1384-1387.
- Hanada, S., Kawase, Y., Hiraishi, A., Takaichi, S., Matsuura, K., Shimada, K. & Nagashima, K.V.P. (1997) *Porphyrobacter tepidarius* sp. nov., a moderately thermophilic aerobic photosynthetic bacterium isolated from a hot spring. *Intl J. Syst. Bacteriol.* **47**, 408-413.
- Hansen, T. A. & van Gemerden, H. (1972) Sulfide utilisation by purple nonsulfur bacteria. *Arch. Microbiol.* **86**, 49-56.
- Hansen, T.A. & Veldkamp, H. (1973) *Rhodospseudomonas sulfidophila* nov. spec., a new species of the purple nonsulfur bacteria. *Arch. Microbiol.* **92**, 45-48.
- Hawthornthwaite, A.M. & Cogdell, R.J. (1991) Bacteriochlorophyll-binding proteins. In: *The Chlorophylls* (Scheer, H., ed.), pp493-528. CRC Press, Boca Raton, Florida.
- Hayashi, H. & Morita, S. (1980) Near-infrared absorption spectra of light-harvesting bacteriochlorophyll protein complexes from *Chromatium vinosum*. *J. Biochem.* **88**, 1251-1258.
- Hayashi, H., Nozawa, T., Hatano, M. & Morita, S. (1981) Circular dichroism of bacteriochlorophyll *a* in light harvesting bacteriochlorophyll protein complexes from *Chromatium vinosum*. *J. Biochem.* **89**, 1853-1861.
- Hayashi, H., Miyao, M. & Morita, S. (1982a) Absorption and fluorescence spectra of light-harvesting bacteriochlorophyll-protein complexes from *Rhodospseudomonas palustris* in the near-infrared region. *J. Biochem.* **91**, 1017-1027.

- Hayashi, H., Miyao, M. & Morita, S. (1982b) Comparative studies of protein properties and bacteriochlorophyll contents of bacteriochlorophyll-protein complexes from spectrally different types of *Rp. palustris*. *J. Biochem.* **92**, 1085-1811.
- Heinemeyer, E.-A. & Schmidt, K. (1983) Changes in carotenoid biosynthesis caused by variation of growth conditions in cultures of *Rhodospseudomonas acidophila* strain 7050. *Arch. Microbiol.* **134**, 217-221.
- Henderson, R. & Shotton, D. (1980) Crystallization of purple membrane in three dimensions. *J. Mol. Biol.* **139**, 99.
- Hermans, J. (1982) Excluded volume theory of polymer protein interactions based on polymer-chain statistics. *J. Chem. Phys.* **77**, 2193.
- Hess, S., Åkesson, E., Cogdell, R.J., Pullerits, T. & Sundström, V. (1995) Energy transfer in spectrally inhomogeneous light-harvesting pigment protein complexes of purple bacteria. *Biophys. J.* **69**, 2211-2225.
- Hess, S., Chachisvilis, M., Timpmann, K., Jones, M.R., Fowler, G.J.S., Hunter, C.N. & Sundström, V. (1995) Temporally and spectrally resolved subpicosecond energy transfer within the peripheral antenna complex (LH2) and from LH2 to the core antenna complex in photosynthetic purple bacteria. *Proc. Natl. Acad. Sci. U.S.A.* **92**, 12333-12337.
- Hiraishi, A., Urata, K. & Satoh, T. (1995) A new genus of marine budding phototrophic bacteria, *Rhodobium* gen. nov., which includes *Rhodobium oriensis* sp. nov., and *Rhodobium marinum* comb. nov. *Int. J. Syst. Bacteriol.* **45**, 226-234.
- Hudson, B.S. & Kohler, B.E. (1974) *Ann. Rev. Phys. Chem.* **25**, 437-460.*
- Hunter, C.N. (1995) Genetic manipulation of the antenna complexes of purple bacteria. In: *Anoxygenic photosynthetic bacteria* (Blankenship, R.E., Madigan, M.T. & Bauer, C.E., eds.), pp473-501. Kluwer Academic Publishers, Dordrecht.
- Hunter, C.N., van Grondelle, R. & Olsen, J.D. (1989) Photosynthetic antenna proteins: 100 ps before photochemistry starts. *Trends Biochem. Sci.* **14**, 72-76.
- Ikedu-Yamasaki, I., Odahara, T., Mitsuoka, K., Fujiyoshi, Y. & Murata, K. (1998) Projection map of the reaction center-light harvesting 1 complex from *Rhodospseudomonas viridis* at 10Å resolution. *FEBS Lett.* **425**, 505-508.
- Imhoff, J.F. (1983) *Rhodospseudomonas marina* sp. nov., a new marine phototrophic purple bacterium. *System. Appl. Microbiol.* **4**, 512-521.
- Imhoff, J.F. (1984a) Quinones of phototrophic purple bacteria. *FEMS Microbiol. Lett.* **25**, 85-89.
- Imhoff, J.F. (1984b) Reassignment of the genus *Ectothiorhodospira* Pelsh 1936 to a new family Ectothiorhodospiraceae fam. nov., and emended description of the Chromatiaceae Bavendamm 1924. *Int. J. Syst. Bacteriol.* **34**, 338-339.
- Imhoff, J.F. (1995) Taxonomy and physiology of phototrophic purple bacteria and green sulfur bacteria. In: *Anoxygenic photosynthetic bacteria* (Blankenship, R.E., Madigan, M.T. & Bauer, C.E., eds.), pp1-15. Kluwer Academic Publishers, Dordrecht.
- Imhoff, J.F. & Trüper, H.G. (1989) The purple nonsulfur bacteria. In: *Bergey's Manual*

- of *Systematic Bacteriology* (Staley, J.T., Bryant, M.P., Pfennig, N. & Holt, J.C., eds.), Vol 3, pp1658-1661. Williams and Wilkins, Baltimore.
- Isaacs, N.W., Cogdell, R.J., Freer, A.A. & Prince, S.M. (1995) Light-harvesting mechanisms in purple photosynthetic bacteria. *Curr. Opin. Struct. Biol.* **5**, 794-797.
- Jay, F., Lambillotte, M. & Mühlthaler, K. (1983) Localization of *Rhodospseudomonas viridis* reaction center and light-harvesting proteins using ferritin-antibody labeling. *Eur. J. Cell Biol.* **30**, 1-8.
- Jay, F., Lambillotte, M., Stark, E. & Mühlthaler, K. (1984) The preparation and characterization of native photoreceptor units from the thylakoids of *Rhodospseudomonas viridis*. *EMBO J.* **3**, 773-776.
- Jenney, F.R. & Daldal, F. (1993) A novel membrane-associated *c*-type cytochrome, *cyt c_y*, can mediate the photosynthetic growth of *Rhodobacter capsulatus* and *Rhodobacter sphaeroides*. *EMBO J.* **12**, 1283-1292.
- Jiminez, R., Dikshit, S.N., Bradforth, S.E. & Fleming, G.R. (1996) Electronic excitation transfer in the LH2 complex of *Rhodobacter sphaeroides*. *J. Phys. Chem.* **100**, 6825-6834.
- Jiraskova, V. & Reiss-Husson, F. (1993) Isolation and characterization of the core light-harvesting complex B875 and its subunit form, B820, from *Rhodocyclus gelatinosus*. *Biochim. Biophys. Acta* **1183**, 301-308.
- Jiraskova, V. & Reiss-Husson, F. (1994) A specific carotenoid is required for reconstitution of the *Rubrivivax gelatinosus* B875 light harvesting complex from its subunit form B820. *FEBS Lett.* **353**, 151-154.
- Jiraskova, V., Reiss-Husson, F., Ranck, J.-L. & Moya, I. (1997) Fluorescence lifetimes and aggregation states of the core light harvesting complex B875 from *Rubrivivax gelatinosus*. *Photosynthesis Res.* **54**, 35-43.
- Joliot, P. & Joliot, A. (1964) Études cinétique de la réaction photochimique libérant l'oxygène au cours de la photosynthèse. *CR. Acad. Sci. Paris* **258**, 4622-4625.*
- Jones, M.R., McEwan, A.G. & Jackson, J.B. (1990) The role of *c*-type cytochromes in the photosynthetic electron transport pathway of *Rhodobacter capsulatus*. *EMBO J.* **12**, 1283-1292.
- Jurnak, F. (1985) Induction of elongation-factor TU-GDP crystal polymorphism by polyethylenc-glycol contaminants. *J. Mol. Biol.* **185**, 215.
- Kam, Z., Shore, H.B. & Feher, G. (1978) On the crystallization of proteins. *J. Mol. Biol.* **123**, 539-555.
- Kämpf, C. & Pfennig, N. (1980) Capacity of Chromatiaceae for chemotrophic growth. Specific respiration rates of *Thiocystis violaceae* and *Chromatium vinosum*. *Arch. Microbiol.* **127**, 125-135.
- Katayama, N., Kobayashi, M., Motojima, F., Inaka, K., Nozawa, T. & Miki, K. (1994) Preliminary X-ray crystallographic studies of photosynthetic reaction center from a thermophilic sulfur bacterium, *Chromatium tepidum*. *FEBS Lett.* **348**, 158-160.
- Kaufmann, N., Reidl, H.H., Golecki, J.R., Garcia, A.F. & Drews, G. (1982)

- Differentiation of the membrane system in cells of *Rhodospseudomonas capsulata* after transition from the chemotrophic to phototrophic growth conditions. *Arch. Microbiol.* **131**, 313-322.
- Kawasaki, H., Hoshino, Y., Hirata, A. & Yamasato, K. (1993) Is intracytoplasmic membrane structure a generic criterion? It does not coincide with phylogenetic interrelationships among phototrophic purple nonsulfur bacteria. *Arch. Microbiol.* **160**, 358-362.
- Kennis, J.T.M., Aartsma, T.J. & Amesz, J. (1994) Energy trapping in the purple sulphur bacteria *Chromatium vinosum* and *Chromatium tepidum*. *Biochim. Biophys. Acta* **1188**, 278-286.
- Kerfeld, C.A., Yeates, T.O. & Thornber, P.J. (1994) Biochemical and spectroscopic characterization of the reaction center-LH1 complex and the carotenoid-containing B820 subunit of *Chromatium purpuratum*. *Biochim. Biophys. Acta* **1185**, 193-202.
- Kingma, H., Duysens, L.N.M. & van Grondelle, R. (1983) Magnetic field-stimulated luminescence and a matrix model for energy transfer. A new method for determining the redox state of the first quinone acceptor in the reaction center of whole cells of *Rhodospirillum rubrum*. *Biochim. Biophys. Acta* **725**, 434-443.
- Kirmaier, C. & Holten, D. (1987) Primary photochemistry of reaction centres from the photosynthetic purple bacteria. *Photosynth. Res.* **13**, 225-260.
- Klug, G., Liebetanz, R. & Drews, G. (1986) The influence of bacteriochlorophyll biosynthesis on formation of pigment-binding proteins and assembly of pigment protein complexes in *Rhodospseudomonas capsulata*. *Arch. Microbiol.* **146**, 284-291.
- Klug, G. & Cohen, S.N. (1988) Pleiotropic effects of localized *Rhodobacter capsulatus* *puf* operon deletions on production of light-absorbing pigment-protein complexes. *J. Bacteriol.* **170**, 5814-5821.
- Koepke, J., Hu, X.C., Muenke, C., Schulten, K. & Michel, H. (1996) The crystal structure of the light-harvesting complex II (B800-850) from *Rhodospirillum rubrum*. *Structure* **4**, 581-597.
- Koolhaas, M.H.C., Frese, R.N., Fowler, J.G.S., Bibby, T.S., Georgakopoulou, S., van der Zwan, G., Hunter, C.N. & van Grondelle, R. (1998) Identification of the upper exciton component of the B850 bacteriochlorophylls of the LH2 antenna complex, using a B800-free mutant of *Rhodobacter sphaeroides*. *Biochemistry* **37**, 4693-4698.
- Koyama, Y., Kuki, M., Andersson, P.O. & Gillbro, T. (1996) Singlet excited states and the light-harvesting function of carotenoids in bacterial photosynthesis. *Photochem. Photobiol.* **63**, 257-264.
- Kramer, H. & Amesz, J. (1996) Antenna organization in the purple sulfur bacteria *Chromatium tepidum* and *Chromatium vinosum*. *Photosyn. Res.* **49**, 237-244.
- Kramer, H.J.M., van Grondelle, R., Hunter, C.N., Westerhuis, W.H.J. & Amesz, J. (1984) Pigment organization of the B800-850 antenna complex of *Rhodospseudomonas sphaeroides*. *Biochim. Biophys. Acta* **765**, 156-165.
- Kramer, H., Deinum, G., Gardiner, A.T., Cogdell, R.J., Franke, C., Aartsma, T.J. & Amesz, J. (1995) Energy transfer in the photosynthetic antenna system of the purple non-sulfur bacterium *Rhodospseudomonas cryptolactis*. *Biochim. Biophys. Acta* **1231**,

33-40.

Kramer, H., Frankc, C., Hunter, C.N. & Ames, J. (1998) The size of the LH1 antenna of purple bacteria. In: *Abstracts of the XIth International Congress on Photosynthesis*. pp11, SY1-2-P15.

Kraulis, P.J. (1991) Molscript - A program to produce both detailed and schematic plots of protein structures. *J. App. Cryst.* **24**, 946-950.

Krinsky, N.I. (1971) Functions. In: *Carotenoids* (Isler, O., Gutmann, H. & Solms, U., eds.). Birkhauser Verlag, Basel.*

Kühlbrandt, W. (1987) Three-dimensional crystals of the light-harvesting chlorophyll *a/b* protein complex from pea chloroplasts. *J. Mol. Biol.* **194**, 757-762.

Kühlbrandt, W. (1988) Two-dimensional crystallization of membrane proteins. *Quart. Rev. Biophys.* **25**, 1-49.

Kühlbrandt, W. (1995) Structure and function of bacterial light-harvesting complexes. *Structure* **3**, 521-525.

Laan, H., Schmidt, T., Visschers, R.W., Visscher, K.J., van Grondelle, R. & Volker, S. (1990) Energy transfer in the B800-850 antenna complex of the purple bacterium *Rhodobacter sphaeroides*: a study by spectral hole-burning. *Chem. Phys. Lett.* **170**, 231-238.

Lacmml, U.K. (1970) Cleavage of structural proteins during the assembly of the head of bacteriophage T4. *Nature* **227**, 680.

Lancaster, C.R.D., Ermler, U. & Michel, H. (1995) The structures of photosynthetic reaction centers from purple bacteria as revealed by x-ray crystallography. In: *Anoxygenic photosynthetic bacteria* (Blankenship, R.E., Madigan, M.T. & Bauer, C.E. eds.), pp503-526. Kluwer Academic Publishers, Dordrecht.

Landau, E.M. & Rosenbusch, J.P. (1996) Lipidic cubic phases: A novel concept for the crystallization of membrane proteins. *Proc. Natl. Acad. Sci. U.S.A.* **93**, 14532-14535.

Lang, H.P. & Hunter, C.N. (1994) The relationship between carotenoid biosynthesis and the assembly of the light-harvesting LH2 complex in *Rhodobacter sphaeroides*. *Biochem. J.* **298**, 197-205.

Lavergne, J. & Trissl, H.-W. (1995) Theory of fluorescence induction in Photosystem II: derivation of analytical expressions in a model including exciton-radical pair equilibrium and restricted energy transfer between photosynthetic units. *Biophys. J.* **65**, 2474-2492.

Lavorel, J., Breton, J. & Lutz, M. (1986) Methodological principles of measurements of light emitted by photosynthetic systems. In: *Light Emission by Plants and Bacteria* (Govindjee, Ames, J. & Fork, D.C. eds.), pp 57-98. Academic Press, Orlando.

Le Maire, M., Kwee, S., Andersen, J. & Møller, J. (1983) Mode of interaction of polyoxyethyleneglycol detergents with membrane proteins. *Eur. J. Biochem.* **129**, 525-532.

Lilburn, T.G., Haith, C.E., Prince, R.C. & Beatty, J.T. (1992) Pleiotropic effects of *pufX* gene deletion on the structure and function of the photosynthetic apparatus of

- Rhodobacter capsulatus*. *Biochim. Biophys. Acta* **1100**, 160-170.
- Lilburn, T.G. & Beatty, J.T. (1992) Suppressor mutants of the photosynthetically incompetent *pufX* deletion mutant *Rhodobacter capsulatus* Δ RC6(p1L2). *FEMS Microbiol. Lett.* **100**, 155-160.
- Loach, P.A. & Parkes-Loach, P.S. (1995) Structure-function relationships in core light-harvesting complexes (LH1) as determined by characterization of the structural subunit and by reconstitution experiments. In: *Anoxygenic photosynthetic bacteria* (Blankenship, R.E., Madigan, M.T. & Bauer, C.E. eds.), pp437-471. Kluwer Academic Publishers, Dordrecht.
- Loach, P.A., Androes, G.M., Maksim, A.F. & Calvin, M. (1963) Variation in electron paramagnetic resonance signals of photosynthetic systems with the redox level of their environment. *Photochem. Photobiol.* **2**, 443-454.
- Madigan, M.T. & Gest, H. (1979) Growth of the photosynthetic bacterium *Rhodospseudomonas capsulata* chemoautotrophically in darkness with H₂ as the energy source. *J. Bacteriol.* **137**, 524-530.
- Matsuura, K. & Shimada, K. (1986) Cytochromes functionally associated to photochemical reaction centers in *Rhodospseudomonas palustris* and *Rhodospseudomonas acidophila*. *Biochim. Biophys. Acta* **852**, 9-18.
- Mauzerall, D. & Greenbaum, N.L. (1989) The absolute size of a photosynthetic unit. *Biochim. Biophys. Acta* **974**, 119-140.
- Mayer, H. (1984) Significance of lipopolysaccharide structure for taxonomy and phylogenetical relatedness of Gram-negative bacteria. In: *The Cell Membrane* (Haber, E., ed.), pp71-83. Plenum Press, New York.
- McDermott, G., Prince, S.M., Freer, A.A., Hawthornthwaite-Lawless, A.M., Papiz, M.Z., Cogdell, R.J. & Isaacs, N.W. (1995) Crystal structure of an integral membrane light-harvesting complex from photosynthetic bacteria. *Nature* **374**, 517-521.
- McElroy, J.D., Feher, G. & Mauzerall, D.C. (1969) On the nature of the free radical formed during the primary process of bacterial photosynthesis. *Biochim. Biophys. Acta* **172**, 180-183.
- McGlynn, P., Hunter, C.N. & Jones, M.R. (1994) The *Rhodobacter sphaeroides* PufX protein is not required for photosynthetic competence in the absence of a light harvesting system. *FEBS Lett.* **349**, 349-353.
- McGlynn, P., Westerhuis, W.H.J., Jones, M.R. & Hunter, C.N. (1996) Consequences for the organization of reaction center-light harvesting antenna 1 (LH1) core complexes of *Rhodobacter sphaeroides* arising from deletion of amino acid residues from the C-terminus of the LH1 α polypeptides. *J. Biol. Chem.* **271**, 3285-3292.
- McPherson, A. (1982) In: *The Preparation and Analysis of Protein Crystals*. John Wiley & Sons, New York.
- McPherson, A. (1990) Current approaches to macromolecular crystallization. *Eur. J. Biochem.* **189**, 1.
- McPherson, A. (1991) Useful principles for the crystallization of membrane proteins. In: *Crystallization of Membrane Proteins* (Michel, H., ed.), pp1-51. CRC Press, Boca

Raton.

Mechler, B. & Oelze, J. (1978) Differentiation of the photosynthetic apparatus of *Chromatium vinosum*, strain DIII. Analyses of spectral alterations. *Arch. Microbiol.* **118**, 109-114.

Meckenstock, R.U., Brunisholz, R.A. & Zuber, H. (1992a) The light-harvesting core-complex and the B820-subunit from *Rhodospseudomonas marina*. Part I. Purification and characterisation. *FEBS. Lett.* **311**, 128-134.

Meckenstock, R.U., Krusche, K., Brunisholz, R.A. & Zuber, H. (1992b) The light-harvesting core-complex and the B820-subunit from *Rhodospseudomonas marina*. Part II. Electron microscopic characterization. *FEBS. Lett.* **311**, 135-138.

Meckenstock, R.U., Krusche, K., Staehlin, L.A., Cyrklaff, M. & Zuber, H. (1994) The six-fold symmetry of the B880 light-harvesting complex and the structure of the photosynthetic membranes of *Rhodospseudomonas marina*. *Biol. Chem. Hoppe-Seyler*, **375**, 429-438.

Meyer, T.E., Cannac, V., Fitch, J., Bartsch, R.G., Tollin, D., Tollin, G. & Cusanovich, M.A. (1990) Soluble cytochromes and ferridoxins from the marine purple phototrophic bacterium *Rhodospseudomonas marina*. *Biochim. Biophys. Acta* **1017**, 125-138.

Meyer, T.E. & Donohue, T.J. (1995) Cytochromes, iron-sulfur, and copper proteins mediating electron transfer from the cyt *bc₁* complex to photosynthetic reaction center complexes. In: *Anoxygenic photosynthetic bacteria* (Blankenship, R.E., Madigan, M.T. & Bauer, C.E. eds.), pp725-745. Kluwer Academic Publishers, Dordrecht.

Michel, H. (1982) Three-dimensional crystals of a membrane protein complex. The photosynthetic reaction centre from *Rhodospseudomonas viridis*. *J. Mol. Biol.* **158**, 567-572.

Michel, H. (1983). Crystallization of membrane proteins. *TIBS* 56-59.

Michel, H. (1991). General and practical aspects of membrane protein crystallization. In: *Crystallization of Membrane Proteins* (Michel, H. ed.), pp73-88. CRC Press, Boca Raton.

Michel, H. & Oesterhelt, D. (1980) Three dimensional crystals of membrane proteins: Bacteriorhodopsin. *Proc. Natl. Acad. Sci. U.S.A.* **77**, 1283-1285.

Miers, H.A. & Isaac, F. (1907) The spontaneous crystallisation of binary mixtures - experiments on salol and betol. *Proc. Roy. Soc.* **A79**, 322.

Mikol, V. & Giegé, R. (1992) The physical chemistry of protein crystallization. In: *Crystallization of Nucleic Acids and Proteins* (Ducruix, A. & Giegé, R., eds.), pp219-240. Oxford University Press, Oxford.

Miller, K.R. (1979) Structure of a bacterial photosynthetic membrane. *Proc. Natl. Acad. Sci. U.S.A.* **76**, 6415-6419.

Miller, K.R. (1982) Three-dimensional structure of a photosynthetic membrane. *Nature* **300**, 53-55.

Miyazaki, T., Morita, S., Hatano, M. & Nozawa, T. (1979) Bacteriochlorophyll *a*-types

- in chromatophore and subchromatophore preparations from *Rhodospseudomonas sphaeroides*. *J. Biochem.* **86**, 1411-1417.
- Miyazaki, T. & Morita, S. (1981) CD and absorption spectra of bacteriochlorophyll types in *Chromatium vinosum* and *Rp. palustris*. *Photosynthetica* **15**, 238-243.
- Michel-Beyerle, M.E., Plato, M., Deisenhofer, J., Michel, H., Bixon, M. & Jortner, J. (1988) Unidirectionality of charge separation in reaction centers of photosynthetic bacteria. *Biochim. Biophys. Acta* **932**, 52-70.
- Mitchell, P. (1961) Coupling of photophosphorylation to electron and hydrogen transfer by a chemi-osmotic type of mechanism. *Nature* **191**, 144-148.
- Molisch, H. (1907) *Die purpurbakterien nach neuen untersuchungen*. Fisher Verlag, Jena.
- Monger, T.G. & Parson, W.P. (1977) Singlet-triplet fusion in *Rhodospseudomonas sphaeroides* chromatophores. A probe of the organization of the photosynthetic apparatus. *Biochim. Biophys. Acta* **460**, 393-407.
- Monshouwer, R., Abrahamsson, M., van Mourik, F. & van Grondelle, R. (1997) Superradiance and exciton delocalisation in bacterial photosynthetic light-harvesting systems. *J. Phys.Chem. B.* **101**, 7241-7248.
- Monshouwer, R., Ortiz de Zarate, I., van Mourik, F. & van Grondelle, R. (1995) Low-intensity pump-probe spectroscopy on the B800 to B850 transfer in the light harvesting 2 complex of *Rhodobacter sphaeroides*. *Chem. Phys. Lett.* **246**, 341-346.
- Nagae, H., Kikitani, T., Katoh, T. & Mimuro, M. (1993) Calculation of excitation transfer matrix elements between the S₂ and S₁ states of carotenoid and the S₂ and S₁ states of bacteriochlorophyll. *J. Chem. Phys.* **98**, 8012-8023.
- Nagarajan, V. & Parson, W.W. (1997) Excitation energy transfer between the B850 and B875 antenna complexes of *Rhodobacter sphaeroides*. *Biochemistry* **36**, 2300-2306.
- Nakagawa, H., Okada, t. & Koyama, Y. (1995) Role of amino-acid sidechains in electron-transfer reactions in reaction center of *Rhodospseudomonas viridis* as revealed by extended Hückel molecular orbital calculations. *Biospectroscopy* **1**, 169-186.
- Neiderman, R.A. & Gibson, K.D. (1976) Isolation and physicochemical properties of membranes. In: *The Photosynthetic Bacteria* (Clayton, R.K. & Sistrom, W.R., eds.) pp. Plenum Press, New York.
- Norris, J.R. & Katz, J.J. (1978) In: *The Photosynthetic Bacteria* (Clayton, R.E. & Sistrom, W.R., eds.), pp397-418. Plenum Press, New York.
- Oling, F., Boekma, E.J., de Zarate, I.O., Visschers, R., van Grondelle, R. Keegstra, W., Brisson, A. & Picorel, R. (1996) Two-dimensional crystals of LH2 light-harvesting complexes from *Ectothiorhodospira* sp. and *Rhodobacter capsulatus* investigated by electron microscopy. *Biochim. Biophys. Acta* **1273**, 44-50.
- Olsen, J.D. & Hunter, C.N. (1994) Protein structure modelling of the bacterial light-harvesting complex. *Photochem. Photobiol.* **60**, 521-535.
- Otte, S.C.M., Kleinherenbrink, F.A.M. & Ames, J. (1993) Energy transfer between the reaction center and the antenna in purple bacteria. *Biochim. Biophys. Acta* **1143**, 84-

90.

- Overfield, R.E. & Wraight, C.A. (1980) Oxidation of cytochromes *c* and *c*₂ by bacterial photosynthetic reaction centers in phospholipid vesicles. I. Studies with neutral membranes. *Biochemistry* **19**, 3322-3327.
- Paillotin, G. (1976) Movement of excitations in the photosynthetic domains of Photosystem II. *J. Theor. Biol.* **58**, 237-252.
- Papiz, M.Z., Hawthornthwaite, A.M., Cogdell, R.J., Wooley, K.J., Wightman, P.A., Ferguson, L.A. & Lindsay, J.G. (1989) Crystallization and characterization of two crystal forms of the B800-850 light-harvesting complex from *Rhodospseudomonas acidophila* strain 10050. *J. Mol. Biol.* **209**, 833-835.
- Papiz, M.Z., Prince, S.M., Hawthornthwaite-Lawless, A.M., McDermott, G., Freer, A.A., Isaacs, N.W. & Cogdell, R.J. (1996) A model for the photosynthetic apparatus of purple bacteria. *Trends Plant Sci.* **1**, 198-206.
- Parkes-Loach, P.S., Springle, J.R. & Loach, P.A. (1998) Reconstitution of the B873 light-harvesting complex of *Rhodospirillum rubrum* from separately isolated α - and β -polypeptides and bacteriochlorophyll *a*. *Biochemistry* **29**, 2951-2960.
- Parson, W.W. (1978) Quinones as secondary electron acceptors. In: *The photosynthetic bacteria* (Clayton, R.E. & Sistrom, W.R., eds.), pp445-470. Plenum Press, New York.
- Parson, W.W. & Cogdell, R.J. (1975) The primary photochemical reactions of bacterial photosynthesis. *Biochim. Biophys. Acta* **416**, 105-149.
- Parson, W.W. & Monger, T.G. (1976) *Brookhaven Symp. Biol.* **28**, 196-212.
- Parson, W.W. & Ke, B. (1982) In: *Photosynthesis* (Govindjee, ed.), pp331-385. Academic Press, New York.
- Peters, J.D. & Drews, G. (1983) The transverse membrane orientation of the light-harvesting and reaction center polypeptides of *Rhodospseudomonas capsulata*. *FEBS Lett.* **162**, 57-60.
- Pfennig, N. (1969) *Rhodospseudomonas acidophila* sp.n., a new species of the budding purple non-sulfur bacteria. *J. Bacteriol.* **99**, 597-602.
- Pfennig, N. (1978) General physiology and ecology of photosynthetic bacteria. In *The photosynthetic bacteria* (Clayton, R.E. & Sistrom, W.R., eds.), pp3-18. Plenum Press, New York.
- Pfennig, N. & Trüper, H.G. (1971) Higher taxa of the phototrophic bacteria. *Intl. J. Syst. Bacteriol.* **21**, 17-18.
- Pfennig, N. & Trüper, H.G. (1974) The phototrophic bacteria. In: *Bergey's Manual of Determinative Bacteriology*, 8th Edition. (Buchanan, R.E & Gibbons, N.E., eds.), pp22-64. The Williams and Wilkins Co., Baltimore.
- Phillipson, K.D. & Sauer, K. (1973) Comparative study of CD spectra of reaction centres from several photosynthetic bacteria. *Biochemistry* **12**, 535.
- Picorel, R., Lefebvre, S. & Gingras, G. (1984) Oxido-reduction of B800-850 and B880 holochromes isolated from three species of photosynthetic bacteria studied by electron

- paramagnetic resonance and optical spectroscopy. *Eur. J. Biochem.* **142**, 305-311.
- Picot, D., Loll, P.J. & Garavito, R.M. (1994) The X-ray crystal structure of the membrane protein prostaglandin H₂ synthase-1. *Nature* **367**, 243-249.
- Price, N.C. (1995) Circular dichroism in protein analysis. In: *Molecular Biology and Biotechnology: A Comprehensive Desk Reference* (Meyers, R.A., ed.) pp179-185. VCH Press, New York.
- Prieur, D. (1997) Microbiology of deep-sea hydrothermal vents. *Trends in Biotechnology* **15**, 242-244.
- Prince, S.M., Papiz, M.Z., Freer, A.A., McDermott, G., Hawthornthwaite-Lawless, A.M., Cogdell, R.J. & Isaacs, N.W. (1997) Apoprotein structure in the LH2 complex from *Rhodospseudomonas acidophila* strain 10050: Modular assembly and protein pigment interactions. *J. Mol. Biol.* **268**, 412-423.
- Pugh, R.J., McGlynn, P., Jones, M.R. & Hunter, C.N. (1998) The LH1-RC core complex of *Rhodobacter sphaeroides*: interaction between components, time-dependent assembly, and topology of the PufX protein. *Biochim. Biophys. Acta* **1366**, 301-316.
- Pucheu, N.L., Kerber, N.L. & Garcia, A.F. (1974) Comparative studies on membranes isolated from *Rhodospseudomonas viridis* grown in the presence and in the absence of yeast extract. *Arch. Microbiol.* **101**, 259-272.
- Pullerits, T. & Sundström, V. (1996) Photosynthetic light-harvesting pigment-protein complexes: Toward understanding how and why. *Acc. Chem. Res.* **29**, 381-389.
- Pullerits, T., Chachisvilis, M. & Sundström, V. (1996) Exciton delocalization length in the B850 antenna of *Rhodobacter sphaeroides*. *J. Phys. Chem.* **100**, 10787-10792.
- Rafferty, C.N., Bolt, J., Sauer, K. & Clayton, R.K. (1979) Photooxidation of antenna bacteriochlorophyll in chromatophores from carotenoidless mutant *Rhodospseudomonas sphaeroides* and the attendant loss of dimeric exciton interaction. *Proc. Natl. Acad. Sci. USA* **76**, 4429-4432.
- Recchia, P.A., Davis, C.M., Lilburn, T.G., Beatty, J.T., Parkes-Loach, P.S., Hunter, C.N. & Loach, P.A. (1998) Isolation of the PufX protein from *Rhodobacter capsulatus* and *Rhodobacter sphaeroides*: evidence for its interaction with the polypeptide of the core light harvesting complex. *Biochemistry* (in press).
- Reed, D.W. & Ke, B. (1973) Spectral properties of reaction center preparations from *Rhodospseudomonas sphaeroides*. *J. Biol. Chem.* **248**, 3041-3045.
- Reiss-Husson, F. (1992) Crystallization of membrane proteins. In: *Crystallization of Nucleic Acids and Proteins* (Ducruix, A. & Giegé, R., eds.), pp175-194. Oxford University Press, Oxford.
- Reiss-Husson, F., Gaucher, J.F., Ducruix, A. & Arnoux, B. (1992) Structural studies of wild type *Rhodobacter sphaeroides* Y reaction center. *Photosynth. Res.* **34**, 85.
- Remsen, C. (1978) Comparative subcellular architecture of photosynthetic bacteria. In: *The photosynthetic bacteria* (Clayton, R.E. & Sistrom, W.R., eds.), pp31-60. Plenum Press, New York.
- Rickle, G.K. & Cusanovich, M.A. (1979) The kinetics of photooxidation of c-type

- cytochromes by *Rhodospirillum rubrum* reaction centers. *Arch. Biochem. Biophys.* **197**, 589-598.
- Robert, B. & Lutz, M. (1985) Structure of antenna complexes of several Rhodospirillales from their resonance Raman spectra. *Biochim. Biophys. Acta* **807**, 10-23.
- Robert, B., Andrianambinintsoa, S. & Lutz, M. (1985) Structural characterization of high 800nm absorbing light-harvesting complexes from Rhodospirillales from their resonance Raman spectra. *J. Biochem.* **98**, 349-354.
- Roth, M., Lewit-Bentley, A. & Michel, H. (1989) Detergent structure in crystals of a bacterial reaction centre. *Nature* **340**, 659-662.
- Roth, M., Arnoux, B., Ducruix, A. & Reiss-Husson, F. (1991) Structure of the detergent phase and protein-detergent interactions in crystals of the wild-type (strain Y) *Rhodobacter sphaeroides* photochemical reaction center. *Biochemistry* **30**, 9403-9413.
- Salisbury, F.B. (1991) Photosynthesis: Environmental and Agricultural Aspects. In: *Plant Physiology*, 4th edition (Salisbury, F.B. & Ross, C.W., eds.) pp249-252. Wadsworth Publishing Co., Belmont, California.
- Sauer, K. (1972) In: *Methods in Enzymology* (San Pietro, A., ed.) Vol 24, pp. 206-217. Academic Press, New York.
- Sauer, K. (1975) In: *Bioenergetics of Photosynthesis* (Govindjee, ed.), Academic Press, New York.
- Sauer, K. & Austin, L.A. (1978) Bacteriochlorophyll-protein complexes from the light-harvesting antenna of the photosynthetic bacteria. *Biochemistry* **17**, 2011-2019.
- Sauer, K., Dratz, E.A. & Coyne, L. (1968) Circular dichroism spectra and the molecular arrangement of bacteriochlorophylls in the reaction centers of photosynthetic bacteria. *Proc. Natl. Acad. Sci. USA* **61**, 17-24.
- Sauer, P.R.R., Lottspeich, F., Unger, E., Mentele, R. & Michel, H. (1996). Deletion of a B800-850 light-harvesting complex in *Rhodospirillum molischianum* DSM 119 leads to "revertants" expressing a B800-820 complex: Insights into pigment binding. *Biochemistry* **35**, 6500-6507.
- Savage, H., Cyrklaff, M., Montoya, G., Kühlbrandt, W. & Sinning, I. (1996) Two-dimensional structure of light-harvesting complex II (LHII) from the purple bacterium *Rhodovulum sulfidophilum* and comparison with LHII from *Rhodospseudomonas acidophila*. *Structure* **4**, 243-252.
- Schägger, H. & von Jagow, G. (1987) Tricine-sodium dodecyl sulfate-polyacrylamide gel electrophoresis for the separation of proteins in a range from 1 to 100 kDa. *Anal. Biochem.* **166**, 368-379.
- Scherz, A. & Parson, W.W. (1986) Interaction of the bacteriochlorophylls in antenna bacteriochlorophyll-protein complexes of photosynthetic bacteria. *Photosyn. Res.* **9**, 21-32.
- Scherz, A. & Rosenbach-Belkin, V. (1989) Comparative study of optical-absorption and circular dichroism of bacteriochlorophyll oligomers in Triton X-100, the antenna pigment B850, and the primary donor P-860 of photosynthetic bacteria indicates that all are similar dimers of bacteriochlorophyll *a*. *Proc. Natl. Acad. Sci. USA* **86**, 1505-1509.

- Scherz, A. & Rosenbach-Belkin, V. & Fisher, J.R. (1991) Chlorophyll aggregates in aqueous solution. In: *The Chlorophylls* (Scheer, H., ed.), pp251-259. CRC Press, Boca Raton, Florida.
- Shinkarev, V. & Wraight, C.A. (1993) Electron and proton transfer in the acceptor quinone complex of reaction centers of phototrophic bacteria. In: *The Photosynthetic Reaction Center* (Deisenhofer, J. & Norris, J.R., eds.), pp194-255. Academic Press, San Diego.
- Singer, S.J. & Nicholson, G.L. (1972) The fluid mosaic model of the structure of cell membranes. *Science* **175**, 720-731.
- Sistrom, W.R. (1978) Control of antenna pigment components. In: *Photosynthetic Bacteria* (Clayton, R.K. & Sistrom, W.R., eds.), pp841-848. Plenum Press, New York.
- Stackebrandt, E., Murray, R.G.E. & Trüper, H.G. (1988) Proteobacteria classis nov., a name for the phylogenetic taxon that includes the 'purple bacteria' and their relatives. *Intl. J. Syst. Bacteriol.* **38**, 321-325.
- Stadtwald-Demchick, R., Turner, F.R. & Gest, H. (1990) *Rhodopseudomonas cryptolactis*, sp. nov., a new thermotolerant species of budding phototrophic purple bacteria. *FEMS. Microbiol. Lett.* **71**, 177-122.
- Staedlin, L.A., Golecki, J.R. & Drews, G. (1980) Supramolecular organization of chlorosomes (chlorobium vesicles) and of their membrane attachment sites in *Chlorobium limicola*. *Biochim. Biophys. Acta* **589**, 30-45.
- Stark, W., Kühlbrandt, W., Wildhaber, I., Wehrli, E. & Mühlethaler, K. (1984) The structure of the photoreceptor unit of *Rhodopseudomonas viridis*. *EMBO J.* **3**, 777-783.
- Stark, W., Jay, F. & Mühlethaler, K. (1986) Localization of reaction center and light-harvesting complexes in the photosynthetic unit of *Rhodopseudomonas viridis*. *Arch. Microbiol.* **146**, 130-133.
- Steffen, H. & Calvin, M. (1970) The origin of the long wavelength absorption bands in purple bacteria. *Biochem. Biophys. Res. Commun.* **41**, 478.
- Steiner, R. & Scheer, H. (1985) Characterisation of a B800/1020 antenna from the photosynthetic bacteria *Ectothiorhodospira halochloris* and *Ectothiorhodospira abdelmalekii*. *Biochim. Biophys. Acta* **807**, 278-284.
- Stetter, K.O. (1996) Hyperthermophilic prokaryotes. *FEMS Microbiol. Rev.* **18**, 149-158.
- Strasser, R.J. (1978) The grouping model of plant photosynthesis. In: *Chloroplast Development* (Akoyunoglou, G., ed.), pp513-524. Elsevier/North Holland Press, Amsterdam.
- Sturgis, J.N. & Robert, B. (1996) The role of chromophore-chromophore coupling in tuning the spectral properties of peripheral light-harvesting protein of purple bacteria. *Photosynth. Res.* **50**, 5-10.
- Sturgis, J.N., Jiraskova, V., Reiss-Husson, F., Cogdell, R.J. & Robert, B. (1995) Structure and properties of the bacteriochlorophyll binding site in peripheral light-

harvesting complexes of purple bacteria. *Biochemistry* **34**, 517-523.

Sundström, V. & van Grondelle, R. (1995) Kinetics of excitation transfer and trapping in purple bacteria. In: *Anoxygenic photosynthetic bacteria* (Blankenship, R.E., Madigan, M.T. & Bauer, C.E., eds.), pp349-372. Kluwer Academic Publishers, Dordrecht.

Sundström, V., van Grondelle, R., Bergström, H., Åkesson, E. & Gillbro, T. (1986) Excitation energy transport in the bacteriochlorophyll antenna system of *Rhodospirillum rubrum* and *Rhodobacter sphaeroides*, studied by low-intensity picosecond absorption spectroscopy. *Biochim. Biophys. Acta* **851**, 431-446.

Takaichi, S., Gardiner, A.T. & Cogdell, R.J. (1993) Pigment composition of light-harvesting pigment-protein complexes from *Rhodopseudomonas acidophila*: Effect of light intensity. In: *Current Research in Photosynthesis, Vol 1* (Murata, N., ed.) pp149-152. Kluwer Academic Publishers, Dordrecht.

Tanford, C. (1980) *The Hydrophobic Effect*. John Wiley & Sons, New York.

Theiler, R. & Zuber, H. (1984) The light-harvesting polypeptides of *Rhodopseudomonas sphaeroides* R-26-1. II. Conformational analyses by attenuated total reflection infrared spectroscopy and possible molecular structure of the hydrophobic domain of the B850 complex. *Hoppe-Seyler's Z Physiol. Chem.* **365**, 721-729.

Thomas, P.E., Ryan, D. & Levin, W. (1976) An improved staining procedure for the detection of the peroxidase activity of cytochrome P-450 on sodium dodecyl sulfate polyacrylamide gels. *Anal. Biochem.* **75**, 168-176.

Thornber, P.J. (1970) Studies of three spectrally different carotenobacteriochlorophyll-protein complexes isolated from *Chromatium*, strain D. *Biochemistry* **9**, 2688-2698.

Thornber, P.J., Trospen, T. & Strouse, C.E. (1978) Bacteriochlorophyll *in vivo*: Relationships of spectral forms to specific membrane components. In: *The photosynthetic bacteria* (Clayton, R.E. & Sistrom, W.R., eds.), pp133-160. Plenum Press, New York.

Trissl, H.-W. (1996) Antenna organization in purple bacteria investigated by means of fluorescence induction curves. *Photosynth. Res.* **47**, 175-185.

Trissl, H.-W. & Lavergne, J. (1995) Fluorescence induction from Photosystem II: analytical equations for the yields of photochemistry and fluorescence derived from analysis of a model including exciton-radical pair equilibrium and restricted energy transfer between units. *Austr. J. Plant Physiol.* **22**, 183-193.*

Trüper, H.G. (1976) Higher taxa of the phototrophic bacteria: *Chloroflexaceae* fam. nov., a family for the gliding, filamentous, phototrophic "green" bacteria. *Intl. J. Syst. Bacteriol.* **26**, 74.

Trüper, H.G. & Pfennig, N. (1978) Taxonomy of the Rhodospirillales. In: *The photosynthetic bacteria* (Clayton, R.E. & Sistrom, W.R., eds.), pp19-27. Plenum Press, New York.

Trüper, H.G. & Pfennig, N. (1981) Characterization and identification of the anoxygenic phototrophic bacteria. In: *The Prokaryotes* (Starr, M.P., Stolp, H., Trüper, H.G., Balows, A. & Schlegel, H.G., eds.), pp299-312. Springer-Verlag, New York.

Ueda, T., Morimoto, Y., Sato, M., Kakuno, T., Yamashita, J. & Horio, T. (1985)

- Isolation, characterization, and comparison of a ubiquitous pigment-protein complex consisting of a reaction center and light-harvesting bacteriochlorophyll proteins present in purple photosynthetic bacteria. *J. Biochem.* **98**, 1487-1498.
- van Gorkom, H.J. (1986) Fluorescence measurements in the study of photosystem II electron transport. In: *Light Emission by Plants and Bacteria* (Govindjee, Ames, J. & Fork, D.C. eds.), pp 267-289. Academic Press, Orlando.
- van Grondelle, R. (1985) Excitation energy transfer, trapping and annihilation in photosynthetic systems. *Biochim. Biophys. Acta* **811**, 147-195.
- van Grondelle, R., Dekker, J.P., Gillbro, T. & Sundström, V. (1994) Energy transfer and trapping in photosynthesis. *Biochim. Biophys. Acta* **1187**, 1-65.
- van Grondelle, R., Kramer, H.J.M. & Rijgersberg, C.P. (1982) Energy transfer in the B800-850-carotenoid light-harvesting complex of various mutants of *Rhodospseudomonas sphaeroides* and of *Rhodospseudomonas capsulatus*. *Biochim. Biophys. Acta* **682**, 208-215.
- van Mourik, F., Hawthornthwaite, A.M., Vonk, C., Evans, M., Cogdell, R.J., Sundström, V. & van Grondelle, R. (1992) Spectroscopic characterization of the low-light B800-850 light-harvesting complex of *Rhodospseudomonas palustris*, strain 2.1.6. *Biochim. Biophys. Acta* **1140**, 85-93.
- van Niel, C.B. (1941) the bacterial photosyntheses and their importance for the general problem of photosynthesis. *Adv. Enzymol.* **1**, 263-328.
- van Noort, P.I., Zhu, Y., LoBrutto, R. & Blankenship, R.E. (1997) Redox effects on the excited state lifetime in chlorosomes and bacteriochlorophyll *c* oligomers. *Biophys. J.* **72**, 316-325.
- Visscher, K.J., Bergström, H., Sundström, V., Hunter, C.N. & van Grondelle, R. (1989) Temperature dependence of energy transfer from the long wavelength antenna Bchl-896 to the reaction center in *Rhodospirillum rubrum*, *Rhodobacter sphaeroides* (Wt and M21 mutants) from 77K to 177K, studied by picosecond absorption spectroscopy. *Photosynth. Res.* **22**, 211.
- Visschers, R.W., Germeroth, L., Michel, H., Monshouwer, R. & van Grondelle, R. (1995) Spectroscopic studies of the light-harvesting complexes from *Rhodospirillum molischianum*. *Biochim. Biophys. Acta* **1230**, 147-154.
- Visser, H.M., Somsen, O.J.G., van Mourik, F., Lin, S., van Stokkum, I.H.M. & van Grondelle, R. (1996) Direct observation of sub-picosecond equilibration of excitation energy in the light-harvesting antenna of *Rhodospirillum rubrum*. *Biophys. J.* **69**, 1083-1099.
- Vredenberg, W.J. & Duysens, L.N.M. (1963) Transfer of energy from bacteriochlorophyll to a reaction centre during bacterial photosynthesis. *Nature* **197**, 355-357.
- Wacker, T., Gad'on, N., Becker, A., Mäntele, W., Kreutz, W., Drews, G. & Welte, W. (1986) Crystallization and spectroscopic investigation with polarized light of the reaction center-B875 light-harvesting complex of *Rhodospseudomonas palustris*. *FEBS Lett.* **197**, 267-273.
- Walz, T. & Ghosh, R. (1997) Two-dimensional crystallization of the light-harvesting I-

- reaction centre photounit from *Rhodospirillum rubrum*. *J. Mol. Biol.* **265**, 107-111.
- Walz, T., Jamieson, S.J., Bowers, C.M., Bullough, P.A. & Hunter, C.N. (1998) Projection structures of three photosynthetic complexes from *Rhodobacter sphaeroides*: LH2 at 6Å and LH1 and LH1-RC at 25Å. *J. Mol. Biol.* **282**, 833-845.
- Wang, R.T. & Clayton, R.K. (1973) Isolation of photochemical reaction centers from a carotenoidless mutant of *Rhodospirillum rubrum*. *Photochem. Photobiol.* **17**, 57.
- Wantanabe, Y., Kameyama, T., Miki, Y., Kuki, M. & Koyama, Y. (1993) The 2^1A_g -state and two additional low-lying electronic states of spheroidene newly identified by fluorescence and fluorescence excitation spectroscopy at 170K. *Chem. Phys. Lett.* **206**, 62-68.
- Wehrli, E. & Kübler, O. (1980) In: *Proceedings of Life Science: Electron Microscopy at Molecular Dimensions* (Baumeister, W. & Vogell, W., eds.), pp48-56. Springer-Verlag, Heidelberg, New York.*
- Welte, W. & Kreutz, W. (1982) Formation, structure and composition of a planar hexagonal lattice composed of specific protein-lipid complexes in the thylakoid membranes of *Rhodospseudomonas viridis*. *Biochim. Biophys. Acta* **692**, 479-488.
- Welte, C., Nickel, R. & Wild, A. (1995) Three-dimensional crystallization of the light-harvesting complex from *Mantoniella squamata* (Prasinophyceae) requires an adequate purification procedure. *Biochim. Biophys. Acta* **1231**, 265-274.
- Wennerström, H. & Lindman, B. (1979) *Phys. Rep.* **52**, 1-86.*
- Wiemken, V., Brunisholz, R.A., Zuber, H. & Bachofen, R. (1983) Topology of chromatophore membrane proteins studied with a chemical marker and with proteinases in *Rhodospirillum rubrum*. *FEBS Microbiol. Lett.* **16**, 297-301.
- Weiss, M.S., Kreuzsch, A., Schiltz, E., Nestel, U., Welte, W., Weckesser, J. & Schulz, G.E. (1991) The structure of porin from *Rhodobacter capsulatus* at 1.8Å resolution. *FEBS Lett.* **280**, 379-382.
- Williams, J.C., Steiner, L.A., Ogden, R.C., Simon, M.I. & Fehrer, G. (1983) Primary structure of the M-subunit of the reaction center from *Rhodospseudomonas sphaeroides*. *Proc. Natl. Acad. Sci. U.S.A.* **80**, 6505-6509.
- Woese, C.R., Stackebrandt, E., Macke, T.J. & Fox, G.E. (1985) The phylogenetic definition of the major eubacterial taxa. *Syst. Appl. Microbiol.* **6**, 143-151.
- Xiao, W.H., Lin, S., Taguchi, A.K.W. & Woodbury, N.W. (1994) Femtosecond pump-probe analysis of energy and electron transfer in photosynthetic membranes of *Rhodobacter capsulatus*. *Biochemistry* **33**, 8313-8322.
- Yeates, T.O., Komiyama, H., Rees, D.C., Allen, J.P. & Fehrer, G. (1987) Structure of the reaction center from *Rhodobacter sphaeroides* R-26: membrane-protein interactions. *Proc. Natl. Acad. Sci. USA.* **84**, 6438-6442.
- Yeates, T.O., Komiyama, H., Chirino, A., Rees, D.C., Allen, J.P. & Fehrer, G. (1988) Structure of the reaction center from *Rhodobacter sphaeroides* R-26 and 2.4.1: Protein-cofactor (bacteriochlorophyll, bacteriopheophytin, and carotenoid) interactions. *Proc. Natl. Acad. Sci. USA.* **85**, 7993-7997.

References

- Zeppenauer, M. (1971) Formation of large crystals. In: *Methods of Enzymology* (Jacoby, W.B. ed.) **253**, 22-. Academic Press, New York.
- Zhang, F.G., van Grondelle, R. & Sundström, V. (1992) Pathways of energy flow through the light-harvesting antenna of the photosynthetic purple bacterium *Rhodobacter sphaeroides*. *Biophys. J.* **61**, 911-920.
- Zuber, H. (1985a) Structure and function of light-harvesting complexes and their polypeptides. *Photochem. Photobiol.* **42**, 821-844.
- Zuber, H. (1985b) Structural organization of tetrapyrrole pigments in light-harvesting pigment-protein complexes. In: *Optical Properties and Structure of Tetrapyrroles* (Blauer, G. & Sund, H., eds.) pp425-441. Walter de Gruyter, Berlin.
- Zuber, H. (1987) The structure of light-harvesting pigment-protein complexes. In: *The Light Reactions, Topics in Photosynthesis, Vol. 8* (Barber, J., ed.), pp197-259. Elsevier Science, Amsterdam.
- Zuber, H. & Brunisholz, R.A. (1991) Structure and function of antenna polypeptides and chlorophyll-protein complexes: Principles and variability. In: *The Chlorophylls* (Scheer, H., ed.), pp627-703. CRC Press, Boca Raton, Florida.
- Zuber, H. & Cogdell, R.J. (1995) Structure and organization of purple bacterial antenna complexes. In: *Anoxygenic photosynthetic bacteria* (Blankenship, R.E., Madigan, M.T. & Bauer, C.E., eds.), pp315-348. Kluwer Academic Publishers, Dordrecht.
- Zulauf, M. (1991) Detergent phenomena in membrane protein crystallization. In: *Crystallization of Membrane Proteins* (Michel, H., ed.), pp53-88. CRC Press Inc., Boca Raton, Florida.
- Zurdo, J., Cabrera-Fernandez, C. & Ramirez, J.M. (1993) A structural role of the carotenoid in the light-harvesting II protein of *Rhodobacter capsulatus*. *Biochem. J.* **290**, 531-537.

